Continental Break-up at the Galicia Margin

Derren James Franklyn Cresswell

A thesis presented for the degree of

DOCTOR OF PHILOSOPHY

UNIVERSITY OF BIRMINGHAM

School of Geography, Earth and Environmental Science

University of Birmingham

UK

November 13, 2018

Abstract

The Galicia margin has been at the forefront of the development and testing of models on the break-up of magma-poor passive margins. It had been previously shown that an important stage in crustal break-up was embrittlement of the pre-thinned crust and continued extension to produce a crustal scale fault that allowed water ingress and serpetinisation of the mantle underlying tilted fault blocks. However, the current paradigm of continental break-up is still largely based on two dimensional observations. The data presented here from a high resolution 3D seismic reflection data reveal in unprecedented detail the complexity of continental break-up. Mapping of structurally important surfaces, including the S reflector and a complex network of interacting faults, has revealed that the S reflector is a slip surface, and that cumulative slip can be observed to occur on S and faults that connect to it. Using the 3D geometry of the faults, analysing fault displacement at a number of different levels, and mapping syn-rift sediments it has been possible to offer a new model of break-up. This model combines elements of previous models but offers a new degree of clarity over the mechanism including fault linkage. Slip initiates at different points on the a weakened serpentinised mantle forming a slip surface that propagates up through a network of faults forming the S reflector, a detachment fault whilst also dissecting the crust, allowing further water ingress and weakening. Progressive slip and weakening rotates slip surfaces, eventually new sites of slip initiation form that propagate through the crust forming a new fault network and ceasing slip on the previous network. Continued weakening and slip eventually leads to break-up. The direction of extension can be seen to change over time, and can be considered to be around a pole of rota-

tion; this may reflect the propagation or a change is stress regime, possible due to proximity to a triple junction. Furthermore, such a rotational opening may also indicate a differential rate of extension along strike, this differential rate may induce break-up of what was (nominally) equal crustal thickness.

Dedication

To my parents, brother and niece, and also to Dawn and Prince.

Acknowledgements

The person I would like to thank most is Dr Gael Lymer, with out the thoughtful discussion about the Galicia dataset over the last 4 years this work would have been much more difficult. Furthermore he has been a source of much encouragement, and no little friendship.

Dr Carl Stephenson and Professor Tim Reston have also been the source of much encouragement and inspiration and I would like to thank them for that and for taking me on in the first place.

The various students and staff in and around the subsurface imaging room have also been extremely supportive.

I thank you all

Contents

List of Figures

List of Tables

Chapter 1

Introduction and Geology of the Galicia Margin

1.1 Introduction

The formation of oceanic basins by rifting the continental crust requires the crust to break apart and thin to zero, enabling the formation of new oceanic crust through seafloor spreading. Rifting and continental break-up is therefore the first stage in the life-cycle of oceanic basins (Wilson, 1963, 1968) and a first order process in the super-continent cycle (Nance and Murphy, 2013; Nance et al., 2014; Murphy and Nance, 2013), thus opening new oceanographic gateways and altering oceanic circulation (Barker and Burrell, 1977). The structures formed on passive continental margins during rifting and breakup will in turn influence the geometry of structures formed when a passive margin enters a phase of compressional tectonics (Reston and Manatschal, 2011; Epin et al., 2017) as the ocean closes at the end of a supercontinent cycle, incorporating large scale structures into regions of the crust where mineral deposits can often be related to large scale structures, for example see Sillitoe (2003).

Classic models of continental extension and rifting were developed from the study of the landward (proximal) portions of the continental shelf or rift basins often from data obtained for

hydrocarbon prospectivity. Figure 1.1 shows the classical model, (a), where tilted blocks forming the continental margin and slope formed brittle failure and steep faults and plastic deformation in the deeper crust. The transition to the ocean is sharp. The West Iberian margin, which pro-

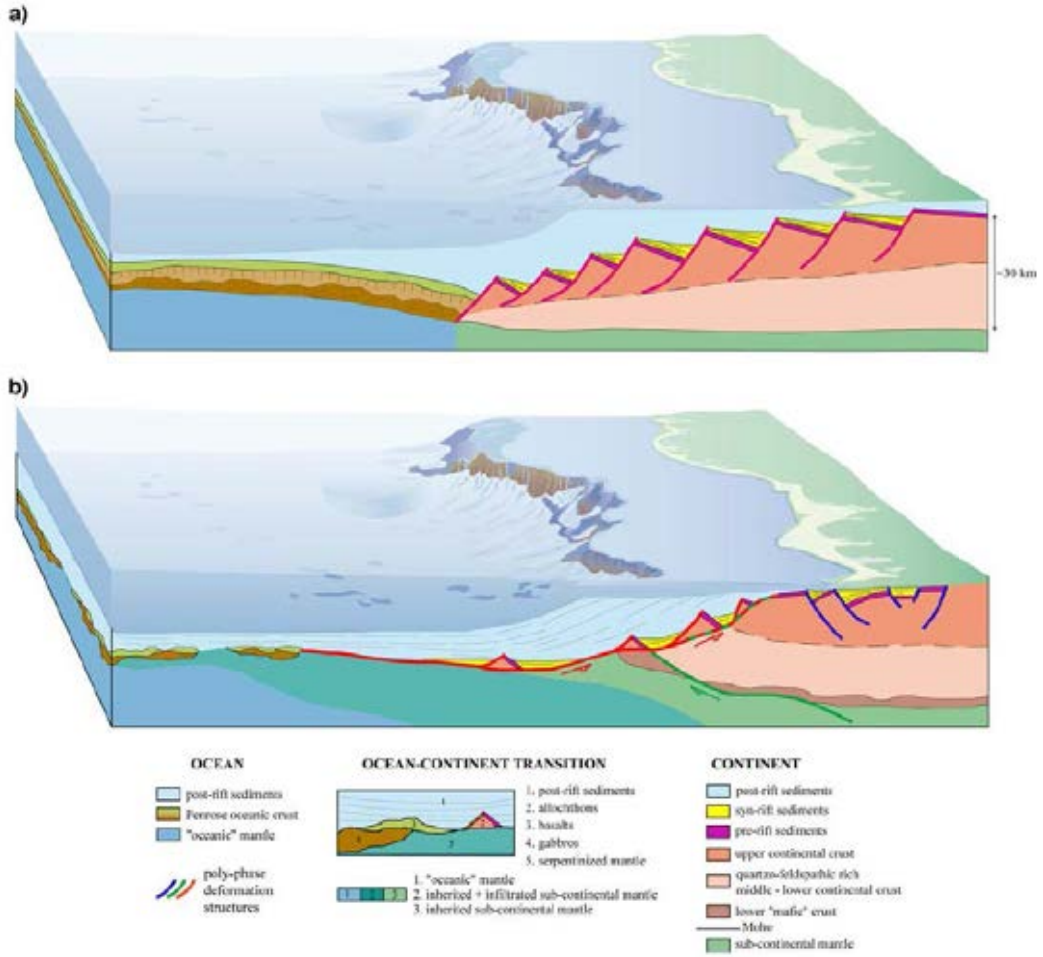

Figure 1.1: *Schematic representation of magma-poor rifted margin: a - classical, b - current paradigm, see text for details (Peron-Pinvidic and Manatschal, 2009, Figure 1).*

vides the focus of this research, provides a small section of the margin formed by the break-up of Pangaea to form the North Atlantic during the Mesozoic (Ziegler, 1989). Detailed study of the west Iberian conjugate (and other) margins through seismic surveying and sampling of the ocean floor geology, via dredge samples and drilling Table 1.1, have led to the recognition that the continental margin and the oceanic-continental crust transition includes a range of structural features and is more geologically complex than previously thought. Features include exhumed

Table 1.1: *Previous data collected on the Galicia Margin, (Sutra and Manatschal, 2012)*

Reference	**Data**
Henning et al., 2004	Seismic Reflection - Iberian Seismic Experiment
Beslier, 1996	Seismic Reflection - LG12
Discovery 215, 1998	Seismic Reflection - CAM144
Zelt et al., 2003	Seismic Refraction same line as ISE1
Dean et al., 2000	Seismic Refraction
Boillot et al., 1987a	Drilling Sites - ODP Leg 103
Sawyer et al., 1994	Drilling Sites - ODP Leg 149
Whitmarsh et al., 1998	Drilling Sites - ODP Leg 173

mantle, allochthonous blocks and possible low angle extensional detachments faults in a zone of hyperextended crust. Figure 1.1b shows a schematic version of these features but (despite the original author's caption) the current paradigm is still only 2D.

A 3D multi-channel seismic reflection dataset acquired in 2013 has allowed, for the first time, a detailed structural interpretation of this zone (Figure 1.2). Three-dimensional interpretation of faults and syn-rift sediments and an analysis of the fault heaves of these data have enabled a range of current evolutionary models of the final stages of rifting to be assessed and refined, providing a greater understanding a key component in global tectonics. It is the mechanism of final breakup of the west Iberian margin that forms the focus of this study.

The formation of ocean basin through extension and break-up of continental crust is of academic relevance as this process underpins much of the understanding required to model and predict the formation and geometry of sedimentary basins formed on oceanic margins. Such sites allow comparisons and contrasts with intra-continental extensional sedimentary basins (e.g. the North Sea, see Cowie et al. 2005). Furthermore, the extensive faulting between and within the tilted blocks seen on heavily thinned passive margins will influence the large scale cycling of fluids: between the the ocean, through sedimentary cover to deeper crustal lay-

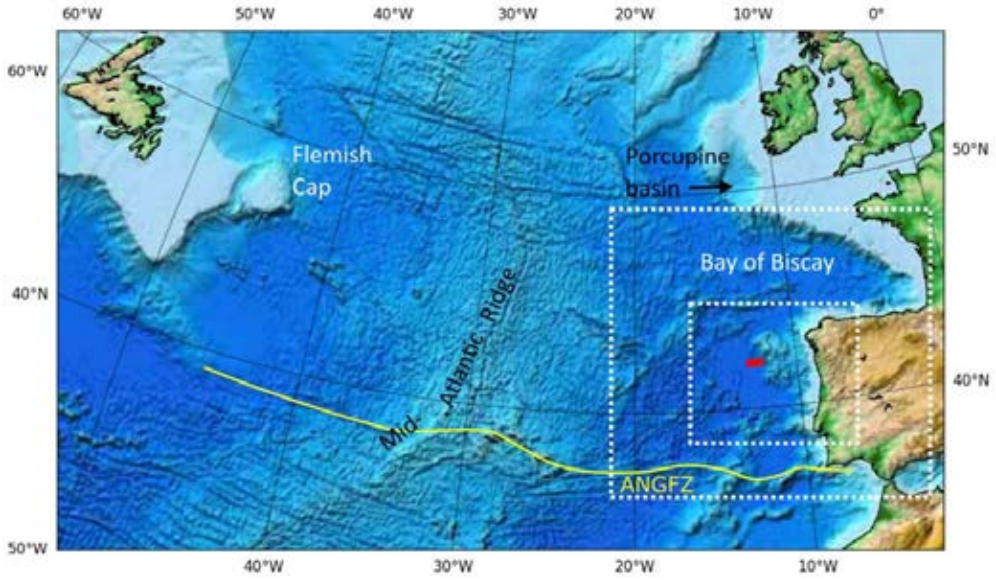

Figure 1.2: *Location of the 3D multichannel seismic survey (red box) on the Iberian passive margin and its context within the north Atlantic and with its Newfoundland conjugate - the Flemish Cap. Small white box shows area of Figure 1.7 and approximate area of 1.3. Large white box shows area of Figure 1.12. ANGFZ = Azores-Newfoundland-Gibraltar Fault Zone (Transform).*

ers. The mode of extension during rifting informs the interplay between brittle and plastic behaviour, and the associated evolution of thermal regimes as extension progresses (for example see McKenzie, 1978; Buck et al., 1988; Brune et al., 2014; Tetreault and Buiter, 2017; Duretz et al., 2016). Commercial interests stem from the move into deeper water offshore areas for exploration (Lentini et al., 2010; Alves et al., 2014) and enhanced understanding at whole reservoir scale for resource exploitation including a better understanding of structure and associated traps, source-migration-reservoir linkage and movement in to and out of the oil window. Furthermore, an enhanced understanding of the 3D structure of a magma-poor margin will facilitate the understanding of the role of crustal thinning and the associated subsidence and heat flows, crucial in developing accurate basin models.

Table 1.2: *Factors differentiating magma poor (hyperextended) and magma sustained margins (Doré and Lundin, 2015)*

Magma Poor Margin	**Magma Sustained**
Magma Poor (mantle melt c. 10%)	Magma-rich
Wide necking zone	Narrow necking zone
Slow rate of extension	Rapid rate of extension
Serpentinised mantle	Seaward-dipping reflectors (SDR)
No Moho - see mantle exhumed	Clear Moho
Deep-water break-up	Subaerial break-up

1.2 Classification of continental margins

On a fundamental level continental margins can be categorised into convergent, divergent and transform (see Twiss and Moores, 2007). Convergent margins are either subduction zones or zones where subduction has proceeded to a state where all the oceanic crust has been subducted and continents have collided. Divergent margins are areas of sea floor spreading (mid-oceanic ridges) or places where the continents are actively rifting. If continental rifting continues the continental crust thins to zero and eventually seafloor spreading will result. Once seafloor spreading begins the thinned edge of the continental margin becomes a passive component of plate tectonics i.e., a passive margin. Two end members of passive margin can be considered based on the volume of intrusive rock emplacement during rifting: magma poor and volcanic (Franke, 2013) or magma sustained (Peron-Pinvidic et al., 2013). Table 1.2 provides a summary of the factors differentiating the two end members. It is the formation of a magma poor passive margin that is the focus of this study. Where tectonic plates move past one another without divergence or convergence they are transform margins. Neither convergent nor transform margins are considered further here.

1.2.1 Conditions required for magma-poor margin formation

The location of rifting often occurs parallel to orogenic terranes exploiting lithospheric fabric and related to the orogeny (Vauchez et al., 1997) with modelling suggesting rifting occurring where the lithosphere is weakest which is where it is thickest (Vink et al., 1984). This highlights the broad role of crustal and lithospheric inheritance. Inherited structures can therefore be considered important in controlling rift structures (Manatschal, 2004), however other evidence suggests that rift evolution may reflect thermal and rheological factors more than structures (Naliboff and Buiter, 2015; Claringbould et al., 2017).

Numerical modelling suggests magma poor margins are related to slower spreading rates and are associated with hyperextension (Brune et al., 2014; Lavier and Manatschal, 2006; Tetreault and Buiter, 2017), and preferentially formed by the rifting of cool craton/post orogenic crust (Pérez-Gussinyé et al., 2001). However, recent modelling and interpretations by Manatschal et al. (2015) suggests that the specific location is less influenced by inheritance.

1.3 Rifting and break-up: the sources of evidence

The modern academic study of the formation of extensional of basins (partly driven by hydrocarbon prospectivity) has a history of drawing up on different sources of evidence; the original concept of pure shear extension was derived from physical principles whereas the simple shear model as applied to crustal scale extension was originally derived from extrapolation of geological field studies (Vann, 1985). More modern studies also use a range of evidence sources to understand the rifting process through to final breakup of the continental crust. The variety of techniques and technologies employed include numerical modelling, field analogue studies, seismic reflection and refraction imaging and rock sampling from ocean drilling programmes. These sources give a variety of observations in terms of geological accuracy and scale. The following section outlines these sources of evidence.

1.3.1 Field evidence

A number of field sites provide evidence of preserved structures of breakup and rifting. These sites are found where post rift compression has uplifted and stacked sediments and structures. Palinspastic sections through the crust may be obtained only once the compressional deformation has been restored. Geological evidence from the Alps (Manatschal and Bernoulli, 1999; Manatschal et al., 2001; Manatschal, 2004; Manatschal et al., 2007) has been at the forefront of developing conceptual models when combined with geophysical evidence obtained by seismic surveys and drilling campaigns (see sections 1.3.2 and 1.3.3).

Key pieces of evidence from field areas include the presence of a zone of exhumed continental mantle from a number of sites that have been dated ranging from Middle Jurassic to earliest Cretaceous. (Manatschal and Müntener, 2009). The Err Nappe (Switzerland) shows a distal margin detachment system (Froitzheim and Eberli, 1990; Masini and Manatschal, 2014) including continental crust and sediments in the hanging wall and serpentinised peridotites in the footwall. The Piz Nair- Samedan basin reveals syn-kinematic sedimentary systems of the distal margin showing syn-sedimentary inter-fingering of mass flow deposits derived from fault footwalls, hanging walls and background sediments (Masini et al., 2012). Facies analysis of the syn/post-tectonic sediment relationships provide an insight into the rifting processes (Mohn et al., 2010, 2012; Masini et al., 2013, 2014).

Other occurrences of previous (now uplifted) magma-poor margins include the Mesozoic basins of the Pyrenees (Tugend et al., 2014, 2015; Masini et al., 2014) and Corsica (Beltrando et al., 2013). More ancient examples include margins the late Pre-Cambrian and Lower Palaeozoic margins exposed in Caledonian-Appalacian belt (for example: Chew, 2001; Chew and van Staal, 2014; Chew and Strachan, 2014; Reston and Manatschal, 2011).

1.3.2 Seismic surveys

The Iberian margin is the most studied with seismic lines on the Newfoundland conjugate margin providing cross sections across the rift on both continental margins (Hopper et al., 2004;

Dean et al., 2015). Figure 1.3 (Sutra and Manatschal, 2012, Figure 1) shows the 2D seismic lines gathered off the Iberian margin (see also Table 1.1). These lines (Figures 1.4 and 1.5) have proven extremely influential in developing conceptual models and in validating numerical models of extension and breakup (Section 1.3.4).

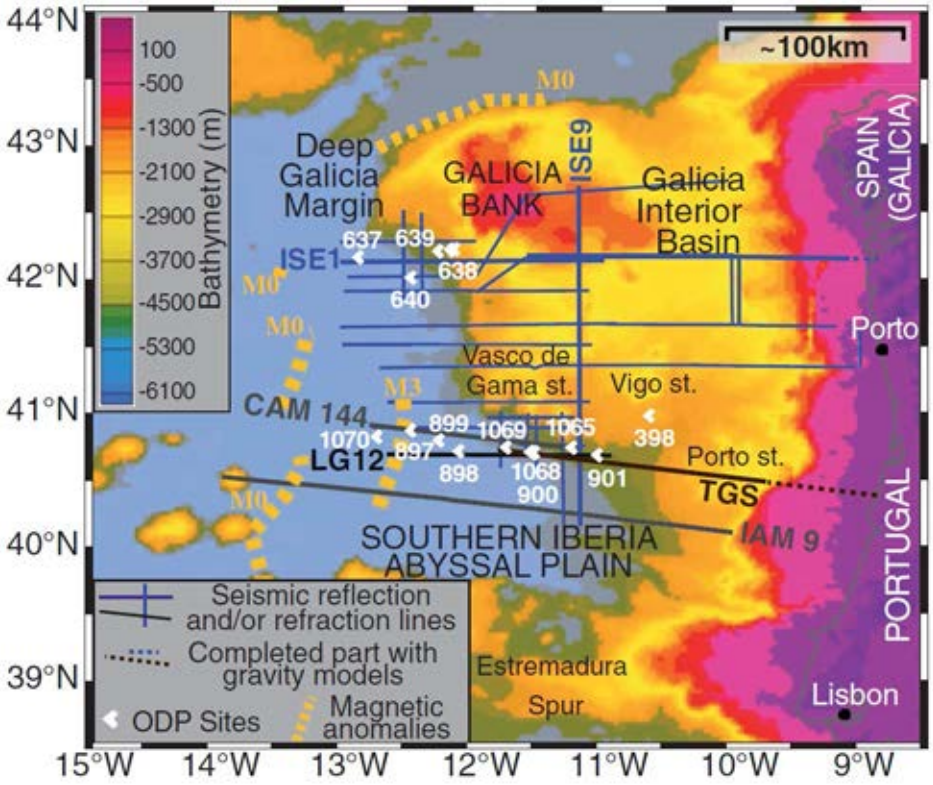

Figure 1.3: *Bathymetric map of the western Iberia margin showing the previous data (Sutra and Manatschal, 2012, Figure 1).*

Seismic imaging from the Galicia Margin and elsewhere reveals a range of structures including normal faults and tilted blocks (Whitmarsh et al., 2000, 2001; Reston, 2009*b*). Some faults and the pre/early syn-rift sediments dip steeply and therefore are hard to image seismically (Reston, 2005). The use of pre-stack depth migration of the seismic data shows improved resolution and more accurate geometries of the structures associated with rifting and their interrelationships (Ranero and Pérez-Gussinyé, 2010; Reston et al., 2007b). An important structure is the high amplitude laterally continuous reflectors that have been interpreted as the crust-mantle boundary, brittle-ductile transition, and a detachment fault at the Galicia Margin (Boillot et al.,

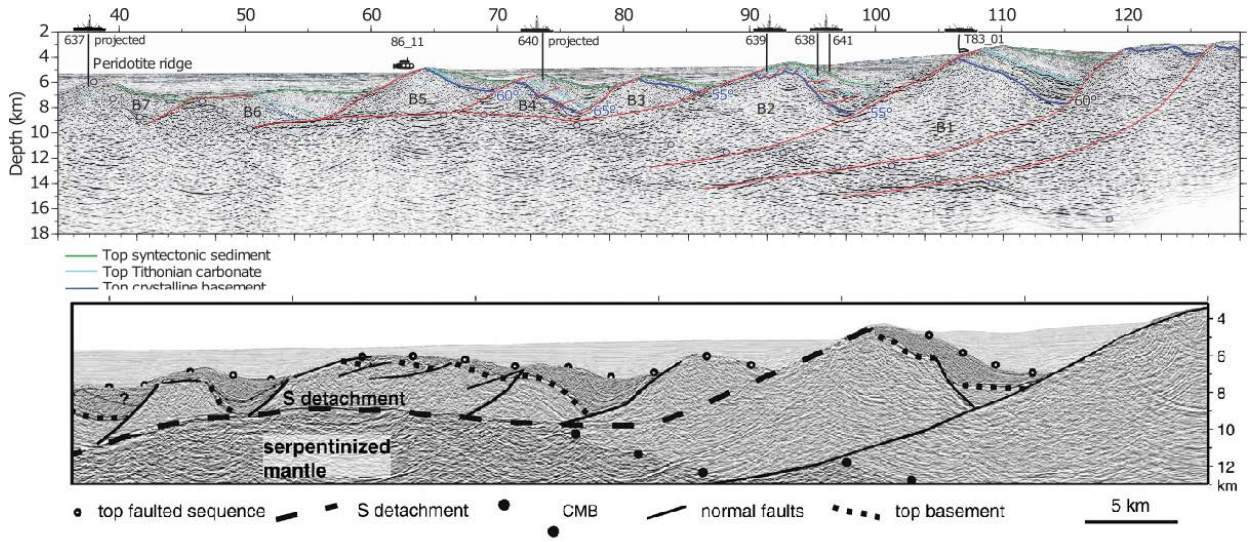

Figure 1.4: *Two seismic lines from the Iberian Margin. Top is interpreted prestack depth migrated sections from Ranero and Pérez-Gussinyé (2010) also showing ODP leg 103 drill sites, bottom is seismic line ISE 4 from Reston (2009*b*)*

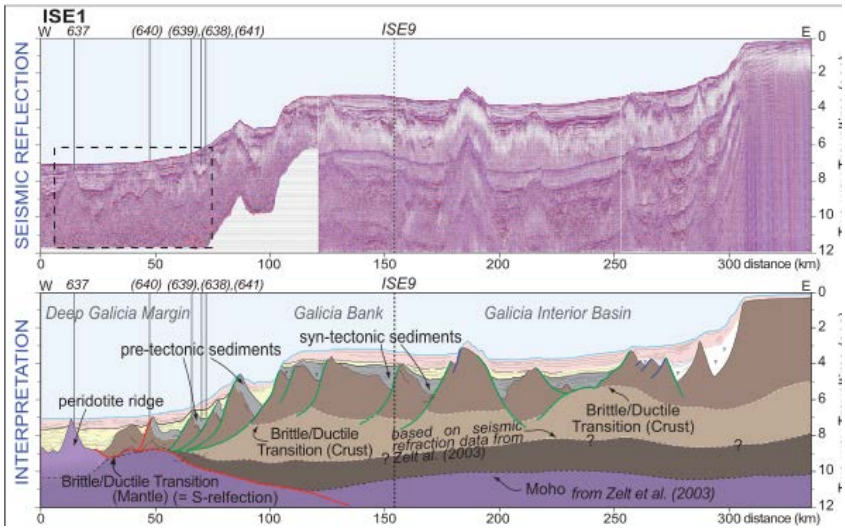

Figure 1.5: *Seismic Section from SIAP showing interpretation - Peron-Pinvidic et al. (2013)*

1989; de Charpal et al., 1978; Sibuet, 1992; Reston et al., 2007b), also see Chapter 2. Figure 1.4 shows two depth migrated lines from the Galicia margin that run through or adjacent to the Galicia 3D dataset. Seismic images such as these have resulted in many of the conceptual models of magma-poor margins and have also been used to compare to numerical models, e.g., line IAM11 (top in Figure 1.4) in Brune et al. (2014). A more detailed discussion of Galician specific data is provided in Section 1.4.

To appreciate the large-scale structural configuration of margins it is necessary to use wide angle seismic data that can give a better idea of structures and velocities a depth. Figure 1.6 provides this view for a number of near conjugate margins including the Iberian Margin (Galicia Bank). Note the extreme thinning of crust toward the continent-ocean transition (COT), believed to be characteristically underlain by serpentinised mantle.

1.3.3 Ocean drilling

Ocean drilling has been undertaken on the Southern Iberian Abyssal Plain (Sawyer et al., 1994; Whitmarsh et al., 1998) and the Galicia Margin (Boillot, Winterer and Meyer, 1987). This drilling (Figure 1.7) has helped constrain the nature of the reflectors seen in seismic datasets by providing a distinct rock type and any associated facies understanding obtainable from the sample. It

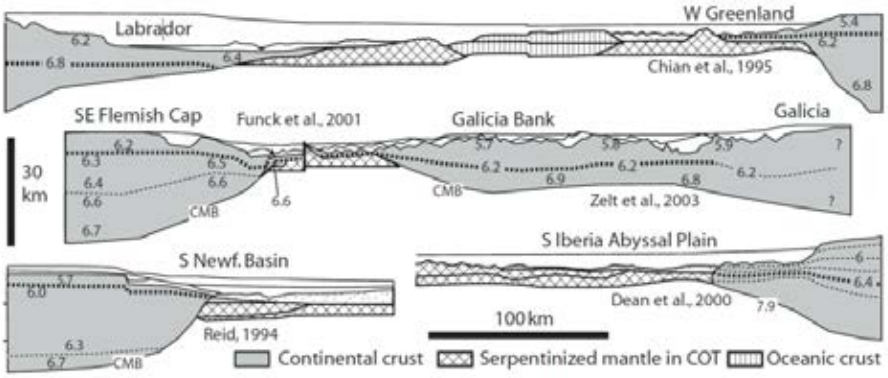

Figure 1.6: *Simplified interpretation across near conjugate magma-poor margins of the North Atlantic, velocity structure shown by contours, CMB is Crust-mantle boundary, (Reston, 2007a)*

has also allowed some constraint on the age of rocks in the tops of the tilted blocks. The geometry of the tilted blocks and the depth of the overlying sediments have made drilling in to syn-rift sediments more difficult, limiting the constraints of age of individual faults. A key finding of the drilling on the Southern Iberian Abyssal Plain (Legs 149 and 173) drilling was the presence of exhumed lower crustal rocks and exhumed continental mantle overlain by sediments (Whitmarsh et al., 1998; Manatschal et al., 2001). This is interpreted as being a deeply penetrating fault on which movement has occurred to the extent that the upper mantle of the footwall surface was tectonically exhumed to form the seafloor (Boillot, Recq and Winterer, 1987; Manatschal et al., 2001). Evidence from sedimentary sequences deposited on the exhumed mantle represent a further tectonic event that changed the nature of the margin after mantle exhumation and led to final lithospheric break up from the Aptian to Albian (Peron-Pinvidic et al., 2007).

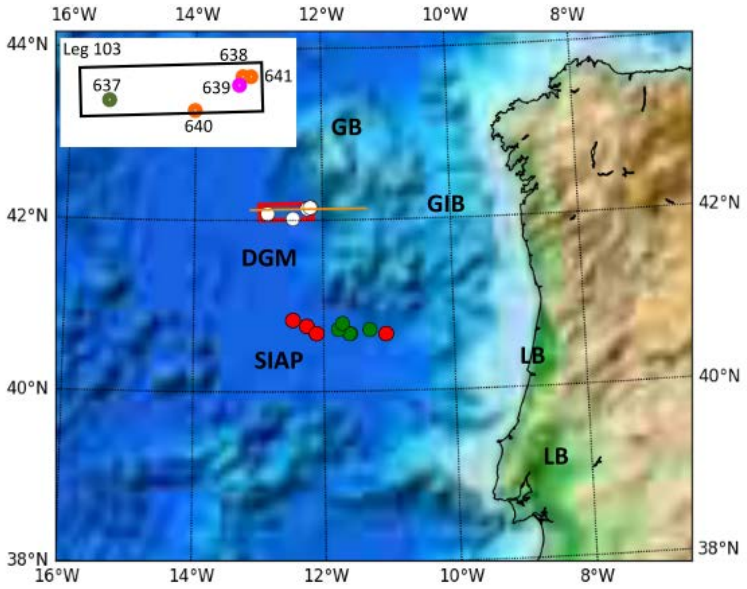

Figure 1.7: *location of 3D multi-channel seismic survey (red box). Drill sites are shown as coloured circles (white - Leg 103, red - Leg 149, green - Leg 173). Inset Leg 103 numbered and coloured according to lithology: Orange (638,640,641) - sediments; magenta (639) - sediments underlain by rhyolitic basement; olive green (637) - peridotite. The Orange line is seismic line IAM11 (Ranero and Pérez-Gussinyé, 2010) shown in Figure 3.10, approximately line 740 from the 3D Galicia data volume. DGM - Deep Galicia Margin, GB - Galicia Bank, GIB - Galicia internal Basin, SIAP - Southern Iberian Abyssal Plain, LB - Lusitanian Basin (onshore, and offshore).*

Table 1.3: *Summary of ODP Leg 103 data, (Boillot, Winterer and Meyer, 1987)*

Hole	637(a)	638(a-c)	639(a-f)	640(a)	641(a-c)
Max penetration depth (m)	286	547	240	232	154
Core recovery %	32	28-49	20-40	18	63-74
Age of base of hole	Late Miocene underlain by peridotite	Valanginian	Tithonian over metadacite/ rhyolite	Hauterivian	Barremian

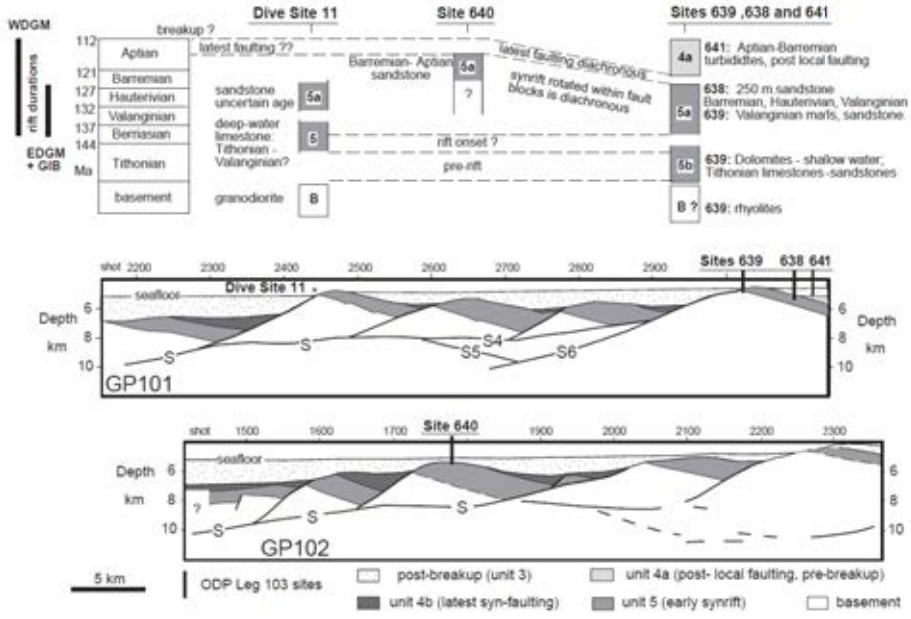

Figure 1.8: *Diagrammatic representation of stratigraphy drilled from the top of different fault blocks derived from ODP Leg 103, see Figure 1.7 for drilling locations (Reston, 2005, Figure 8)*

A summary of the core data provided from the various holes of ODP Leg 103 sampling is provided in Table 1.3. The recovered core wan also analysed for: Lithothology (see Figure 1.8), biostratigraphy, Palaeomagnetics, geochemistry (rock and interstitial water), bulk density, thermal conductivity, compressional seismic velocities. In addition Geophysical logging was undertaken within the holes and consisted of: sonic induction, gamma-ray, caliper, lithodensity, neutron density and natural gamma.

Dating of samples from Leg 103 has provided a constraint on the age of extension in the Galicia Interior Basin and the deep margin from Berriasian before focusing oceanward until break up (Barremian/Aptian) (Boillot, Winterer and Meyer, 1987; Boillot, Comas, et al., 1988; Reston, 2005). Figure 1.8 shows the age and facies of the drill sites and can be correlated to Figure 1.4. Of particular note is the diachronous nature of the top of the syn-rift sediments: Barremian proximally and Aptian more distally, with the most recent faulting seen with in the fault blocks suggesting that deformation is localising or migrating oceanward. Also of note, however, is the interpretation of the Tithonian sediments being deep water distally, at dive site 11 (Boillot, Comas, et al., 1988). Whilst the Tithonian sediments are shallow proximally (holes 638, 639 and

641) when they are interpreted as being pre-rift or maybe rift onset more distally, suggesting that even pre-rift these sediments were in deeper water (sections 3.1 and 4.1.1 provide more precise locations of drill/dive sites within the data volume).

1.3.4 Numerical models

A range of numerical models have been published (for example see Huismans and Beaumont, 2003; Lavier and Manatschal, 2006; Brune et al., 2014; Choi et al., 2013); these, when allied with other sources of evidence especially seismic data can aid in understanding the fundamental processes at work during rifting and break up. Models use rheological variables thermal variables or both and are commonly two dimensional. The following section briefly discusses some of the key variables and types of modelling. It then presents a number of important findings that are used when the modelling is integrated with other sources such as drilling and seismic data. Modelling is focused on work that is deemed to be important or influential on the development of concepts that inform the later stages of rifting and break-up; where possible models with more convincing analogues taken from field or seismic evidence are favoured.

Modelling inputs

Numerical models use empirically derived values for a layered crust or lithosphere (e.g. Figure 1.9). The 'classic' model based on variation of lithosphereic strength with depth is one in which listric normal 'faulting' occurs in the upper crust. The listric faulting and associated tilted blocks resulting from flow in a sufficiently thick lower viscous layer, shear stress on the base of the crust or stress refraction across rheology contrasts (Brune and Ellis, 1997).

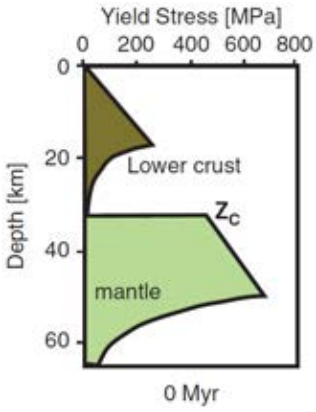

Figure 1.9: *Basic lithospheric strength profile from Pérez-Gussinyé (2013), crust strength from (Tullis et al., 1991), mantle strength from (Newman and White, 1997)*

The incorporation of a range of physical and rock properties can be investigated in a dynamic way - with the variables changing during different stages of the rift for a comprehensive list see Brune et al. (2017, p 259). In addition the rise in computational power over the last decade or so have made the ability to undertake complex 2D models and 3D models much more possible. Gerya (2009) outlines that numerical modelling involves conserving mass, momentum and energy by solving equations of continuity, motion and heat. Rheological properties, elastic for brittle and ductile flow or plastic deformation, are used to represent the behaviour or rocks. It is also necessary to impose boundary conditions in terms of rate of movement (extension of rifting). Common modelling methods include thermo-mechanical finite element modelling (Lavier et al., 1999; Huismans and Beaumont, 2002, 2003, 2011, 2014; Naliboff et al., 2017; Tetreault and Buiter, 2017), finite difference modelling (Lavier and Manatschal, 2006; Manatschal et al., 2015; Duretz et al., 2016), whereas Driscoll and Karner (1998); Mohn et al. (2015) use numerical forward modelling with sequence stratigraphic data.

Key modelling results

Numerical modelling of rifting and extension has produced a plethora of results in recent years, far too many to cover here. However, see Brune et al. (2017) for a good introduction and an comprehensive list of work. Significant modelling results that have direct relevance to the Iberian

margin and the break-up of the continental crust (and thus this work) include:

- that the processes that may localise deformation leading to the narrowing of rifts, include the loss of cohesion in brittle layers, lithospheric necking and magmatism, whereas wide (de-localised) rifts result from viscous flow in the lithosphere and occur where there is relatively high heat flow and thick crust (Buck et al., 1999).

- that asymmetry within rifts may occur due to low velocity coupled (brittle/frictional plastic) rifting between the upper crust and lower crust and mantle (Huismans and Beaumont, 2002).

- that the balance of lower crustal flow and upper crustal brittle faulting may result in the migration of rifting (Brune et al., 2014) shown in 1.10.

- the possibility that steep brittle faulting rotates to low angles at high offsets (Lavier et al., 1999), see Figure 1.11. This rotation is modelled to be more likely if strength is reduced by over 10%, resulting in flexural response of the lithosphere. Flexure of the fault footwall occurs as it is exposed thus flattening the fault surface until a point where it is mechanically favoured to form a new fault by carving a 'slice' off of the hanging wall (Buck, 1988a; Choi et al., 2013).

A numerical model with parameters based on field evidence from the Alps identified three stages of rifting: stretching; thinning and exhumation; the presence of 'concave-down detachments' in brittle layers (including an under-plated lower crust) during the thinning phase of rifting, with these two brittle layers being de-coupled by the plastic middle crust acting as a shear zone whilst being attenuated (Lavier and Manatschal, 2006). Pérez-Gussinyé et al. (2006) showed that magma poor rifted margins are characterised by mantle that was either depleted in basaltic components or was approximately 50°C cooler than average (less than 1250°C). Naliboff et al. (2017) shows that the complex architecture seen on rifted margins is related to increasing extension velocities and also the inheritance of previous structures, especially the rotation of faults and the incision of these by higher angle faults (that may be the reactivation of faults)

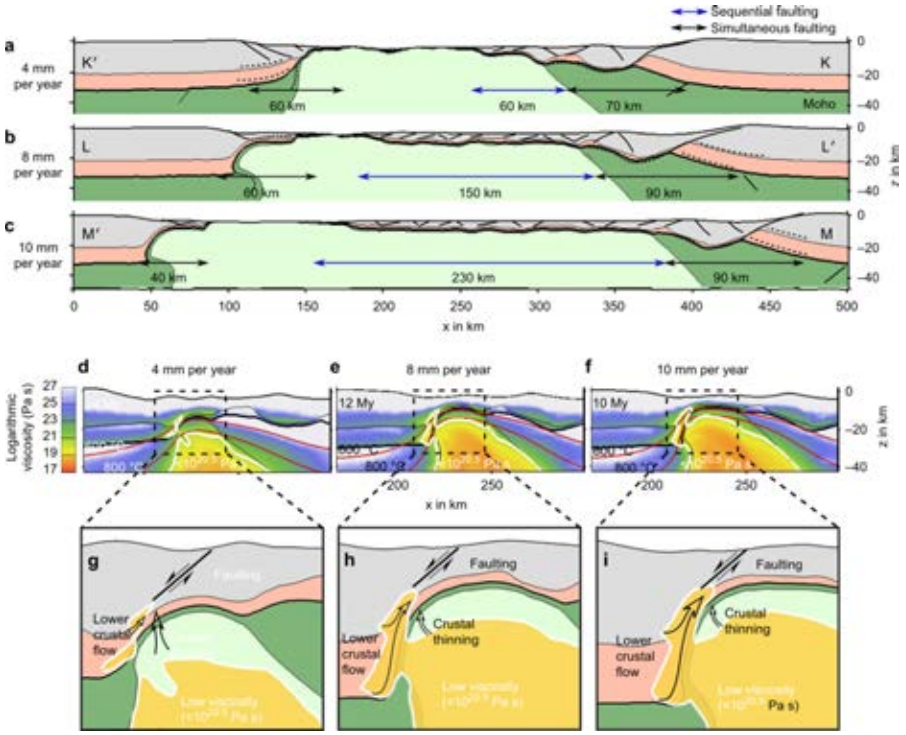

Figure 1.10: *Determining the influence on margin structure of rift velocity using modelling (3 different full extension velocities). The modelling predicts a change from simultaneous faulting to sequential (blue and black arrows) increasing rift velocities leads to advection of the isotherms to shallower depths forming an exhumation channel, lower crustal flow therefore counteracts fault-controlled crustal thinning prolonging rift migration leading to a wider margin (Brune et al., 2014).*

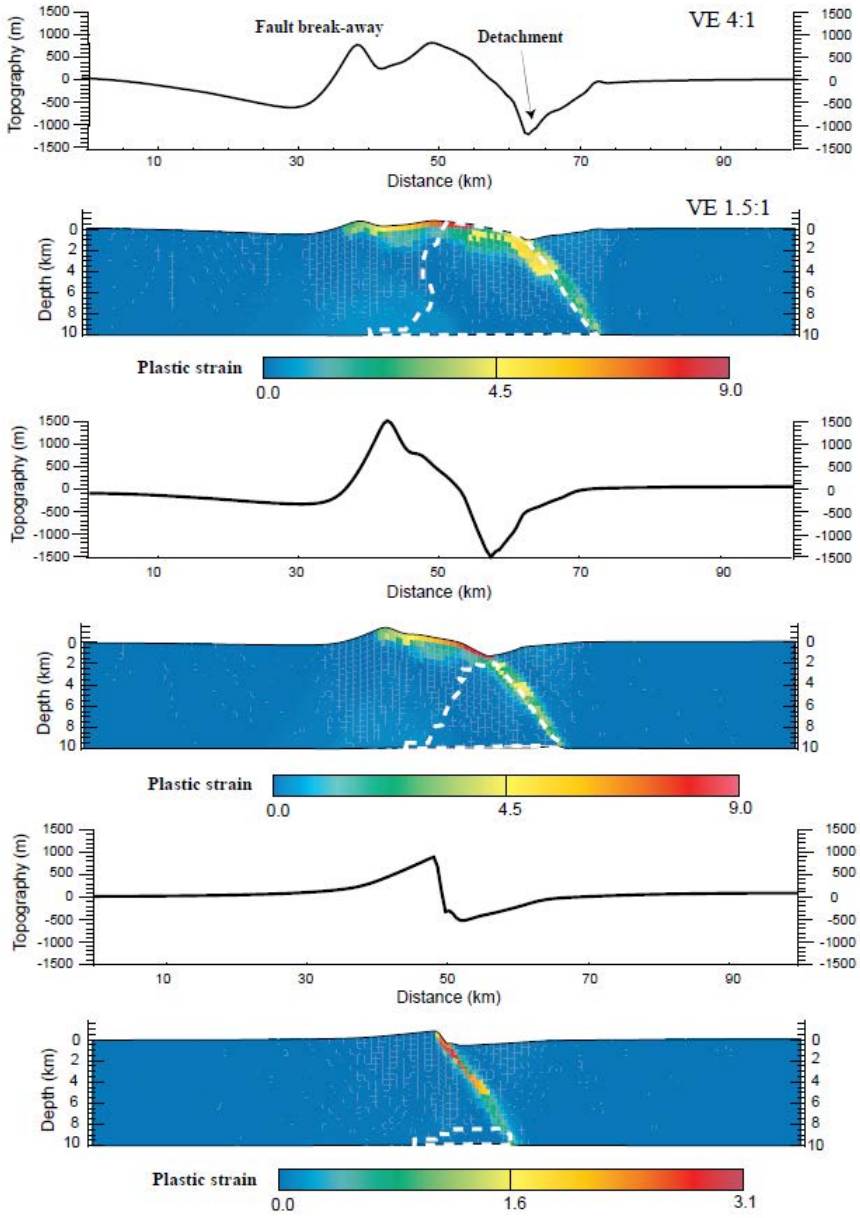

Figure 1.11: *Modelled topography and plastic strain. Three steps in evolution of a model, for the last step (upper panel) modelled fault offset is 27 km. White dashed contour on plastic strain profile bounds uplifted lower crustal material. Inactive footwall rotates to horizontal as extension increases. VE is vertical exaggeration. (Lavier et al., 1999, Figure 2).*

in the hanging wall. Furthermore, high strain is seen at the top of mantle, and compariosons are made with the magma-poor mid-Norwegian margin (Osmundsen and Ebbing, 2008). Another important aspect is recognising that the strength and rheology of the crust and lithosphere changes as a rift develops. Modelled rising asthenosphere during rifting may reduce the yield strength of lithosphere prior to breakup with the rheology of lower crust and upper mantle changing during the rifting process (Manatschal and Bernoulli, 1999). Furthermore, the crust when thinned to approximately 10 km becomes entirely brittle and therefore couples (brittle) deformation with the upper mantle (Pérez-Gussinyé and Reston, 2001).

Despite all the detailed work; the contribution of numerical modelling to understanding the final stages of breakup is limited to testing simple ideas. Almost by definition, being a model, this results in oversimplifications of the natural world. The following section provides the geological context for the Iberian margin based primarily on geophysical and drilling data.

1.4 Geology of Western Iberia

Observations and interpretations from seismic surveying of passive margins, especially the Iberian margin, combined with field studies, numerical modelling and drilling have produced a range of conceptual models of the late stages of rifting and continental break-up at magma-poor passive margins. This section brings together the key features and places them in the structural and stratigraphic context of the Galician margin.

A number of bathymetric features can be seen on the western flank of Iberia (Figure 1.7). These bathymetric features are controlled by the gross structural architecture of the margin and include the (largely onshore) Lusitania Basin, Galicia Interior Basin, Galicia Bank, Iberian Abyssal Plain, Deep Galicia Margin. In addition to seismic evidence other geophysical data can support and be used to underpin and support findings from other data sources.

1.4.1 Gravity and magnetics

Gravity (Sandwell et al., 2014) and magnetic (Maus et al., 2009) maps are shown in Figure 1.12. These maps allow the gross structure of the margin to be determined suggesting transitions between the continental and oceanic crust.

Figure 1.12A (top) shows the clear magnetic polarity reversals in the western area outlining the area where seafloor spreading occurs; from about 500 km off shore the reversals are less consistent but can be seen to swing from N-S to being E-W in the bay of Biscay. A swathe of negative polarity is seen for approximately 300 km offshore with a few small positive zones that are 50-100 km in radius located to the south and east of the Galicia Bank. Considering the gravity map, Figure 1.12B (bottom), gravity lows marking fragments of continental crust (pink/red) are shown to form the Galicia Bank off the NW coast of Iberia, whereas the south Iberian Abyssal Plain is marked by a gravity high, higher than ocean crust seen in the NW area of the map, and determined from clear magnetic polarity reversals. Detailed analysis of gravity data by Druet et al. (2018) reveal a range of zones, the Galicia 3D dataset spans the necking and hyper-extended/exhumed zone with the serpentinised mantle ridge in the west of the dataset running from 43°N southward to at least 40°N on the South Iberian Abyssal Plain.

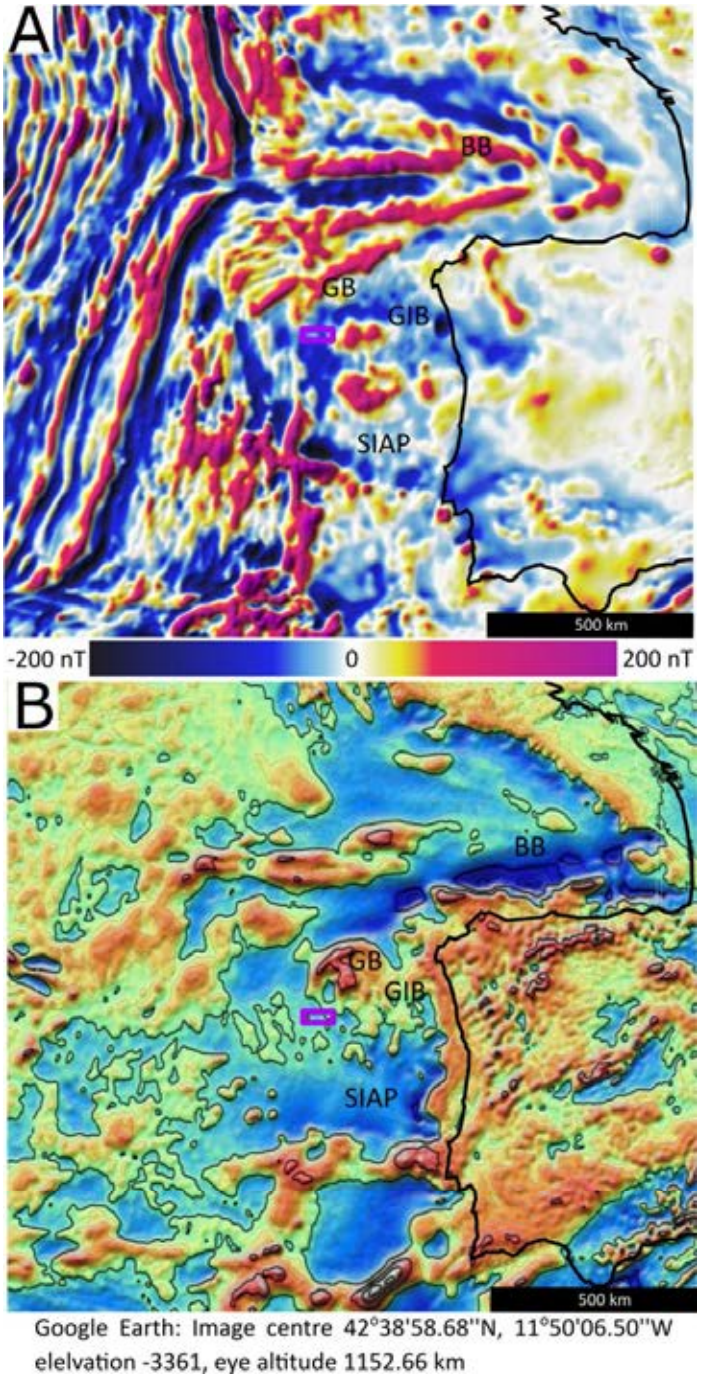

Figure 1.12: *A: Magnetic (Maus et al., 2009), and B: Gravity (Sandwell et al., 2014) anomaly maps of the Iberian margin, displayed on Google Earth via .kmz files*

1.4.2 On-shore and near shore field evidence

As the study site for this work lies over 200 km offshore (Figure 1.2 the correlation with onshore geology is circumspect at best. ODP drilling has occurred and is summarised in Section 1.4.3. The onshore geology of Galicia consists of a number of Variscan structural zones that trend NW-SE and curve round to east-west into the bay of Biscay. These zones are separated from the offshore geology by Cordobia-Badajoz-Tomar Lineament, which off Galicia trends offshore. To the east of this lineament, and onshore, lies a deformed zone of Precambrain and Lower Palaeozoic rocks (schists with complex mafic materials) of the Galicia-Tras-os-Montes zone (Téllez et al., 1993).

To the north of Lisbon some onshore and offshore hydrocarbon exploration wells have been drilled allowing the stratigraphy of the Lusitanian basin to be determined. Wells reach Hercynian basement overlain by Upper Triassic rocks, and pass through a Jurassic and Cretaceous sediments including notable unconformities in Oxfordian, Barriasian and the Aptian. Evidence of Neogene compression is also seen in the basin (Wilson et al., 1989). The partly segmented Lusitanian basin (Figure 1.7) runs NNW-SSE across the coast of Portugal and is considered to be the southern equivalent of the Galicia Interior Basin (Wilson et al., 1989; Pérez-Gussinyé et al., 2003).

1.4.3 Off-shore geology: seismic surveys and ocean drilling

The lack of intrusive and extrusive igneous activity on the west Iberian margin mean that seismic reflection imaging does not have to deal with the difficulties of strong reflections and limited transmission posed by igneous bodies (especially sills). Thinner sedimentary cover compared to other margins also facilitates both seismic imaging and drilling as limited post rift sediments requires much less time and expense to reach syn-rift sediments and basement rocks. Therefore, a number of 2D seismic surveys lines (see Figures 1.3, 1.4 and 1.5) and three previous drilling programmes (Figure 1.7) have made it the 'type' section for 'magma-poor' passive margin.

The geological evolution of the margin can be considered as part of the northward and step-

wise opening of north Atlantic (Murillas et al., 1990) resulting in three phases of rifting (Figure 1.13) representing different stages in the evolution of the margin (Peron-Pinvidic and Manatschal, 2009; Peron-Pinvidic et al., 2013). The initial 'stretching' phase occurring during the latest Palaeozoic with left lateral strike slip faults occurring to the to the north and south of the Iberian margin (Bay of Biscay and Gibraltar fault zones (Ziegler, 1989). These late Hercynian faults were reactivated during extension in the Mesozoic (Ziegler, 1989) with the second 'thinning' phase occurring during the Jurassic and continuing into the third 'hyperextension' phase culminating in the Upper Cretaceous. Of the three phases of extension shown in Figure 1.13 it is the latest phase of extension during the Cretaceous that is considered to be 'syn-rift' in this work (for example in Chapter 5) 'pre-rift' is considered to be sediments that may have been deposited during the earlier two phases of extension in the Triassic and Jurassic.

Tucholke and Sibuet (2012) merge the two later stages of extension, highlighting that the two later rifting phases proposed by (Peron-Pinvidic and Manatschal, 2009; Peron-Pinvidic et al., 2013) are separated to fit their staged model of rifting. Numerical and geodynamic modelling of the Iberian margin (Brune et al., 2016) suggests that rifting rapidly increased in rate c. 145 Ma (Jurassic-Cretaceous boundary) and that this increase in rate is associated with a change to a more oblique angle of rifting. This Mesozoic opening resulted in numerous abandoned rifts (the Bay of Biscay, the Rockall Trough and the Labrador Sea) and changes in spreading axes (and plate boundaries) resulting in a range of graben systems in 'V-shaped' basins (Peron-Pinvidic and Manatschal, 2010; Ziegler, 1989). The Galicia Interior Basin velocity structure suggests that the basin formed at a Palaeozoic terrane boundary (Peron-Pinvidic et al., 2013), again highlighting the importance of inherited structure for the gross margin configuration. The Galicia Interior Basin has been interpreted as the northern extension of the Lusitania basin (Murillas et al., 1990; Wilson et al., 1989).

The Porcupine Basin may have been initially linked to Galicia and Lusitanian basins with the former being offset as the North Atlantic and Biscay triple junction opened (Tankard and Balkwill, 1989). The lack of clear sea floor spreading anomalies west of the Iberian margin suggests the transition to sea floor spreading occurred during the Cretaceous Normal Superchron (Re-

ston et al., 2007b; Granot et al., 2012), reducing the clarity of anomalies on the Southern Iberian Abbysal Plain and the Deep Galicia Margin (Figure 1.12A). Sibuet et al. (2007) suggests that these cruder magnetic anomalies are symmetrical within the transitional crust on the Iberian and Newfoundland basins, and are related to serpentinisation and therefore ultra-slow to slow spreading from Late Berriasian to Late Valanginian-Early Hauterivian and Late Valanginian-Early Hauterivian to the Aptian-Albian boundary respectively. If these serpentinisation processes are related to exhumation, the exhumation occurs as continued extension occurred on the more proximal continental margins.

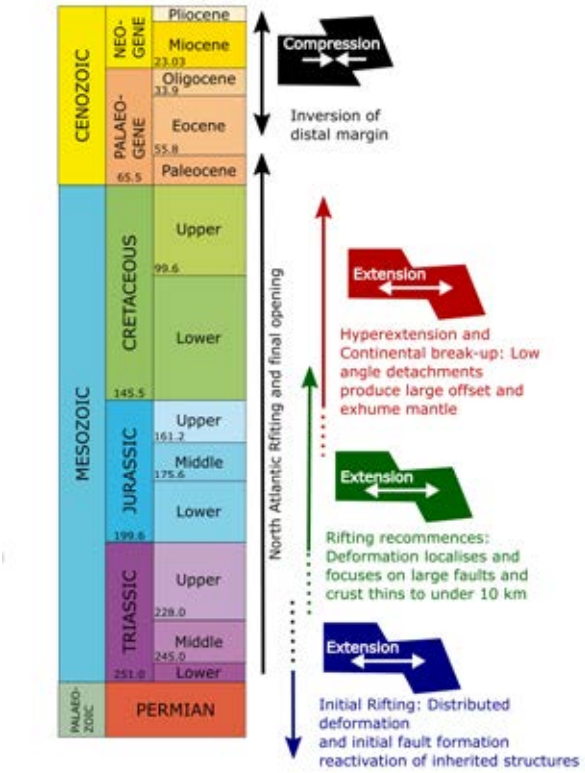

Figure 1.13: *Stratigraphy and Tectonic History of the Iberian Margin after Peron-Pinvidic et al. (2013)*

The Iberian-Newfoundland conjugate is bounded on the southern side by the Newfoundland-Gibraltar fault zone (transform margin). The northern limit is the NW tip of Iberia and the NE tip of Flemish Cap. Figure 1.14 shows a pre-stack depth migrated seismic interpretation of the

Newfoundland margin at the Flemish Cap shows no detachment suggesting an asymmetrical conjugate (Hopper et al., 2004) with the Moho (M) aligning with the S reflector from the Iberian conjugate margin. The continental crust thins quickly and abuts a thinned (3-4km) oceanic crust. Oceanic crust also thins seaward to (<1.3km) - suggesting limited magmas (like ultra-slow spreading). The structural fabric defined by gravity and magnetic geophysical data on the Newfoundland side of the margin appears to have controlled rift basin development (Tucholke and Sibuet, 2007). The northern margin of the Iberian - Newfoundland conjugate underwent compression in the Cenozoic. A recognition of the importance of large scale structural inheritance is highlighted by the Iberian basement being formed during the Variscan orogeny and the Newfoundland basement formed the Appalachian orogen. These terranes of crust were assembled during the closing of the Iapetus and Rheic Oceans during the Palaeozoic (Tucholke and Sibuet, 2007, 2012). Extension occurred in the GIB and deep margin from Berriasian before focusing oceanward until break up in the Barremian/Aptian (Reston, 2005). Figure 1.15 shows the location of the Galicia 3D seismic volume in relation to the tectonic elements of necking and the hyperextended and exhumed mantle zones (HME). Work from this thesis and from Davy et al. (2017) suggests that the continent-ocean boundary is further west than indicated here: west of the serpentinised mantle (peridotite) ridge is still transitional crust.

Figure 1.16 shows the plate reconstruction for the margin at the M0 Chron at the end of rifting but prior to large scale seafloor spreading. Note how the dataset lies close to the triple junction between North America, Iberia and Eurasia, the eastern arm of the junction forming the Bay of Biscay. This reconstruction therefore provides the local-regional scale plate tectonic setting at or near the break-up of the continental crust.

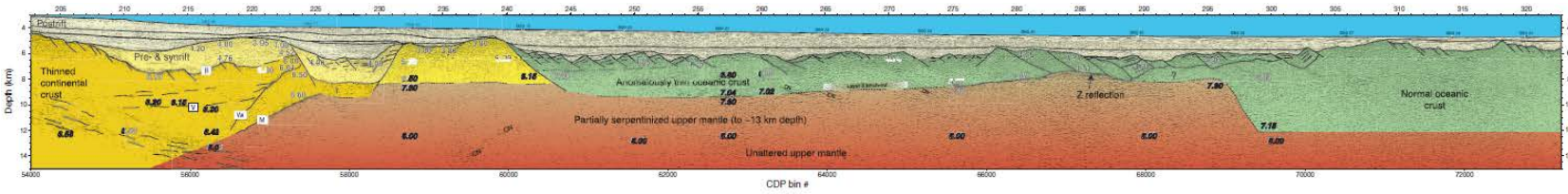

Figure 1.14: *Screech1 pre-stack depth migrated line from Flemish Cap (Hopper et al., 2004).*

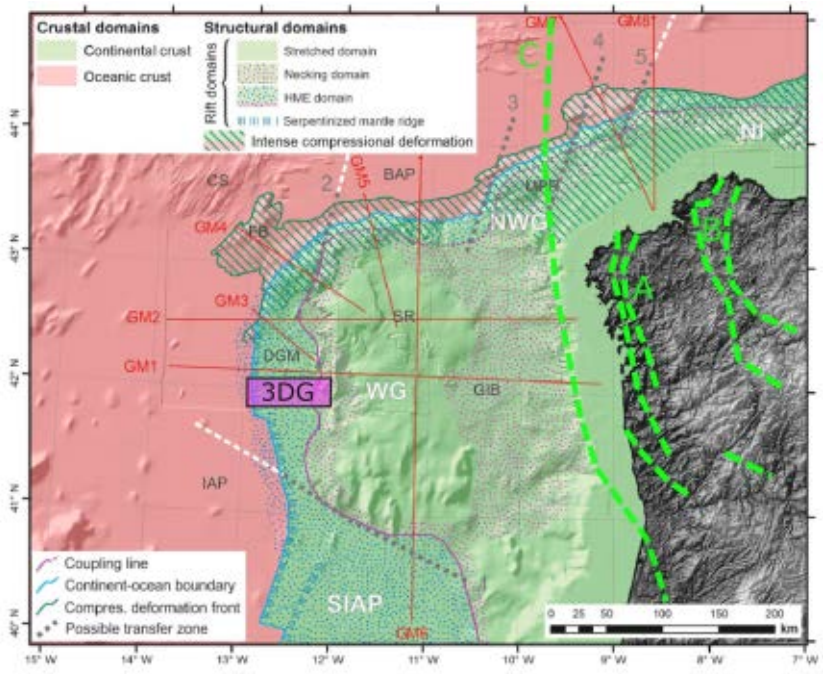

Figure 1.15: *Tectonic setting of the Galicia 3D dataset (3DG - magenta box) from Druet et al. (2018) incorporating detail from Téllez et al. (1993) and from within Tankard and Balkwill (1989): CS, Coruña seamounts; BAP, Biscay abyssal plain; MPR, marginal platform region; FB, Finisterre bank, SR, seamount region; DGM, deep Galicia margin;GIB, Galicia interior basin; IAP, Iberia abyssal plain. Dashed white lines indicate approximate limits between the different segments of the margin: SIAP, south Iberia abyssal plain segment; WG, west Galicia segment; NWG, northwest Galicia segment; NI, north Iberia segment. Dashed green lines indicates onshore lineations: A, Galicia-Tras-os-Montes zone; B, Ollo de Sapo domain; C, Porto-Badajoz-Cordoba Suture. The Hercynian front is speculated to be along the line of continent ocean boundary.*

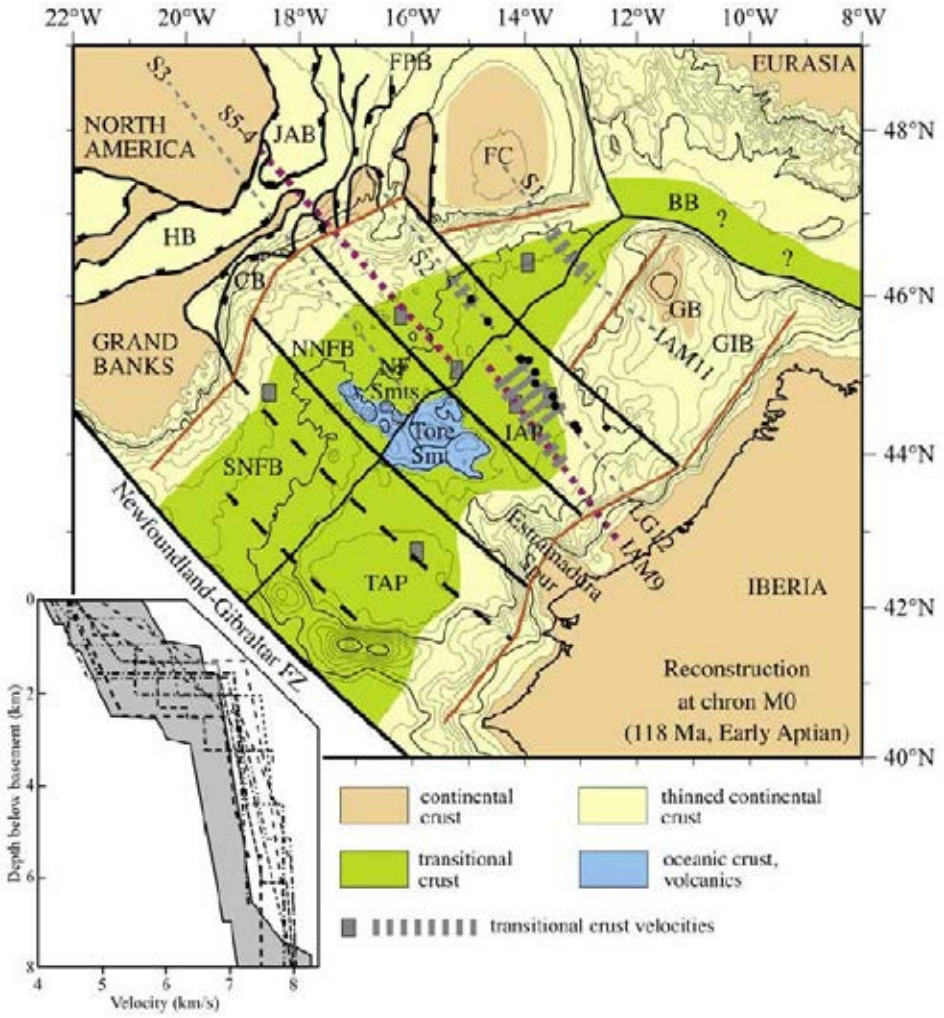

Figure 1.16: *Plate reconstruction at c. 118Ma, from Sibuet et al. (2007, Figure 1). The seismic line IAM11 passes through the 3D Galicia dataset.*

1.5 Scope and Outline

It has been shown in the previous sections that the Iberian margin including the Deep Galicia margin led understanding of the later stages of rifting and break up of magma-poor passive margins due to data collected there and models that have used these data. This thesis aims to use the Galicia 3D seismic reflection dataset to constraint the mechanism of breakup through detailed mapping of faults and specific structural horizons. Chapter 2 considers in more detail the current paradigm of magma-poor margins with particular reference to continental break-up. First it covers the basic ideas of continental extension and the specific terminology and

processes that has been developed. Secondly, it provides detail on to the competing theories of the final stages of rifting and break-up. Finally, as this work has looked in in detail at the faulting within the Galicia 3D dataset, a brief introduction into the geometries growth of faults and fault networks is provided. Chapter 3 introduces the methodologies that have been used, from the seismic reflection data acquisition and processing to interpretation of horizons and faults and the measurement of displacement on these faults.

Chapters 4 and 5 present the results of mapping a number of horizons within the dataset that provide a uniquely detailed insight into the break-up of a magma-poor margin. Of particular importance is the relationship of these horizons to the faulting seen within the Galicia 3D dataset. Chapter 6 provides an analysis of the faults with reference to understanding the development and interactions with each other and in so doing builds on the background provided in Chapter 2. Chapter 7 presents how this work has moved the knowledge of continental break-up forward.

Chapter 2

Current Paradigm for Magma Poor Margins

This chapter presents the current paradigm of the final stages of rifting through to break-up of the continental crust. This paradigm has been developed from observations on the Iberian margin, field data from uplifted passive margins (e.g. Alps) and from numerical, and to a lesser extent analogue, modelling of rifting. This will lay the foundation and provide context with which to understand the Galicia 3D data and the nature of the break-up captured on the Galicia Margin. It also provides the background on the formation of and growth of extensional normal faults. An understanding of how faults grow and develop over time will provide important information on the kinematics of faults within the Galicia 3D data allowing the various mechanisms presented in this chapter to be assessed.

2.1 Theories of extension

Two concepts of deformation within rocks are pure shear and simple shear (Figure 2.1), both retain original area however simple shear has an element of rotation (albeit one that may move), whereas pure shear has no element of rotation. At a crustal scale, this comparison does not

preclude the presence of faulting rather that in simple shear there is an element of asymmetry resulting from this faulting resulting from this rotation.

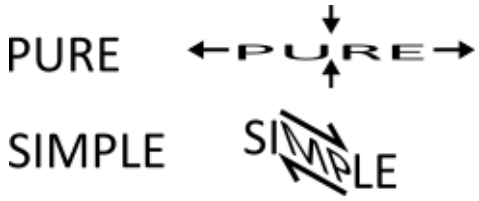

Figure 2.1: *Diagrammatic representation of pure and simple deformation*

The concept of pure shear and simple shear as applied to extension are summarised in the following sections, along with a hybrid model are shown on Figure 2.2 from Lister et al. (1986). Other models also exist for example, Heterogeneous Stretching, a type of pure shear (Reston, 1990; Reston and Pérez-Gussinyé, 2007c) and the the flexural cantilever model of Kusznir et al. (1991), a hybrid model incorporating aspects of both simple shear and pure shear. Although these models are large-scale lithospheric models they provide the context with which to understand the nature of the thinning of the continental crust prior to final rifting and break-up.

The basic models of extension initiated a renewed attempt at obtaining a physical understanding of the gross mechanisms associated with crustal extension. However, to apply these models to crustal deformation under extension it is necessary to consider the general structure of the crust and how this impacts its strength. Figure 1.9 shows a typical strength profile, with the yield stress plotted against depth. The straight line in the upper c. 18 km of the crust highlights a region where brittle failure dominates. The reduction in strength of the lower crust (in this case an aggregate of dry anorthosite and quartz) is a region of the crust where the rapid strength reduction results in plastic deformation. At the Moho (Zc) the mineralogy used for the profile changes to (dry) olivine resulting a a strong brittle upper mantle. The reduction in strength at c. 50 km marks the transition into the asthenosphere from the mantle lithosphere. The strength profiles are based on empirically derived mineral properties at different temperatures and pressures. The profiles form some aspects of the boundary conditions for numerical modelling of extension (see Section 1.3.4). The basic strength profile highlights that the lower

crust provides a 'weak' zone. Understanding how deformation in the upper and lower crust interact is an essential aspect of understanding how the crust thins to zero and finally breaks up.

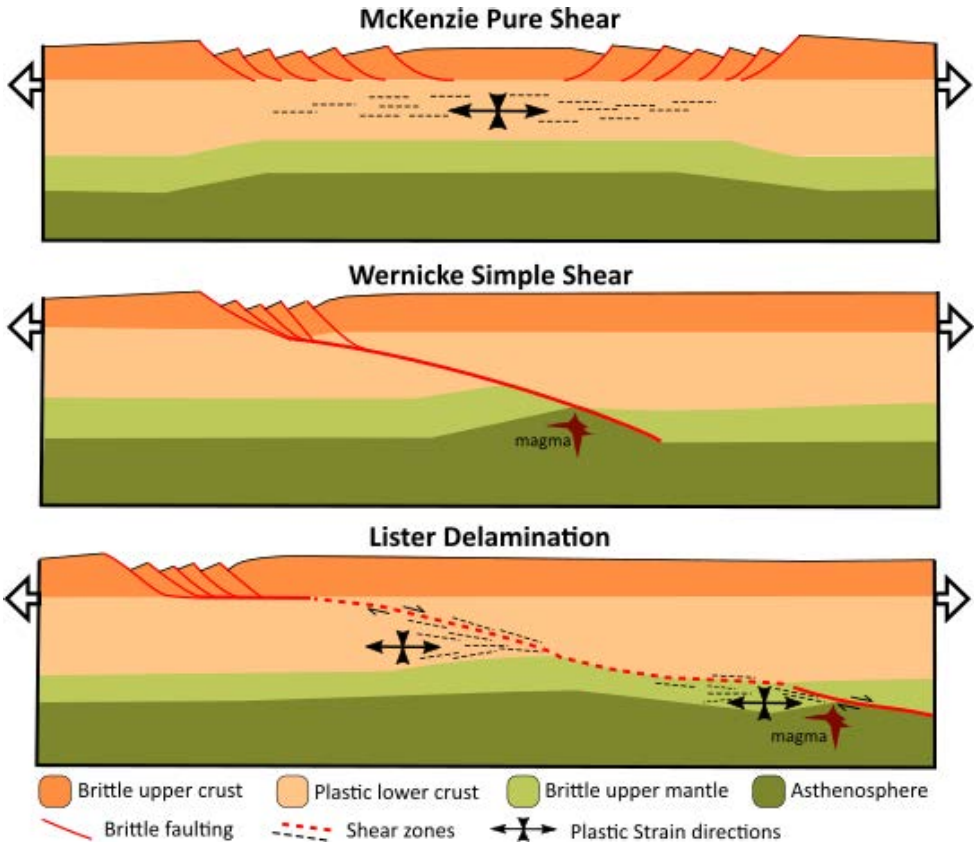

Figure 2.2: *Three proposed models of crustal extension after Lister et al. (1986)*

The following sections provide a basis for understanding more detailed and complex modelling that has been developed and forms an integral part of the current understanding along with seismic and field observations.

2.1.1 Pure shear

Initially proposed to understand the development of sedimentary basins, McKenzie (1978) provided the first example of stretching (extension) that incorporated the thermal consequences. The amount of stretching was modelled as being instantaneous and the results provided a good fit for some sedimentary basins such as the North Sea (Wood and Barton, 1983; White, 1990), c.f.

Ziegler (1989).

The pure shear model invokes a symmetrical structure in which the upper brittle crust is thinned by normal faulting with the lower crust deformation being more plastic and possible over a larger area White and McKenzie (1988). The McKenzie model is widely accepted and successfully outlines how the crust might respond to an instantaneous stretching event in terms of subsidence and thermal profile. It was not designed to explain the detailed structure that have been revealed by advances in seismic imaging and the hyperextension seen at the edges of the margins (Reston and McDermott, 2014; Huismans and Beaumont, 2014), specifically low angle detachments (see Section 2.5.2), embrittlement of the crust (Pérez-Gussinyé and Reston, 2001) and mechanisms of crustal separation (see for example Brune et al., 2014; Ranero and Pérez-Gussinyé, 2010; Reston and McDermott, 2011).

2.1.2 Simple shear

In contrast to the pure shear model the Wernicke (1985) 'uniform simple shear' model incorporates a large penetrating fault or shear that results in extension that, on the gross scale, is asymmetric. The Wernicke model also allows the lateral separation of crust and mantle (Tankard and Balkwill, 1989). The model was originally developed in the Basin and Range region of the United States but has since been related to rifted continental margins, for example by Lister et al. (1986). The resultant structure of a rift has a distal area that has syn-tectonic uplift (with almost equal amount of post-rift subsidence) whereas a proximal area undergoes syn-rift and post-rift subsidence (Wernicke and Axen, 1988); the terms proximal (near to surface) and distal (deeper) are with reference to the site of surfface extension. This provides the idea of upper and lower plate (Lister et al., 1986) with switching (at transform faults) along strike of conjugate margins. The footwall has isostatic uplift by folding / faulting. As extension continues a 'wave' of isostasy (Wernicke and Axen, 1988) passes through the footwall in the direction of extension in a model that shows some similarity in terms of footwall deformation with the 'rolling hinge' of Buck (1988a). The footwall goes through two periods of vertical shear - one on the breakaway side up as it pass from beneath the footwall and in opposite sense as the footwall is progressively

uncovered (Figure 2.3). The through-going fault can be considered a detachment fault. The dip of the detachment when active is more than its final dip and its initial dip as it may begin as a sub horizontal shear zone in the plastic zone (mid – lower crust) that moves up into brittle domain as a rolling hinge (Buck, 1988a; Choi et al., 2013), shown in Figure 2.4. The initiation of deformation in the plastic domain leading to faulting in the overlying brittle field may could explain lack of seismicity a low angles (Wernicke, 1995; Jackson and White, 1989). Two versions of cross lithospheric detachments have been proposed (Lister et al., 1986): the Wernicke and the Delamination models (Figure 2.2). The latter has the detachment that is subhorizontal at the base of the crust prior to cutting the brittle upper mantle spatially distant from the Wernicke model.

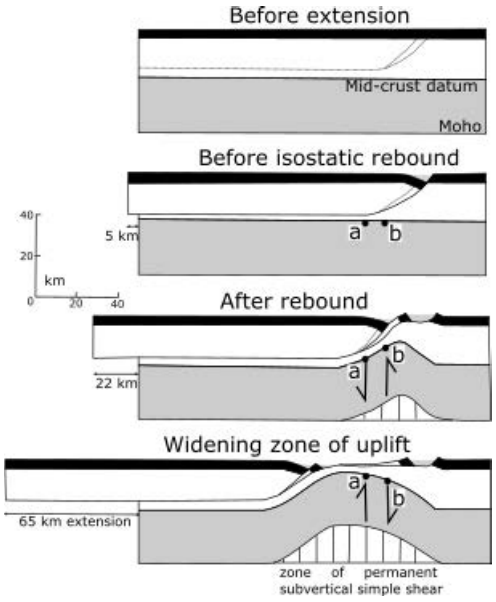

Figure 2.3: *Conceptual model of an evolving breakaway zone. Note migration of footwall strain and reversal of shear sense between points a and b, redrawn from Wernicke and Axen (1988)*

2.1.3 Hybrid models

In addition to the variation to the Wernicke model offered by the delamination model (Lister et al., 1986), see Figure 7.1, there have been a number of other theories postulated to account for rifting many of which contain features of the pure and simple extension models, i.e., hy-

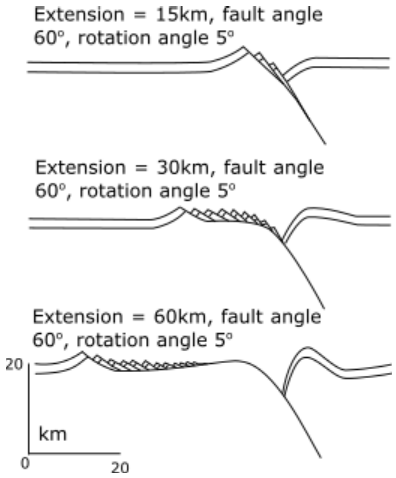

Figure 2.4: *Rolling hinge model showing resultant topography and abandoned faults with a flexural rigidity of 0.5 km. Redrawn from Buck (1988a)*

brid models. Etheridge et al. (1988) reviews simple shear models of detachments with reference to different conjugates and include areas where pure shear may account for deformation above and below the detachments (in the lower crust and/or upper mantle). The key to such hybrid models is the asymmetry of conjugates in terms of their structure. A sequential and 'genetic' link between pure and simple shear through extension episodes has been proposed incorporating a transition from pure to simple shear: Initially plastic deformation controls lower crustal deformation with brittle in upper crust and mantle, essentially pure and distributed (Whitmarsh et al., 2001). As thinning progresses so too does the rheology of the lower crust; progressively changing to enable more brittle behaviour. This rheological change initiates a switch to a décollement (detachment) along the crust mantle boundary and faults cutting into the mantle (Pérez-Gussinyé et al., 2003), once the crust has thinned to approximately 10 km thick. (Reston and Pérez-Gussinyé, 2007c). Thus, thinning from 30 down to 12 km is by pure shear (Manatschal et al., 2001; Reston and Pérez-Gussinyé, 2007c) switching to simple shear thereafter.

When considering the influence of heat flow, both pure and simple shear can be invoked at different times in a margin's evolution as shown by 2D modelling of heat flow (Buck et al., 1988). A change from pure to simple shear may account for the late rifting asymmetry of distal

margins of the western Iberia and the Tethyan Adriatic with the associated detachments giving rise to high level of extension and resulting in mantle exhumation that may be indicative of the 'lower plate' of the simple shear model (Wilson et al., 2001). A change from symmetrical pure shear to asymmetrical simple shear may accompany the movement of the rift location from the area of initial stretching to the heavily thinned edge of the continental margin. This switch in both location and style is considered to be in response to the lithosphere's thermal state (Manatschal and Bernoulli, 1999) and conicides with the embrittlement of the crust (Reston and Pérez-Gussinyé, 2007c).

Whitmarsh et al. (2000) suggests a simple of evolutionary picture may not reflect the possible complexities of the later stages of rifting. Changes in the deformation process from pure to simple and the angle of normal faults and sequence of faulting may change over time due to a change in stress field and temperature dependent rheology of lithosphere. Furthermore, such changes in the mechanism of extension highlight uncertainties as to whether the centre of the rifting migrates oceanward as rifting proceeds, or whether dissipated pure shear gradually focuses to a simple shear detachment at the centre of the rift. The switch from pure to simple shear also suggests that an original decoupled crust where brittle and plastic deformation occurs discretely as a response to extension is replaced by a coupled crust in which brittle deformation occurs and penetrates the whole, previously thinned crust (Huismans and Beaumont, 2002; Reston and Pérez-Gussinyé, 2007c; Reston, 2009*b*).

2.2 Key structural elements and terminology

A number of, often related, structural elements have been interpreted from 2D seismic lines and, where relevant, field analogues. These elements are interpreted on different continental margins and may be considered important in explaining the processes that result in hyperextension and eventual breakup of the continent. This section compares and contrasts elements from different seismic lines (and other evidence) within and outwith the study area. A discussion on the nature of the elements and their alternative interpretations is provided. This discussion provides the

background on the various mechanisms of late stage deformation and break-up presented in later sections; and to the work presented in Chapters 4 and 5.

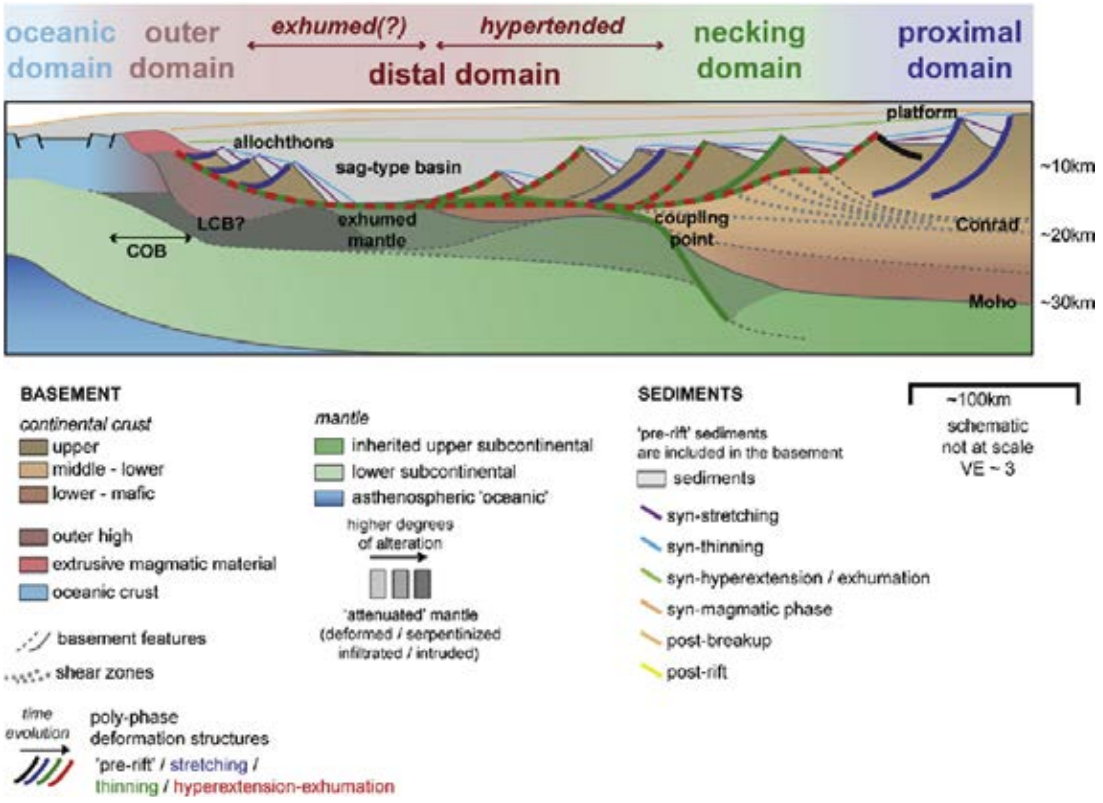

Figure 2.5: *Domains of magma-poor margins (from Peron-Pinvidic et al., 2013, Figure 3)*

In order to provide context for the interpretation of the 3D Galicia data, it is useful to have an overview of the key terminology of concepts and structural elements. This section draws on the synthesis of work based on field evidence and 2D seismic sections and drilling results from Iberia (Peron-Pinvidic and Manatschal, 2009) and also from other passive margins (Peron-Pinvidic et al., 2013; Reston, 2009*b*). Often specific structures relate to specific processes of deformation during the evolution of passive margins (see Peron-Pinvidic et al., 2013; Sutra et al., 2013; Naliboff et al., 2017). The evolution of a margin from initial rifting through to break-up results in distinctive zones or 'domains' on the margin which have been classified (Peron-Pinvidic et al., 2013; Sutra et al., 2013; Tugend et al., 2014). Figure 2.5 shows the domains of Peron-Pinvidic et al. (2013) which is used below. The proximal domain relates to stretching of the crust in the early stages of rifting, and can be approximated by the basic pure shear model (section 2.1.1).

The necking domain results when extension has continued resulting in the first fault that extends deep enough to couple with the mantle (the breakaway fault) and therefore represents the onset of simple shear (Section 2.1.2). The hyperextended (distal) domain consists of a number of tilted fault blocks, the lower portion of these faults connecting to either the breakaway fault or the mantle. The exhumed (distal) domain is a zone of exhumed mantle at the (palaeo)seafloor but before the true seafloor spreading of the oceanic domain.

Continental 'neck'

Forming the boundary between the proximal and necking domain (Figure 2.5), the continental neck consists of a wedged shaped portion of continental crust; the lower boundary is the Moho where it has flexed upwards due to thinning of the crust to under 10 km. The upper surface is formed by the 'breakaway' faults: faults that are the first to cut through the whole crust and reach the mantle. The neck is not a smooth transition but is composed of graben and half graben and is formed by brittle failure in the upper crust and plastic extension and thinning in the lower crust. The intersection of Moho and breakaway faults has been termed the coupling point - where deformation of crust and mantle become coupled. The neck is the equivalent to the taper break of Osmundsen and Ebbing (2008).

Continental blocks

The process of rifting can occur in different stages over geological time and rifts can be heavily influenced by previous tectonic cycles whether these be previous rifting or orogenic episodes. Previous rifting can thin the crust, which in turn may then be underplated by the addition of (eventually strong) mafic crust. Rifted margins in the current continental configuration and over geological history are considered to have a hierarchy, based on the size of continental fragments that constitute the transition from un-thinned (say 30 km thick) continental crust to true oceanic crust. Within this scheme each type of block is linked genetically to a domain on the margin. These blocks range in size, from large to small: Micro-Continent, Continental Ribbon, H - Block and tilted blocks including allochthons (Peron-Pinvidic and Manatschal, 2010).

Micro-continents and continental ribbons - proximal domain

These larger blocks are essentially failed rift episodes on one side of a conjugate margin that partially separated a strip of continent from the bulk of the continent. Modelling has suggested that for these rift 'jumps' to occur a period of quiescence in extension of 20-60 my is required (Naliboff and Buiter, 2015). According to the extensional configurations of Lister et al. (1986) continental ribbons and micro-continents result from two detachments, with the opposite dip toward one another giving a marginal plateau and opposite dip away from each other forming a continental ribbon. The Galicia Bank (Figure 1.7) may be considered a continental ribbon. However, Pérez-Gussinyé et al. (2003) show seismic imaging that shows brittle faulting reaching down in to the lower crust and a switch within the Galician Interior Basin from pure shear to simple shear. The simple shear faults do not couple with the mantle. A different velocity structure within the Galicia Bank compared to that seen on the western flank of the Galician Interior Basin suggest that the Galician Interior Basin may represent an inherited Palaeozoic terrane boundary.

H - Block

The 'H' block concept was derived primarily from modelling (Whitmarsh et al., 2001), but has also been suggested from restoration and fieldwork (Manatschal et al., 2001, 2007). It is considered to be a relic of conjugate (proto) detachment prior to localisation on one of them. The surface is underlain by both continental and mantle therefore the detachment cuts from crust to the mantle (Manatschal et al., 2001). It has been suggested that despite only approximately 5km crustal thickness the H-block shows delayed subsidence on a continental margin until the footwall of the underlying faults are pulled out from beneath the H block (Peron-Pinvidic and Manatschal, 2010).

Tilted blocks - necking domain

Tilted blocks and allochthons consist of the rotated hanging walls of basement/pre-rift blocks and are often postulated to evolve sequentially ocean-wards (Peron-Pinvidic and Manatschal, 2010; Ranero and Pérez-Gussinyé, 2010; Manatschal, 2004). When considering the tilted blocks it is important to consider the degree of tilting and nature of the top surface and pre-rift / syn-

rift stratigraphy (Peron-Pinvidic and Manatschal, 2010) as this provides key structural-stratal relationships providing evidence of deformation mechanisms (Manatschal and Bernoulli, 1999). Wilson et al. (2001) suggests the only way to identify syn-rift is by features that are diagnostic of fault block rotation i.e., divergence of stratigraphy (rocks or seismic) into footwall, and their rotation. Wilson et al. (2001) further comments that other workers have failed to report this (or do not do it well), arguing that previous studies of syn-rift (described by reflection divergence) are not thickening into growth faults, they are compactional drape over half grabens due to influxes of post-rift turbidites after sediment supply routes have been re-established. Wilson et al. (2001) furthermore suggest the absence of syn-rift sediments seen on seismic reflection data being due to sediment starvation as fault blocks formed. Re-sedimentation of eroded sediments means chaotic looking seismic sections.

Allochthonous blocks - hyperextended distal domain

Allochthons are tilted blocks that are isolated from other crustal blocks and can be seen in seismic reflection data and can also inferred from bathymetry. These are generally considered to be crustal units overlying detachment faults (Manatschal, 2004). Their geometry and location to other features suggest such blocks have been considered to be the final part of a continuum of slices of continental crust formed during break-up (Peron-Pinvidic and Manatschal, 2010).

Continuous high amplitude reflectors - hyperextended distal domain

First recognised by de Charpal et al. (1978) in the Bay of Biscay and beneath the Galicia margin, a strong predominantly continuous un-displaced (un-faulted) reflector is seen to be located beneath overlying fault blocks, this is the S reflector (Figure 2.6). Other reflectors have also been recognised: H on the Southern Iberian Abyssal Plain (Krawczyk et al., 1996) and P from the Porcupine basin (Reston et al., 2001).

The high amplitude reflectors were initially considered to be the brittle-ductile transition (de Charpal et al., 1978). Alternative explanations include the crust-mantle boundary (Boillot et al., 1989) and also as a low angle detachment fault within the crust (Sibuet, 1992), or at the base of the crust overlying serpentinised mantle (Reston et al., 2007b).

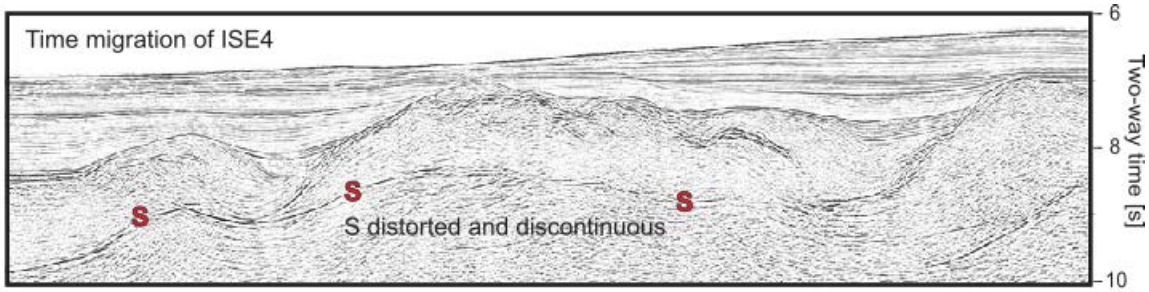

Figure 2.6: *The S reflector on Line ISE4 from Reston et al. (2007b)*

The presence of the S reflector well above the brittle-plastic transition for crustal rocks at <3 km from seafloor suggests it is a brittle structure (Pérez-Gussinyé and Reston, 2001). The reflector is sharp boundary with high amplitude (Reston, 1996). Geophysical data and waveform analysis (Reston, 1996) and waveform inversion (Leythaeuser et al., 2005) have been used to interpret the S reflector as a detachment fault. The waveform inversion (Leythaeuser et al., 2005) suggests S is thin layer (c. 50 m) and that it is fundamentally a step increase in velocity and density beneath a slightly lower velocity and density layer and is interpreted as a damage zone. Data from the 3D Galicia volume (the dataset used within this work) suggests that the S is the base of similar interval: a damage zone underlain by a step increase in velocity and density with a predominantly 20 ms thickness (in two-way travel time +/- 5 ms) that results in a zone 60 - 70 metres thick with the thickest portion more oceanward with the velocity used for time to depth conversion being 5100m/s (Schuba et al., 2018). The S reflector is therefore interpreted as being the boundary between crystalline basement and serpentinised mantle. The volume of water (>150km^3) required for serpentinisation suggests that it was derived on faults connecting mantle and the seafloor (Reston et al., 2007b; Reston, 2007a). Evidence from the uplifted passive margin seen in the Alps also suggests the presence of detachment faults that juxtapose mantle and continental crustal rocks (Froitzheim and Eberli, 1990; Masini and Manatschal, 2014).

Zone exhumed continental mantle - distal domain

Initially described as tectonic denudation (Boillot, Recq and Winterer, 1987), one consequence of a large offset detachment fault that cuts through the lower crust and onto the mantle is the

exhumation at the palaeo-seafloor of lower crustal rocks and in places the continental mantle. These zones of exhumed continental mantle (ZECM) are topped by a detachment fault overlain by fault derived breccia and reworked basement, i.e., mantle and lower crustal rocks are exposed by faults, with the fault surface forming the top of the basement (Figure 2.7). These areas have been shown by drilling on the Deep Galicia Margin and the Southern Iberian Abyssal Plain (Boillot, Winterer and Meyer, 1987; Sawyer et al., 1994; Whitmarsh et al., 1998).

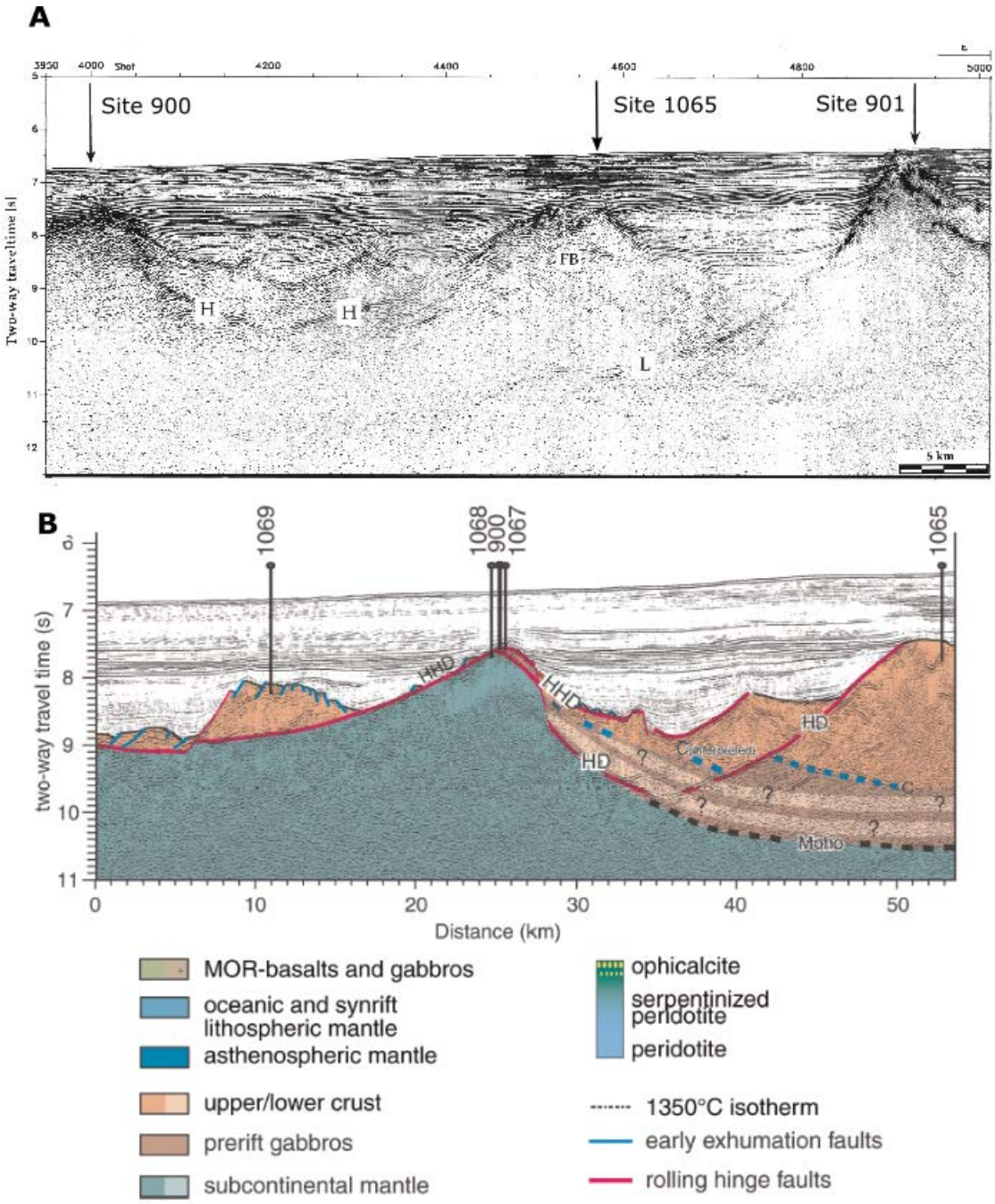

Figure 2.7: *Examples of exhumed continental mantle from the Southern Iberian Abyssal Plane. A: Seismic line LG12 (Krawczyk et al., 1996) and further interpretation on same line from further drilling (Manatschal et al., 2007). Sites refer to ODP drill sites where site 1068 was one of the sites to reveal the presence of serpentinised peridotite*

2.3 Other magma-poor margins

A number of modern examples magma-poor margins have also been studied. These include: The Bay of Biscay (de Charpal et al., 1978) East India, (Pindell et al., 2014); the South China Sea (Savva et al., 2013; Li et al., 2014), the NW Australian and the Brazil-Angola conjugate (Franke, 2013). Reston (2009*b*) provides a synthesis of the occurrence and common features of those within the Atlantic.

In addition, a comparison of the South-East Tethys margin (Adria), which has been thrust on to continental crust in the modern day Alps, has been compared in terms of structural architecture and tectonic evolution with modern day Iberia (e.g. Manatschal et al., 2001). Other occurrences of ancient magma-poor hyper extended margins that have been uplifted due to being caught up in an orogenic cycle include the Pyrenees (Tugend et al., 2014, 2015; Masini et al., 2014) and Corsica (Beltrando et al., 2013), and more anciently the Appalachian-Caledonian belt (Chew, 2001; Reston and Manatschal, 2011; Chew and van Staal, 2014; Chew and Strachan, 2014).

2.4 Stretching factors

Continental lithosphere stretching factors provide a simple way to measure the extension (stretching) seen within a sedimentary basin. The level of extension can be measured using the β factor:

$$\beta = L_o/L_i$$

where L_o is the measured length after extension and L_i is the original length. A β factor of 2 therefore results if stretching has occurred to twice the original length. In the case of crustal scale tectonics where it is difficult to assess the original length prior to extension wide angle seismic profiles can be used assess thinning (Barton and Wood, 1984) with thinning being related to β by the relationship:

$$\beta = 1 - 1/\beta$$

Stretching factors allow a comparable measure of the amount of extension seen between different rifts and between different parts of a rift. However such comparison, especially at higher

stretching factors need to take into account how this extension is measured. In the upper crust it can be measured in the field or more likely on seismic images. On seismic images the stretching factor measured is that determined from faulting ($\beta_faulting$), rather than full stretching of the upper crust ($\beta_uppercrust$), due to the limitations of seismic resolution to reveal all the brittle faulting present. The resolution of seismic data and the difficulty in imaging faulting at deep (basement) structural levels means that at the margin scale other methods are used, such as thinning often based on wide angle seismic data, for example Figure 1.6.

2.5 Mechanisms of hyperextension and break-up

A number of mechanisms have been suggested to account for the structural elements and other strands of evidence seen on the west Iberian margin and magma-poor margins elsewhere. This section reviews the various mechanisms and highlights the key findings and areas of uncertainty. The focus is on how 3D interpretation [and where possible restoration] may help validate mechanisms, may offer refinement, or propose new mechanisms of continental break-up. In order to undertake this review of mechanisms a summary of structural styles and their changes over time is required. Figure 2.8 shows the various mechanisms that are considered. The following sections outline these various mechanisms and primarily refer to the key works that provided the original evidence.

2.5.1 Depth-dependent stretching

Figure 2.8 A

Extension by depth-dependent stretching Driscoll and Karner (1998); Davis and Kusznir (2004); Kusznir and Karner (2007) or depth dependent thinning (as the models that invoke it are determined by the variation in whole crustal or lithospheric thickness due to rifting) consists of extension by upper crustal brittle fracture and lower crust ductile flow, similar to that proposed by de Charpal et al. (1978). A conceptual example of depth dependent thinning DDT is provided in Figure 2.8A and a discussion of the theory's in relation to the extension discrepancy is

provided in 2.6.

A characteristic aspect of DDT is that the extension in these rheologically different layers varies with depth, resulting in one or more of the layers being attenuated more rapidly than the other(s). Viscous flow may initiate prior to brittle failure as lower levels of stress are needed to deform them. However, the overlying layers would also need to be extended and would therefore thin. This suggested variation of extension with depth presents a 'space problem' common in structural geology when trying to balance sections. If more thinning occurs in one layer, the thinned area must be preserved and move elsewhere; in the case of passive margins this would be either toward the (proto) ocean, toward the continent or laterally along the margin. Reston (2009*b*) provides evidence that none of these are seen to the extent needed to explain the discrepancy. Numerical modelling has also been instrumental in developing depth dependent stretching of the lithosphere (Huismans and Beaumont, 2002, 2003, 2011, 2014) and Brun and Beslier (1996) provides an example from analogue modelling research, however the inability to change rheology as extension proceeds makes the direct application of analogue modelling problematic.

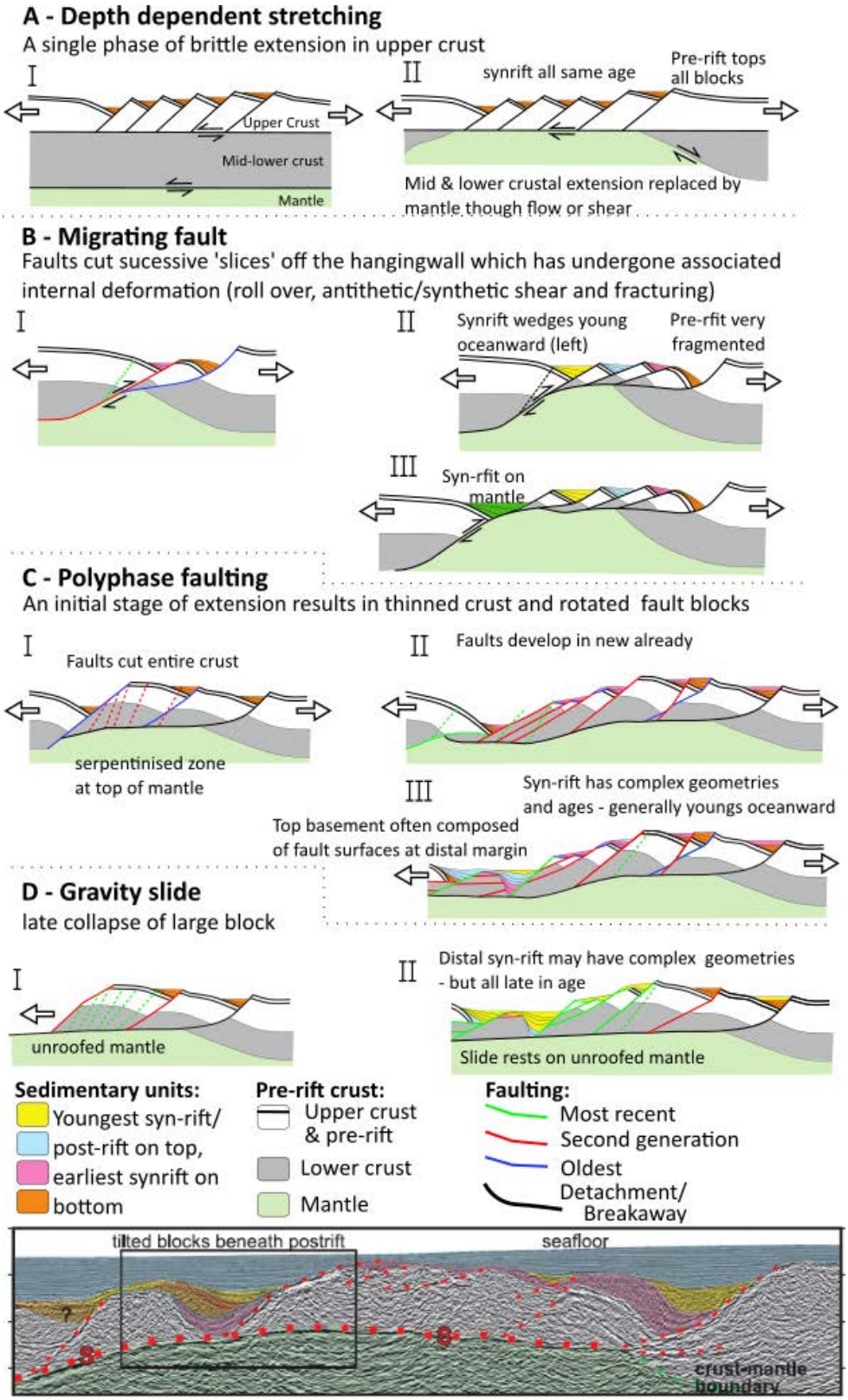

Figure 2.8: *Conceptual models of the breakup of the continental crust and formation of the S reflector, developed by Reston et al. (2007b) and pers. comm.*

Although low angle detachments are recognised within DDT, sequence stratigraphy and kinematic basin modelling are used to understand lithospheric deformation and sedimentology. The results of modelling and analysis of seismic data from Carnarvon Basin (Driscoll and Karner, 1998) South China Sea, Iberian Margin, Mid-Norwegian margin, Angolan Margins (Davis and Kusznir, 2004; Kusznir et al., 2005; Kusznir and Karner, 2007) suggests that the amount of extension varies vertically with more plastic lower crust and mantle accommodates greater extensional strain than the brittle upper crust. Extension in the upper crust has to be same as extension in lithospheric mantle but not necessarily spatially coincident (Driscoll and Karner, 1998). Driscoll and Karner (1998) arguing that a zone of "strain partitioning" creates a diffuse detachment between brittle and plastic layers in the lithosphere. Their modelling suggests that subsidence was regional and had limited relation to brittle faulting/thermal and related to lower crust/upper mantle extension. The balancing of upper crustal extension is assumed to occur where a detachment breaches crust, with the detachment being a ramp-flat that dips continent-wards. The lower crustal extension is dominant during later stages of extension - due to asthenosphere upwelling with little upper crustal brittle deformation, but this still does not account for the space problem outlined above. This model in considered to be similar to other margins including Iberia (Driscoll and Karner, 1998; Davis and Kusznir, 2004). Evidence for DDT includes the lack of sub-aerial erosion within basins suggesting any significant isostatic response to thinning is absent (c.f. Wernicke and Axen, 1988; Lavier et al., 1999). Using similar data, Kusznir and Karner (2007) proposed a model of diverging athenospheric upward flow to provide a driving mechanisms of DDT, with the variability of the flow field explaining the lack of brittle upper crustal deformation. Arguments on the validity of the DDT model to fully represent the nature of brittle deformation and therefore crustal break-up are provided in Section 2.6.

2.5.2 Migrating fault

Figure 2.8 B

A number of different models have been proposed that essentially use similar observations to invoke a range of mechanisms. They have been grouped together here as they do have some common features and may not be mutually exclusive in terms of providing a break-up mechanism.

Rolling hinge

The rolling hinge (Figure2.9) is a conceptual and numerical mechanism that includes flexural response of the footwall that flattens the fault surface until a point where a new 'slice' is cut off the hanging wall (Buck, 1988a; Choi et al., 2013). Initially used to explain continental core complexes, it has also been proposed at passive margins (Manatschal et al., 2001; Reston et al., 2007b) due to its ability to exhume lower crustal and mantle at the surface, in the footwall with isostacy resulting in non-active shears become listric (Buck, 1988a).

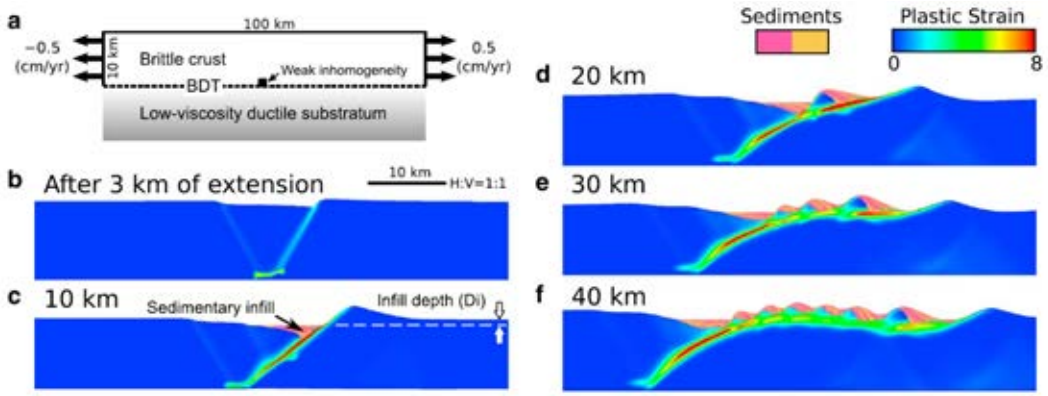

Figure 2.9: *Rolling hinge model (Choi et al., 2013) showing model set up (a) and different stages of extension (b-f)*

Detailed field and theoretical assessment of the rolling hinge in a continental setting suggest that is possible that faulting may continue at low angles (<35°) (Axen and Bartley, 1997), However, there are inherent mechanical problems of movement at this angle (Anderson, 1905, 1951; Axen and Bartley, 1997). Late stage concave-down faults interpreted on the Iberian Abyssal

Plain, can be considered to also follow the rolling hinge model (Manatschal et al., 2001; Whitmarsh et al., 2001). These detachments have been explained by a localisation on upper crustal and upper mantle detachments. The faults flatten and 'pull' footwall from beneath hanging wall with rotation of detachment faults dips during activity, this is evidenced by rock samples collected on the fault surface suggest low angle detachment active during sedimentation. Field tests for footwall and hanging wall have been proposed to assess the presence of rolling hinge mechanism (Axen and Bartley, 1997). In essence this mechanism is essentially the same as the rolling hinge. Downward concave is used to explain cutting into lower crust and mantle that is seen at the (paleo) sea floor from drilling samples (Manatschal, 2004). The amount of extension, the large offset and the excessive thinning leading to lower crustal/mantle exhumation, is argued to be by conjugate concave down faults rather than multiple normal faults (Lavier and Manatschal, 2006). Such concave-down faults initiate as straight steep faults dipping to c. 70° and only become concave due to rolling hinge (Lavier et al., 1999). The difference between exhumation of the mantle at rifts and at continental core complexes in that crust is already heavily thinned at the final stages of rifting.

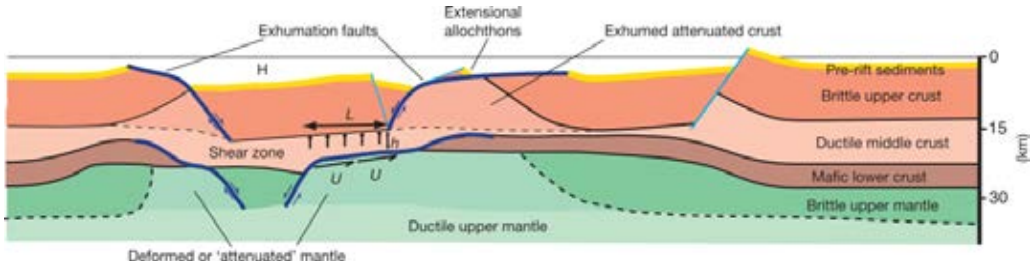

Figure 2.10: *Complex model for the thinning phase during continental break-up. We note that thinning is accommodated by the simultaneous exhumation of middle crust and extension of the upper mantle (Lavier and Manatschal, 2006).*

Some version of a rolling hinge style detachment have faults in the lower crust / upper mantle and separate detachments in the upper crust during the thinning phase with the final break-up of the crust an uncertain mechanism (see Figure 2.10). Further evidence for rolling hinge (concave-down) detachments is the lack of large amplitude rift-related topography which

is paradoxical unless a rolling hinge detachment is invoked (Wilson et al., 2001).

Low angle detachments

Possible low angle detachments have been observed on seismic data: the S reflector, described by de Charpal et al. (1978) in the Bay of Biscay (Goban Spur) and Deep Galicia Margin (see also Reston, 1996; Reston et al., 2007b; Sutra et al., 2013), the H reflector (Krawczyk et al., 1996) in the Southern Iberian Abyssal Plain. Field studies in the Alps has also revealed possible low angle detachments (Mohn et al., 2012; Manatschal, 2004). These detachments therefore have been recognised as a potential mechanisms that plays an important role in large scale extension and thinning.

Three main questions arise from the interpretation of low-angle detachment faults:

- a) did the detachment faults form at low angle?
- b) did the detachments form at a steep angle but then remain active at a low angle during and after rotation?
- c) did the detachments form steep and remain steep when the were active, and were then subsequently passively rotated.

In one interpretation (Manatschal et al., 2001) initial detachment changes dip at 12 km depth suggesting a number of possibilities: lower most crust is weak and quartz rich, the lowermost crust is hot allowing for the deformation feldspar, the upper most mantle is weak (serpentinised), or the upper mantle/lower most crust are under-plated by hot gabbro. In addition high amounts of displacement are seen on the most oceanward detachments and form basement at/near surface and rotation of the faults occurs whilst they are still active 30-17° (Manatschal et al., 2001).

Extension during the latter stages of rifting is considered to be by simple shear on top-to-the-ocean low angle detachments on one side of the conjugate. On the other side the sense of shear is top landward: the footwall of the fault is pulled out form under the continent. The scale of deformation seen on these detachments juxtaposes post rift sediments on exhumed mantle as well

as draping fault blocks. The timing of these detachments suggests that they are late structural features in the extension and rifting process. Footwalls are upper crustal granites/gneisses to serpentinised mantle (Manatschal and Bernoulli, 1999). The S reflector and the Alpine detachments have geometrical similarities (but there is no kinematic data). Similarities are: 1) they are rift related, 2) they occur and are active in the shallow crust 3) they can be traced to exhumed mantle, and 4) they are overlain by rotated fault blocks (Manatschal and Bernoulli, 1999).

Pérez-Gussinyé and Reston (2001) describe the formation of these detachments in reference to modelled changes in the rheology of the continental crust, controlled by temperature and pressure: as extension continues, cooling and reduced thickness leads to a switch from plastic to brittle behaviour. The plastic layers at the base of the upper crust and within the lower crust gradually become brittle until the whole crust is embrittled (Figure 2.11). Stretching factors (β) to reach embrittlement increase with high strain rates. This embrittlement of whole crust is seen at β factors of 3-5, with the variation being dependent on rate. In addition, at high amounts of extension, embrittlement enables seawater ingress leading to serpentinisation at the crust-mantle boundary (see also Reston et al., 2007b; Bayrakci et al., 2016). As the mantle does not contain enough water for serpentinisation, it must be derived from the sea/sedimentary pile via faults. This serpentinisation weakens the faults at the top of within/the mantle producing a detachment faults that spans from the now embrittled upper crust to the mantle thus moving away from pure shear (seen at low β), to asymmetric simple shear.

Serpentinisation may give local simple shear. Initially brittle and plastic deformation coexist, as extension continues, more crust deforms brittle and faults penetrate into upper mantle and slip onto the décollement on the serpentinised zone. The plastic layer in the lower crust being relatively thinner for a stronger crustal rheology, and a stronger rheology at high extension rate (Pérez-Gussinyé and Reston, 2001).

To summarise the process from embrittlement to the formation of a detachment:

1. embrittlement of the mid/lower crust ductile zone couples upper crust and mantle

2. embrittlement allows water ingress to the mantle

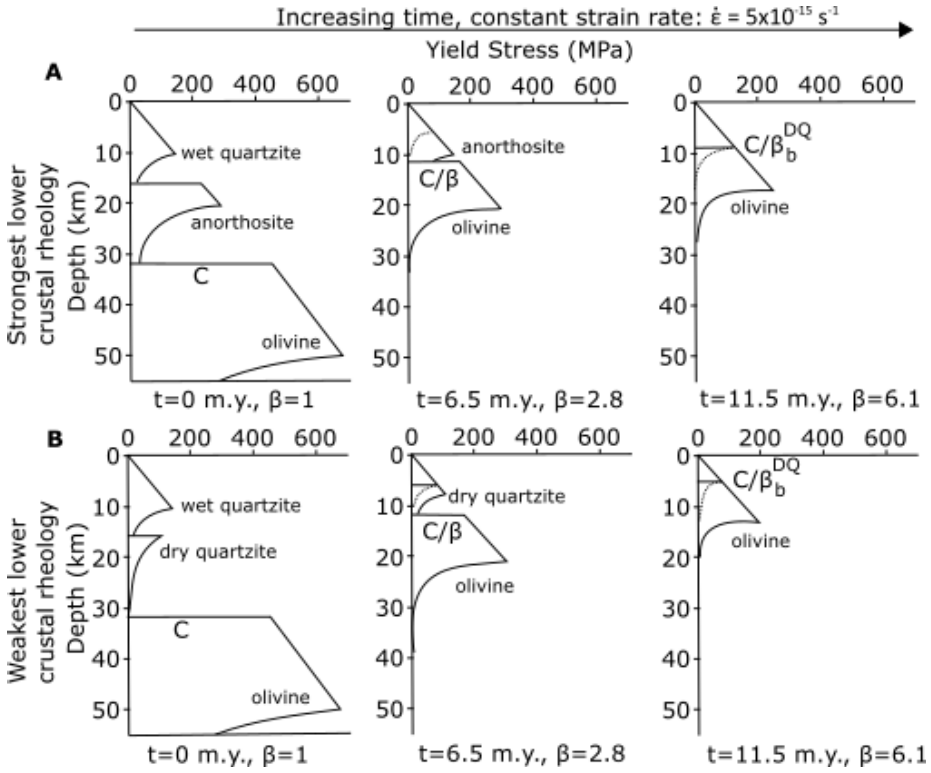

Figure 2.11: *Temporal evolution of the the lithospheric yield strength for a given strain rate for two different lithologies. C/β is crustal thickness, C = initial thickness, β_b = stretching factor of embrittlement*

3. reaction between water and mantle produces serpentinites

4. serpentinisation leads to weakening and slip

5. slip results in detachments faults forming.

Initial models of the formation of low-angle detachments drew similarities with continental core complexes (Boillot, Recq and Winterer, 1987; Lister et al., 1986). However, there are differences; continental core complexes have thick crust and a hot Moho despite large lateral variations in extension. This suggests that the lower crust is very weak, whereas continental margins had a thin brittle crust prior to detachment formation (Pérez-Gussinyé and Reston, 2001; Pérez-Gussinyé et al., 2001).

An analysis of syn-kinematic sediments has shown that movements (Reston et al., 2007b) on the ramp-flat geometries formed by steeper faults soling on to an underlying detachment and on newer faults cutting rotated older faults is relatively slow therefore ruling out catastrophic events such as submarine landslides (see also Section 2.5.4). Comparing the angle of the base of the syn kinematic wedges and the S reflector, it is postulated that, at the commencement of the most recent displacement, S dipped at approximately 30°. However, from looking at the top of the interpreted syn-kinematic wedges it is estimated that S was active at angles near 10°. Geometries of syn-kinematic wedges suggest that S was active at angles of under 15° when the next hanging wall fault short cut formed (Reston et al., 2007b).

Reston et al. (2007b) suggested a variety of models of slip on the S reflector including that the displacement along S was a hybrid of two end member models: the rolling hinge, where initially steep faults rotate as displacement occurs and eventually lock allowing sequential migration of the faults into the hanging wall, and a 'classical' model where all faults are active above S at the same time and progressively extend. Movement at low angles is explained by presence of serpentinite along the fault zone reducing the friction coefficient. Moreover, a cycle of water influx, serpentinisation (volume increase and increased temperature), sealing, overpressure and further rupture are also suggested in an anastomosing fault zone. This cycle would rotate local stress in fault zone and reduce the angle of slip-initiation that is possible on a detachment to

approximately 10°(see Reston et al., 2007b, Figure 7).

Detachment faulting is important in late extension in already thinned crust (Manatschal et al., 2001). If the order of the movement of the faults that cut down on to the low-angle detachment are to be determined, it is important to understand the stratigraphy of the syn-rift sequences (Wilson et al., 2001).

Sequential faulting

A relatively simple model based on geometric principles and area balancing sequential faulting (Ranero and Pérez-Gussinyé, 2010) is reminiscent of tilt block interpretation of passive margins (Figure 2.12).

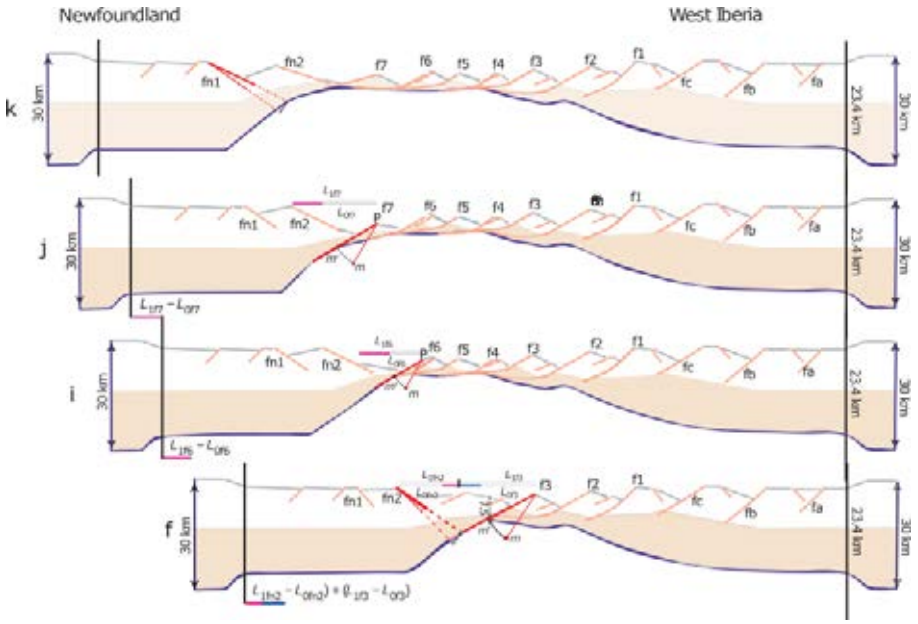

Figure 2.12: *Three of the later stages of the sequential faulting model (Ranero and Pérez-Gussinyé, 2010) showing important faults seen within the Galicia 3D dataset: Faults 3, 4, 5 and 6*

Steep angled Andersonian normal faults, that become slightly listric with rotation of their lower portion, form sequentially ocean-wards in the gradually thinning brittle crust. This allows asthenospheric upwelling and isostatic readjustment; in addition the lower crust is ductile. These factors gradually reduce the dip of the active fault, which locks mechanically and another steeply dipping fault form in the thinned crust. This results in gradually smaller slices being

carved off the hanging wall and therefore a reduction in the size of blocks oceanward. The S reflector would be made up of the down dip portions of each of the sequential faults. In many respects therefore this model bears a close resemblance to a rolling hinge. Sequential faulting of the Iberian margin was used by Brune et al. (2014) to support modelling that balanced upper crustal brittle failure with lower crustal plastic deformation (flow) due to higher thermal gradients.

2.5.3 Polyphase faulting

Figure 2.8 C

In contrast to the relatively simple mechanisms and geometries proposed by DDT and migrating fault models, polyphase faulting Reston (2005); Reston and McDermott (2014) highlights the complex nature of magma-poor margins seen in seismic data. As a starting point the model considers simultaneous movement on rigid domino blocks, but acknowledges this is an oversimplification and incorrect, in that the blocks are not rigid, they internally deform sub-seismically, move progressively, may not be equally sized. Furthermore rifting is 3D in nature and may show polarity switches from east to west dipping normal faults bounding rotated blocks (Reston, 2005). The model is developed further using depth migrated data to ensure correct tilted block geometries, the seismic images show a clear inflection (convex-up) of the fault surfaces which suggest faulting, rotation then further faulting. 2D restoration of tilted blocks combined with recognition of up to three phases of faulting seen on the Deep Galicia margin (including a at least an extra, earlier one in the Galicia Interior Basin) based on syn-rift stratigraphy seen in drill and submersible data and along with footwall faulting. Displacement at the root of the blocks occurs on serpentinised mantle and faulting is seen to focus oceanward over time, from the Galicia Bank to more distal areas.

An important factor of the polyphase faulting model is the sub-seismic faulting within the crustal blocks deformation, which in part explains the extension discrepancy. This discrepancy is more common at margins than basins as there is much more extension on margins that seen

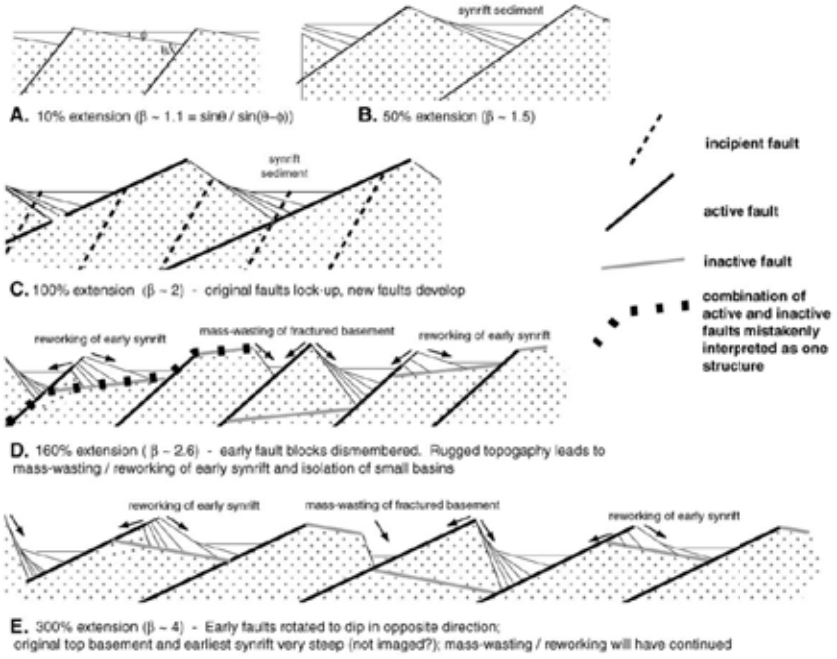

Figure 2.13: *Illustration of the variety of structures produced by polyphase faulting in a domino model. Note that early syn-rift sediment is likely to become hard to recognise and subject to mass-wasting. Also note that parts of early and later faults may be misinterpreted as a single phase of faulting.*

in continental basin (i.e. margins have higher β factors). This greater extension would provide difficulty in identifying marker horizons with which to measure extension. The obvious marker horizon to choose, top basement, can be rotated fault slip surfaces that are then offset by later faulting or subject to mass wasting, or both. Initially steep (angles of 60-70°) Andersonian (Anderson, 1905, 1951) extensional faults 'lock-up' at approximately 30° and new ones form at stretching (β) factors of approximately 2 (Figure 2.13). Extension beyond this may make interpretation too difficult. Additionally large scale low angle detachments which may also be difficult to interpret in terms of offset as they flex upwards and may be mistaken for crustal blocks. Furthermore, the detachment itself may be faulted and extended. On seismic profiles it is generally the latest phase of faulting that most obvious but, it is not that clear cut as to when they become preferentially interpreted (Reston, 2005, p 564). In addition if a later stage of faulting is relatively undeveloped it may not be imaged seismically but still results in internal deformation and rotation of blocks. As stretching proceeds toward the rift centre there is

greater potential for an extension discrepancy especially, as fault blocks become smaller and dismembered (Reston and McDermott, 2014).

Some aspects of other models can be considered to support elements of polyphase faulting: despite the different exhumation mechanism (convex-up detachments), numerical modelling (Lavier and Manatschal, 2006) outlines that deformation occurs in three overprinting phases. Rolling hinge models also have overprinting faults as the footwall undergoes fault bend fold as dip lessens by small vertical shears or flexure failure (Axen and Bartley, 1997). Where more simple detachments provide the mechanism, older detachments are seen to be cut by younger ones with faults showing cataclasis not mylonitisation suggesting they were in the brittle regime and not lower crustal ductile shear zones. Polyphase faulting takes into consideration many of the difficulties seen in interpreting seismic data whilst providing a conceptual model with which to consider such interpretation, however such a method places little focus on lithospheric scale processes (Manatschal and Bernoulli, 1999).

2.5.4 Gravitational collapse

Figure 2.8D

Multichannel seismic reflection data and ocean bottom seismometer reflection/refraction data on a N-S line (margin parallel) from Galicia Bank in South Iberian Abyssal Plain (SIAP) were interpreted by (Clark et al., 2007) as gravitational collapse. Clark et al. (2007) considered that these data provide evidence that the N-S section along the Galicia Bank – SIAP section is similar in appearance to margin perpendicular sections. This includes tilted fault blocks that deepen and widen away from the Galicia Bank and are listric at depth and sole onto a (speculative) detachment surface. The scale of structures and magnitude of extension is similar to that seen on margin parallel (E-W) sections and therefore cannot be along strike slip (which would be much smaller). Two possible interpretations are suggested i) two sets of detachment faults one top-to-west the other top-to-south, ii) one detachment with top-to-SW with displacement between 22-39°. The latter explanation is argued against due to greater weight of evidence from

paleogeographies and dominant E-W extension trend seen elsewhere (e.g., immediately north in Galicia Interior Basin). A gravity collapse mechanism is inferred across an E-W transform fault between GB and SIAP. This would waste the initial steep bathymetry between the two sections of the margin. The gravity collapse hypothesis would suggest why there are low volumes of accumulated sediment, relatively low time periods between mass wasting events would only allow limited time for accumulation.

2.6 The extension discrepancy

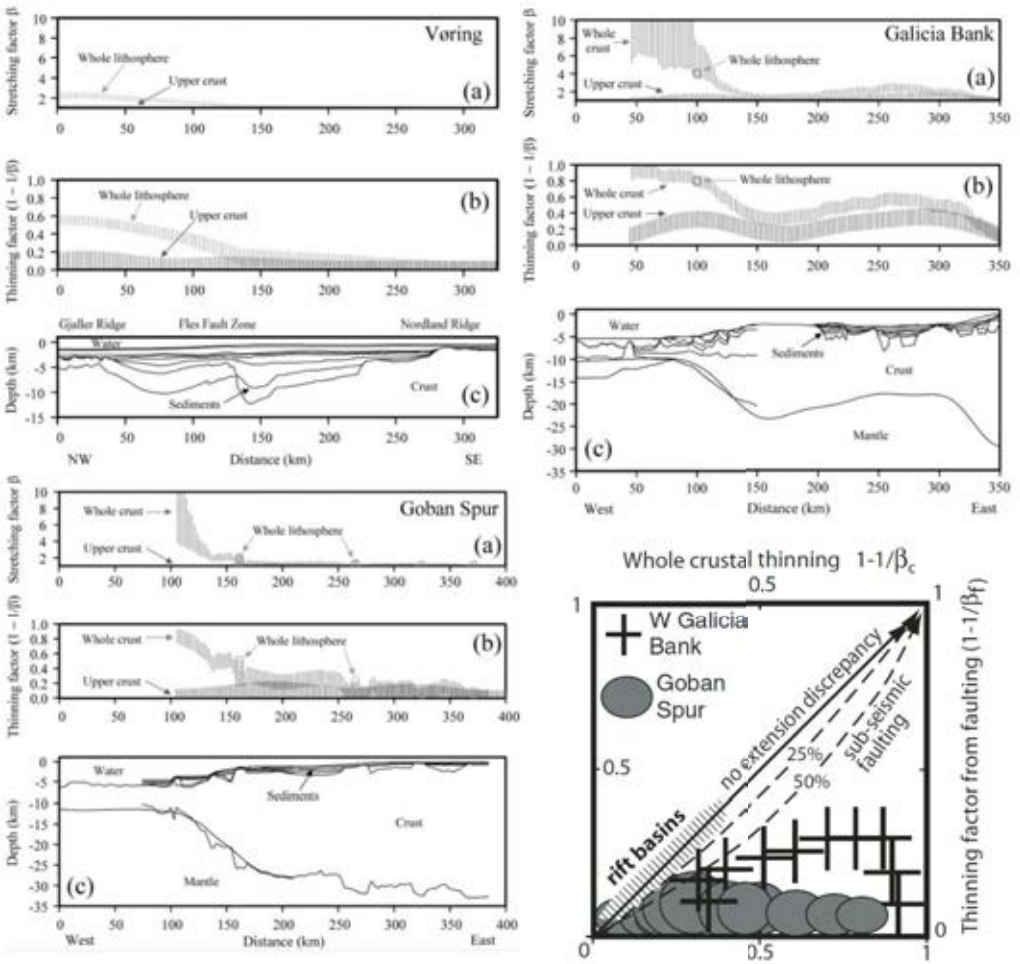

Figure 2.14: *Three plots from Davis and Kusznir (2004) showing stretching factors and thinning factors for three magma-poor margins. Graphical plot shows these data plotted against each other (Reston, 2007a), see text for description*

An important aspect of understanding the mechanisms that result in crustal hyperextension and final crustal break-up is the extension discrepancy; where the extension seen in the brittle upper crust is not enough to account for the extension of the lithosphere that has led to rifting and can be assessed from crustal thinning (Reston, 2005, 2007a). In areas of limited crustal extension (e.g. the North Sea) this extension discrepancy may be explained by sub-seismic deformation (Wood and Barton, 1983; Marrett and Allmendinger, 1992). However, relative to rift basins the extension is much higher at the edge of the continents and sub-seismic deformation alone is not enough to explain the discrepancy.

Depth-dependent thinning has been proposed to provide an explanation for the extension discrepancy. Figure 2.14 (Davis and Kusznir, 2004) for example shows different amounts stretching and thinning for the upper crust, which is derived from measuring the extension on faults, shown alongside this is whole crustal thinning. Figure 2.14 also includes is a cross plot of fault derived upper crustal thinning versus whole crustal thinning (Reston, 2007a); the plot clearly shows the extension discrepancy (crosses and circles) plot away from the diagonal line, which also incorporates possible levels of sub-seismic faulting not measured when measuring the brittle faults (Marrett and Allmendinger, 1992).

Depth-dependent thinning (e.g. Davis and Kusznir, 2004) however does not explain the extension discrepancy. Reston (2009*b*) provides a variety of evidence on why this is the case:

- DDT is incompatible with the evolving rheology of extending crust, especially at a heavily thinned margin (such as the Deep Galicia Margin) where embrittlement means that there would be no plastic lower crust to attenuate (Pérez-Gussinyé et al., 2003).
- The depth distribution of extensional faults within the crust does not support DDT.
- The explanation of the extension discrepancy by DDT is not supported by numerical modelling (Figure 2.15) or compatible with rifted margin velocity structures.
- The scale of DDT required to explain the extension discrepancy would result in an inverse discrepancy adjacent to the margin (Figure 2.16).

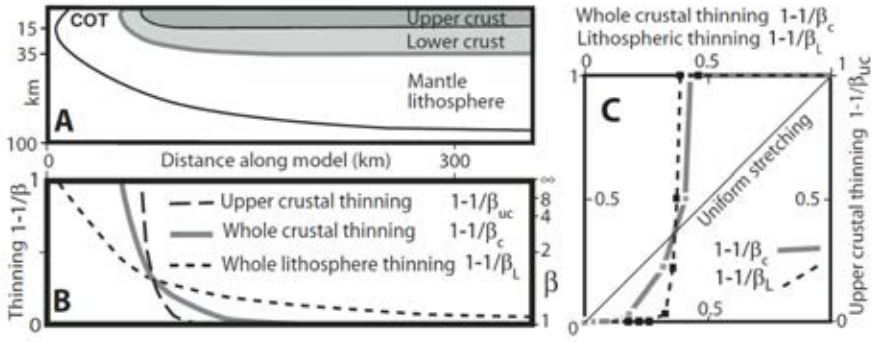

Figure 2.15: *Using depth-dependent thinning models to produce crustal and lithospheric thinning plots (Reston, 2009a).*

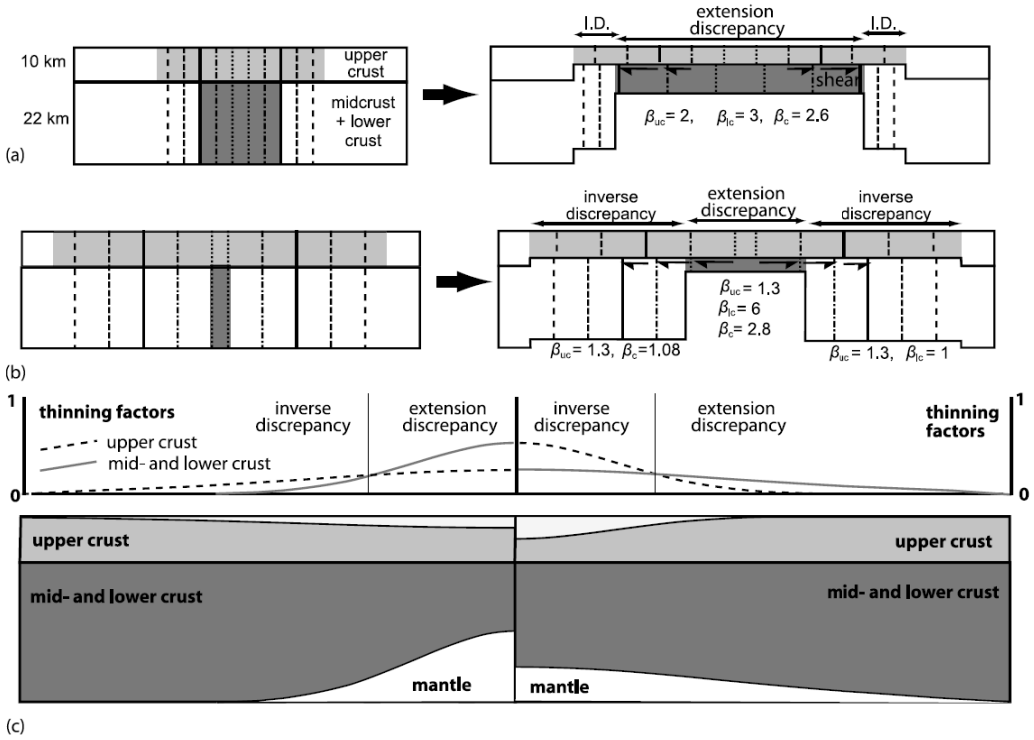

Figure 2.16: *Illustrations of crustal depth-dependent stretching and depth-dependent thinning, see text for further discussion. a) 50 km of extension could result in a zone of extension that is 50 km wide in the upper crust and 25 km wide in the lower crust (shaded zones). Relative displacement between upper and lower crust is shown by the passive markers. b) shows the case for 30 km of extension with deformation zones being 100 and 5 km wide for upper and lower crust respectively. c) shows a smoothed model: upper crust thinned over a wider area than the lower crust with a reduced thinning factor (left–hand panel); upper crust thinned over a narrower area than the lower crust with a increased thinning factor (right-hand panel) (Reston, 2009a).*

Figure 2.15A of Reston (2007a) shows modelled unroofed continental mantle and lower crust at the continent ocean transition (COT) and depth-dependent stretching as a result of mantle upwelling ((Davis and Kusznir, 2004; Kusznir et al., 2005; Kusznir and Karner, 2007)). Figures 2.15B and C uses the this model to produce and plot thinning factors across different lithospheric levels (whole lithosphere - β_L, whole crust - β_c, upper crust - β_{uc}). The cross plot of upper crustal thinning against whole crustal and lithospheric thinning (C) highlights that this model only produces a minor extension discrepancy (to right of diagonal line) which is offset by an inverse discrepancy at thinning factors above 0.35. This inverse discrepancy is further highlighted in Figure 2.16 which shows how varying amounts of discrepancy (extension and inverse) can be produced by different amounts of stretching/thinning depending on the relative widths at which extension occurs in the upper and mid/lower crust (Reston, 2009*a*).

Figure 2.16a shows how an extension discrepancy develops over the majority of the crust ($\beta_{lc} = 3$, $\beta_{uc} = 2$). However, on the flanks of the basin produced by the extending crust an inverse discrepancy (I.D.) develops ($\beta_{lc} = 1$, $\beta_{uc} = 2$). Figure 2.16b shows a case with lower extension and different extension zone widths in the upper and lower crust; here the basin flanking inverse discrepancy is very wide which is rarely observed in nature (Reston, 2009*a*). In Figure 2.16c the thinning varies smoothly and is differently distributed between lower and upper crust, in both cases an extension discrepancy needs to be balanced by an inverse discrepancy.

This interplay between the extension discrepancy is further highlighted in Figure 2.17 which cross-plots upper crustal thinning against whole crustal thinning for 14 magma-poor margins. Figure 2.17 shows that for the margins plotted there is no significant extension discrepancy (no margins plot in the bottom right corner). An explanation of the extension discrepancy is that cross-cutting (polyphase) faulting obscures true upper crustal extension (Reston, 2005, 2007a; Reston and McDermott, 2014). The result of these arguments suggest that although a number of models can be used to explain the extension discrepancy, depth-dependent thinning is not one of them.

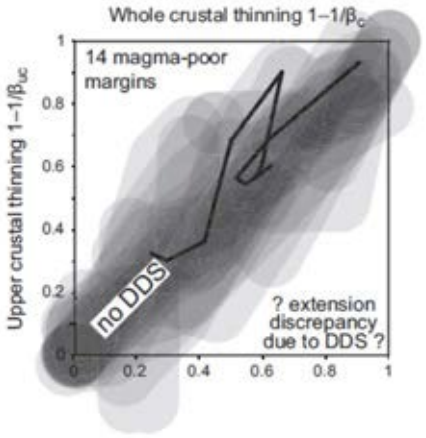

Figure 2.17: *Estimated range of upper crustal thinning factors, derived from seismic velocity models (Reston, 2009*b*) plotted against whole crustal thinning factors for the 14 best constrained magma-poor margins [W Galicia-Flemish Cap; Labrador–W Greenland; Rockall Trough (2) Porcupine Basin (2); N NewfoundlandBasin – S Iberia Abyssal Plain; S Newfoundland Basin; Nova Scotia (2) – Morocco], from Reston and McDermott (2014)*

2.7 Discussion - testing the mechanisms

An important test for the various mechanisms proposed for final break-up is the relative ages of the syn-rift sediments (Figure 2.8). One of the benefits of having the 3D seismic data is that it is possible to map reflectors (a geophysical representation of sedimentary units) to provide a surfaces (horizons) within the volume to possibly derive relative ages - if these surfaces are syn-rift and can be correlated then relative timings of their formation can be obtained.

For depth-dependent stretching the top of the syn-rift would be of the same age, meaning also that the same post rift stratigraphy would onlap the base of the post-rift unconformity across its entire surface. Additionally, fault blocks be tilted at a similar angle throughout the lower crust and would have relatively planar surfaces. For a migrating fault, the majority of syn-rift, and all of the latest syn-rift, sediments would young oceanward. The rolling hinge model specifically would require that fault dips on the block bounding faults decrease landward as the non-active fault is back rotated away from the active fault due to flexure of the footwall from isostatic unloading (i.e. it is moved through the hinge). The dip of the sediments within

the blocks should increase in dip landward. The nature of the rolling hinge would also suggest that evidence of sub-vertical shear be seen within the blocks and the syn-rift sediments (Axen and Bartley, 1997). As with the rolling hinge, the geometric methodology of the sequential faulting model (Ranero and Pérez-Gussinyé, 2010, supplementary material) also requires back rotation of the blocks and associated reductions and increases in the landward dip of the faults and sediments, respectively. It also suggests that there is a decrease in the size of the blocks oceanward and that the S reflector would be made up of the lower portions of the faults as they form sequentially, step-wise toward the future ocean. The syn-rift geometries of polyphase faulting are likely to be complex, however, as the faulting is considered to focus oceanward the syn-rift will also young oceanward (McDermott and Reston, 2015). Another primary test is the presence of faults that cut across earlier faults resulting in faults that have fault-bounded (flat) tops and possibly geometries (sharp-angled convex-up) which indicate that the toes (lower portions) of blocks have been removed by a subsequent fault. For a gravity slide distal syn-rift would be all the same age and for such a large scale slide it would be expected to see a large zone of compressional deformation at the distal end of the slide (toe thrusts).

2.8 Fault growth, fault networks, and rift development

This study focuses on how faulting of the brittle crust may have resulted in hyperextension and final break-up of the continental crust. In order to understand the mechanisms of how faulting brings about this break-up, it is useful to understand the nature of faulting at different scales and how faults form and interact with each other. The following sections provide a brief overview of the current understanding of faulting and how this applies to the evolution of rifting. The previous sections have outlined the state of knowledge regarding continental break-up with special reference to the Iberian Margin. The acquisition of the Galicia 3D seismic data have provided an opportunity to undertake detailed and rigorous interpretation of faults, structural horizons and syn-rift sediments. To understand these new fault data, it is necessary to have an understanding of faulting. The size and displacement of faults, fault network development and how

faults interact within sedimentary basin during extension has proved important when considering the impact of such features on hydrocarbon exploration and exploitation. These factors include the movement, storage and baffling of fluids in relation to the formation of structures, and the role that structures play in provide in determining sediment geometries that influence the the movement, storage and baffling of fluids (Peacock and Sanderson, 1994; Yielding et al., 1996; Torabi and Berg, 2011). The principles of understanding relative timings of fault formation and fault network development, especially within the syn-kinematic sediments, may also help determine the mechanisms of extension at the hyper extended margin. For example the role of fluids within the fault system possibly changing effective pressures and allowing slip at reduced stress. Additionally, fluids may provide the flux of the necessary components for alteration of fault wall rocks thus providing aspects of weakening or healing. A major example being the ingress of seawater via large faults that can serpentinise and weaken the mantle, allowing changes in the angle of slip, or even rate of slip (Pérez-Gussinyé et al., 2001; Bayrakci et al., 2016; Prada et al., 2017). In addition to considering the impact on fluids, the techniques used when understanding sedimentary basin development are also applicable to understanding the formation of hyperextension and break-up.

2.8.1 Fault scaling

Faults are observed at a range if scales (Dawers et al., 1993; Walsh and Watterson, 1987; Scholz and Cowie, 1990); laterally extensive faults may be viewed on maps from field studies, satellite imagery or aerial photographs, or as imaged and interpreted on seismic reflection image time or depth slices. The geometric properties of faults observed and measured in a population may be 'self-similar' and display fractal geometry (Zhang et al., 1991; Schlishe et al., 1996) providing fault populations with numerically defined scaling relationships, where fault displacement is mathematically related to other aspects of fault geometry usually fault length or height (Figure 2.18I). The relationship developed is a power function (Torabi and Berg, 2011; Kim and Sanderson, 2005) where:

$(D_{max} = cL^n)$

Where: D_{max} is the displacement, the maximum linear movement measured on the fault parallel to the slip direction; L is the fault length; n provides the measure of the scale dependent geometry and c is a constant and is the ratio D_{max}/L. If the exponent n = 1 the relationship is a linear scaling law, with self similarity at all scales. The range of the exponent n recorded is between 0.5 and 2 (Torabi and Berg, 2011; Kim and Sanderson, 2005). Nicol et al. (1996) presents evidence that the exponent is not a power law but is a faults scaling law dependent on a faults size (Figure 2.19). This geometric relationship between displacement (D) and length (L) suggests that faults grow as their displacement grows has provided much of the understanding of fault growth and development (Childs et al., 2017; Elliott, 1976; Watterson, 1986).

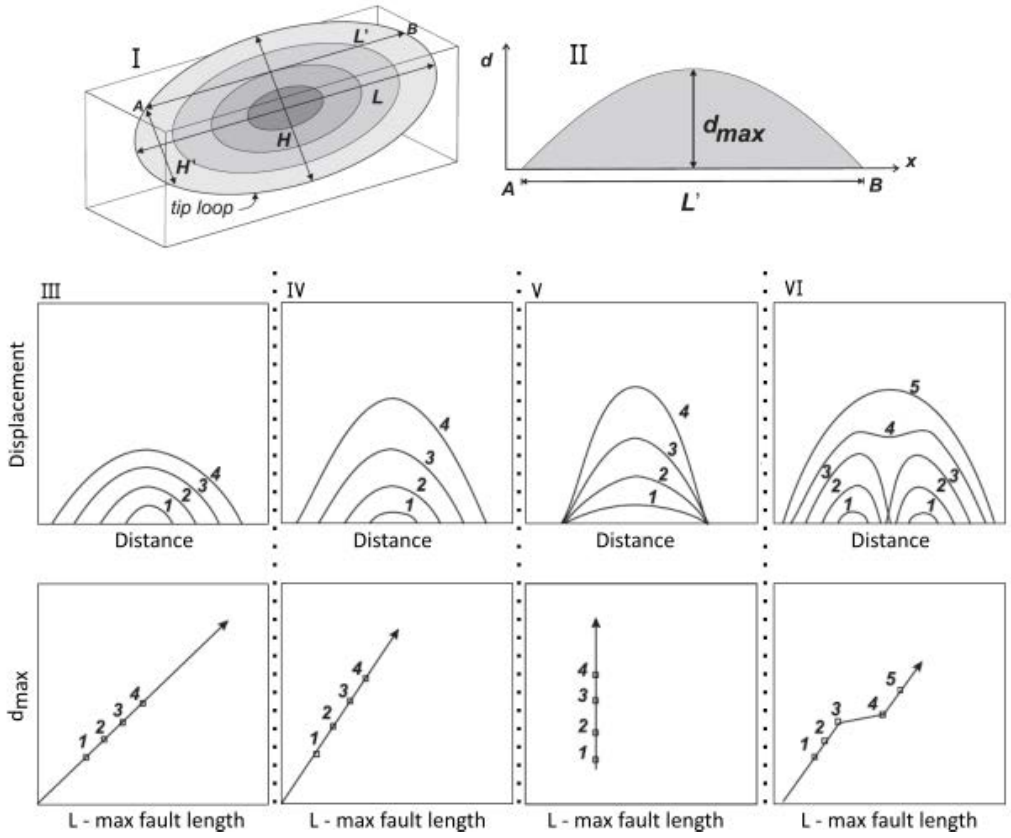

Figure 2.18: *Idealised displacement distributions and fault growth models - after (Kim and Sanderson, 2005, Figures 1, 7). In sub-figure I darker shading relates to larger amounts of slip. See text for description and further references*

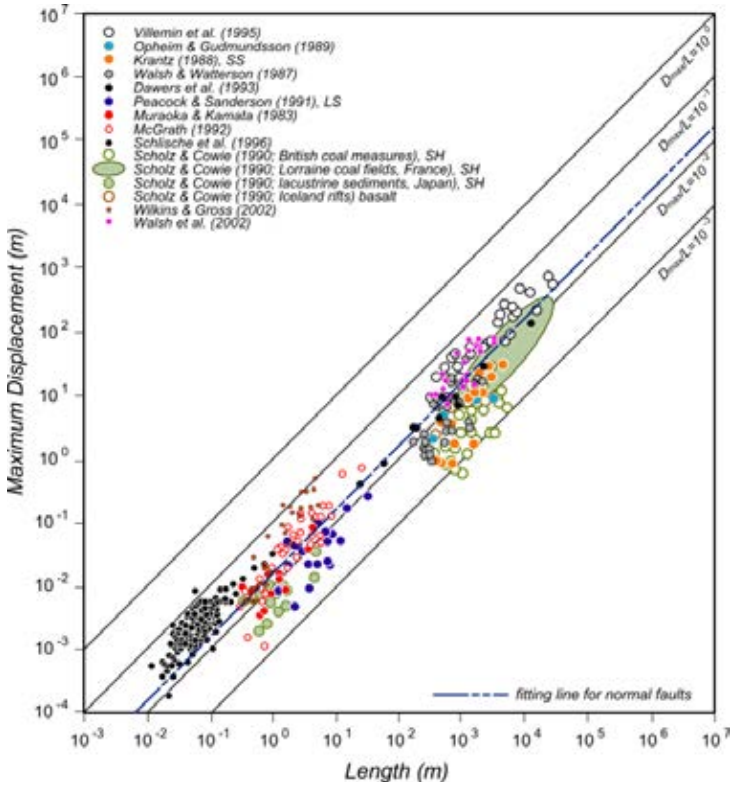

Figure 2.19: *Maximum displacement (d_{max}) versus fault length (L) for Normal Faults from Kim and Sanderson (2005)*

2.8.2 Fault growth models

Considering a single fault plane in the geological record, Walsh and Watterson (1989) showed that they may consist of linked segments that have a kinematic relationship, meaning they behaved as a single fault prior to any segment linkage. Two end members can be considered in the development and growth of an individual fault from segments, see Childs et al. (2017) for a clear albeit brief overview; it is the classification of Childs et al. that is used here. Similar reviews can also be found (see for example: Kim and Sanderson, 2005; Jackson et al., 2017). These idealised models of fault growth use elliptical slip planes (Figure2.18I) that grow with increasing extension, with maximum slip being in the centre of the ellipse and decreasing to the edge of the ellipse or fault 'tip'. This isolated fault shows a displacement length profile (2.18II) where maximum displacement in in the centre of the fault.

The first end member considers propagating **isolated** faults (Figure 2.20), the second the

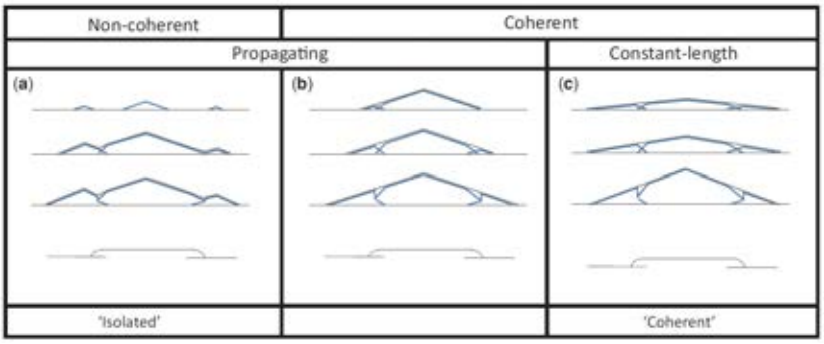

Figure 2.20: *Classification of models of fault growth based on displacement length profiles. Solid lines are the displacement profiles for individual faults and the dashed lines are profiles of cumulative displacement.*

constant-length **coherent** faults, a third combined model is the coherent- propagating fault, but is 'less commonly invoked' (Childs et al., 2017, Figure 1 caption p2) - the emboldened text provides how they are commonly referred to.

Considering the 'isolated' fault, as extension continues the faults develop by tip propagation, increasing in length as fault displacement also increases (Walsh and Watterson, 1987, 1988; Cowie and Scholz, 1992a,b). Further extension leads to further displacement on the faults, the tips of the faults continuing to propagate laterally (2.18III, IV). In isolated fault systems faults propagate as their displacement increases, faults that are approximately along strike therefore merge. This provides a constant straight line on the D-L plot. In the constant-length coherent model the D-L profile ends up in the same place, however in a stepped fashion.

The alternative 'coherent' model (Walsh and Watterson, 1991; Walsh et al., 2002) is that further extension simply produces increased fault displacement with fault tip propagation and therefore lateral fault growth remaining limited (2.18V); an explanation for this is that during extension faults form at a variety of lengths, and due to an initially rapid tip propagation and linkage, the fault population include some that are laterally extensive, but with very little displacement. Eventually as displacement increase faults will display the observed fault scaling relationships (section 2.8.1). The constant-length coherent model establishes the map view of the fault system early and it essentially remain the same, bar the formation of linkage and relay

structures (Childs et al., 2017). An essential feature of this model is that in map view the fault network is established relatively early in the evolution of the fault system with changes only due to interaction of faults (Childs et al., 2017). Nicol et al. (2017) presents data on an outcrop scale suggesting that the coherent model is applicable at a small scale.

Lateral propagation of the fault tips is considered to be retarded due to interaction of the fault tips and produced a large reduction in displacement gradients close to fault tips (Cartwright et al., 1995). An *a priori* assumption may exist in that the development of the initial faults form in response to underlying faults. This model was developed to bridge a gap in understanding of the scaling relationships seen between faults from the geological record and modern-day faulting observed through earthquakes. The irregular aggregate (cumulative) displacement profile is characteristic of non-coherent faults that were initial isolated. A single 'triangular' displacement profile for cumulative displacement suggests the faults were kinematically linked i.e. had geometric coherence (Figures 2.18VI stage 4, and 2.20). It may be the case that at the scale of observation the is no geometric link; the link being via distributed strain within fault wall rock. In the case of the Galicia data (or other seismic data) this distributed strain may also include sub-seismic scale deformation .

When considering the development of faults and their relationship to displacement-length plots, they can be considered as individual faults (Barnett et al., 1987; Cowie and Scholz, 1992a,b; Walsh and Watterson, 1987; Walsh et al., 2002) or as series of linked fault segments (Cartwright et al., 1995; Dawers and Anders, 1995; Peacock, 2002), with the style of fault growth and fault interaction influencing the displacement-length characteristics as plotted over time (Figure 2.18VI).

Walsh et al. (2002) suggests that the kinematics (i.e. the temporal and spatial movement) of faults are important as geometric analysis of the final shape alone cannot determine fault growth models. Where two faults have developed and their tips are in close proximity to one another the displacements are impacted: as extension in the area is likely to be similar (or the same) the cumulative displacement on the two faults remains the same resulting in a potentially large displacement gradient (Cartwright et al., 1995) at fault tips. Furthermore, this interaction and displacement gradient results in deformation around the fault tip and between the tips of

the two faults, resulting in a change from from propagation to displacement due to fault system "saturation" (Nicol et al., 2017).

2.8.3 Fault interaction and relay zones

The discussion above highlighted that the importance of faults interacting and linking along strike. Where faults do interact they may not (initially or even eventually) directly link. Where they do interact the area around them is termed a fault 'relay', that fundamentally consists two faults tips separated by a 'relay ramp' (Figure 2.21). The beaching of relay ramps provides the most efficient way of lengthening faults (Fossen and Rotevatn, 2016). Areas where overlapping faults interact (see Figure 2.18VI) are often characterised by relay ramps which transfer deformation by small scale faulting, fracturing and ductile deformation of the bedding planes (Fossen and Rotevatn, 2016; Childs et al., 2016). The exact nature of the deformation depends on the geometric relationship of the faults. At higher amounts of extension, the relay zone can become breached, resulting in faults that can significantly vary in strike direction compared to the general extension perpendicular trend (Cartwright et al., 1995).

Figure 2.21 shows a spectrum of structures defined by the variation in the aspect ratio of segment overlap to distance between faults (normal to dip). The front face of each block diagram illustrates a characteristic cross-sectional geometry. Faults with a large aspect ratio (a and d) result in beds within the relay zone showing no tilting. Low aspect ratio results in beds within the relay dipping in the direction of the fault. Where there is no overlap (i.e. they underlap) a monocline forms by fault propagation (arrow in f) (Childs et al., 2016). In addition to along strike linkage 3D discrete modelling (Finch and Gawthorpe, 2017) has highlighted fault growth by down dip linkage and propagation. This results in displacement being variable along strike and displacement maxima migrating as segments link, therefore final displacement maximum may not correlate with initial fault segment maximum. Furthermore the down dip linkage may mask the interaction of faults at different levels and provide misleading geometric relationships at these levels (Giba et al., 2012; Long and Imber, 2012). The nature of the country rock however can influence this down dip linkage as weak sedimentary layers can inhibit vertical propagation,

resulting in the formation of parallel faults that widen the fault zone (Roche et al., 2017).

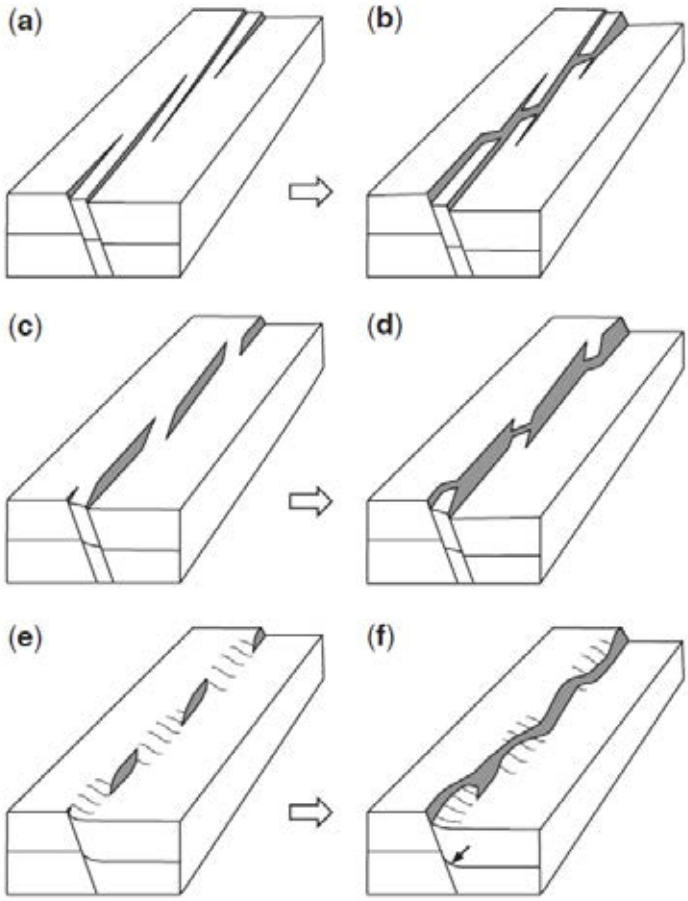

Figure 2.21: *Sketches illustrating (a, c, e) a spectrum of segmented fault geometries and (b, d, f) the fault zone structure that develops from them when displacement increases and fault segments become connected (Childs et al., 2016).*

2.8.4 Use of syn-rift sediments to determine fault growth

Where faults reach the free surface and influence the sedimentation of the basin, they can be considered growth faults with the resultant sediments being growth strata (Childs et al., 2003). Jackson et al. (2017) reviews a range of techniques to determine the kinematics of faults using growth strata. The techniques in include:

- Expansion index analysis which is the ratio of hanging wall to footwall sedimentary thick-

ness across a fault plotted against time (relative or geological),

- Isochron/Isopach mapping (depending on whether the data source is in time, for time migrated seismic data, or depth, for depth migrated seismic data, data derived from boreholes or field studies, respectively) of the syn-sedimentary growth strata. In seismic data growth strata is seen to thicken into (or adjacent to) the fault with the maximum thickness relating to maximum fault displacement,

- Displacement backstripping, where for, growth strata, the displacement at a shallower structural horizon from that displacement at a deeper structural horizon at the same point along the strike of the fault, and

- Relay zone backstripping uses the same technique as displacement backstripping but in the relay zone of linked faults, thus determining fault growth.

An example of Isopach analysis has been used to test the models of fault growth (Jackson and Rotevatn, 2013) resulting is evidence for both models but with fault segments reaching maximum length before significant displacement was seen, with down dip linkage, and therefore propagation also being important. Field studies reproducing isopach analysis at the field scale Khalil and McClay (2017) on the margin of the Red Sea have highlighted hanging wall synclines that have axial traces sub-parallel to faults but are also segmented and plunge into depocentres, i.e., show longitudinal (parallel to fault) and transverse synclines (perpendicular to fault). These complex hanging wall synclines are due to fault interaction or linkage along strike, with the synclines being formed by fault propagation folds. Jackson et al. (2006) also presents hanging wall folding or bed tilting of syn-rift strata adjacent to faults at a range of scales (m - km). In addition to the presence of synthetic and antithetic faulting the hanging wall of the major faults, these faults (and mini fault blocks) rotate into the major faults. These structures represent responses to vertically propagating normal faults. Lateral variations in sediments and structures laterally suggests complex interactions of the faults segments at different scales. These are of interest as they provide deformation at the scale that may usually may not be resolvable at the seismic scale.

The high resolution 3D dataset used in this study means that it is possible to interpret faults at a number of different scales from the seismic resolution up to a maximum of 20 kilometres (the N-S width of the dataset for faults that predominantly strike N-S - see Section 3). The interaction of faults at different scales within the 3D data therefore provides an as yet unexplored set of evidence in understanding the mechanisms of continental break-up at the Galicia margin. Isopach mapping and a simplified version of displacement backstripping have been used in data for the 3D Galicia dataset and are presented in Section 5.2 and Chapter 6.

2.8.5 Rift evolution

Continued extension of the continental crust results in the development of a rift. From the previous section(s) it is clear that as faults develop and grow a network of parallel laterally extensive, large offset faults form the edges of these rifts. Seismic imaging and well drilling undertaken during hydrocarbon exploration of the North Sea basin has resulted in extensive datasets. These data have been utilised to study the evolution of rift basins (Cowie et al., 2005). Rifts are seen to evolve by focusing strain at the rift axis; this strain being accommodated in the upper brittle crust by faulting: initially faulting is distributed across the rift, however, as the rift evolves, extension becomes localised, with faults in the rift axis undergoing greater displacement. This localisation is explained by coupling of the upper and lower crust with increased geothermal gradient of the lithosphere due to thinning resulting in lower crustal plastic deformation. Of interest here is that the evolution rifts tend to localise (focus) to the rift centre (see also Reston and McDermott, 2014), whereas the migrating fault models of break-up suggest that deformation predominantly migrates taking successive slices off the rift hanging wall.

2.9 Discussion

The purpose of this preliminary discussion is two-fold: first, to summarise the observations of the late stages of rifting and continental break-up at magma poor continental margins, and second to highlight the key areas of uncertainty. This latter purpose will require an analysis

of possibly conflicting mechanisms and models that have been presented. From this analysis a number of key questions will be raised, which the interpretation and analysis of the Galicia 3D seismic dataset may help resolve. The presence of large offset structures including break-away faults linking to a possible detachment structure (e.g. the S Reflector) that have been both imaged (e.g. Reston et al., 2007b; Ranero and Pérez-Gussinyé, 2010; Peron-Pinvidic and Manatschal, 2009; Sutra et al., 2013) and modelled (e.g. Lavier and Manatschal, 2006; Brune et al., 2014) suggest that late stages of rifting and break-up have an element of simple shear and that deformation in the upper crust, lower crust and eventually the upper mantle become coupled. This in turn suggests embrittlement of the lower crust and the upper mantle (Pérez-Gussinyé and Reston, 2001). Such brittle behaviour is relative to the strain rate of the extension and the rheology of the upper lithosphere (continental crust and upper mantle) at elevated temperatures associated with rifting: if the strain rate is higher than that possible due to plastic deformation, then brittle faulting will ensue. The coupling of the various depths within the lithosphere is recognised due to cooling and thinning, however the exact nature of the coupling, and the geometries it forms in 3D, are less clear. Slow rifting may result in sufficient time for heat loss to produce embrittlement despite the influence of any asthenospheric upwelling resulting from initial pure shear rifting and continued extension and thinning.

Coupling can also be invoked where extension in the more plastic lower crust has resulted in this plastic layer being so thinned as to be negligible (Lavier and Manatschal, 2006), leaving only upper brittle portions of the crust and brittle mantle. This however does not take onto account the embrittlement of the lower crust (Pérez-Gussinyé and Reston, 2001). Furthermore, attenuation of a plastic lower crust also suggests an element of depth-dependent thinning and results in a space problem when a whole margin is considered, as this lower crustal material must go somewhere. This is the main problem associated with the depth dependent thinning models of late stage rifting. Increased heat flow in the centre of an established rift has been postulated to result in a higher isotherm that effectively couples upper crustal brittle processes and plastic processes into a localised zone of deformation for which the rheological regime varies over time. Earlier stages of rifting within a basin are seen to move from a period of dispersed deformation

that over the duration of the rift period localises toward the rift axis (Cowie 2005). If this axis were to continue then localisation due to thermal weakening would reinforce coupling of deformation within the lithosphere. Despite the mechanism of formation of this localised coupling zone or structure, it is apparent from observations from different sources: seismic, field and numerical modelling that they play a key role in late stage extension and final breakup

The representation of these coupling structures in the upper crust at the thinned edge of continental margins that are possible to image seismically provides, possibly, the best way to understand their role in continental break-up at the scale of the whole margin (10-100's km). Numerical modelling may constrain what is physically plausible and suggest idealised patterns of structures. In addition, plate tectonic reconstructions can give the whole margin scale spatial and temporal constraints but contribute little to the mechanisms of break-up, other than maybe variations in rate over million-year timescales (Brune et al., 2016). Field analogues enable observations at the millimetre to kilometre scale that can elucidate how structure may physically interact. Three main mechanism will be considered here: polyphase faulting, sequential faulting and the rolling hinge. The possibility of gravitational collapse is not considered as a primary mechanism as no compressional component is seen in what would be the equivalent to toe thrusts seen in large submarine slides. Furthermore, the gravitational collapse to occur there needs to be sufficient accommodation space for the collapsed material to move into – which in itself requires that an element of tectonic breakup had already occurred.

Sequential faulting and the rolling hinge model both require that, as the continental crust hyperextends, brittle normal faults carve consecutive slices from the hanging wall of a fault cutting through the continental crust to the mantle. In the rolling hinge model, the location of the faults 'root', remains a common point, in the sequential faulting model the root migrates underneath the hanging wall. Both models require upwelling of the asthenosphere to fill in the space resulting from the thinning of the continental crust. Both models require that the faults form, dipping toward the rift axis, at a relatively high angle 50-60° and then rotates to shallower angles of c.25-45°. In the rolling hinge model, this rotation is due to flexural unloading of the footwall and can be quite large as the elastic thickness of the plate is reduced due to previous thinning

(extension) of the continental crust and mantle lithosphere. In the sequential faulting model, this rotation of the faults is based geometrically on the angles based on the extension factor and the preservation of area, with no real reference (directly) to any flexural or isostatic mechanism. Furthermore the model has a requirement that each fault forms sequentially oceanward without a change in mechanism and with no 'fixed hinge' rather the locus of faulting migrates and therefore differs from the rolling hinge mechanism. Neither the rolling hinge model or the sequential faulting require movement on a low angle detachment.

In terms of interacting faults systems, a 3D study of fault displacements has never been undertaken on a hyperextended margin and this study will highlight how faults interact both along strike, perpendicular to strike and also in the down dip direction; whilst also being underlain by a possible detachment fault. Taking the idea of fault growth into the hyperextended zone may shed new light onto the applicability of current models.

Chapter 3

Methodologies

3.1 The seismic dataset: acquisition and processing

The location of the seismic dataset used in this work is shown in Figures 1.2 and 1.7. The seismic data were collected in 2013 with the RV Marcus Langseth, towing two 3300 cubic inches tuned airgun arrays, firing alternately every 50 m (Figure 3.1). The data were received by 4 digital hydrophone streamers, each 6 km in length, containing 480 channels and towed 200 m apart, producing a 68.5 km x 20 km volume down to 14 s TWT with a nominal inline spacing of 6.25 m and a cross-line spacing of 50 m (Figure 3.2). Seismic processing (Yilmaz, 2001) was carried out commercially by the hydrocarbon service company Repsol. Processing consisted of editing, despiking and low cut filtering, wavelet shaping including zero phase conversion, multiple suppression (surface related multiple elimination and radon demultiple), static correction to correct for variation in water velocity (Krahmann et al., 2008) during the experiment, offset plane Fourier regularisation and binning to 12.5 m inline and 25 m crossline spacing, 3D pre-stack time migration after tomographic and residual moveout velocity analysis, and bandpass filtering (Yilmaz, 2001). Amplitude-preserved data, i.e. without any automatic gain control, were used in all interpretation undertaken for this work. This aspect is of importance as the preserved amplitudes were used in attribute analysis for some of the interpreted horizons (see

Sections 4.1.1 and 4.2.4)

The data consists of 800 (numbered from south to north from 70 to 870) in-lines and 5500 cross lines (numbered from west to east from 7000 to 12500). Only every other cross line was included in the data. The data line spacing therefore was effectively a 25 x 25 m grid. The in-lines represent acquisition sail lines and are orientated a few degrees anticlockwise of due east-west. The (almost east-west) sail lines were selected to be perpendicular to the continental margin and is therefore considered to be the tectonic transport direction during rifting, this orientation is also parallel to the transform faults on the Mid-Atlantic Ridge (Figure 1.2). Previous 2D lines (Sutra and Manatschal, 2012; Ranero and Pérez-Gussinyé, 2010; Reston, 2007a) have also shown that the main faults on the margin have a significant dip to the west supporting the interpretation of east-west extension. However, given the nature of 2D seismic surveys the actual tectonic transport direction was unknown as was its development temporally and spatially.

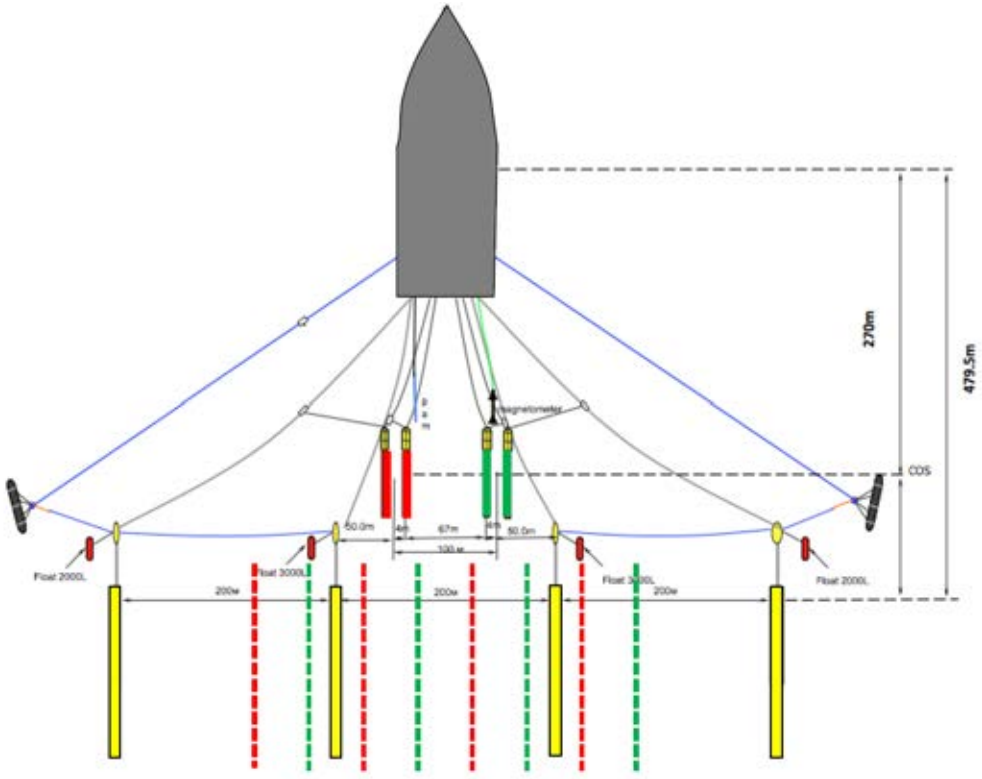

Figure 3.1: *The deployment of the instruments used to acquire the Galicia 3D dataset.*

Table 3.1: *Table showing the latitude and longitude of the Galicia 3D multichannel seismic data volume.*

	Lattitude (degrees N)	Longitude (degrees W)
northwest corner	42.18119	12.985384
northeast corner	42.01281	12.150003
southeast corner	42.00117	12.979664
soutwest corner	42.19279	12.153368

Figure 3.3 shows the corner coordinates of the 3D volume's bounding box in Universal Trans Mercator Projection (UTM). The latitude and longitude of the dataset are presented in Table 3.1. The slightly inclined red box is the the survey area, and the red numbers indicate the inline and cross line numbers; the inclined box marking the data volume will be used throughout this work to provide location information. The tectonic setting of the data volume is shown in Figure 1.15. The trace of lines 700 and 370 (Section 4.1.2) are also shown. Table 3.1 shows the latitude and longitude coordinates of the four corner of the data volume.

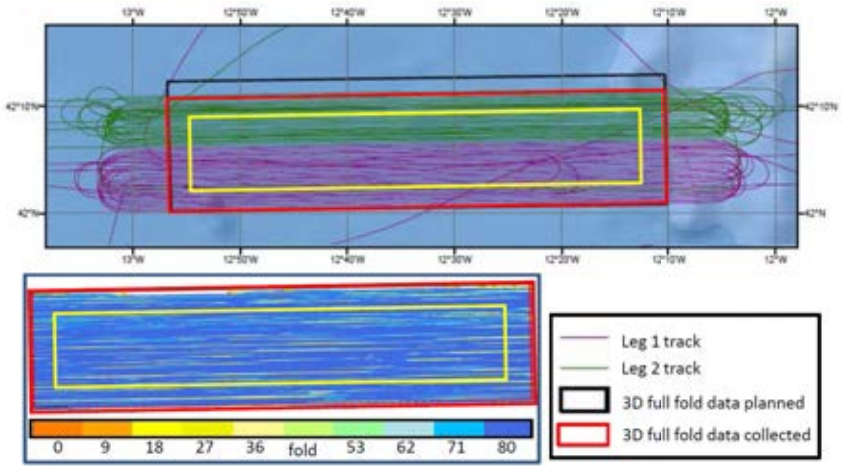

Figure 3.2: *The sail lines used to acquire the 3D Galicia dataset. The green sail lines were acquired after the RV Marcus Langseth returned to port to replace a broken engine*

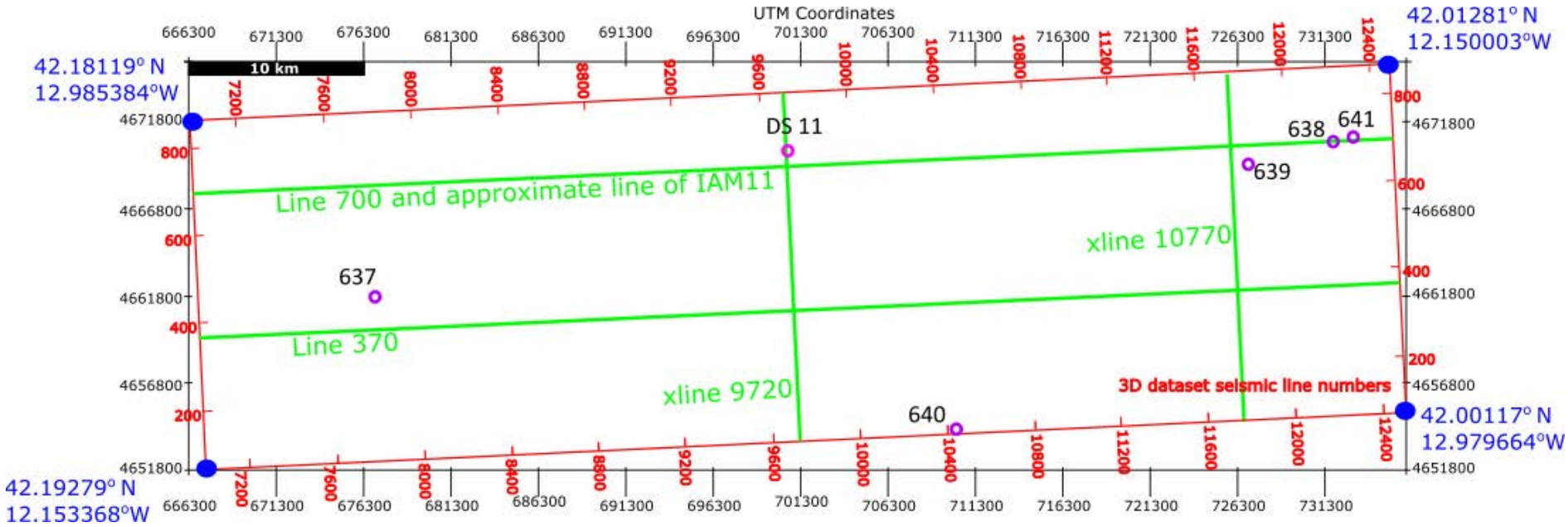

Figure 3.3: *Location of seismic lines (red), corresponding UTM grid (black) and latitude and longitude of the corners (blue) for the dataset. Lines 370 and 700 are shown in Figure 4.1, crosslines (xlines) 9720 and 10770 are shown in Figures 4.2 and 4.3 respectively. Pink circles show numbered ODP Leg 103 drill sites, DS 11 is dive site 11 (Boillot, Comas, et al., 1988)*

3.2 Seismic interpretation

Bacon et al. (2007) provides a thorough introduction to 3D seismic interpretation. All Interpretation in this work was undertaken using a petroleum industry standard package IHS Kingdom Suite software (version 8.1). Works-flows used were taken from the software training manual.

3.2.1 Horizon picking

Rationale for picked horizons

A number of structural horizons were considered important interpretation targets in addition to the sea floor, which acts as an upper bound to any geological interpretation. The seismic data do not benefit from significant well data and the stratigraphy extends deep within each fault block and cannot therefore be correlated beyond the tops of each block any the interpretation presented here does not use the known stratigraphic horizons. Given the nature of the dataset and the desire to understand the mechanism of continental break-up, three key horizons were considered essential interpretation targets:

- the S Reflector, given its possible role as a detachment structure and in possible mantle serpentinisation (Section 2.2),
- base post-rift (top of the syn-kinematic sedimentary sequences) by definition is a surface below which sediments that were deposited have been deformed by movement associated with extension and break-up of the crust, and
- the acoustic basement, that is known from drilling to be granodioritic or rhyolitic in composition and forms the core of the tilted blocks seen on the margin (Section 1.3.3).

In addition to the essential targets listed above, to fully understand the mechanisms of break up the interrelationships of a number of syn kinematic horizons was also considered important. The nature, geometry and relative timing of these syn-kinematic sequences would provide evidence of tectonic history. In addition, syn kinematic horizons would provide important markers if any structural restoration was to be undertaken.

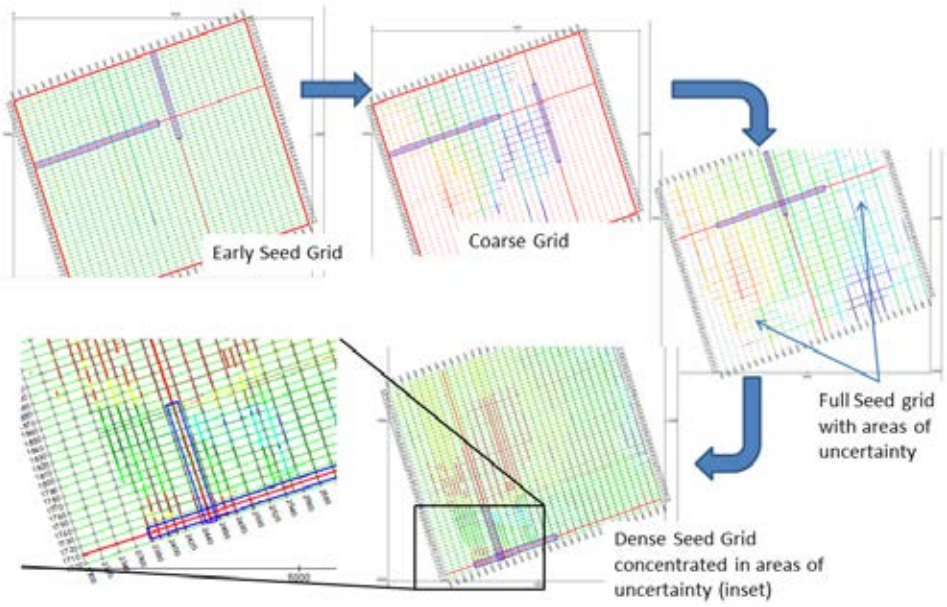

Figure 3.4: *An example of tying the loop during seismic interpretation to produce a 'seed pick' ready for auto-picking or interpolation*

Horizon picking methodology

A common method of picking geological horizons in a 3D dataset (or 2D grid) is by 'tying the loop': picking one's target horizon on a seismic line and then using perpendicular lines to create a 'seed pick' that can then be used to autopick or, less commonly interpolate, between the picked lines (see Figure 3.4 for an example). Interpretation of horizons within the Galicia 3D dataset was undertaken using this method. However the strucutural complexity of many of the horizons at the hyperextended margin meant that 5 x 10 (inline x cross line) seed pick was used (125 x 125 m). However, the requirement of detailed and accurate picking for the heavily deformed (faulted and folded) syn-kinematic sediments meant that horizons were sometimes followed line by line (25 metres on both in lines and cross lines) to ensure interpretation across faults was as constrained as possible given that the data had such good resolution.

All horizons were primarily picked on seismic lines (in and cross) using the 'F' function in Kingdom Suite which snaps to the seismic wavelet within the data. The picking can follow peak,

trough, or zero phase parts of the wavelet, although zero phase was not used for any horizon. Although Kingdom Suite has the function to auto pick horizons on individual seismic images, the nature of the surfaces of interest made this inappropriate as most of the horizons were either complex in nature (parts of the S reflector, top acoustic basement) or unconformities (base post rift, intra syn-rift, intra post-rift). Interpolation of the horizon seed picks allowed 3D surfaces to be generated using the 3D Seeker tool, which, uses the wavelets of the picked horizons to hunt through the 3D volume and auto-picks similar wavelets. In order to provide complete 3D surfaces, horizons were picked along faults, rather than terminating at them in order to provide footwall and hanging wall cut offs. This proved useful in obtaining a true geometry of the fault by snapping to the wavelet, which for many faults was a positive reflector, and not just interpreted based on reflector terminations. The horizons picked in this study are provided in Table 3.2.

3.2.2 Fault picking

The main thrust of this work is that understanding complex faulting provides a method with which to understand the final breakup of continental crust. It was therefore important to capture as many of the faults as possible so where a fault showed a degree of lateral continuity within the 3D data they were picked, essentially this resulted in faults being picked if they had a length of over approximately 125 metres (15 inlines). Initially the main block bounding faults were interpreted followed by small intra-block faults.

As with horizons, faults were picked every 5 inlines as often the path of the fault was either relatively clear as it showed clear offset of a horizon or other consistent reflector. Picking on cross lines was more limited, as the tectonic transport direction is approximately E-W faults were difficult on the N-S cross lines. Faults solely within the acoustic basement were not so clear and are generally less constrained. The use of arbitrary seismic lines across the data were useful in understanding fault geometries. Given the complex pattern of faulting seen in the hyperextended margin, being able to view seismic images in any orientation was important to understanding the cross cutting relationships of the faults.

Table 3.2: *Interpreted horizons presented or utilised in this study*

Horizon name	**Use within thesis**	**Section cross references**
S Reflector	Structural Analysis Depth Conversion	4.2.4
Moho	Structural Analysis, Depth Conversion	NA
Top acoustic basement (TAB)	Structural Analysis Depth Conversion	4.2.3
Top Package A	Structural Analysis Depth Conversion	5
Base post-rift unconformity (BPR)	Structural Analysis Depth Conversion	4.2.1
Post Rift 1	Depth Conversion	NA
Post Rift 2	Depth Conversion	NA
syn-rift - Block 4 B4 - 1.5, 2.0, 3.0, 6.0, 7.0	Fault movements	5
syn-rift - Block 5 B5 - 0.5, 1.0, 1.2, 1.3	Fault Movements	5

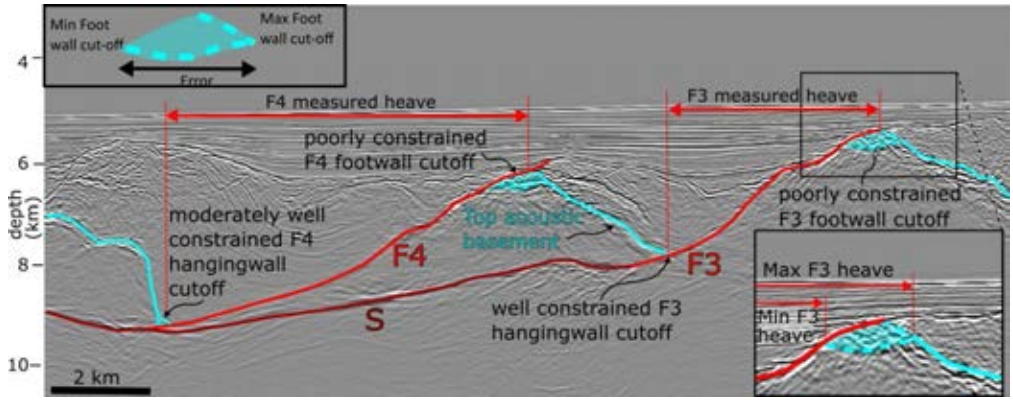

Figure 3.5: *Diagrammatic representation of how the heave errors (min and max) were derived. It is important to recognise that the heave measurements had uncertainty, but the primary measurement (i.e. not the min or max represents the most geologically considered measurement), whereas the min and max represents the geologically possible extremes and as such are much less likely to be realistic, given the high resolution of the 3D.*

In addition to interpreting faults, the heave on these faults has also been measured. As with all measurement there is some uncertainty and the uncertainty (error) on measuring fault heave was, to a large extent, due to picking the fault especially in the footwall as some footwall degradation may have occurred or the may be minor faulting in a 'damage' zone. Figure 3.5 highlights some of the uncertainties (and therefore errors) in determining heave. Heave was measured on surfaces by deleting a portion of the horizon along a particular line and then measuring length (heave) of the missing segment using the ruler in the interpretation software. Figure 3.6 shows the method used within Kingdom Suite to measure heaves. The precision of the actual measuring is to within a few metres, much better than error based on interpreting hanging wall and footwall cut-offs. This rigorous picking of faults has led to a comprehensive fault network in the central portion of the seismic dataset. This fault network, given the resolution of the dataset and fine spatial scale on which the faults have been interpreted provides unique data over an hyperextended margin.

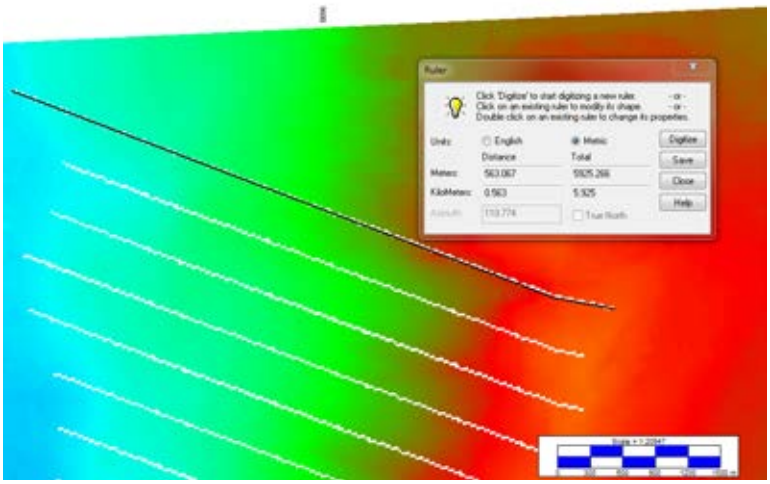

Figure 3.6: *Map view of an horizon showing the method used for measuring heave using in-built ruler in Kingdom software. White lines are fault heaves, measured heave is black line, window shows measured length and level of precision can be determined*

Horizon attributes

Kingdom Suite software provides numerous tools with which to interrogate the seismic attributes of interpreted horizons. The amplitude of the trace envelope function (amplitude) provides an important tool in understanding the nature of horizons and the interaction of the geophysical properties of the rocks that are juxtaposed either side of the horizon (Figure 3.7). The amplitude map that produced by using the attribute therefore provides the detail of the relative amount of energy that is reflected from an interpreted surface. A similar method is the root mean squared (RMS) amplitude which works on a volume of seismic data on a window about the target horizon. Further attributes were trialled in order to reveal aspects of the dataset. These included similarity (coherence) to assess the presence of faults particularly in the basement, however the results did not provide any more information than seen in the amplitude data. similarity, dip and maximum curvature were investigated on the S horizon; the results did not reveal anything that was not seen in the trace-envelope data.

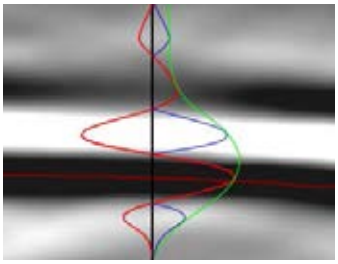

Figure 3.7: *Trace Envelope Function - negative parts of a seismic trace (red) are 'flipped' to the positive side (green) - an envelope curve is then fitted to encompass both curves on the positive side (Taner et al., 1979; Barnes, 2007)*

Time to depth conversion

The time migrated dataset has also been depth converted to produce a depth version of the 3D volume. Depth conversion used the results of initial interpretations of the key structural horizons (Section 4) an horizon within the syn-rift (Section 4.2.2) and two horizons within the post rift. The horizons were used to build a velocity model with which to undertake a time-depth conversion. The horizons used in the velocity model were: Sea floor, Intra-post-rift, base post-rift, intra syn-rift, top acoustic basement and top mantle. The top mantle horizon consisted of a fusion of a number of interpreted surfaces: the S detachment, the Moho interpreted beneath the continental crust to the east of the breakaway faults, and the interpreted exhumed mantle that form the Peridotite Ridge in the west of the data volume. The horizons are used to separate the seismic data into a distinct number of packages that are then assigned a velocity. Figure 3.8 shows the various packages and Table 3.3 shows the relationship between surfaces and velocity packages.

In order to undertake the depth conversion, the horizons used to provide the upper and lower boundaries of the velocity packages have to be present throughout the volume. This adds added layer of complexity as the heavily faulted nature of the hyperextended crust means that in places the different horizons have the same interpretation, i.e., the different horizons occupy the same 3D space. For example where a fault cuts more than one horizon in the the fault forms part of the surface of two horizons. In order to provide a clear configuration of the horizons

in the velocity model, a basic mathematical function was used to ensure that structurally lower horizons always appeared lower in the velocity model, and that where appropriate, horizons shared the same interpretation in 3D space. This mathematical functions merges surfaces based on their maximum or minimum depth (in time). For example on top of the tilted block in Figure 3.8 the top of the dark green package is also the same as the top of the light green package. Both horizons were seed picked and the auto-picked, but this left two surfaces that were inter woven over the crest of the block. To ensure a single surface for the velocity model a merge maximum function was used so that over the crest of the block both surfaces used the pick for the horizon at the top of the dark green package. Before carrying out the time to depth conversion the horizons are smoothed.

The interval velocities used were based on knowledge of rocks based on the results of four drilling survey contained within the areal extent of the dataset. This meant that we could assign a lithology for the basement and also recognised that the sediments were mixed clastic and carbonate mud (marl) sequences . Common seismic velocities based on these rock types and burial depths were then assigned to each velocity interval (Table 3.3) each interval being between two interpreted horizons. These velocities were then validated using the wide-angle survey data collected using ocean-bottom seismometers that were deployed as part of the data acquisition programme. These wide angle data were processed to provide 3D tomographic and 2D full wave form inversion models of the 3D seismic data volume (Davy et al., 2017; Bayrakci et al., 2016). Figure 3.9 shows the velocity model of Davy *ibid.* along line 420 (c.f Figure 3.8), this image was therefore used to ensure that velocities assigned to each interval (Table 3.3 and Figure 3.8) were the same/similar to those obtained by the detailed geophysical investigations of Davy et al. (2017). As the Galicia dataset is a 3D volume it was possible to use cross lines and arbitrary lines to intersect line 420 to enhance the confidence that that the 3D velocity model used for the time to depth conversion was valid and correlated with that produced by Davy et al. (2017).

The resultant seismic images obtained from the time-depth conversion process compare favourably with those produced by 2D pre-stack depth migration (Ranero and Pérez-Gussinyé, 2010) therefore validating the simplified method used in the depth conversion (Figure 3.10).

Table 3.3: *Table showing relationship between interpreted horizons and the velocities used for different packages in the seismic data see also Figure 3.8.*

Horizon	Velocity package	Velocity (m/s)
	Sea	1500
Seafloor	———————-	————————
	Late post-rift	2200
Post rift 1	———————-	————————
	Early post-rift	3000
Base-post rift	———————-	————————
	Late syn-rift	3750
Top Package A	———————-	————————
	Early syn-rift	4450
Top Acoustic basement	———————-	———————-
	Acoustic basement	5500
S Reflector/mantle	———————-	————————
	Mantle	6000

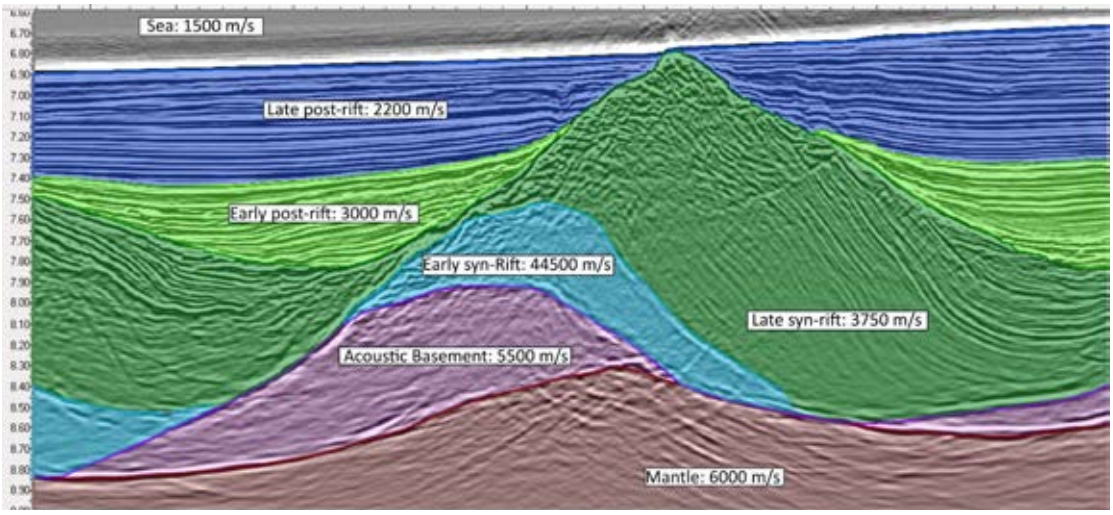

Figure 3.8: *Seismic section (part of line 420) showing velocities used in the time to depth conversion. Velocities were validated with Figure 3.9.*

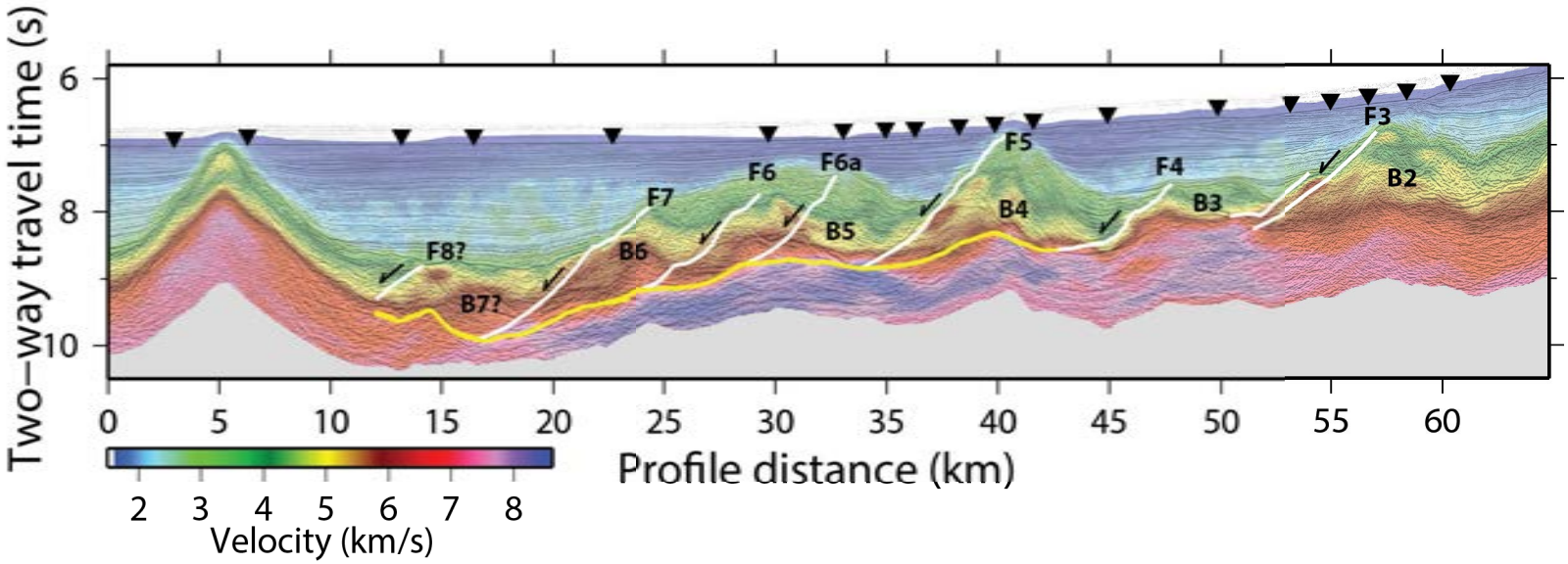

Figure 3.9: *Full wave form Inversion Velocity model on line 420 used to validate depth conversion (Davy et al., 2017, Figure 14B-01)*

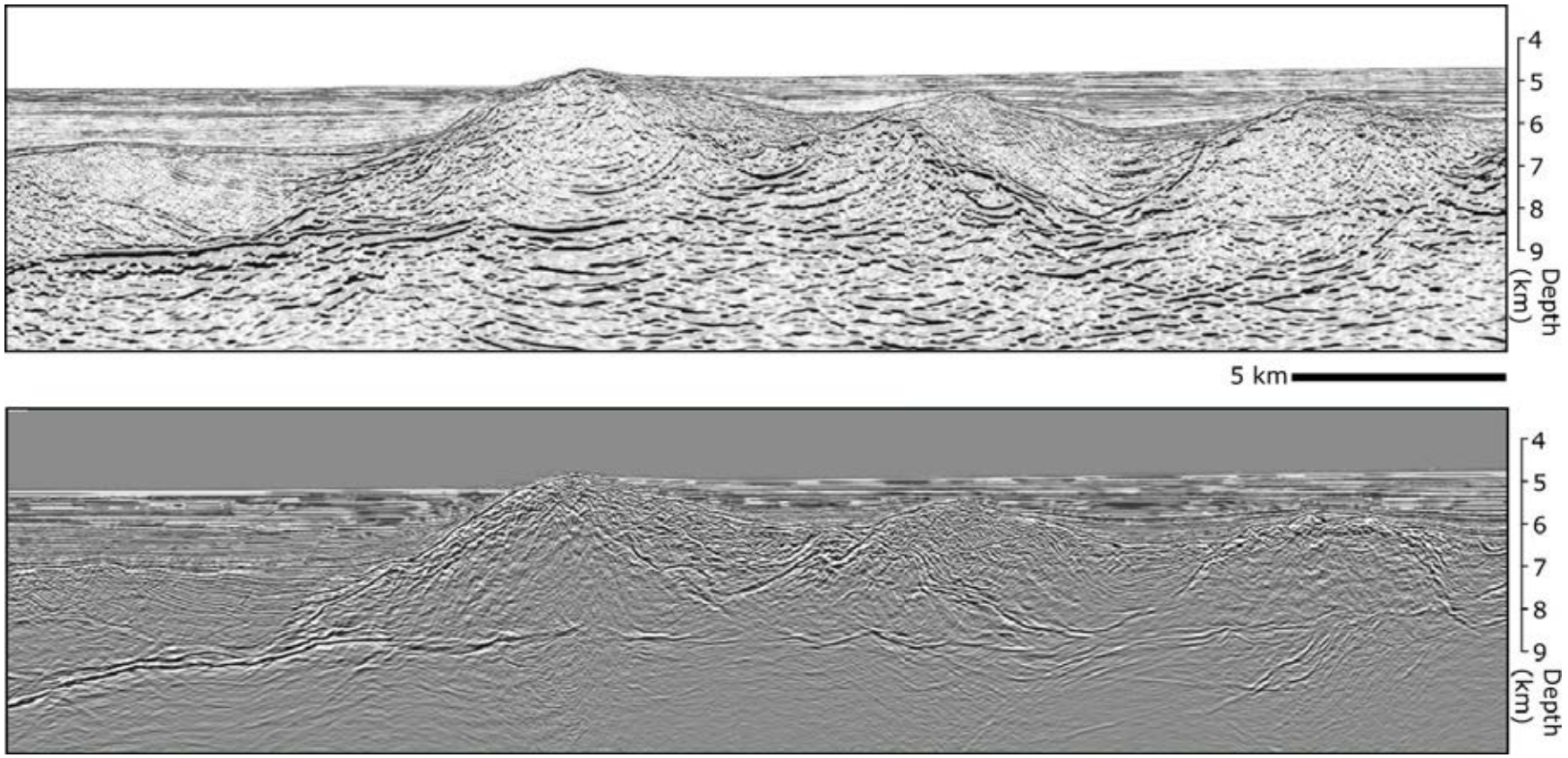

Figure 3.10: *Comparison of 2D pre-stack depth migrated vertical seismic section (IAM11, top) with the corresponding depth converted section from the 3D dataset (bottom)*

3.3 Restoration

An arbitrary line seismic section was exported from Kingdom Suite and imported into Midland Valley's Move™ software in order to undertake a 2D seismic section restoration. Interpretation of faults and horizons withing Kingdom Suite were used to build a model within Move™ ready for reconstruction. The model used the main blocks bounding faults in addition to key structural surfaces. The aim of the restoration was two-fold. First to assess if the various fault blocks that had been interpreted could be re-assembled (in two dimensions) to a relatively consistent thickness of crust. Second, to ascertain if by undertaking the restoration any further evidence could be obtained for the mechanism of continental break-up.

Move™ manipulates lines and surfaces based on a range of geologically derived algorithms. Move™ also uses polygons on the seismic image to move and where necessary transform the geometry of the seismic image. These polygons form discrete packages of the seismic image that are bounded by an upper and lower horizon and where appropriate (which is almost everywhere in the hyperextended Galicia margin) faults. Due to the hyperextended margin and the focus of this study on the sin-rift, the validation of restoration models via line length was less applicable than other simpler restorations. The initial part of the restoration involved backstripping and decompaction (Sclater and Christie, 1980) of the overlying sediments and was undertaken in order to provide geometries present prior to deposition of the post-rift sediments. Backstripping was undertaken with adjustment for Airy isostacy, with flexural isostacy considered to be more suitable to regional scale studies (Watts, 2001).

Two restoration techniques were used in this work: block restoration and move-on-fault. Block restoration treats each fault block as a coherent rigid unit enabling 'jigsaw fitting' of the various blocks. Move-on-fault restoration transposes fault blocks along faults using geologically constrained algorithms. In this process it is possible to internally deform the hanging wall block. Within this work the *fault parallel flow* method (Egan et al., 1997; Kane et al., 1997) was used as it is considered suitable for more complex fault geometries. Unfortunately, deformation of the hanging wall cannot be accommodated. However, an additional step used in restoration was the

translational tool 'unfolding' (in this work however the tool was used to fold). Certain portion of the restoration were folded in order to recreate the rolling hinge model. This method was used in an attempt to mimic footwall deformation.

Chapter 4

3D Seismic Interpretation of the Galicia Margin: Observation and Analysis

The 3D seismic reflection data used in this study provide images of the thinned crust of the Galicia margin vastly superior to previous 2D surveys. They provide a clarity of imaging previously unseen from 2D datasets of the Galician margin, or elsewhere over such thinned continental crust. This exceptional imaging allows for a high confidence of interpretation. The structure of the Galicia margin revealed by the data is in both two-way travel time data and in depth-converted data (Section 3.2.2) based on initial two-way travel time interpretations. The geometries seen in the depth-converted data are considered to be more geologically accurate interpretations as the influence of vertical and horizontal velocity variations associated with the complex structures are diminished compared to geometries seen in two-way travel time data. It is therefore these depth-converted data in conjunction with time data that are used to provide the detailed analysis provided in Section 4.2.

4.1 General structure of the Galicia margin

The following section briefly outlines the general structure of the margin seen within the data: the distribution of crustal blocks, the block bounding faults and the associated half-grabens and mini-basins and their sedimentary fill. The description of this general structure uses four interpreted horizons in conjunction with example seismic sections.

4.1.1 Galician margin structure in two-way travel time

Viewing inline seismic sections approximately parallel to the expected tectonic transport direction (i.e. perpendicular to the coast and the Mid-Atlantic Ridge and parallel to the closest ocean transform faults, albeit they are a long way offshore, see Figure 1.2) reveals the general structure of the margin (Figure 4.1). As with previous 2D studies of the Galicia margin, the thinned continental crust, seen within the 3D volume consists of a number of rotated crustal blocks above a strong, often sub-horizontal, reflector termed the 'S' (Section 1.3 and Figure 4.1).

The crustal blocks defined in these data are separated by faults that dip oceanward and are seen to connect with the S reflector, but do not significantly offset it. These block bounding (inter-block) faults have been be traced and interpreted along strike (approximately north-south). The crustal blocks shown in Figure 4.1 are composed of a lower, often-wedge-shaped, portion of acoustic basement identified from an upper surface consisting of strong positive reflector with limited reflectivity below this. The top acoustic basement seen on the western flanks of the tilted blocks consists exclusively of fault planes. This basement has been sampled by drilling (Boillot, Winterer and Meyer, 1987; Boillot, Winterer et al., 1988) and by submersible (Boillot, Comas, et al., 1988) and found to be rhyolitic or granodioritic, respectively. In addition this interpretation of acoustic basement has been verified by tomographic full waveform inversion (Bayrakci et al., 2016; Davy et al., 2017). The wedge-shaped nature of the crustal blocks form half-grabens that are infilled with a number of seismic packages interpreted to be pre-rift and syn-rift sediments (see Chapter 5). These sediments are characterised by strong layering that most commonly dips toward the landward block bounding fault. These sedimentary sequences

are faulted by intra-block faults and are also gently folded. The geometry of the crustal blocks and structures within the pre-rift and syn-rift sediments suggests that tilting of the crustal blocks was controlled by the block-bounding normal faults, with the offset on these faults being in the order of a few (c. 5) kilometres (see Section 6.1 for an analysis of fault displacements).

Above the rotated crustal blocks, composed of basement, pre-rift and syn-rift sediments, is a strong unconformity that has significant topography. Filling in this topography and onlapping onto the unconformity are sequences of relatively undeformed, approximately layer cake strata that are interpreted to consist of post-rift sediments. The unconformity beneath these post-rift sediments has been termed the base of the 'base post-rift unconformity' and marks the top of syn-kinematic sediments associated with the local faulting within each fault block. The base post-rift unconformity surface is considered to be diachronous, i.e., of different ages between different half-grabens (see Figure 4.1). This diachronistic nature is supported by the onlapping sediments and is also derived from drilling on the margin (see Section 1.3.3). In the west is a N-S trending ridge that has been drilled and shown to be serpentinised peridotite of sub-continental mantle origin, (Boillot, Winterer et al., 1988).

Viewing crosslines through the 3D data highlights the lateral variation of deformation and across the crustal blocks (Figure 4.2) whilst also emphasising the lateral continuity of half-graben sediments (Figure 4.3).

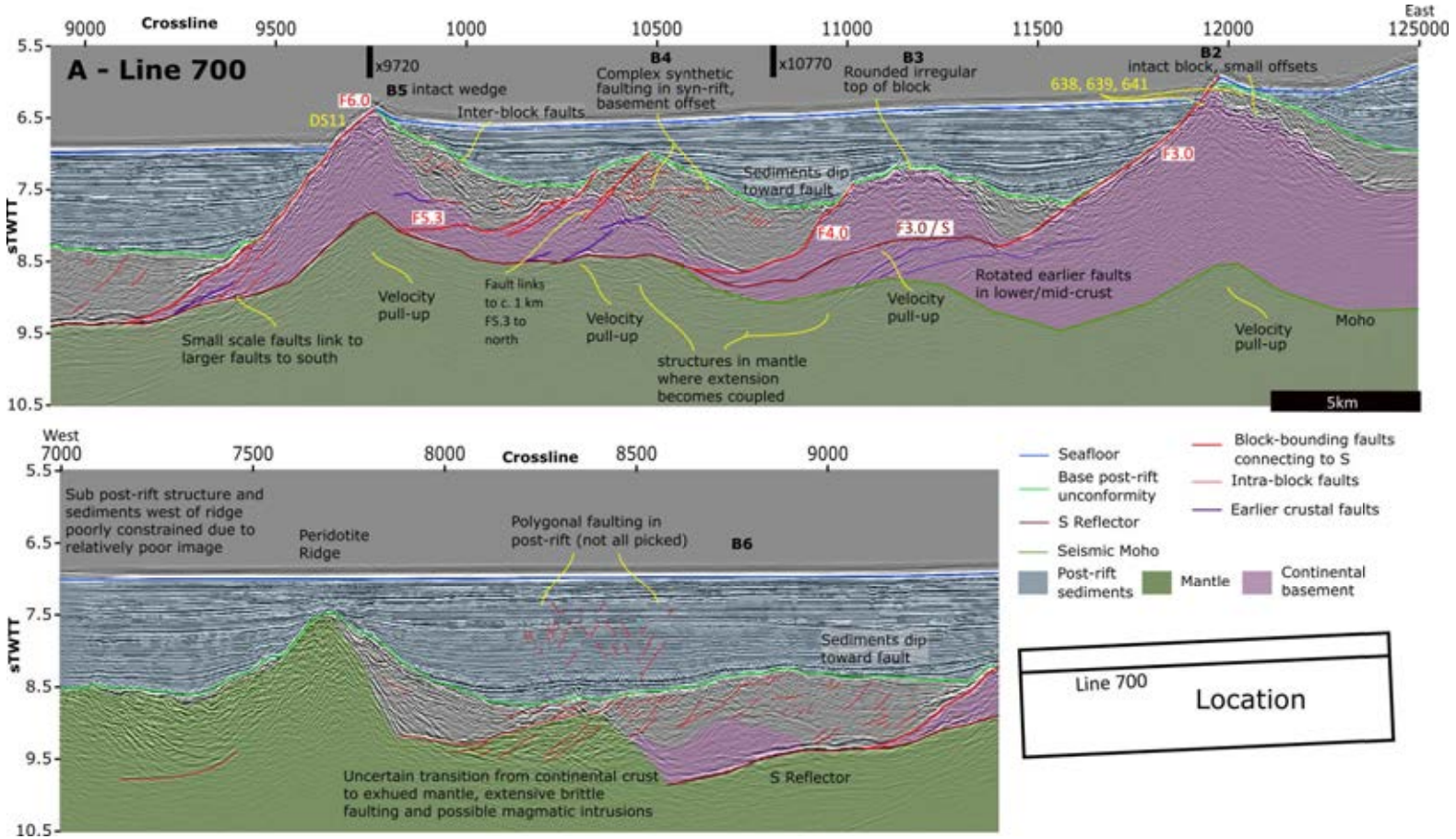
A - Line 700
Crossline
East
West
sTWTT
x9720
x10770
B5 intact wedge
B4
Complex synthetic faulting in syn-rift, basement offset
B3
Rounded irregular top of block
B2
intact block, small offsets
638, 639, 641
F6.0
D511
Inter-block faults
F5.3
F4.0
F3.0 / S
F3.0
Sediments dip toward fault
Velocity pull-up
Fault links to c. 1 km FS.3 to north
Small scale faults link to larger faults to south
structures in mantle where extension becomes coupled
Rotated earlier faults in lower/mid-crust
Moho
5km
Sub post-rift structure and sediments west of ridge poorly constrained due to relatively poor image
Peridotite Ridge
Polygonal faulting in post-rift (not all picked)
B6
Uncertain transition from continental crust to exhued mantle, extensive brittle faulting and possible magmatic intrusions
S Reflector
Seafloor
Base post-rift unconformity
S Reflector
Seismic Moho
Post-rift sediments
Mantle
Continental basement
Block-bounding faults connecting to S
Intra-block faults
Earlier crustal faults
Line 700
Location

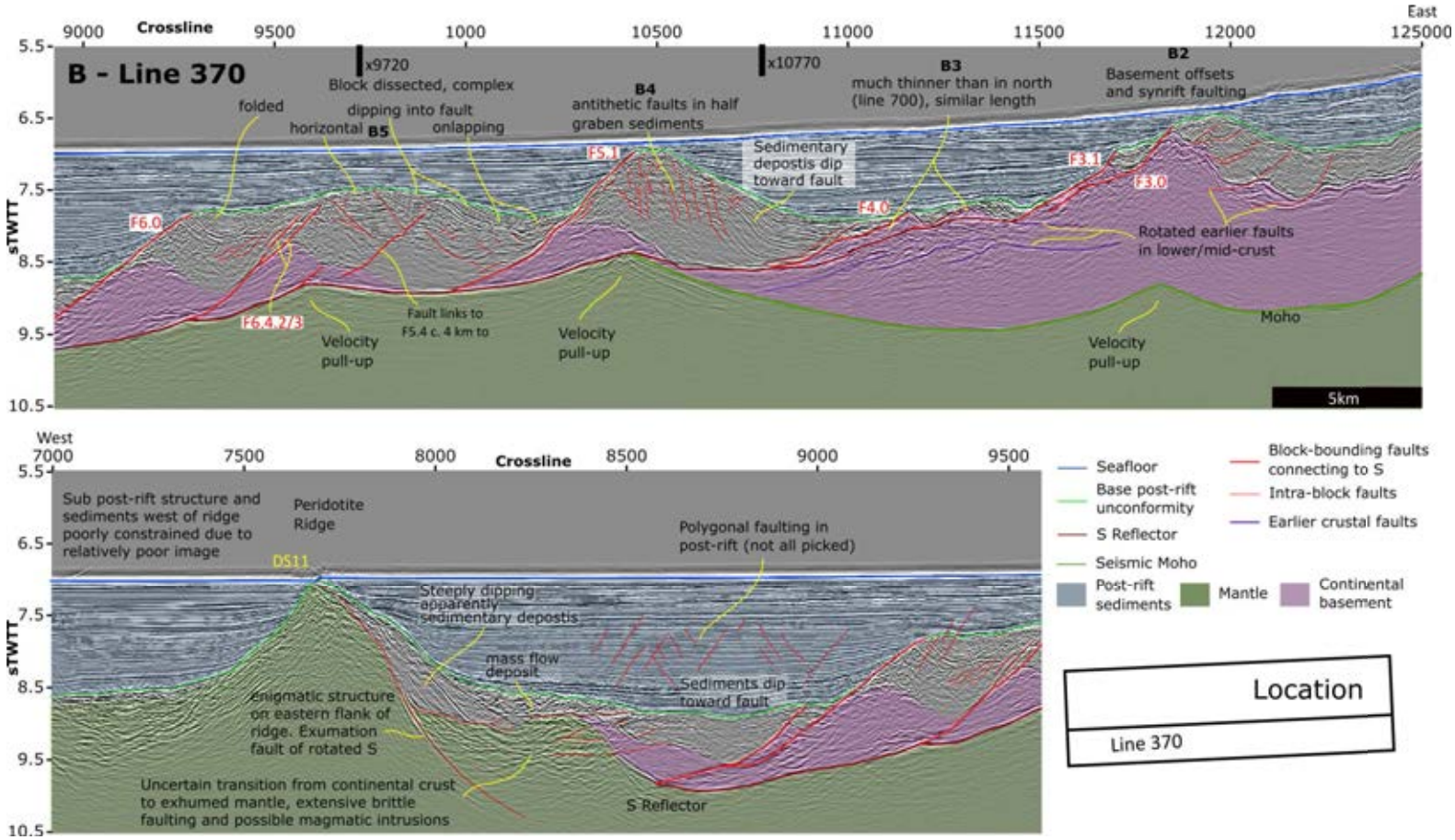

Figure 4.1: *A:**Previous Page:** Line 700 showing main structural elements in the north of the data volume. B: Line 370 showing main structural elements in the south of the data volume. Red numbers give refer to faults and black numbers to blocks, after Ranero and Pérez-Gussinyé (2010). x9720 and x10770 are crosslines 9720 and 10770 shown in Figures 4.2 and 4.3, respectively. Yellow numbers refer to ODP Leg 103 sites. Location map shows position in dataset, see Figure 3.3.*

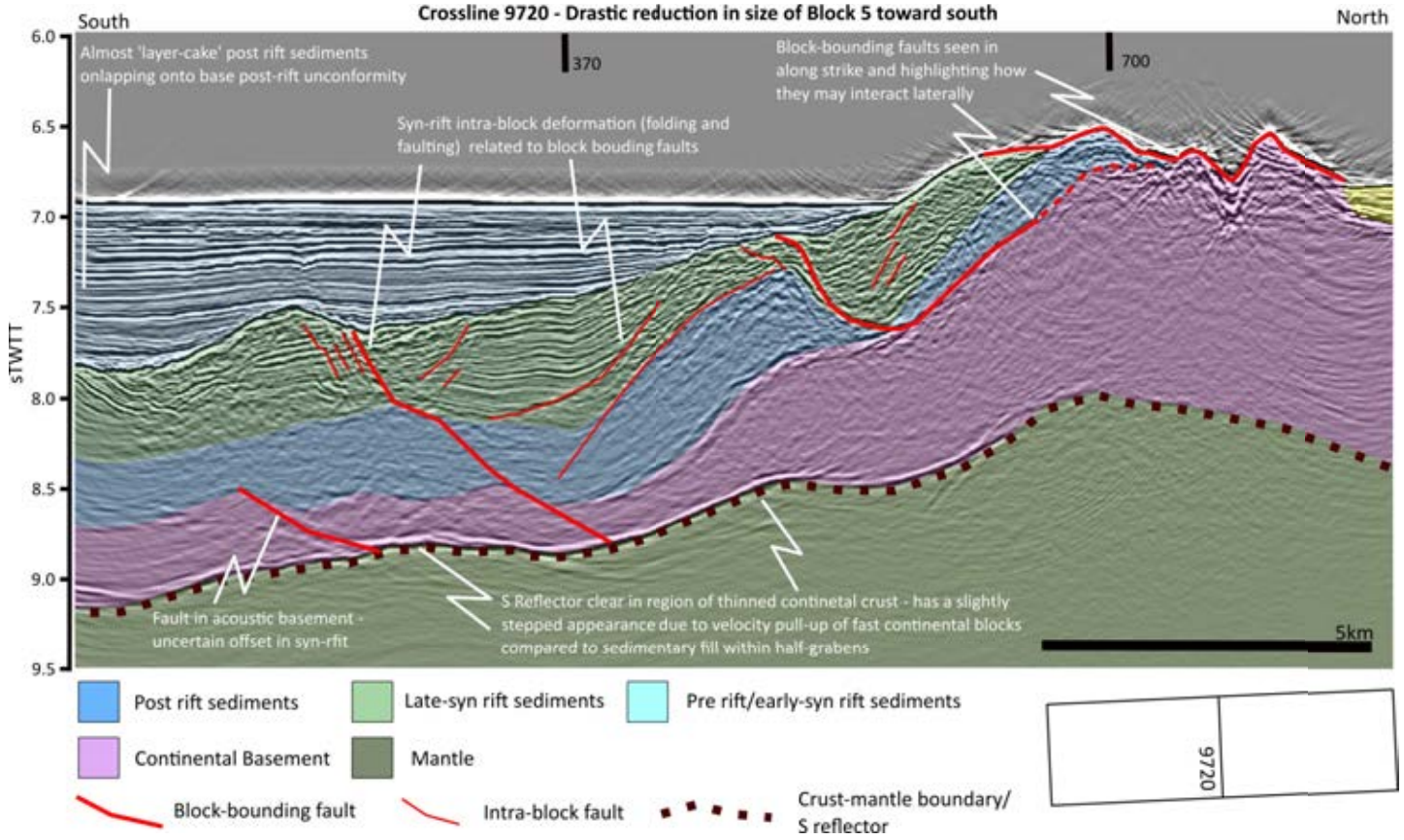

Figure 4.2: *Crossline 9720 showing the large reduction in size of Block 5 to the south. Location map shows position in dataset, see Figure 3.3*

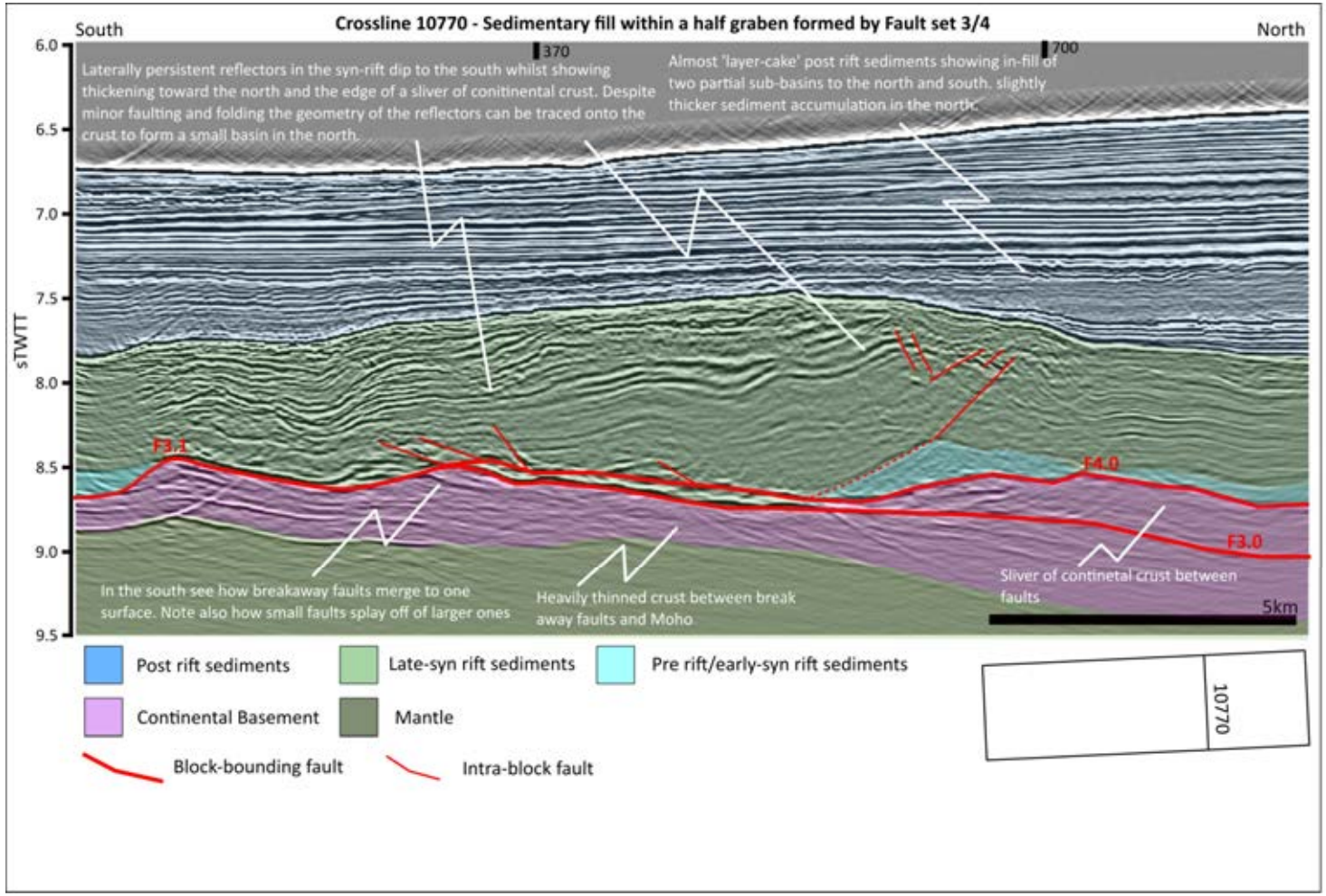

Figure 4.3: *Crossline 10770 showing laterally continuity of the sediments within the half-graben. Location map shows position in dataset, see Figure 3.3*

To fully understand the mechanisms of continental breakup it is necessary to identify and map the key sedimentary and structural horizons to provide evidence of the structural development seen within the 3D volume. The resulting maps display four of the important horizons: Seafloor, base post-rift unconformity, top acoustic basement and the S reflector (see Figure 4.1). A description of the key features of these horizons are presented below; a detailed analysis, especially their relationship with fault network is given in Section 4.2.

Seafloor

The seafloor marks the present-day extent of the sedimentary fill of the basins that resulted from continental rifting and the post tectonic thermal subsidence of the margin. Using the interpreted time structure map of the seafloor (Figure 4.4) alongside seismic images (Figures 4.1, 4.2 and 4.3), it is possible to make a number of important observations on the key structural components within the dataset that are expressed at the present day seafloor. The westernmost edge of the Galicia Bank forms the eastern margin of the dataset and represents continental crust that has been thinned to approximately 10 km. Two ridges which are formed by the tops of two tilted fault blocks formed during breakup are still observed: One (Block 3 - B3) is proximal to the edge of the Galicia Bank and is the site of drilling and/or submersible sample collection (Figures 1.7and 1.3) that confirmed the core of the tilted blocks seen in seismic images is granodiorite or rhyolite and also provided ages for some of the syn-rift sediments (Boillot, Winterer and Meyer, 1987; Boillot, Winterer et al., 1988). The other block (B5) is the northern central area of the study area, and forms a ridge that is not laterally continuous; it forms a feature 5 km long trending north-south. The western flanks of the ridges are formed by fault scarps of intra-block faults (drilled just south of the 3D volume).

A clear channel exists running approximately east-west in the central eastern area of the data volume. This channel is interpreted as being the modern-day sediment delivery system to this part of the continental margin. The channel cuts across the proximal ridge (B3), highlighting that this block must be discontinuous or smaller in vertical extent in its central portion for this sediment delivery channel to be active. Analysis of the seafloor map suggests that the

underlying structure may be more complex than simple N-S trending fault blocks (Ranero and Pérez-Gussinyé, 2010, Figure 1b) based on the bathymetry.

Arguably the predominant feature is the Peridotite Ridge, a prominent peak within the bathymetry, that drilling (ODP Leg 103, site 637) has shown to be exhumed continental mantle (Boillot, Winterer and Meyer, 1987; Boillot, Winterer et al., 1988). The Peridotite Ridge in highest in the south and decreases in size moving northward until it is not seen above the seafloor approximately half way through the data volume.

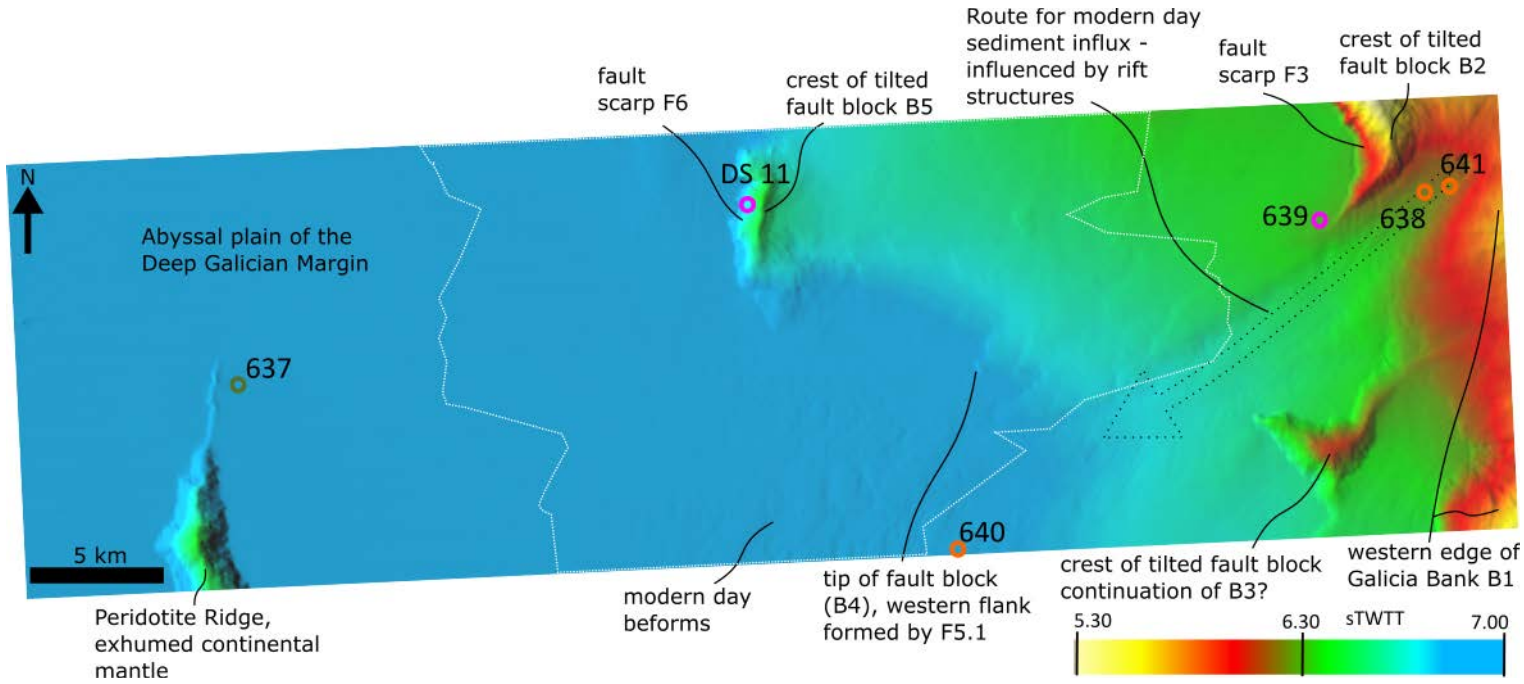

Figure 4.4: *Time structure map of the Seafloor showing a number structural features expressed at the seafloor. White dotted line shows the well constrained S reflector (Section 4.2.4). Numbered circles indicate ODP Leg 103 drilling/dive locations coloured according to lithology: Orange (638,640,641) - sediments; magenta (639) - sediments underlain by rhyolitic basement; olive green (637) - peridotite.*

Base of post-rift unconformity - BPR

The interpreted surface that forms the base of the post-rift sediments is a diachronous unconformity, or series of unconformities (Figure 4.1). Between the sea floor and the BPR are sediments that have a predominantly layer cake seismic stratigraphy and as such are interpreted as being undeformed by tectonic processes that occurred due to the rifting and breakup of the continental crust between Iberia and the Flemish Cap, and as such are interpreted to be post-rift. These post-rift sediments show clear evidence of polygonal faulting (Puttock, 2015) possibly due to dewatering or differential compaction (Figure 4.5). These sediments do, however, show some lateral variation and contain a number of unconformities that may document some of the post tectonic development of the margin. Some of the lower (deeper) unconformities that occur in the proximal portion of the dataset may reveal evidence of tectonic processes that occurred further outboard, although there may be future research potential of these unconformities, they are not considered further here.

Sediments beneath the base post-rift surface are deformed by tectonic processes; it is this change from predominantly undeformed to deformed seismic sequences that mark the BPR surface. The deformation below the BPR consists of a complex interplay of tilting, folding and faulting within three identified packages (A, B and C) which will be discussed in Chapter 5. Previous drilling within the study area would put an age of the BPR surface as Aptian (see Figure 1.8), but the exact age may vary from one location to another due to the migration or focusing of faulting on the margin.

One of the aims of this work is to understand the relative timing of faulting and syn-sedimentary deformation that has captured the break-up of the continent; the base post-rift surface reveals the 3D geometry of these crustal blocks as this breakup occurred. The time structure map of the base post-rift surface (Figure 4.6), alongside seismic sections (Figure 4.1), shows a series of approximately N-S trending blocks, B2-5, numbered after Ranero and Pérez-Gussinyé (2010), moving proximally to distally. Proximally, a discontinuous block (B2) runs north-south. The western flanks of B2 are cuspate faults, meaning that in places the arêtes of the blocks also

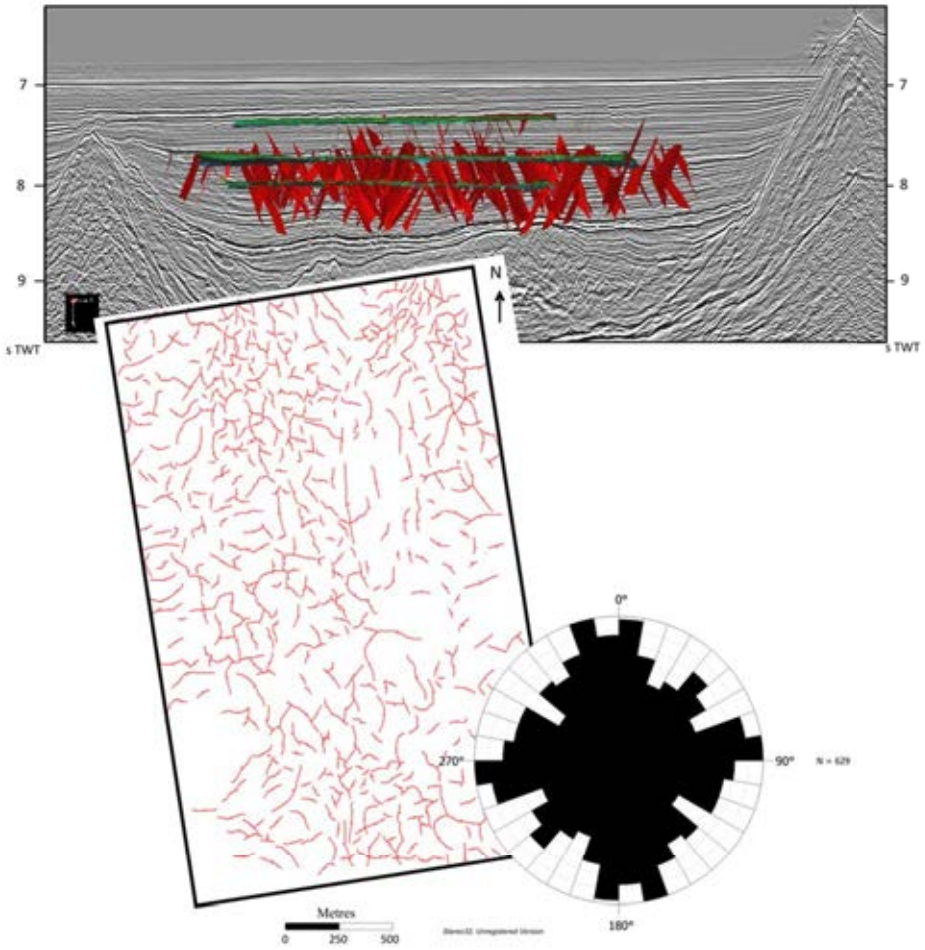

Figure 4.5: *3D model of faults with three mapped horizons with inline 685. Fault map of Horizon 2 (middle one in 3D view) showing multi-directional orientations in the rose diagram, N = 629 faults.*

trend more NE-SW and NW-SE. Moving oceanward, in the north of the volume, a smaller N-S trending block (B3) reduces in size southward until it pinches out, resulting in a 8-9 km wide southern graben. Further oceanward there is a complex set of blocks: B4 runs the whole width of the volume (N-S) but varies in vertical extent. Moving outboard, the next block is B5, which also trends N-S. It is the largest block in the volume in the north but gradually reduces in vertical extent moving south. In the north B5 has a oceanward (west) dipping eroded fault scarp (now partly covered by post-rift sediments) that shows erosion of the blocks has contributed to the basin fill (see Section 4.2.3). Between B4 and B5 in the north of the volume is an *en échelon* series of NE-SW trending small blocks that links the two larger blocks (B4 and B5), this arrangement is reminiscent of breached fault relays seen at lower amounts of extension (Section 2.8). Oceanward of B5 is a large 12-15 km wide basin that gives way to the Peridotite Ridge. Two large mass flow deposits are interpreted to underlie the base post-rift horizon on the eastern flank of the Peridotite Ridge.

Analysing the base of post-rift horizon (Figures 4.6 and 4.1), it is clear that the structure of the edge of the continental crust is composed of a series of linked and rotated crustal blocks that vary in size laterally and result from displacement on a network of crustal scale faults. The blocks seen this base post-refit level are distinct (albeit linked) and are separated by faults. Block 4 is separated by faults from Blocks 2 and 3, faults separate block 4 from block 5, even where they almost merge in the north, faults also form the western flanks of Block 5.

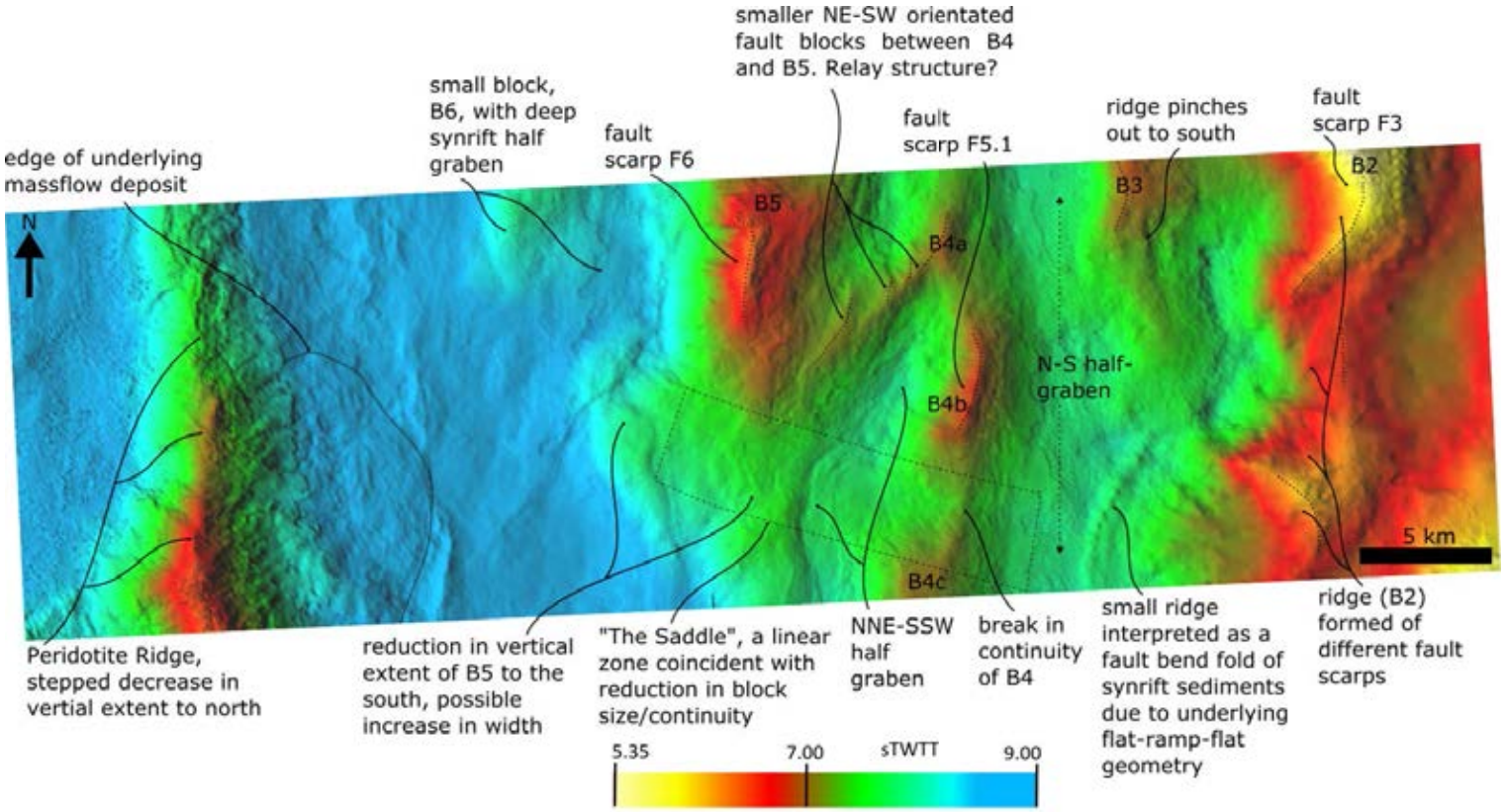

Figure 4.6: *Time structure map of the diachronous (see text) base post-rift unconformity showing gross structural architecture of the edge of the Continental crust.*

Dotted lines on top of blocks to emphasis fault scarps indicated

Top of acoustic basement - TAB

Moving lower in the 3D volume the next important and ubiquitous structural horizon is the top acoustic basement (TAB). Figure 4.7 unsurprisingly bears close resemblance to the base post-rift time structure map (Figure 4.6). This is unsurprising as there is relatively thin pre-rift and syn-rift sediment thicknesses over much of the volume and they are deformed by the same faults. Acoustic basement has been mapped as continental crust and as exhumed mantle in the region of the Peridotite Ridge. There are areas where displacement on the intra-block faults has thinned the continental crust to zero thickness, resulting in basement windows exposing the mantle rocks that are directly covered by syn-rift sedimentary fill. These windows trend N-S to NE-SW.

It is useful to consider the relative sizes of the continental blocks as this may have implications for the mechanism of break-up, for instance the oceanward reduction in block size suggested by the sequential faulting model (Section 2.5). Block 5 (B5) is, in the north, large when compared to all other blocks in the central area of the data volume that are expressed at both the top acoustic basement and base post-rift levels. The size of B5 at top acoustic basement level is partly due to a relative lack of syn-rift sediments. The size of B5 rivals the size of the proximal margin within the data volume (B1 and B2), which form the footwalls of the breakaway faults that cut the through the crust and reach the mantle.

Clearer expression of the fault bound nature of blocks is seen by sharp edges to blocks and relatively flat tops of blocks, for example: B4 and the small 'relay' between B4 and B5. As with the blocks seen as the base post-rift level, the distinct (albeit linked) blocks seen at this level are separated by the same faults as seen at the base post-rift level.

In the south of the graben between B5 and the Peridotite Ridge three small NE-SW trending ridges have been interpreted. The interpretation here is less constrained as the highly positive polarity basement reflection seen in other areas is almost absent, possibly due to large thickness of sedimentary fill or the fact that basement is heavily dissected, and therefore possibly heavily fractured, reducing the acoustic impedance contrast with overlying sediments. Despite this

reduction in the strength of the positive polarity top basement reflector, faulting in the overlying sediments and more subtle basement reflections can be seen and it is has been therefore possible for the basement ridges to be interpreted. However, the exact size of the blocks is difficult to fully constrain. Although beyond the scope of this work, it is useful to consider the transition from continental crust to the exhumed mantle of the Peridotite Ridge. From the end of the S reflector (see next section) to the flank of the ridge there is a zone of very complicated reflections that highlight the complex nature of this area (see annotations in 4.1). What is apparent is that there is a large amount of brittle faulting in relatively high velocity rocks (Bayrakci et al., 2016; Davy et al., 2017); either fractured mantle or heavily dissected continental crust. The presence of some strong discontinuous reflector also suggests that there may be a number of igneous intrusions that reduce the clarity of the images. The Peridotite Ridge has the same geometry as seen in base post-rift map, due to limited sedimentary cover of such a feature.

In the southern central area of the volume an important feature is apparent: 'The Saddle', is marked by rapid reduction in size of blocks 4 and 5 where they cross it. It also coincides with a zone of high amplitude seen on the S reflector (see Section 4.2.3 and Figure 4.8). The saddle trends WNW-ESE at its proximal end and swings to NW-SE at its distal end therefore making it perpendicular to the strike of the crustal blocks and basement windows (N-S/NE-SW). The zone is 15-20 km long (E-W) and 4-5 km wide.

Figure 4.7 also shows a number of lineations (marked with arrows) on the western flanks of faults blocks, which may represent slip indicators as at these points these surfaces are fault planes. The direction these indicators follow the slightly arcuate trend of the saddle. These lineations extend for 4-5 km suggesting periods of extended slip and are preserved under syn-rift sediments.

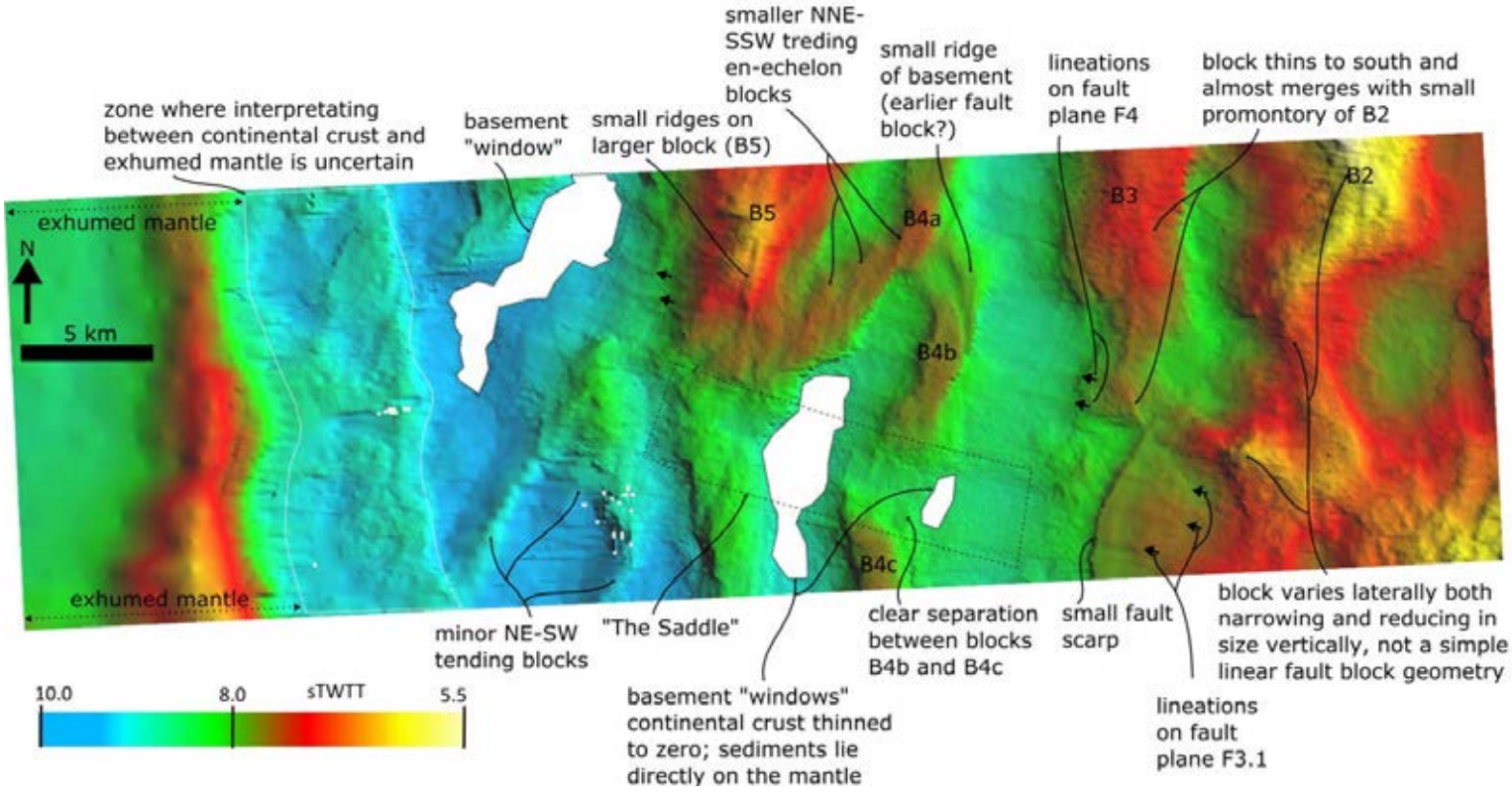

Figure 4.7: *Time structure map of the top acoustic basement surface. Black arrows show lineations that are interpreted as fault slip indicators*

The S reflector

The S reflector is imaged as a largely continuous structure within the central region of the 3D dataset (Figure 4.1). In the east of the time structure map of the S reflector (Figure 4.8) are the breakaway faults that cut the crust and reach the mantle (with B2 forming the footwall). The time structure map of the S reflector (Figure 4.8) appears to have 'topography' of a series of interconnected ridges and a distinct 'saddle' as seen at the base post-rift unconformity and top acoustic basement levels (Figure 4.7). This topography is primarily due to velocity pull-up of the sub-horizontal S reflector (see Figure 3.10 for a comparison with pre-stack depth migrated data) surface below the higher velocity cores composed of granodiorite of the crustal blocks compared to the sediment filled half-grabens. Lineations trending NW-SE in the north west and approximately E-W in the east (shown by arrows in Figure 4.8) are interpreted as being slip indicators on a detachment surface as observed on other major slip surfaces (Cann et al., 1997; Resor and Meer, 2009; Edwards et al., 2018). Figure 4.8 also shows a trace envelope (amplitude) map which shows that a number of the higher amplitude areas are associated with features seen on the time structure map including bright amplitude zones that correspond to some topographic highs and also the NW-SE and c. E-W trending slip indicator lineations (arrowed). Section 4.2.4 provides more detail on relationships between the S reflector, faults and other structural elements of the dataset.

The S reflector stops abruptly in the west (see Figures 4.1), its westward structural continuity is uncertain; S may flex upward to run parallel to the eastern flank of the Peridotite Ridge or it may be offset by landward-dipping normal faults. Alternatively, the crustal extension it provided was replaced by large scale disseminated faulting and possible igneous intrusions due to final break-up (see Lymer, Picazo, Cresswell et al., in prep).

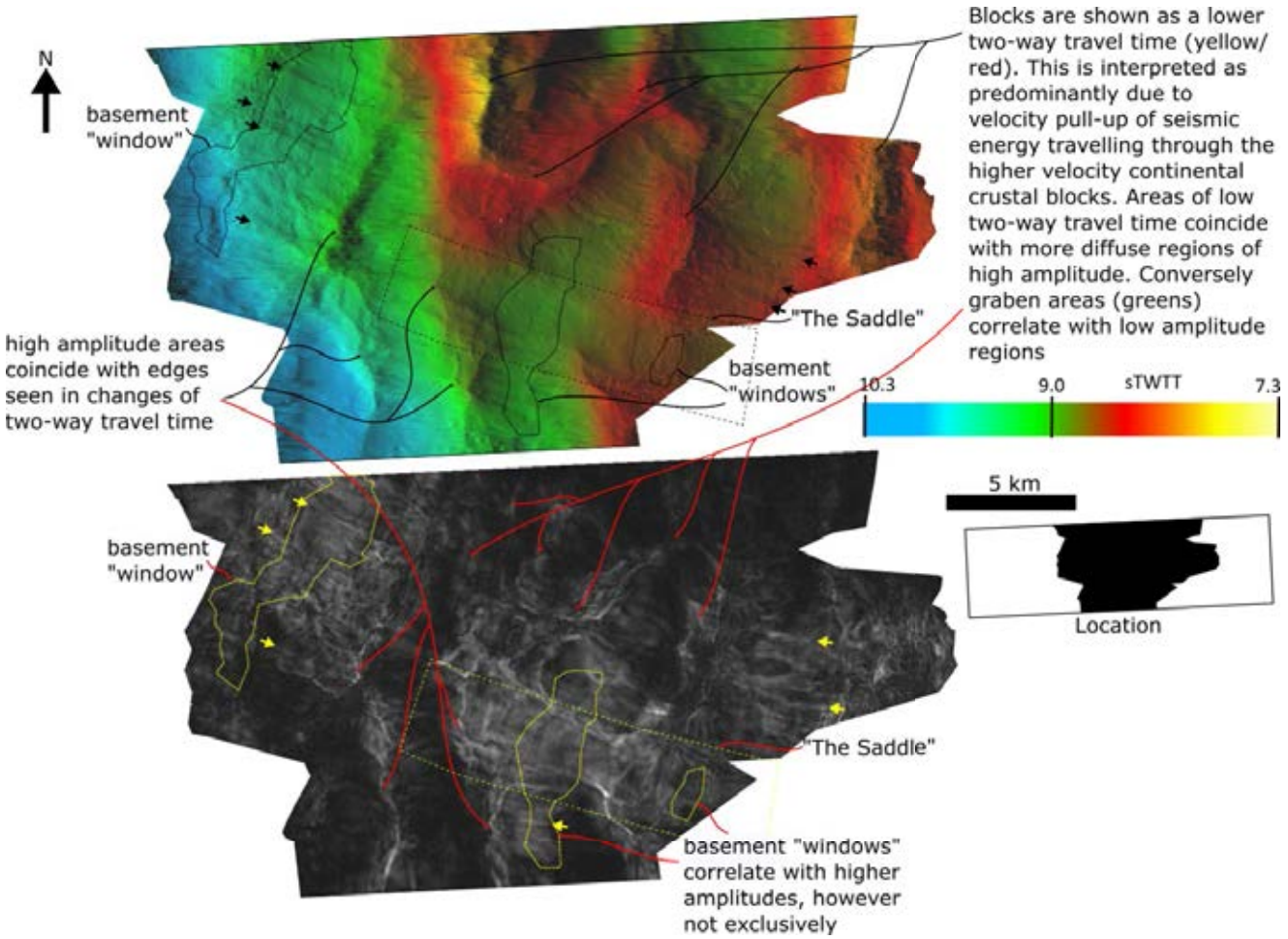

Figure 4.8: *Two maps of the S reflector. Top: Time structure map, bottom: Trace envelope amplitude map. Arrows show corresponding lineations. Location map shows position in dataset, see Figure 3.3.*

4.1.2 Summary of the general structure

The following list provides a summary of the general structure obtained from the seismic images and the time structure maps of the four horizons considered above:

- aspects of the margin structure are expressed at the seafloor, and may still influence modern day sediment transport on the margin
- the margin consists of a number of tilted fault bounded blocks overlying a bright reflector - the 'S'
- the tilted blocks are laterally discontinuous and are seen to connect (merge) with each other; this connection is revealed at different structural levels
- the tilted blocks are formed by faults that, like the blocks, merge laterally.
- where merged faults result in the separation of the blocks, these faults are considered as fault 'sets', in Figures 4.6 and 4.7 these fault sets separate B4 from Blocks 2 and 3, separate B4 from B5, and also form the western flanks of B5.
- the acoustic basement is so thinned that in three discrete windows it has thinned to zero allowing sediments to lie directly on the mantle
- the western edge of the tilted blocks are fault surfaces that may show fault slip lineations
- the S reflector displays corresponding features lineations on both amplitude and time maps the including E-W to WNW-ESE lineations interpreted as being slip corrugations on faults. Other features seem to coincide with fault-S intersections

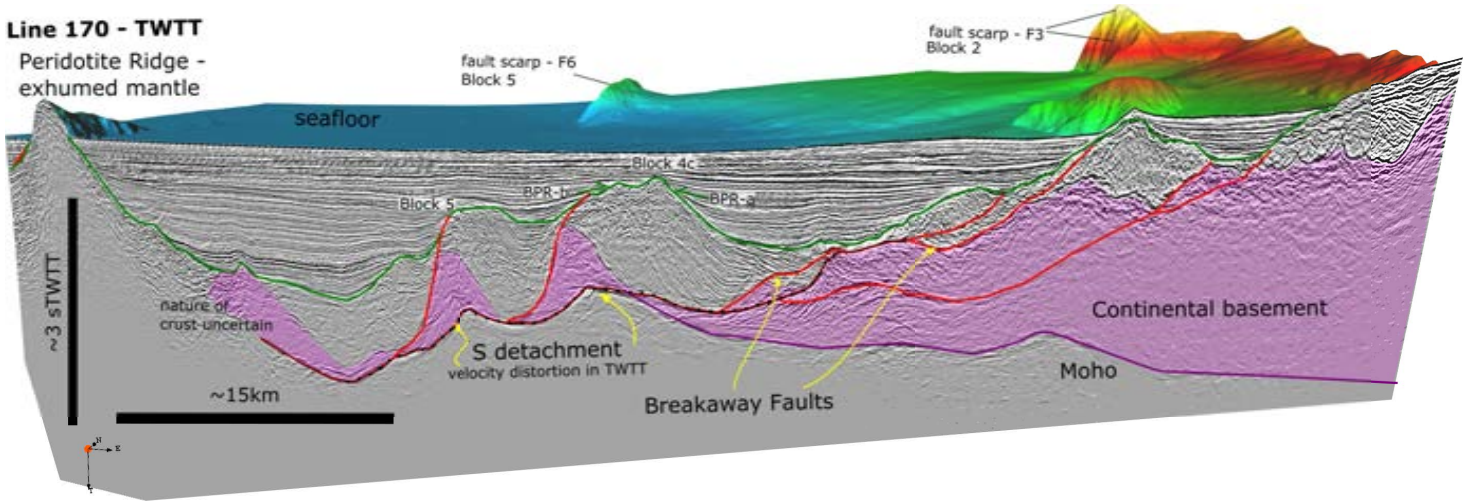

Figure 4.9: *3D block diagram of the Galicia margin. Note onlap of the the post-rift sediments (BPR-a and BPR-b) onto the base post-rift unconformity (green line) suggesting diachronous nature of the horizon, and the faults linking onto the S reflector.*

4.2 Detailed analysis

In order to understand the mechanism of hyperextension and breakup, a detailed analysis of the relationship between each of the structural horizons and the main block bounding faults is presented. To ensure block geometries are geologically realistic, much of this analysis has been undertaken on the depth-converted data. Figures 4.10 and 4.11 shows three depth inlines and a depth slice, respectively. The inlines show multiple phases of faulting, which overlap spatially and temporally, dissecting the crustal blocks. Pre- and syn-rift sediments are rotated and faulted in various directions and by various amounts. For example, Block 5 (hangingwall of Fault 6.0/6.1) is heavily dissected towards the south and shows very complex and rotated syn-rift sediments. The depth-slice (Figure 4.11) shows the observed variation of trends of the intra-block faults when compared to the main block-bounding faults.

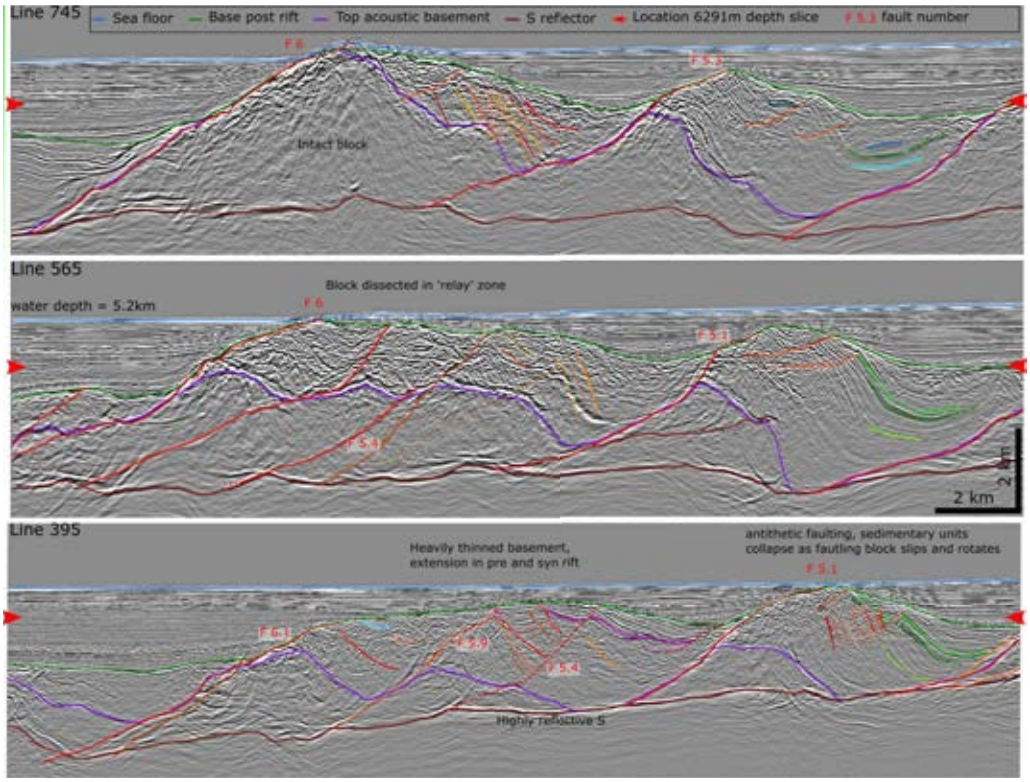

Figure 4.10: *Three depth inlines showing structural complexity of the Galica margin. Red arrows indicate depth slice Figure 4.11 note the flatter S reflector, c.f. Figure 4.1, but also the irregularity where some faults intersect. See Figure 4.11 for location lines within the dataset.*

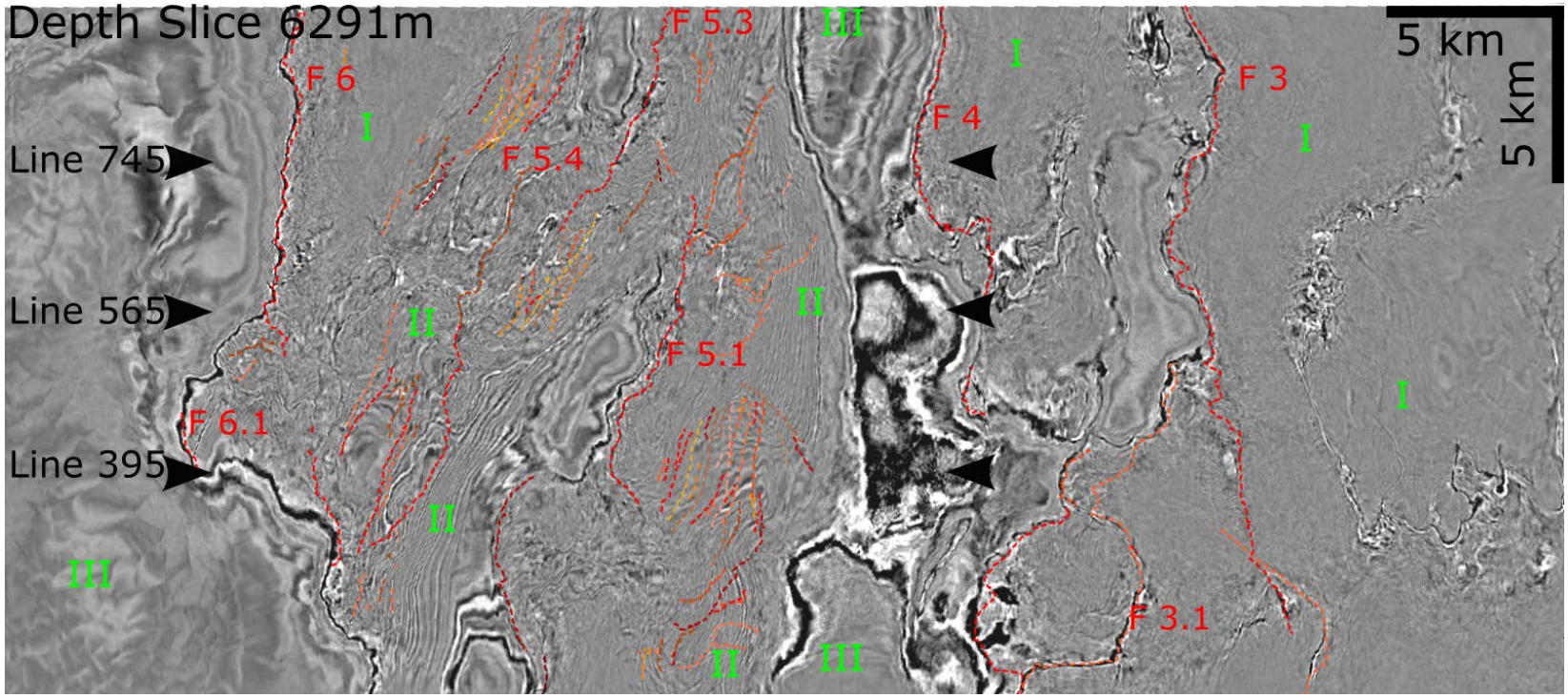

Figure 4.11: *Depth slice at 6291 msTWTT, black arrows show inlines shown in Figure 4.10. Green numerals indicate: I-Acoustic basement blocks, II- pre-rift/syn-rift sediment atop rotated blocks, III-post-rift sediments with polygonal faulting. Arrow heads mark extent of lines shown in Figure 4.10.*

As the emphasis of this study is the nature of the mechanisms of hyperextension and break-up of the continental crust, the sequences between the sea floor and the base of the post-rift unconformity will not be considered in any detail. Furthermore, the focus on break-up limits the extent of the study to the region between the breakaway faults in the east (faults 3.0 and 3.1) and the western limit of the S reflector (see Figures 4.1 and 4.8). In addition to the horizons outlined above, there are also some syn-rift packages (between top acoustic basement and the base post-rift unconformity) that have been interpreted in order to help constrain the relative fault kinematics (Childs et al., 2017; Jackson et al., 2017). These syn-rift packages are covered in more detail in Section 4.2.2. The earliest of these packages (Package A) is interpreted as early or pre-rift syn-rift and forms a distinctive horizon than covers much of the data volume and has therefore been included in this more detailed analysis. The following sections present a more detailed analysis of the geometries of four horizons and their relationships with the main faults. The horizons are:

- Base post-rift unconformity (BPR)
- Top 'Package A' - a distinctive marker horizon that it laterally extensive within the synrift sediments
- Top acoustic basement (TAB)
- S reflector - incorporating some of the breakaway faults (F3.0 and F3.1), the most proximal faults that couple crustal deformation with the mantle

The acoustic basement at the 'core' of the crustal blocks once formed the un-thinned continental crust; any sediments on the top of the basement blocks may be syn-rift and therefore not unequivocally part of the pre-rift crust (for example deep water marls at dive site 11 on Block 5 - see Sections 1.3.3 and 1.4). As the geometries of the blocks are formed by the different phases of crustal extension and they are a record of the rifting and breakup of the continents, allowing the mechanisms of breakup to be more clearly understood.

4.2.1 Base post-rift unconformity

The diachronous unconformity at the base of the post-rift sediments marks the upper surface within the dataset that provides direct evidence of hyper extended continental crust and may therefore reveal aspects of the mechanism of hyperextension and continental break-up. The overall geometry of the BPR surface was introduced in Section 4.1. Considering the surface in more detail, in both two-way travel time and depth (Figures 4.6 and 4.12 respectively), reveals a number of fault scarps and the related rotated crustal blocks in the fault hanginwalls. Rather than simple margin-parallel (north-south) ridges (Ranero and Pérez-Gussinyé, 2010; Lavier and Manatschal, 2006, Figure 2), a complex connected fault scarp network exists. Scarps of large inter-block faults that reach the S reflector on the seismic sections (often) coincide with the expression of these faults on the BPR surface, consequently such faults are considered to be the latest phase of faulting. This interpretation is non-trivial: faults expressed at this surface are considered to be the faults that were active during the final breakup of the continental crust, the fact that these faults also intersect with the S reflector at depth suggests that there is a common genesis between the deformation expressed at the BPR level, the faults and the S reflector. Analysis of the three dimensional BPR surface therefore provides an essential element in understanding final breakup.

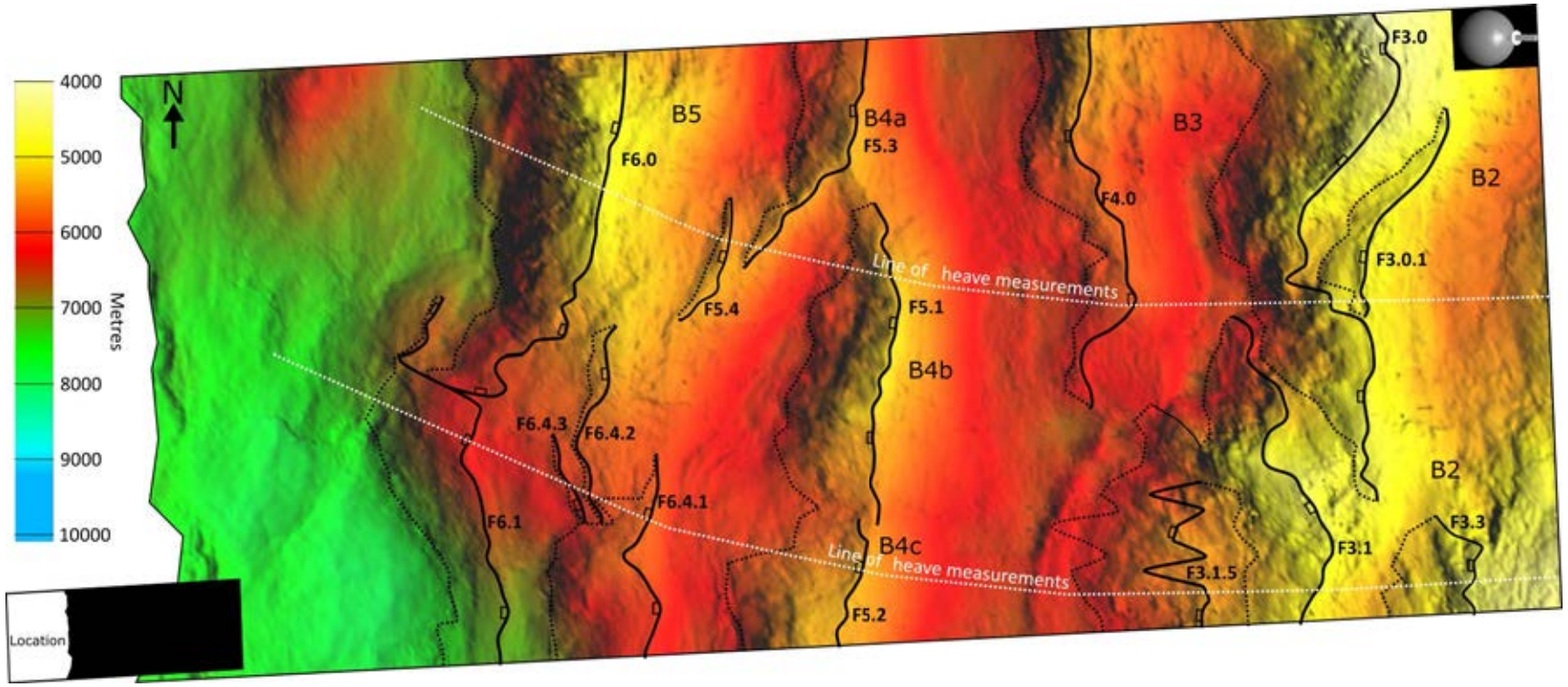

Figure 4.12: *Depth Map of base post-rift unconformity showing fault network at this level. Hangingwall cutoffs solid line, footwall cutoffs broken line, tick denotes down-throw. Location map shows position in dataset, see Figure 3.3.*

The major fault hanging wall and footwall cut-offs are shown in Figure 4.12, which focuses on the eastern and central area of the data volume. The area between these cut-offs is a fault scarp or heavily deformed sediments lying directly on a fault surface (see labelled faults in Figure 4.1). Figures 4.6 and 4.12 show that the crustal blocks composed of acoustic basement and graben fill trend approximately N-S with some, usually smaller, blocks trending NE-SW. As the blocks are formed by oceanward dipping faults similar trends to those seen for the grabens are observed in the faults scarps. Furthermore, the post-rift sediments onlap on to the interpreted fault scarps (Figure 4.1). These faults scarps would have formed part of a palaeo-seafloor surface and as such been liable to erosion, meaning that the interpreted fault surface may not be the line of original faulting. This erosion of fault scarps leads to rounding of the footwall blocks, or even flattening of the footwall block if near palaeo-sea surface (Davis and Kusznir, 2004). Post-rift seismic stratigraphy suggests that this erosion provided fill material for the accommodation space created by the rifting and breakup. Field evidence for this is seen within the post-rift and syn-rift sediments in the uplifted hyperextended margin exposed in the Swiss Alps (Masini et al., 2013, 2014). Evidence for movement on the fault is also apparent by deformation seen within the syn-rift sediments (Chapter 5).

In the east of the volume, the BPR surface has a semi-continuous N-S trending block (B2) that has three main fault scarps, labelled F3.0, F3.1 and F3.1.5 (two subsidiary faults also link these three). The fact that these faults are linked suggests that they have some kinematic coherence. They are therefore considered a 'fault set', this criteria will be used henceforth to determine and refer to fault sets. Faults in fault set 3 form the breakaway fault which couples brittle deformation within the crust with deformation at/in the mantle. In the north, Fault 3.0 (F3.0) forms a single fault scarp 4-5 km wide (E-W); the footwall cut-off is curved, trending N-S in for approximately 2 km in the very north, but gradually swinging NE-SW for 5 km. The width of the scarp reduces southward to where the scarp of F3.1 begins. This occurs approximately halfway along the ridge, which also coincides with a reduction in the height and width of the ridge; at this point the scarps of F3.0 has reduced to a width of 2 km. The combined width of the scarp where they overstep is approximately 4 km, which reduces southward. The southern half of both fault

scarps trend predominantly NNE-SSE apart from a 2 km section of the scarp of F3.1 that trends NE-SW and forms a NW facing scarp of the crustal block and may result from a fault linking (possibly via a breached relay) two NNE-SSE segments. A scarp (of F3.1.5) further dissects the crustal block to the south where it links directly with F3.1. The convoluted plan view form of faulting relates to both the heavy dissection of the block 3 and that the fault and the BPR surface intersect at a low angle.

Moving west (oceanward) the scarp of F4.0 forms the western flank of Block 3. The scarp has a maximum width of 2 km to the north of the data volume and gradually reduces in width to the south where both block and scarp are no longer expressed on the BPR surface, resulting in a 15 km wide basin. Seismic sections (Figure 4.1B, between cross lines 11000-11500) reveal that F4.0 merges with F3.1. Moving west, a discontinuous block (B4) spans the width (N-S) of the volume. Within the 'saddle' the fault scarp cannot be interpreted in the seismic volume; instead this area is dominated by heavily deformed (faulted) syn-rift sediments.

This gap in the continuity of Block 4 forms part of the 'saddle' (Figure 4.13). To the south of the saddle lies the scarp of F5.2 and to the north the scarp of F5.1. The footwall cut-off for both of these faults is predominantly linear and trends between NNE-SSW and N-S with the maximum width of the scarp being 2 km. The scarp of F5.1 is 15 km long. To the north a 7 km long discrete fault scarp (F5.3) with a width of 1-2 km flanks the western edge of block 4 and has a concave to the west footwall cut-off. However the footwall cut-off of Fault 5.3's southern edge trends NE-SW and forms part of a series of small NE-SW trending *en échelon* blocks that link the northern part of block 4 with the central portion (within the data volume) of Block 5. These *en échelon* blocks have small (approximately 1km) scarps also trending NE-SW.

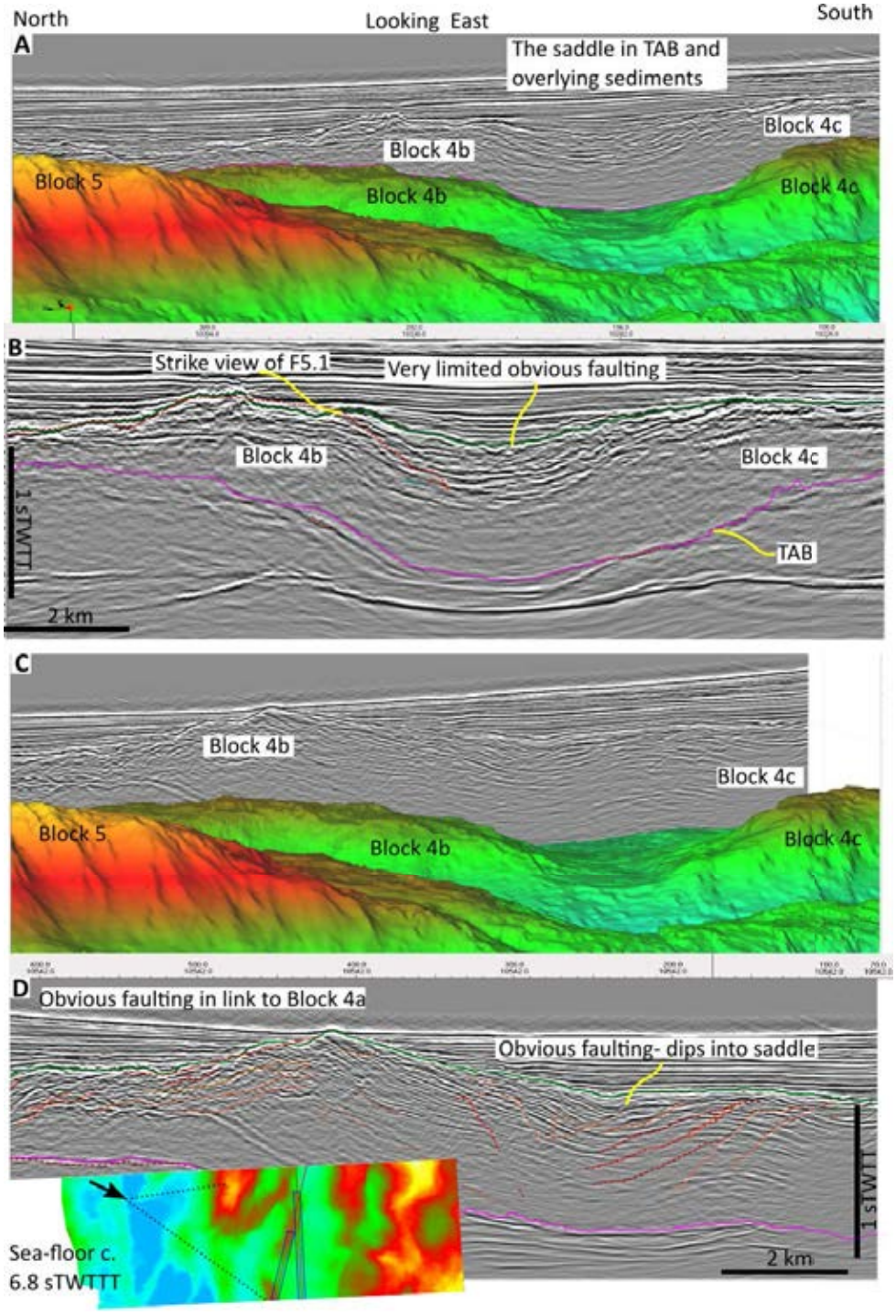

Figure 4.13: *2D and 3D view of the 'saddle' looking east (toward the continent). A and B show arbitrary line directly across the saddle. C and D show inline slightly further east and shows greater deformation in the graben. Deformation is concentrated in the syn-rift is composed of extensional structures dipping into the saddle. 3D surface in A and C is the top acoustic basement.*

In north of the data volume Block 5 has a fault scarp (formed by F6.0) up to 6 km wide, 12 km long. This scarp tapers to the south to be replaced by three smaller blocks and fault scarps; the transition being at the 'saddle' (see Figure 4.6). The westernmost of the smaller southern fault scarps (and therefore blocks) trends distinctively NE-SW and extends across the line of the 'saddle'. The central one (F6.2) is easily the largest with a scarp width of up to 4 km and lies SW of the northern scarp of Fault 6.0. The eastern one lies directly south of Block 5, a smaller scarp (F6.4.2) lying to the south-eastern side of the block forming the southwestern most of the line of *en échelon* blocks that link blocks 4 and 5. Fault 6.4.2 merges with two smaller faults in the south to form a scarp of 3-4 km width. The footwall cut-off linkage between F6.0 and F6.1 shows a convoluted geometry with the northern end of F6.1 seemingly being displaced to the NW. The geometries results from an interaction of faults at depth (below BPR). For example, Figure 4.14 shows a series of time slices that show how the faults link at depth and can explain the strong deviations in fault geometry seen at the BPR level, c.f. depth maps presented in the following Sections 4.2.3 and 4.2.2.

In summary the fault network at the base post-rift unconformity has a range of interactions: direct linkage, over-stepping relays and *en échelon* faults. These interactions result in a complex fault network, especially when smaller faults that connect with the block bounding faults are considered. Capturing this complexity at a surface that marks the end of active tectonic extension is a key contribution of this study. This complexity suggests that a simple localisation or migration of active faulting is not clearly seen when deformation within the 3D volume is considered. Deformation, both faulting and folding, of the sedimentary packages between the base post-rift unconformity and the top acoustic basement may reveal more detail of this complexity. The following section presents the fault network interaction with an horizon within the syn-rift sediments; further details are provided in Chapter 5.

4.2.2 Syn-rift horizon - package A

Three distinct syn-rift packages can be seen in the data. Figure 4.15 shows these three packages (see also Figure 4.2), which have been interpreted based on the following characteristics (oldest

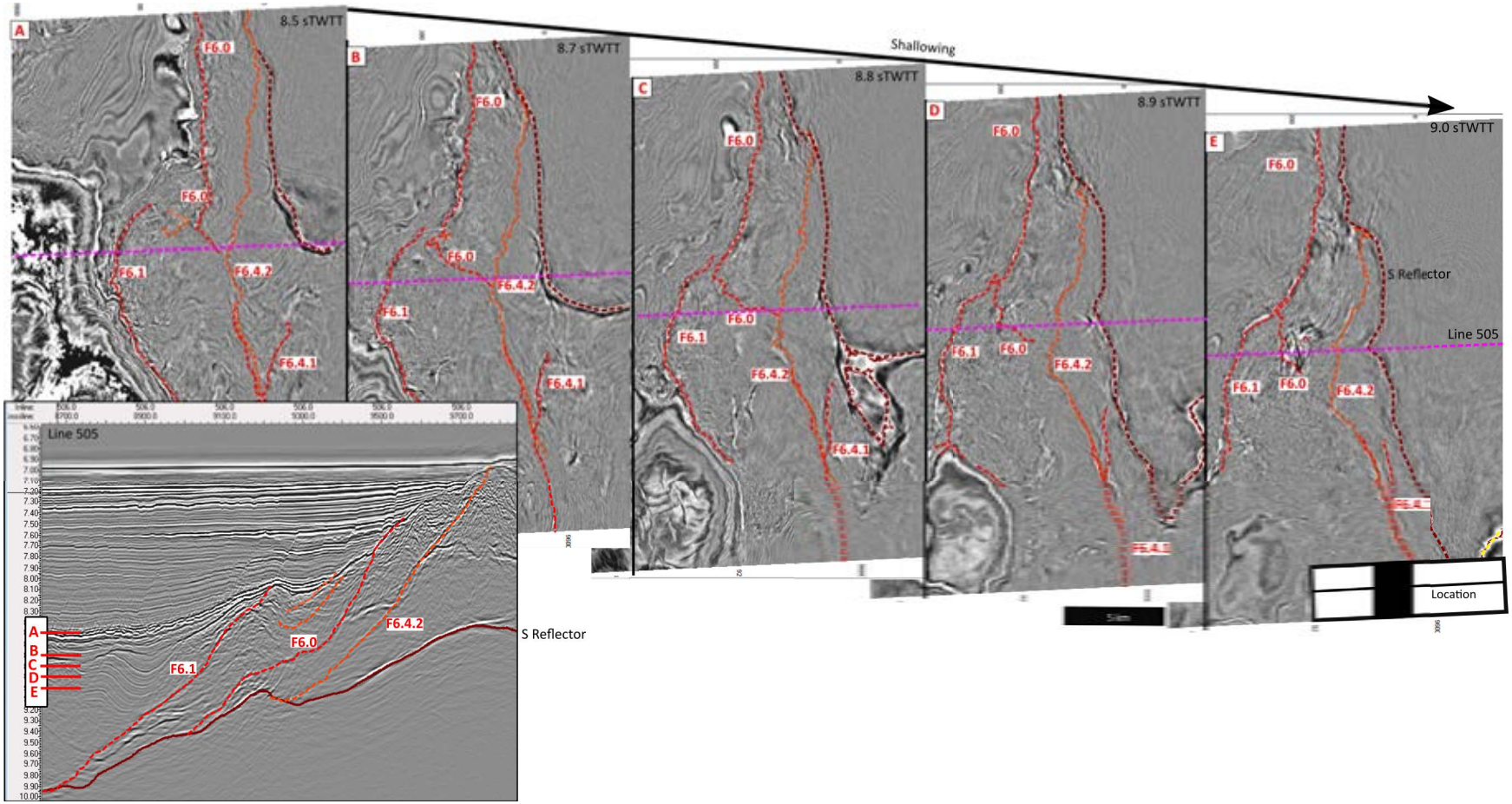

Figure 4.14: *Time slices through linkage between faults 6.0 and 6.1 explaining their linkage at depth*

first):

Package A: Topped by a bright negative polarity reflector: black-WHITE-black (capitals indicates largest amplitude of waveform). Laterally extensive and beneath which is a package of limited reflectivity. The top of this package has been mapped throughout the central area of the dataset (Figure 4.16).

Package B: Numerous reflectors that can be laterally extensive but often contains significant (usually) minor faulting within both the hanging wall and footwall of the main faults. Reflectors can be seen to thicken into major block bounding faults and are truncated by these faults, or faults adjacent to them. Sometimes reflectors are seen to onlap onto faults or form a damage zone in the fault hanging wall. The sediments are often folded (usually tilted, open synclines) in the half-grabens.

Package C: Highly reflective package that infills small basins on top of package B. Package C is not offset by major faults and often laps onto minor faulting, sometimes displaying minor fault bend folds.

The presence of a continuous reflector between the breakaway faults in the east (F3.0/3.1) and the hanging wall of Fault set 6 in the west has provided a 'marker' horizon (top package A) within the syn-rift sediments which has been mapped out. It is important to mention that other than package A (due to the top of package A's distinctive negative polarity), it is not possible to confidently interpret other reflectors in the data between the different half-grabens. The top of package A forms a horizon that provides a mappable structural level between the base post-rift unconformity and the top acoustic basement. Fault cut-offs can therefore also be mapped on this horizon (Figure 4.16). The continuity of the top of package north-west of the line of faults formed by 6.0 and 6.1 is however, less constrained, but a similar horizon in terms of seismic character was interpreted and is used here.

Figure 4.16 shows the depth map of the top of package A. A distinctive feature in the east of the map is that the areas between the hanging wall and footwall cutoffs for F3.0, F3.1 and F3.1.5 and F4.0 form a continuous network: the surfaces are geometrically linked, providing increased confidence of considering these faults to be part of a set. Of particular note is the merging of

F3.1.5 and F4.0 giving a fault surface of 10 km width in the dip direction (c.f. Figure 4.12).

Fault set 5 has a similar geometry to that seen at the BPR structural level: direct linkage of F5.1 and F5.2, significant overstep of F5.2 and F5.3. Fault 5.4 has a lateral extent of over 10 km (but a width of approximately 0.5 km) and almost links with F6.4.1, whilst runs parallel to and oversteps F6.4.2 for much of their length. In the south west there are 3 sub parallel fault strands (F6.1, F6.2 and F6.3) in stead of the single one expressed at the BPR structural level. Maximum offset for fault set 6 is approximately 7 km on F6.0.

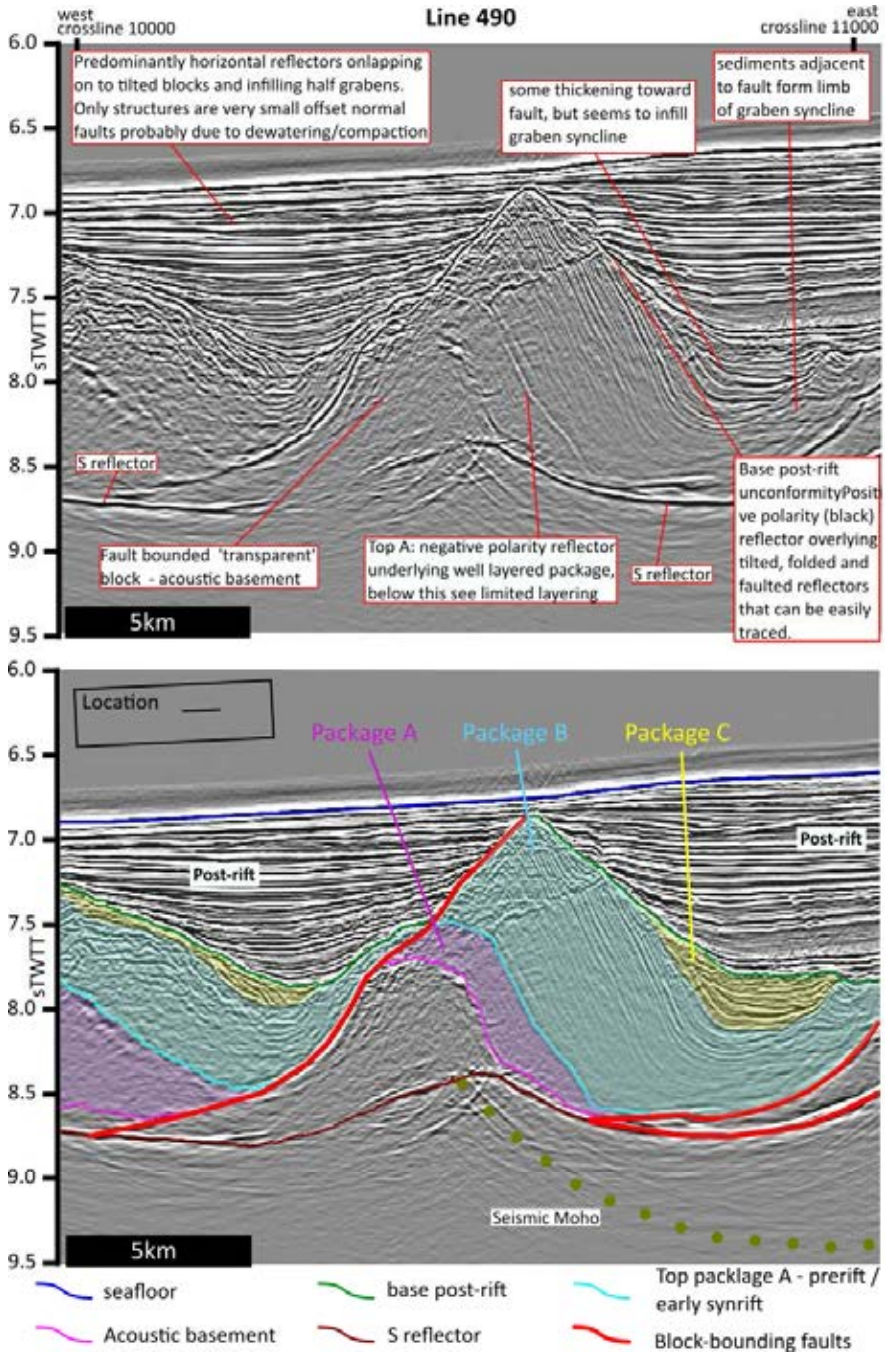

Figure 4.15: *Seismic image of a portion of Line 440 highlighting three syn-rift packages that can be seen in the half-grabens throughout much of the data volume*

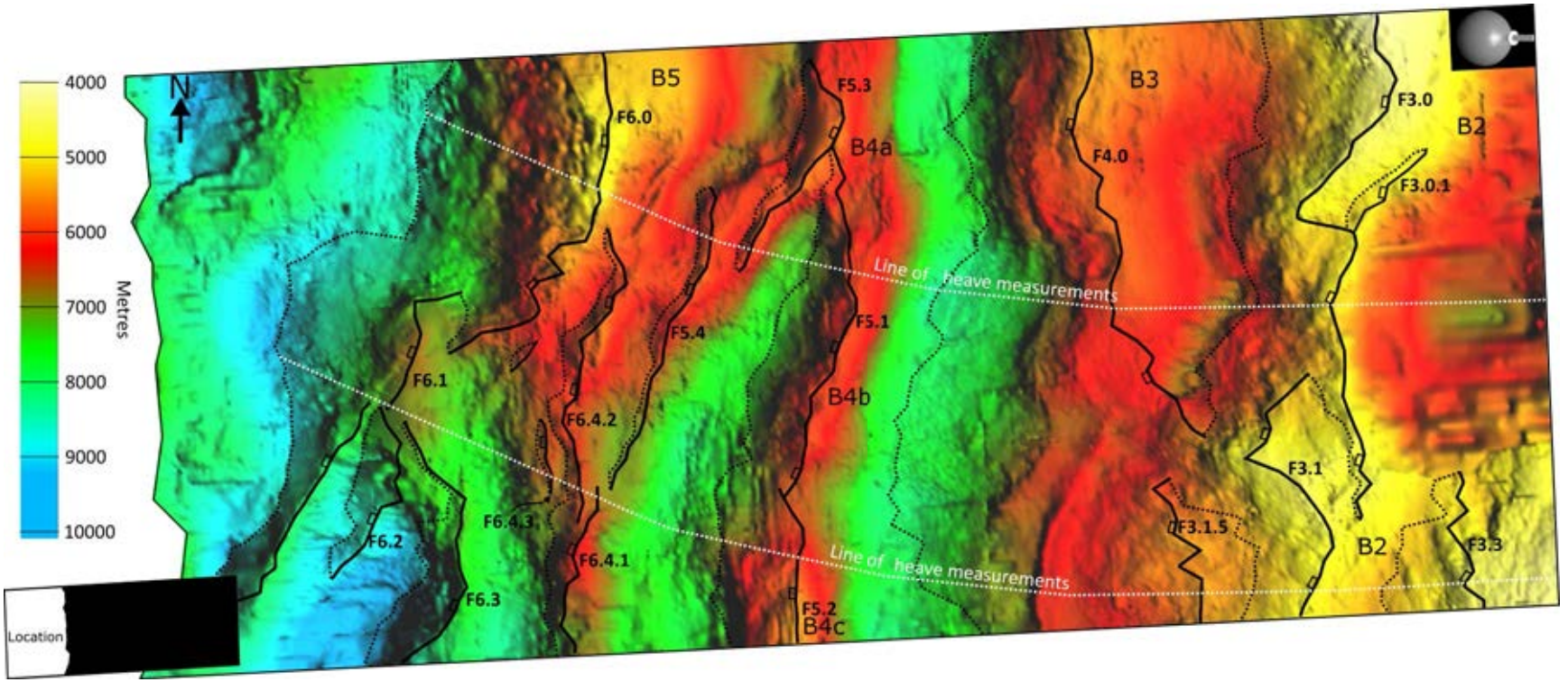

Figure 4.16: *Depth map of the top of package A (early syn-rift) showing fault network at this level. Hanging wall cutoffs solid line, footwall cutoffs broken line, tick denotes down-throw. Location map shows position in dataset, see Figure 3.3.*

4.2.3 Top acoustic basement

Interpretations of the depth-converted map of the top acoustic basement (Figure 4.17) reveals a number of notable features with regard to the expression of the faults at the surface and the network of faults. In the east (as with the top package A) the F3.0, F3.1 and F4.0 form one linked surface between the hanging wall and footwall cut offs with a maximum offset of over 10 km. The linkage of offsets for F5.1 and F5.2 in the south, and the overstep of F5.1 with F5.3 and F5.4 toward the north, are similar to that seen at higher structural levels (Figures 4.16 and 4.12). However there is significantly larger offset, up to 4 km for F5.1, F5.2 and F5.3; Fault 5.4 remains low, $<$1 km. The near linkage between Fault 5.4 and 6.4.1 is not as apparent as it was at the top package A level. Fault set 6 in the west forms a connected network with in a single fault in the north (F6.0) dividing into 5 distinctive strands in the south - of which the western ones (F6.1 and F6.2) trend NNE-SSW and the more easterly one trending N-S. Maximum offset between fault cutoffs being up to 10 km on F6.0 (as opposed to approximately 7 km at top package A). In summary fault sets 3/4, 5 and 6 form a continuous surface of linked faults.

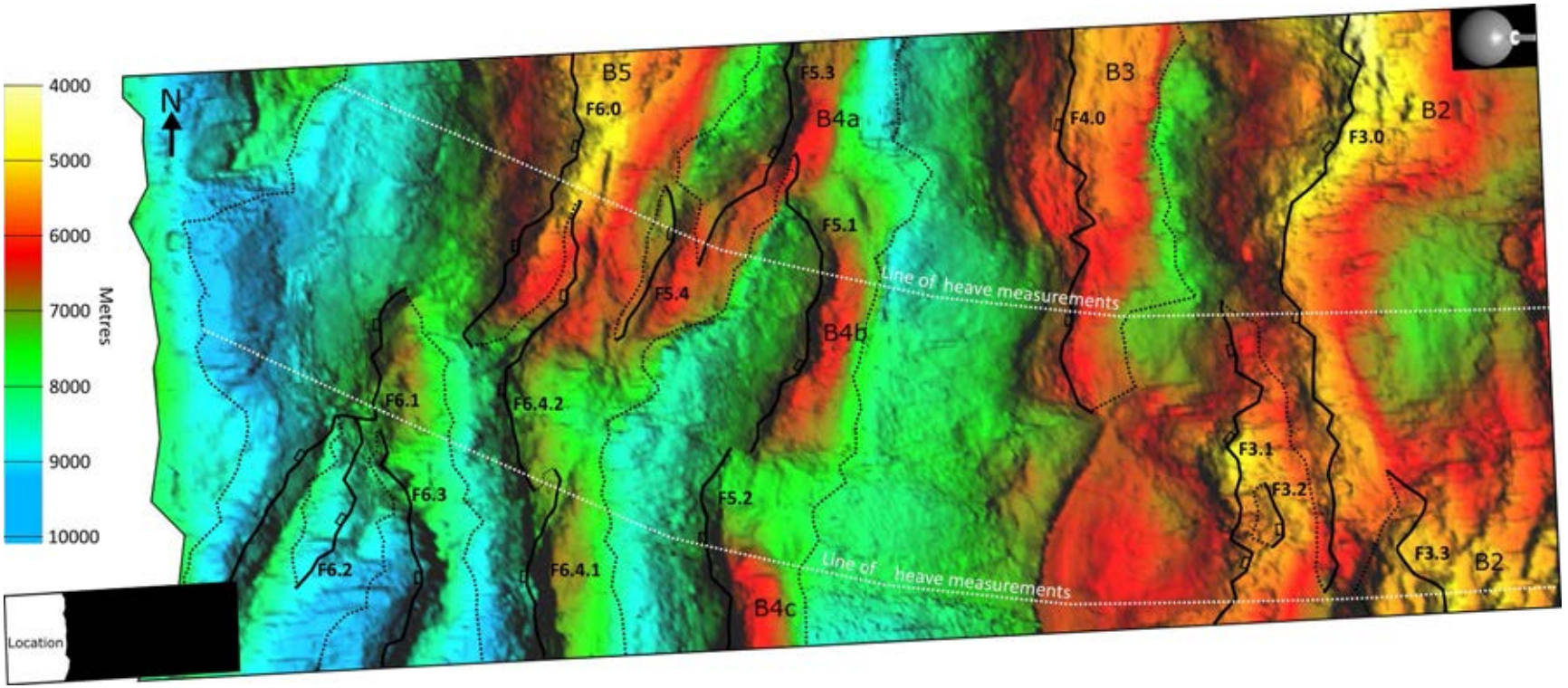

Figure 4.17: *Depth map of the top acoustic basement showing fault network at this level. Hanging wall cutoffs solid line, footwall cutoffs broken line, tick denotes down-throw. Location map shows position in dataset, see Figure 3.3.*

The small scarp seen in the time structure map of the top acoustic basement (Figure 4.7 at the southern end of F4.0 is still a distinctive feature of the what is a fault slip surface. This scarp also coincides with a 'jog' in the fault bounded block. The saddle between Blocks 4b and 4c is very pronounced and shows a clear separation, however crust must still underlies the majority of the saddle as there is only a small basement window (Figure 4.7). A smaller saddle-like feature also occurs where Block 4b merges with 4a. Block 5 is still very pronounced in the north due to the limited syn-rift, however clear fault related ridge (F6.4.2) divides the blocks to the south where it becomes progressively dissected especially the south of the saddle where it form three distinct blocks with deeper grabens.

Figure 4.18 shows the amplitude of the top acoustic basement (TAB). That the TAB consists of a number of fault surface is clearly displayed by the amplitude lineations, interpreted as corrugations due to fault slip. Note also the very high amplitude of the eroded scarp of Fault 6.0 and the high amplitudes of Block 3 (F4.0) which suggest erosion of these scarps that form the footwall of the faults. This erosion will have provided some sediment to half-grabens formed by the fault. However, the fact that these footwall scarps can be mapped and are not consistently flat-topped suggests this footwall erosion was submarine not sub-aerial or close to wave action.

Additionally basement thickness maps and thinning factor maps (Figure 4.19) have been derived which clearly show the nature of thinning and highlights the basement windows, and emphasises the lateral variations of deformation in seen within the blocks.

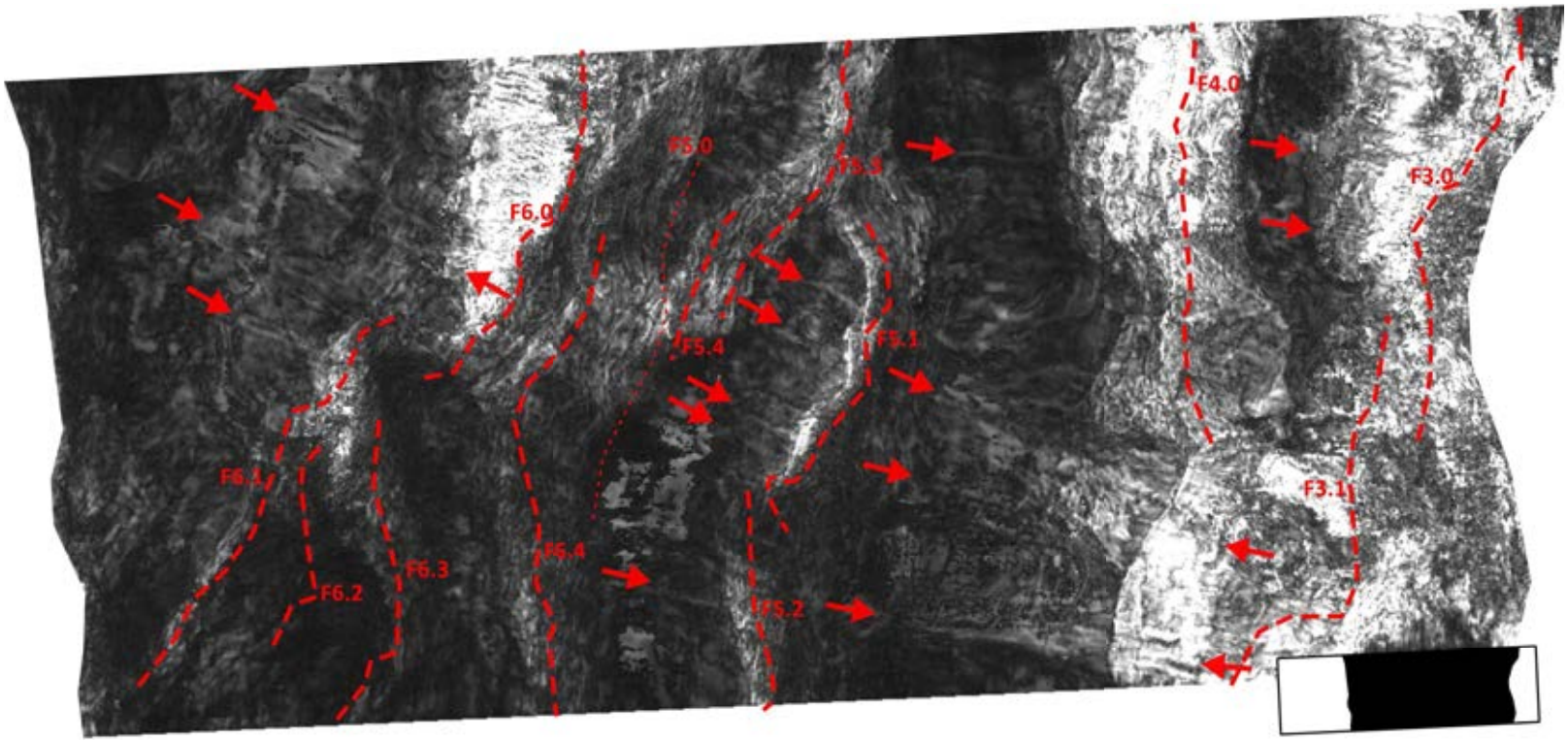

Figure 4.18: *Amplitude map of the top acoustic basement showing fault footwall cutoff network and lineations, interpreted a corrugations indicating fault slip (arrows), these corrugations all occur where top acoustic basement is composed of a fault surface. Note F5.0 is not expressed at BPR level. Location map shows position in dataset, see Figure 3.3.*

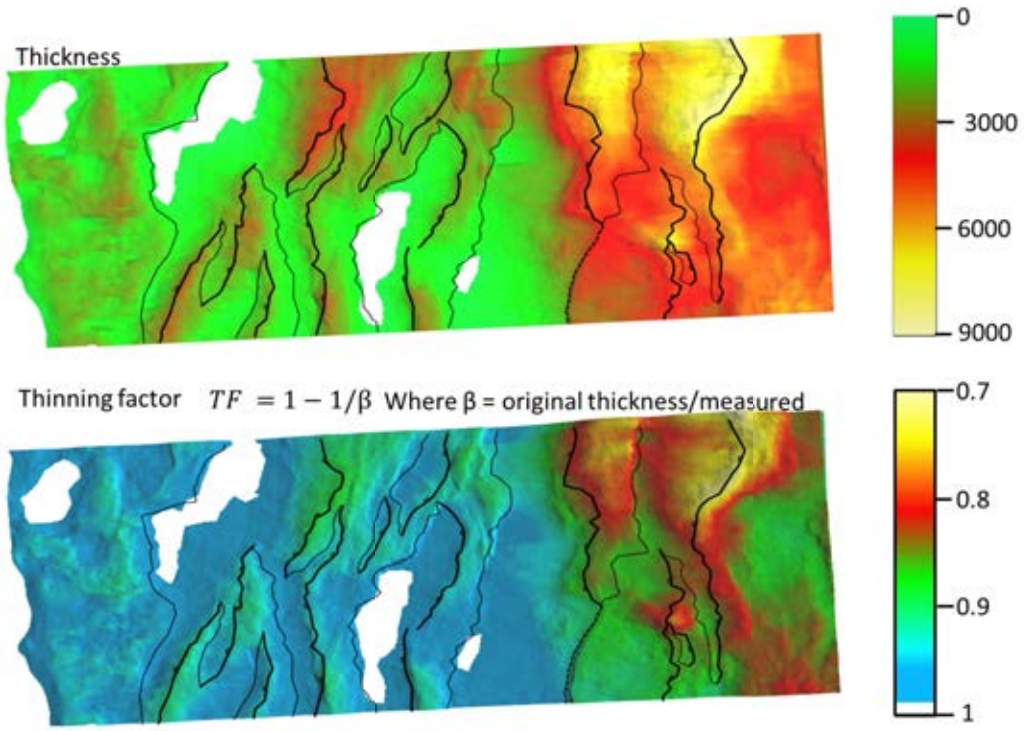

Figure 4.19: *Acoustic basement thickness and thinning factor maps where β is derived from thinning rather than extension. Location in Figure 4.18.*

4.2.4 The S reflector

The majority of the S reflector (Figure 4.8) is interpreted as top of the mantle that has been serpentinised by water ingress down faults that are seen to cut from the paleo-seafloor to the mantle (Pérez-Gussinyé and Reston, 2001; Bayrakci et al., 2016). To the east, the interpreted S surface consists of the breakaway faults (F3.0, 3.1 and 4.0) that cut through the crust and couple paleo-seafloor and the mantle; whereas in the the west S reflector stops abruptly. Thus the east and west lateral extent of a clear reflector is limited to the central area of the data volume. This central area is limited to where faults are observed to cut through the continental crust and reach the mantle (Figure 4.1). The velocity pull-up seen of the time map of S (Figure 4.4 is confirmed when compared with the depth-converted S map (Figure 4.20); the apparent topography seen in the time surface is not seen in the depth surface. In depth the S reflector is sub-horizontal across its entire extent west of the breakaway faults (Figure 3.10).

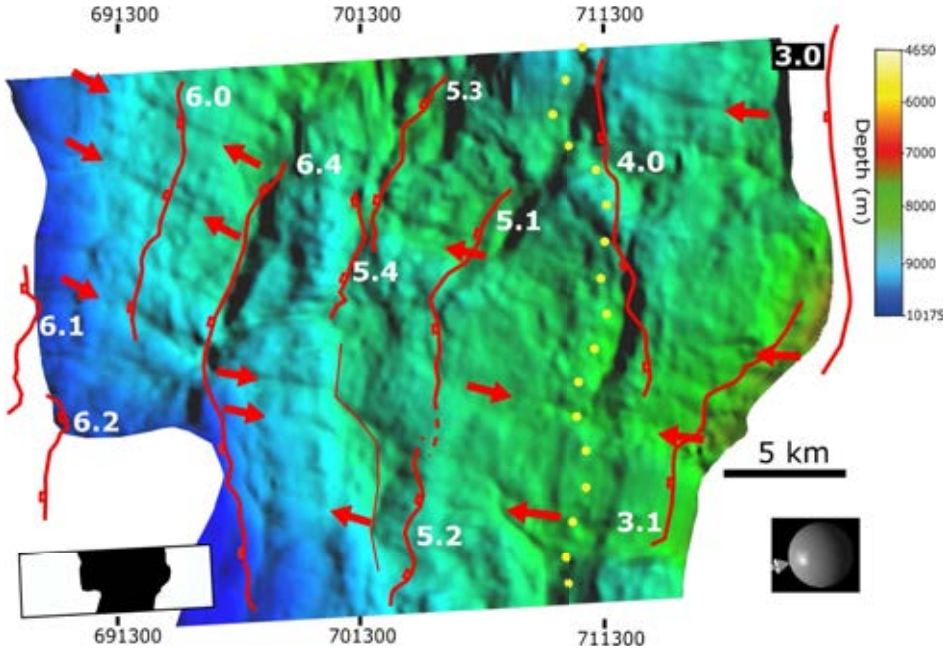

Figure 4.20: *Depth map of S rReflector, showing intersection of main block-bounding faults (red lines, numbered white), slip indicator corrugations (red arrows), seismic Moho-S intersection (olive dots), thus to east of Moho-S intersection is the lower portion of breakaway faults. At at this level the breakaway faults are not interpreted to link with each other. Location map shows position in dataset, see Figure 3.3.*

A detailed texture map of the S amplitudes, including the lower parts of the the breakaway faults is shown in Figure 4.21 and provides a structural context for the amplitude variations seen in Figure 4.8. The amplitudes seen on the S surface highlight variability in the nature of the surface. These variations may reflect the the ease of interpretation the S reflector in different parts of the volume (Sections 3.2.1 and 3.2.2) related (perhaps) to processes that generated S. Further comparison can be drawn between the location of the ridges in two-way travel time, in depth and in the discrete, approximately N-S trending high amplitude features (Figures 4.8, 4.21, and 4.20, respectively). These features coincide where the current block bounding faults root on the S. It is also clear that the high amplitude swathe running WNW-ESE coincides with the 'saddle' and associated basement windows. A distinctive amplitude pattern (Figure 4.21) also signifies where the Moho intersects the S, i.e., where the breakaway fault cuts down to

mantle coupling crustal extension and brittle deformation at mantle level.

Lineations trending E-W to WNW-ESE on both maps (Figures 4.8 and 4.20) are clearly in the hanging wall of the landward fault and are aligned perpendicular to fault strike providing evidence that they are slip indicators on a detachment surface and can be considered corrugations similar to those seen on other faults (Cann et al., 1997; Resor and Meer, 2009; Edwards et al., 2018). The amplitude maps of the top acoustic basement Figure 4.18 where this surface consists of faults shows further lineations interpreted as corrugations on a slip surface, providing further evidence that S is a slip plane: corrugations on S have the same orientation and coincide spatially with those on the faults. This is especially the case for F6.0 where the corrugations are an up-dip continuation of those on S. Given that S is demonstrated to be a slip surface, faults that connect with S can also the expected to be slipping with S forming part of that slip plane.

The alignment of corrugations on the S Reflector and F6.0 suggests a single genesis: either S forms as the lower portion of a fault as it propagates down-dip from within the acoustic basement, suggesting that faults are initiating and propagating within the basement. Alternatively, the faults are propagating upwards from S. The latter suggests fault nucleation occurs within the mantle or at a continental crust-mantle interface. Importantly, the structures seen on S and the faults are the same but derive from the interpretation of different surfaces.

The intersection of the current block bounding faults with S maps as relatively simple lines with occasional changes in orientation, or as jogs that may have resulted from fault linkage (see Section 2.8). Generally, in the east and north of the volume the fault-S intersections trend N-S whereas in the south and west they trend more NE-SW.

To assess the influence on basement thickness in producing the amplitude variations, the amplitude of the trace envelope was plotted against basement thickness. Basement thickness was calculated by subtracting the depth-converted top acoustic basement depth from depth-converted S depth (the dataset used the less extensive amplitude map shown in Figure 4.8 to avoid the very high amplitudes shown in Figure 4.21). The resulting Figure 4.22 shows a point cloud with a skewed normal distribution with a number of peaks. The skew suggests that thicker continental crust (higher than 9 km) has low amplitude (less than lower quartile)

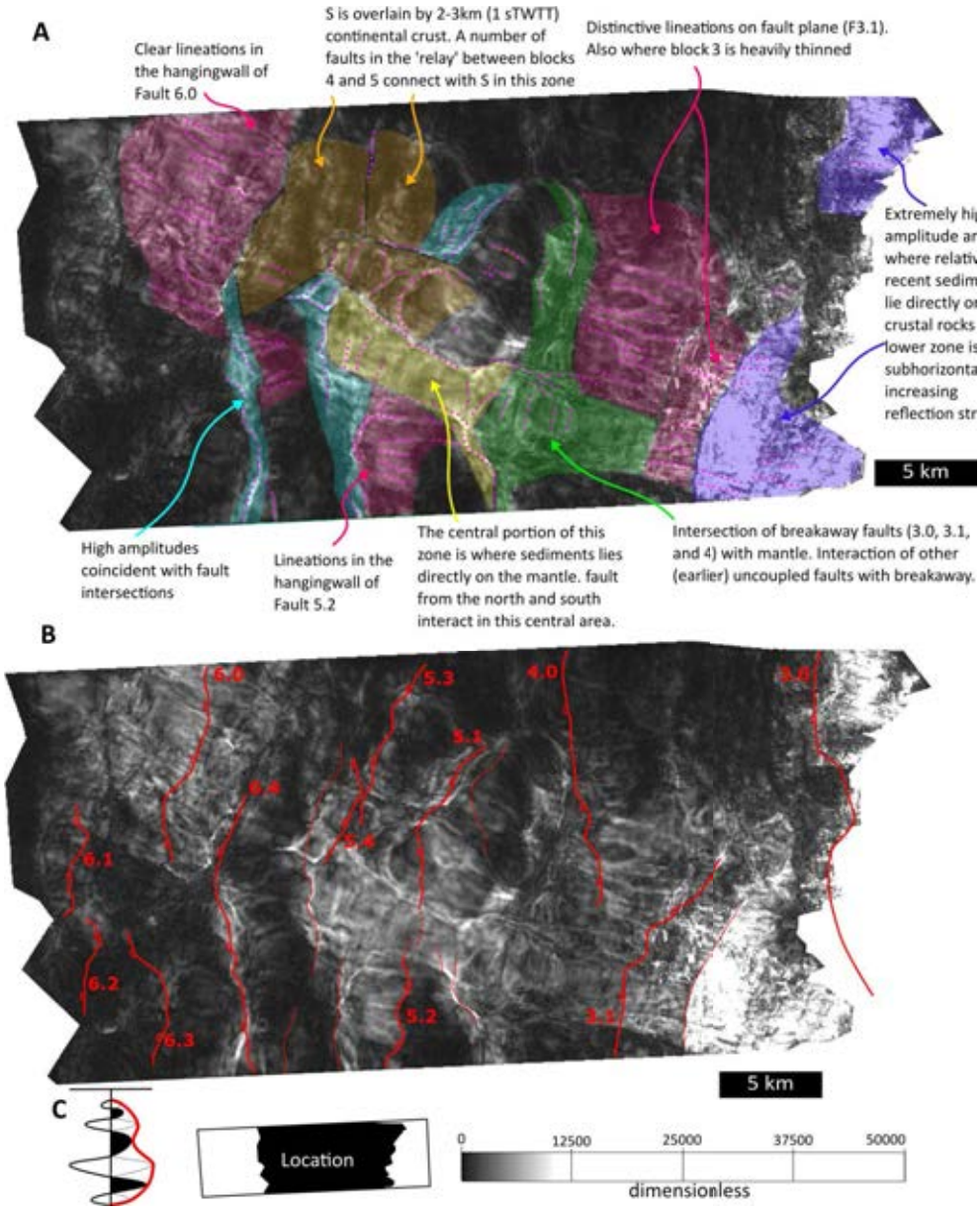

Figure 4.21: *Structural analysis of the S reflector and breakaway faults. A: Zoned maps of distinctive amplitude patterns and lineations with annotations relating to observations from the 3D data volume. B: Amplitude map of S Reflector and breakaway faults showing intersections of block bounding faults. C: Diagrammatic representation of trace envelope function (see also Figure 3.7) that produces the amplitude map (Taner et al., 1979).Location map shows position in dataset, see Figure 3.3.*

.

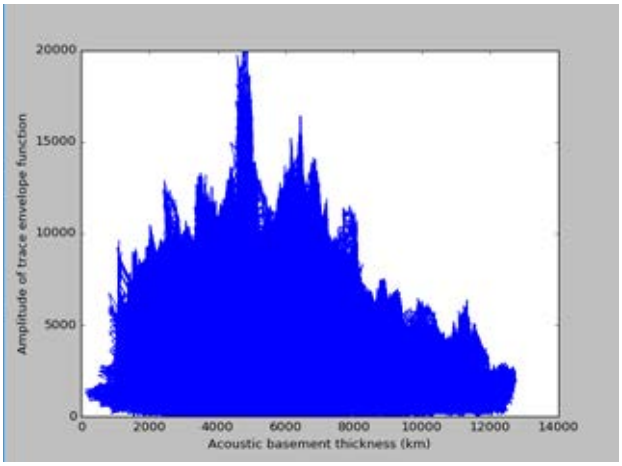

Figure 4.22: *Point cloud plot of acoustic basement thickness versus trace envelope amplitude of the S reflector*

4.2.5 Summary

Interpretation of the 3D volume has allowed these features to be mapped and has revealed the complexity of fault linkage both laterally and vertically (up and down dip). This understanding of the nature of fault linkage in the hyperextended zone is an important aspect of the work presented here, as previous studies based on 2D data envisaged laterally extensive faults and fault blocks (e.g. Lavier and Manatschal, 2006) during the later stages of rifting and break-up. Furthermore, the variation in trend along strike reveals the limitations of 2D models of break-up especially where these are based on 2D geometries. Where not discussed the length (along strike) of the fault scarps cannot be provided as they extend out of the data volume.

4.3 Restoration

Two 2D line restorations (Figures 4.23 and 4.24) have been undertaken on an arcuate arbitrary line that follows the tectonic transport direction determined from the slip indicators seen on the S reflector and faults that make-up top acoustic basement (Figures 4.20 and 4.18). This arbitrary line is in the north of the data volume approximately along the line of 2D pre-stack depth migrated line IAM11 (see Figure 3.10 and Ranero and Pérez-Gussinyé 2010). Restorations were undertaken with the most distal block being restored first and then working landward block by block, thus invoking the migrating fault models (Figure 2.8), and in line with the current paradigm that deformation moves oceanward. The first restoration (Figure 4.23) used a basic method ((Section 3.3) of jigsaw fitting the different tilted blocks. The blocks are treated as rigid objects, i.e. without any attempt to restore an internal sub-seismic faulting or ductile deformation bought about by, for example, cataclastic flow (Rutter, 1986). The initial stages of restoration in Figure 4.23 show this initial interpretation (A), the removal of water and post-rift sediments and the subsequent isostatic readjustment (B), and the removal of the syn-rift sediments for B7 and the subsequent isostatic readjustment (C). This latter step provides a surface displacement surface that is straighter between the fault (F6.0) and the top of the mantle (S reflector), highlighting the that these are the same slip surface and suggesting that (at least in places) S is the lower portions of slip surfaces. Figure 4.23D shows B7 restored on F6.0 to top basement level and the syn-rift removed on the other fault blocks producing a slightly accentuated topography on the top of the mantle (S reflector). Figure 4.23E-F show restoration of the subsequent blocks (B5, B4 and B3) to the top basement level. Once all the blocks have been restored (F), the geometries of lower surfaces of the blocks mean that there is still considerable space within the restored basement. Further, slight rotation of the blocks to allow some overlap that can be considered represent the sub-seismic or cataclastic flow within the blocks provides a much closed fit and balances out the remaining space. Given the hyperextended nature of the data, even a basic rigid block restoration produces a consistently thick, approximately 7 km, crust with some 'initial' topography.

Figure 4.24 uses a an algorithm to bend the mantle below the the tilted block before each stage of restoration in order to create geometries at the base of the crust similar to those proposed by migrating fault models, specifically those produced by the rolling hinge of Choi et al. (2013). The initial interpretation and first two restoration steps (A and B) are the same as Figure 4.23. Step 3 (Figure 4.24C) shows the mantle and lower portion of the footwall of F6.0. The subsequent of step of the restoration (D) shows restoration of Block 4 and rolling hinge offset landward (to the east) to align with F5.1. The final stage including a small amount of overlap to reduce space between the blocks (to account for an element of cataclastic flow). The final restoration on F3.0 used the *fault parallel flow* (see Egan et al., 1997; Kane et al., 1997) algorithm to recognise an element of intra-block deformation through movement on the rolling hinge. A numerical rolling hinge model of Choi et al. (2013) is shown as comparison in inset F. Inset G shows the location of the arbitrary line (also used in Figure 4.23) and IAM11.

As with Figure 4.23 the final stage of Figure 4.24 shows a consistently thick crust with a small amount of topography, which either reflects the uncertainties in the restoration or highlights that the this approximately 7 km thick crust has already undergone significant thinning (extension). Figures 4.23 and 4.24 show that even relatively simple methods can be used to sequentially restore the complex geometries, especially if a rolling hinge model is invoked and only a small amount of internal block deformation is assumed. This restoration is along the line of IAM11 which was forward modelled by Ranero and Pérez-Gussinyé (2010) to fit the interpretation of the 2D pre-stack depth migrated line.

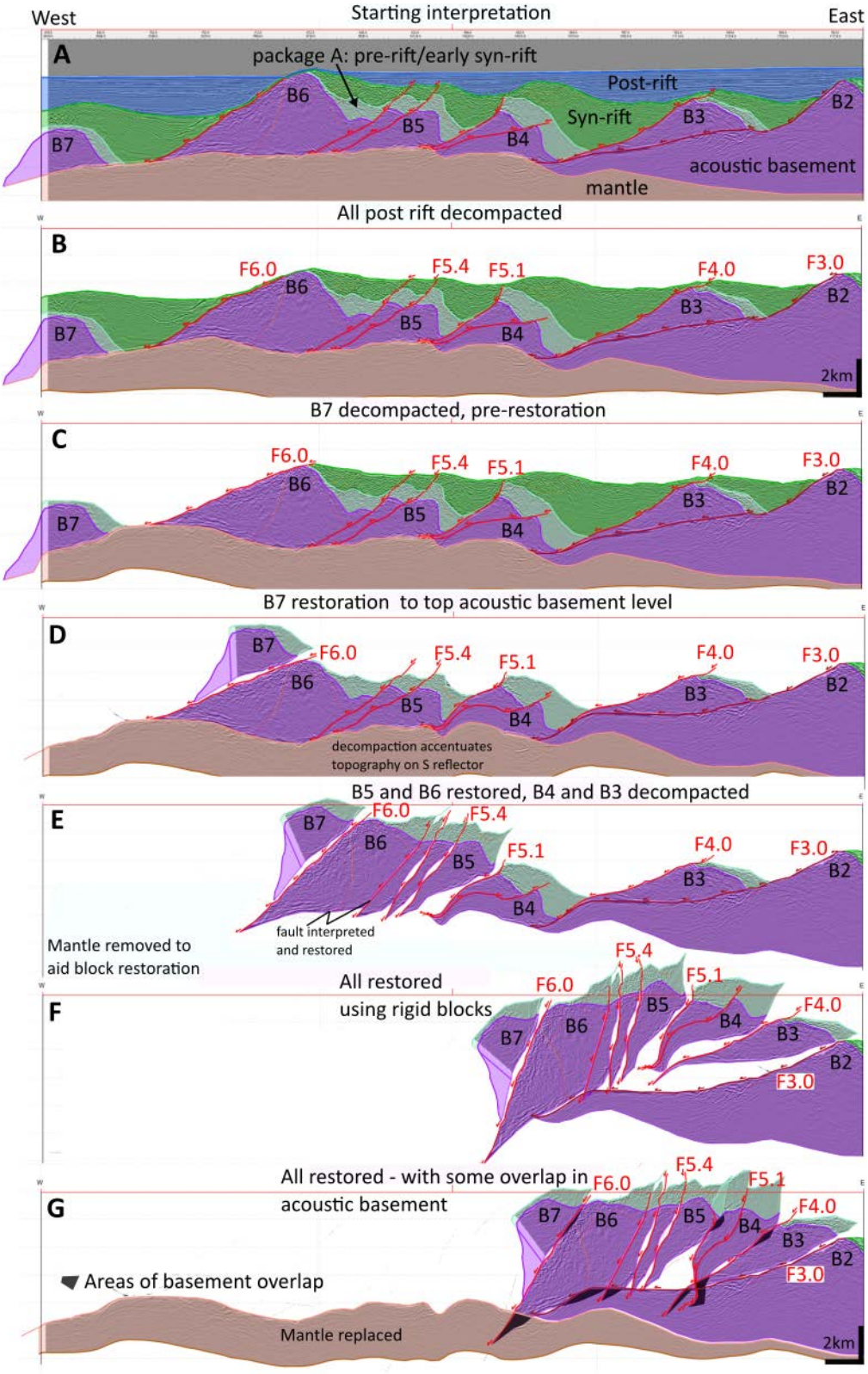

Figure 4.23: *2D rigid block restoration*

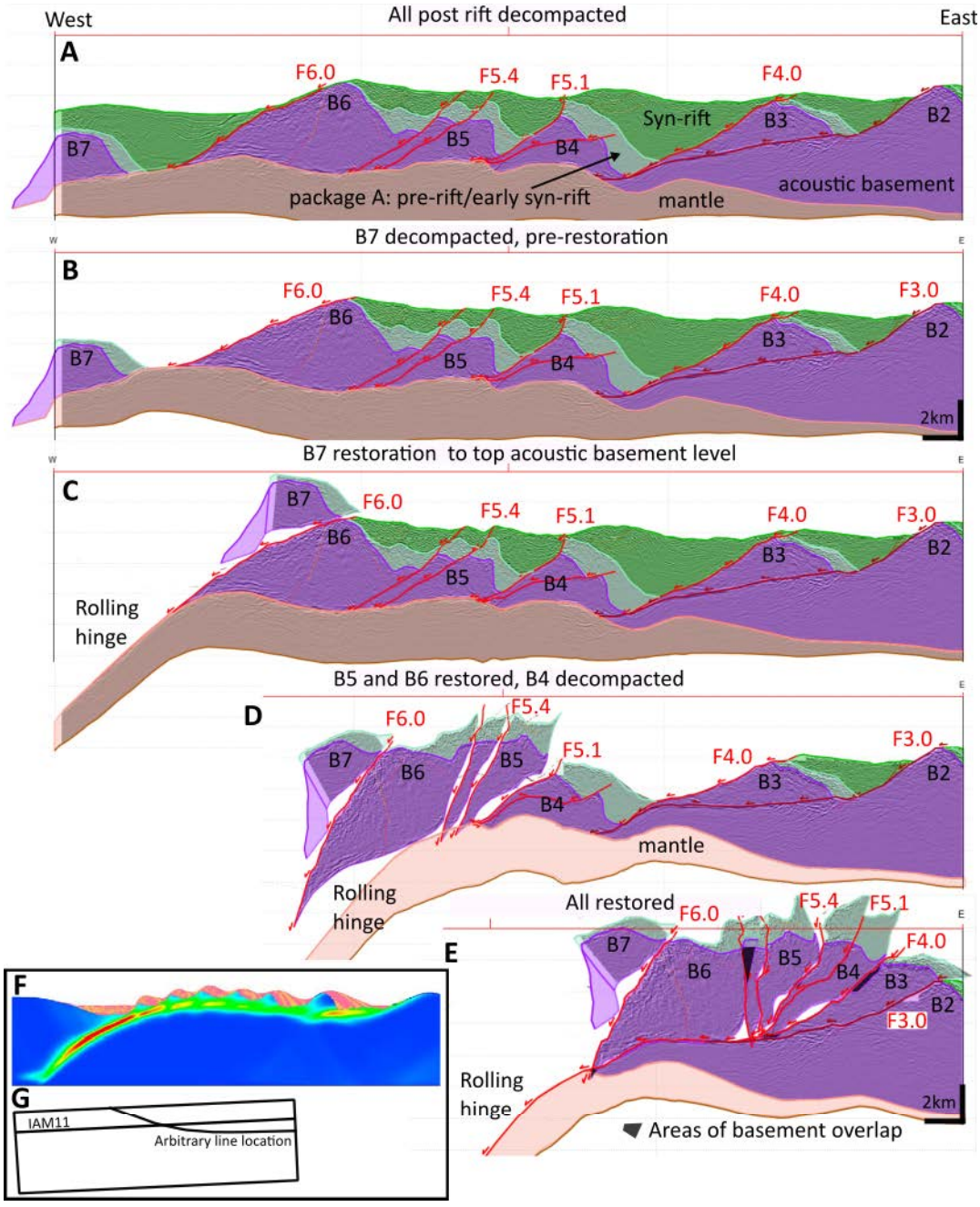

Figure 4.24: *2D rolling hinge style restoration. A-E shows restoration steps. F shows rolling hinge of Choi et al. (2013) for reference, G shows arbitrary line and line of IAM11 within the dataset.*

Chapter 5

Pre and Syn-rift Sediments

The 3D volume allows horizons within the syn-rift packages to be mapped out. Three main packages (A, B and C, see Section 4.2.2) within the syn-rift can be determined using a combination of seismic stratigraphy and the geometric relationships of the reflectors.

5.1 Time structure of the syn-rift

Between the top of the package A horizon and the base post-rift unconformity many of the syn-rift sediments have reflectors that can be mapped out in the half-grabens in which they accumulated, however it is not possible to follow reflectors between half-grabens. The syn-rift sequences on top of B4 (in the hanging wall of F3.1 and F4.0) can be interpreted throughout the half-graben (See Figure 4.3). However, the linked nature of faulting between fault sets 5 and 6 have resulted in intense deformation within B5, and as such only the southern section of this half-graben (in the hanging wall of F5.1 and F5.2) has reflectors that can be mapped confidently over any lateral extent (Figure 4.2).

Where possible, syn-rifts sediments have been carefully interpreted and mapped on every fifth inline and fifth crossline, creating a 125m x 125 grid (see Section 3.2.1), occasionally, for instance across intra-block faults, interpretation was undertaken every line. These horizons were mapped in order to understand the relative motions of the underlying faults that formed the

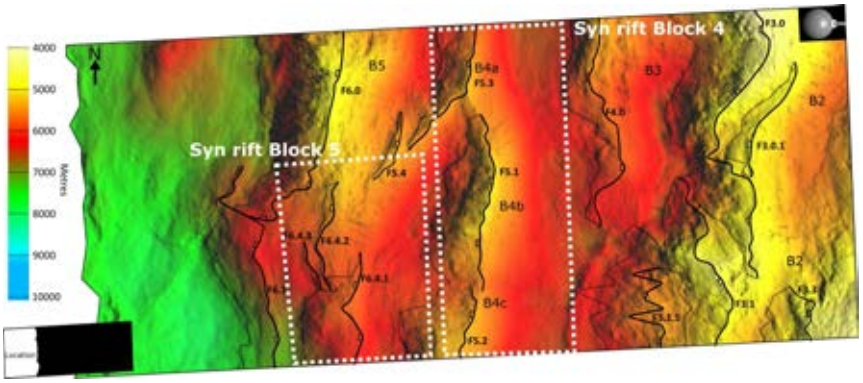

Figure 5.1: *Location of the half-graben basins within each block (B) and their relation to faults (F) on the base post-rift horizon. Areas used for analysis of the syn-rift sediments are shown by white dashed rectangles: Block 4 is shown in Figures 5.3 and 5.6; Block 5 is shown in Figures 5.4 and 5.7. Surface originally shown as Figure 4.12. Location map shows position in dataset, see Figure 3.3.*

half-grabens. In addition this interpretation also mapped deformation from intra-block faults related to the motion of the main block bounding faults. As the sediments that produce the interpreted reflectors are syn-kinematic the faulting and folding is related to the adjacent faults their geometry may capture the development of the fault network.

Figure 5.1 shows how the dataset was divided in to blocks that are separated by fault sets, based on the original numbering of Ranero and Pérez-Gussinyé (2010). Figure 5.2 shows these horizons in a seismic section, and Figures 5.3 and 5.4 show the time structure maps for a number of horizons within B4 and B5, respectively (hanging wall of Faults 4.0/3.1 and hanging wall of Faults 5.1/5.2, respectively). These maps also show the fault polygon network that deforms these surfaces.

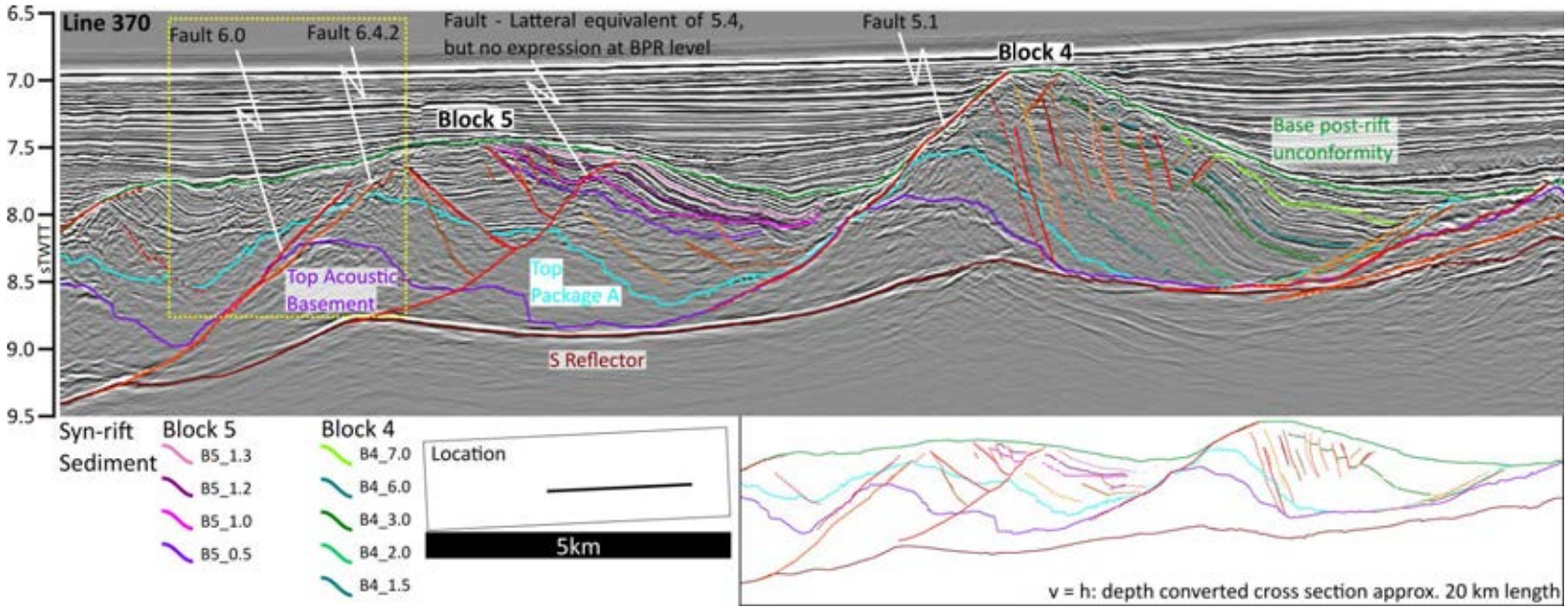

Figure 5.2: *Seismic section of line 370 that cuts through both sets of the mapped syn-rift sediments, Figures 5.3 and 5.4. Lower right panel is depth-converted section showing dips of faults. Location map shows position in dataset, see Figure 3.3.*

Block 4 - Figure 5.3

Considering the time structure of the syn-rift horizons on B4 a monoclinal, structure can be seen which dips steeply to the east, with reflectors at the top of the block (west) and in the direct hanging wall off Fault 4.0 / 3.1 (east) having lower dips. This pattern is consistent at all of the mapped syn-rift levels.

Faulting of the syn-rift horizons is focused in two areas. In the south regularly spaced (0.5 - 1 km) N-S antithetic faults dipping 70-80° to the east, which appear to be more abundant and more laterally pervasive in the mid to late syn-rift (horizons B4-H3.0 and B4-H6.0). This more abundant and pervasive nature may be partly due to difficulty in interpreting faults in the deep syn-rift's less reflective packages. Alternatively this faulting maybe accommodated partly by inter-layer slip of the deep syn-rift where the reflectors (strata) are steep and therefore the faults may be bed-parallel, on weak layers. Such slip is noted on the top of Package A horizon on various parts of the 3D volume. The top syn-rift horizon (B4-H7.0) onlaps across faults rather than be offset by them, is also seen on the base post-rift unconformity. This suggests that this distributed antithetic faulting formed toward the end of the deposition of the syn-rift sediments.

Block 5 - Figure 5.4

The four mapped syn-rift horizons in B5 show a consistent dip to the ESE in the south of the half-graben and toward the SE in the north. In the very south of the there are distinctive synclines in the earliest syn-rift (horizon B5-H0.5) and also in the latest (B5-H1.3).

An important feature on all four maps is the presence of the west dipping (synthetic to block bounding faults) F5.0, that links laterally to F5.4, but is not expressed at the base post-rift unconformity and therefore not mapped as the most recent set of faulting. It is worth noting that the offset on F5.0 is limited. Other faults that cut the mapped syn- rift horizons are all antithetic and often link to F5.0 at depth. The dip of the faults is c. 55-70° (to the east), lower than in B4. All faults trend between N-S and NNE-SSW. Faulting clearly reduces as the horizons become younger - indicating that deformation is reducing over time, or that the deformation is propagating up from depth.

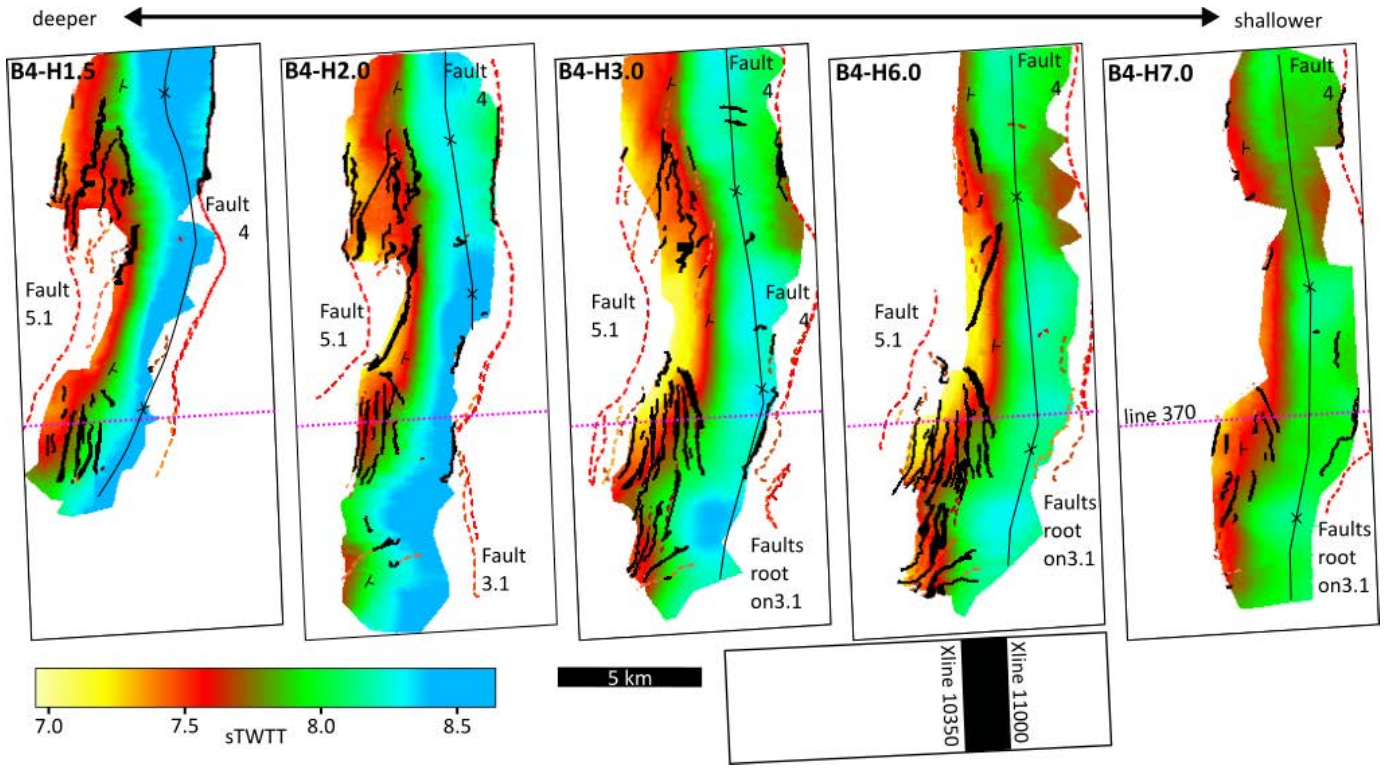

Figure 5.3: *Time structure maps of syn-rift horizons in Block 4, black polygons indicate fault offsets. Location map shows position in dataset, see Figure 3.3.*

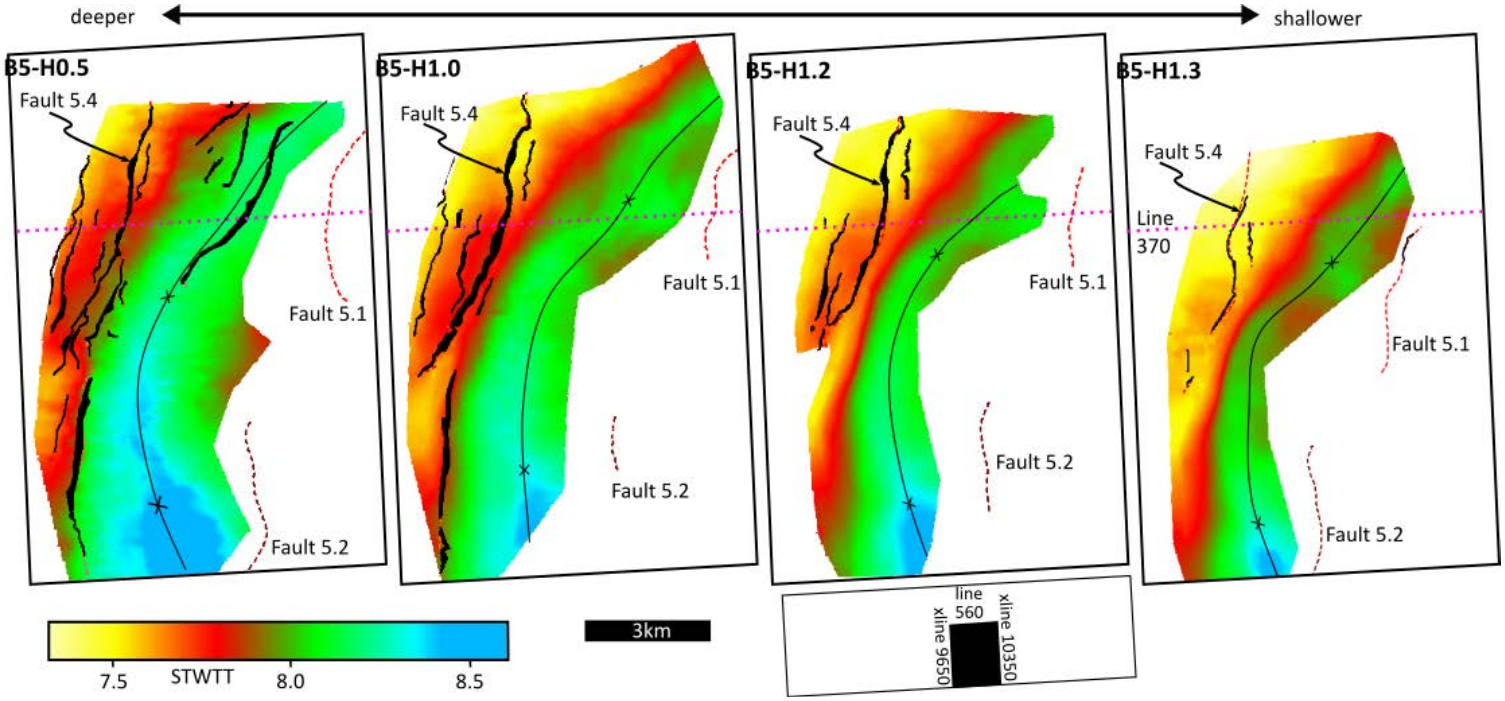

Figure 5.4: *Time structure maps of syn-rift horizons in Block 5, black polygons indicate fault offsets. Location map shows position in dataset, see Figure 3.3.*

In summary:

- The dips of the strata (reflectors) in Block 4 is steeper than Block 5 and is more monoclinic than synclinal.
- The dip of faults are steeper in Block 4 than Block 5
- The interaction (deformation) if the sediment with the underlying fault

5.2 Syn-rift isopach maps

Syn-rift sediment thickness (isopach) maps can provide evidence of the growth and kinematics of faults (see, for example Jackson et al. (2017) and Section 2.20). Figure 5.5 shows two isopachs. The first for the pre-rift to early syn-rift package A and the second for the later syn-rift packages B and C. Looking at the depth of sediment accumulation at different time periods may provide evidence of the nature of the fault growth. The fault network shown in Figure 5.5 is taken from that expressed at the top of the top of package A (Figure 4.16).

Considering first the isopach maps for the whole syn-rift (Figure 5.5) the early syn-rift (package A) has the three linked depocentres with 2500-3000 m of sediments. These depocentres are form part of B4 and were formed by accommodation space generated by displacement on F4.0 in the north and F3.1 (F3.1.5, is a small fault splaying off F3.1 within the syn-rift) in the south. Even at this early stage the faults are linked with a recognisable depocentre extending out of the data to the south. Later syn-rift (packages B and C) show that the three depocentres become more linked as fault displacement increases, as shown by a large dominant depocentre in the south. A similar pattern is followed by the syn-rift sediments on B5: linked depocentres in the early syn-rift that become more extensive in the late syn-rift, however the depth and width of the depocentres in smaller and reflects the more limited displacement seen on fault set 5. Isopachs in the hangingwall of fault set 6 show a more distal depocentre in the early syn-rift followed by one closer to the fault cutoff. This pattern of isopach development suggests that coherent faults within each set that gradually accumulate displacement with greater sediment accumulation in

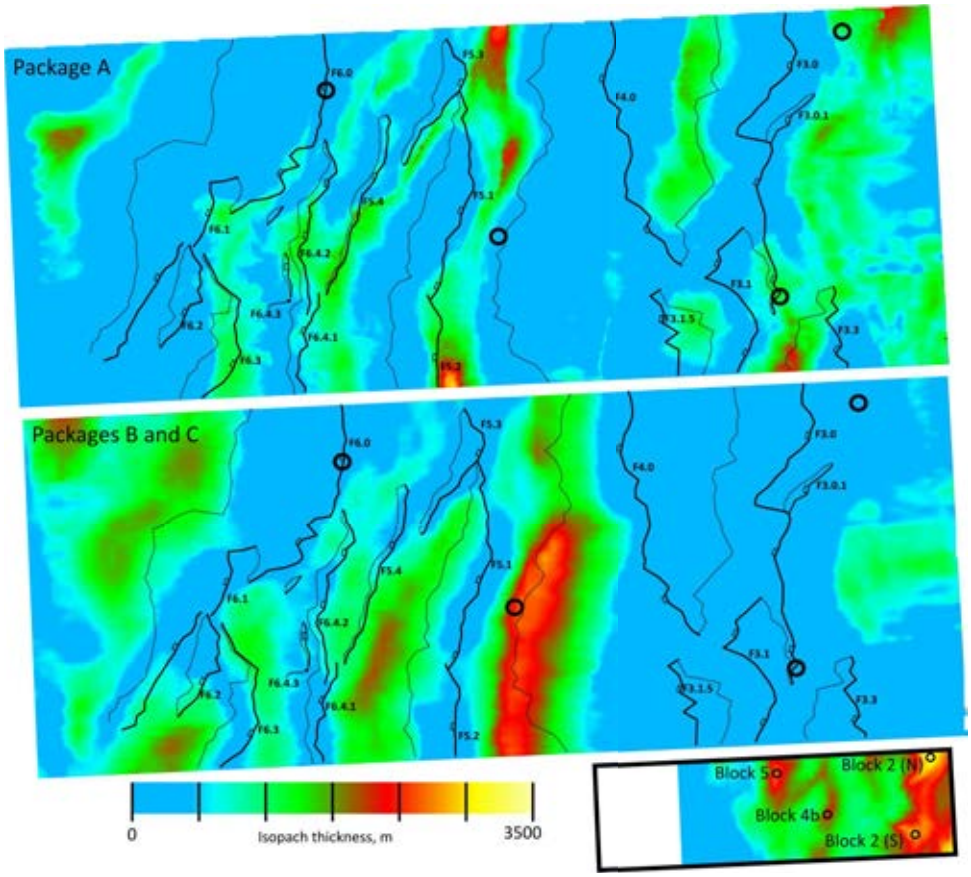

Figure 5.5: *Isopach maps of pre-rift/early syn-rift, package A and of later syn-rift packages B and C. Fault network is also shown.Location map shows position in dataset, see Figure 3.3.*

the south. The more detailed analysis of the syn-rift seen in B4 and B5 (Figures 5.3-5.7) highlight the folded nature of the sediments within packages B and C and also highlights the linkage of depocentres that concentrate sediment in the south.

In addition to mapping out syn-rift horizons in B4 and B5 (Figures 5.3 and 5.4), Isopachs were also generated using a constant velocity of 3750 m/s used in the depth conversion (see Table 3.3). The resulting Isopach maps are shown in Figures 5.6 and 5.7 for B4 and B5, respectively.

Block 4 Isopachs - Figure 5.6

Working from the early to late syn-rift a number of interesting features are revealed. The earliest syn-rift shows two isolated depocentres (a and b) both with depths of approximately 1000m. The largest is in the centre of the half-graben at the southern end of F4 (close to where F4.0 merges with F3.1, see Figure 5.3) and the smaller one in the north. Moving up through the syn-rifts

these depocentres grow and and become deeper (c and d) and by isopach B4-H3.0 - B4-H2.0 the northern depocentre is no longer as deep whereas the central one (e) is much more extensive and is still over 700 m thick for an area 30 km long and c. 6 km wide. The two latest syn-rift isopachs are much thinner with the depocentres much more isolated but still up to 700 thick (g). Isopach BPR - B4-H7.0 shows two isolated depocentres (h and i) that appear to lie in 'jogs' in the basement geometry. The main sediment accumulations appear in the centre and south of the graben.

Block 5 Isopachs - Figure 5.7

Working from early to late syn-rift - a wide early depocentre can be recognised that is up to 1000 m thick. There appears to be a slight segmentation between the very west of the mapped Isopach (a and c) and the central portion (b and d), which is where F5.1 and F5.2 link. Moving to the later syn-rift a curved (concave to east) depocentre (e and f) that is relatively thin (max 500 m). By the latest syn-rift the depocentre has moved to the east of the mapped area next to F5.2 and is 700 m thick (g).

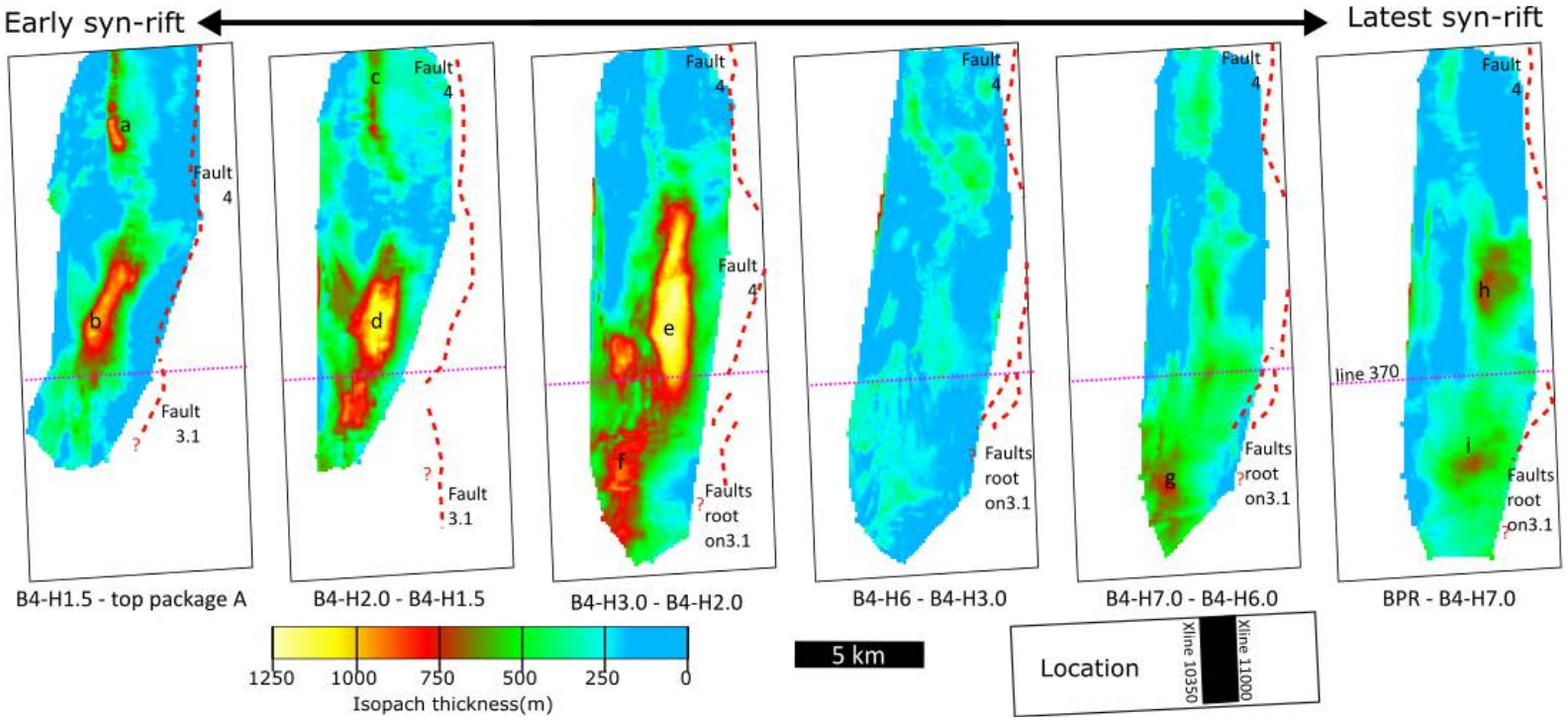

Figure 5.6: *Isopachs showing the development sediment thickness between 5 horizons interpreted in Block 4 revealing the accommodation space provided by displacement on block bounding faults. The red '?' indicates that the fault does not stop, rather the isopach data make it difficult to map any further. Location map shows position in dataset, see Figure 3.3.*

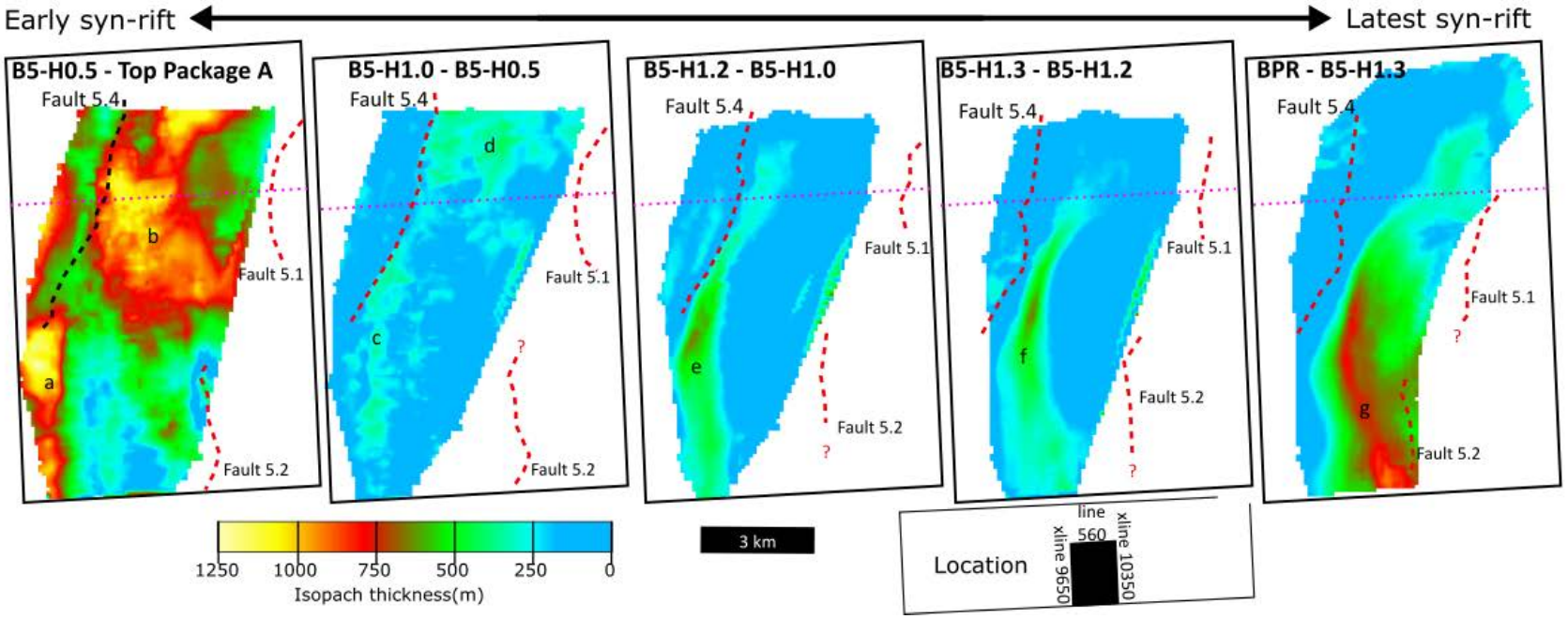

Figure 5.7: *Isopachs showing the development sediment thickness between 5 horizons interpreted in Block 5 revealing the accommodation space provided by displacement on block bounding faults.The red '?' indicates that the fault does not stop, rather the isopach data make it difficult to map any further. Location map shows position in dataset, see Figure 3.3.*

5.3 Angles of the syn-rift deposits

Assuming that the block-bounding faults and S reflector act as a slip surface, the angles of the syn-rift units can be used to established the angles of slip on S, which is important in determining the mechanism of final break-up (Section 2.5). Figure 5.8 (Lymer et al., 2018, submitted) shows the measured dips of the angles of the syn-rift in relation to the S reflector and the fault that slipped and provided the accommodation space for the syn-rift to form. Figure 5.9 shows the geometric methods used to to determine angles. It can be seen that S can be considered to have commenced slipping at 32°- 37° and ceased slipping at 20°- 26°, the faults are calculated to have ceased slipping at at 38°- 45°.

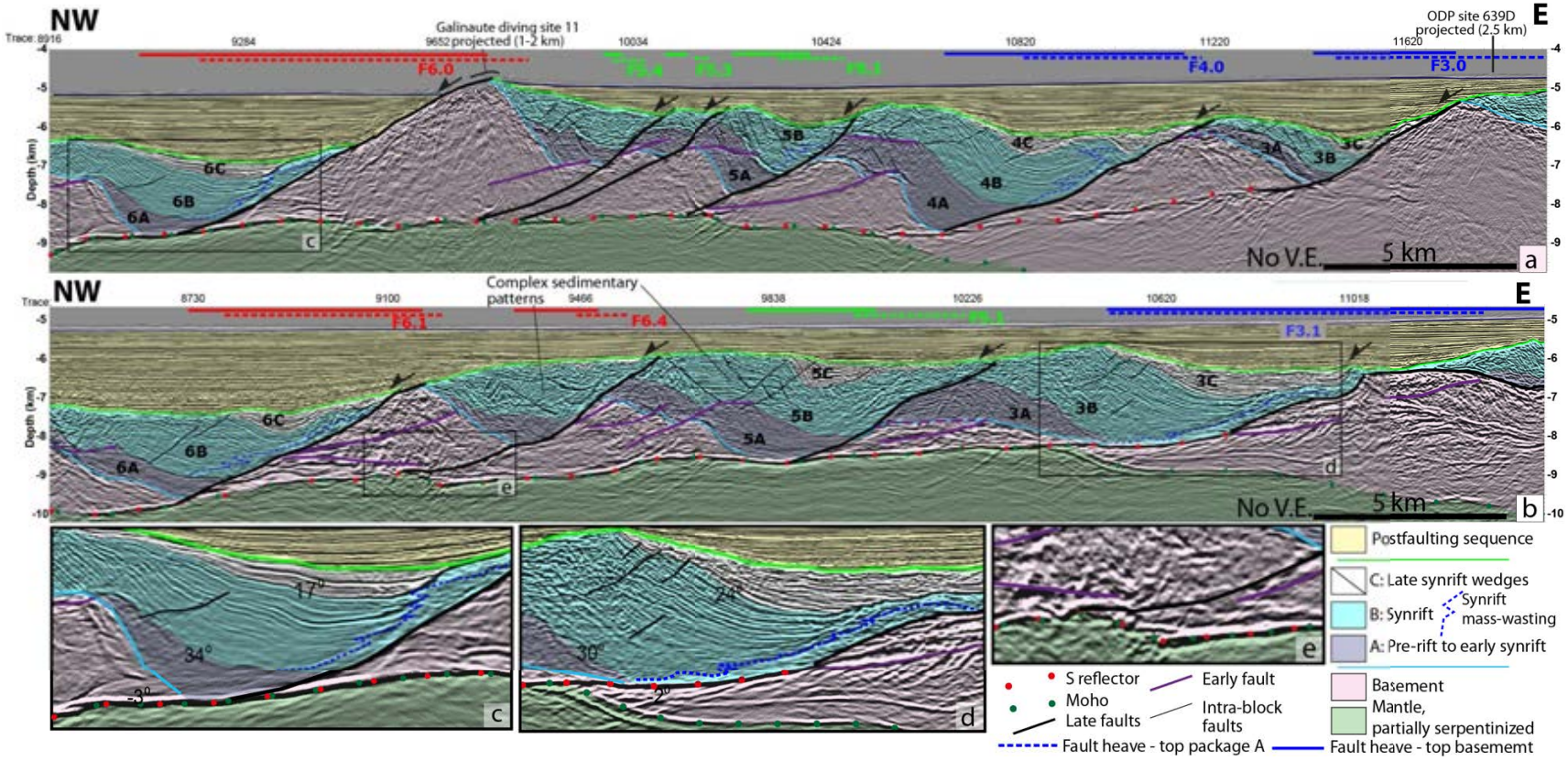

Figure 5.8: *Two depth sections (a and b) showing angles measured on syn-rift for two faults (c and d). Sections are arbitrary lines shown in black in Figure 6.1*

Fig 4C

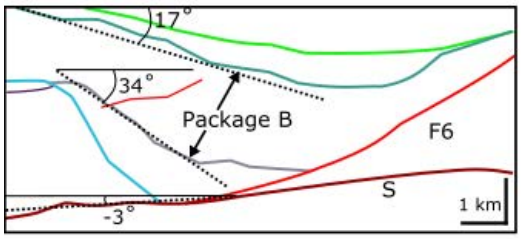

Rotate base package B to horizontal to give **dip of S** at commencement of slip on F6 and correlative portion of S
= -34° + (-3°) = -37° (37°west).

Rotate top package B to horizontal to give **dip of S** at cessation of slip on F6 and correlative portion of S
=-17°+ (-3°) = -20° (20°west)

NB: Positive angles to east, negative to west

Fig 4D

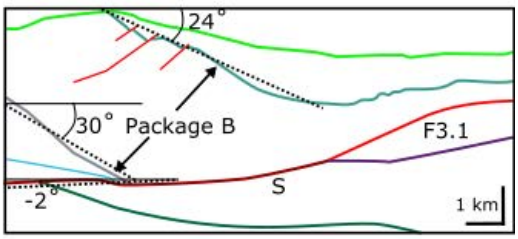

Rotate base package B to horizontal to give **dip of S** at commencement of slip on F3.1 and correlative portion of S
= -30° + (-2°) = -32° (32°west).

Rotate top package B to horizontal to give **dip of S** at cessation of slip on F3.1 and correlative portion of S
=-24°+ (-2°) = -26° (26°west)

Alternative method

Cessation of slip on F6, top package B horizontal: S at 20°, F6 at 38°

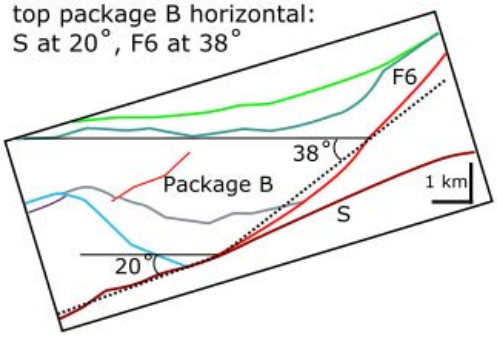

Cessation of slip on F3.1, top package B horizontal: S at 26°, F3.1 at 45°

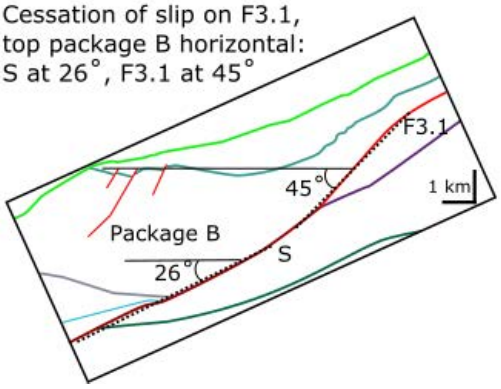

Figure 5.9: *Method used to determine angles of slip on S and faults using syn-rift sediments*

5.4 Discussion of syn-rift

Explanations for the monoclinal structure of the syn-rift in Block 4 (Figure 5.3) include a roll over anticline, however, this does not necessarily explain the flattening of strata (reflectors) near the fault which has provided the accommodation space in which the sediments have been deposited. Fault drag does not seem appropriate at the scale of the observations being made or the degree of overstep between the Faults 4.0 and 3.0/3.1 (Childs et al., 2016). Another possibility is that the low-dip strata near the fault, if rotated anticlockwise, as if the movement of the underlying fault was being restored, would dip in the same direction and the fault and curve convex toward the fault - suggestive of a fault propagation fold as described by Jackson et al. (2006), for example. The steep dips on the monocline therefore representing the original horizontal surface of deposition. A similar argument would also account for the syncline seen in Block 5. However, the more *en échelon* nature of fault set 5 may result in a hanging wall monocline if the original fault segments were seen to under step (Childs et al., 2016).

5.5 Summary of observation and analysis

Figure 5.10 shows a 3D block diagram from the seismic volume highlighting the main interpretations and observations outlines in this chapter:

- Fault sets form geometrically connected networks suggesting kinematic linkage for at least part of the growth and evolution
- The fault networks vary laterally
- The S reflector is slip surface (detachment fault) that connect to slip of faults to dissect the crust
- S slipped at 20-26° and faults slipped at 28-45° (Lymer et al., 2018)
- Isopachs suggest that linked faults with discrete depocentres of sediment accumulation evolved over time an migrated toward the hangingwall fault.

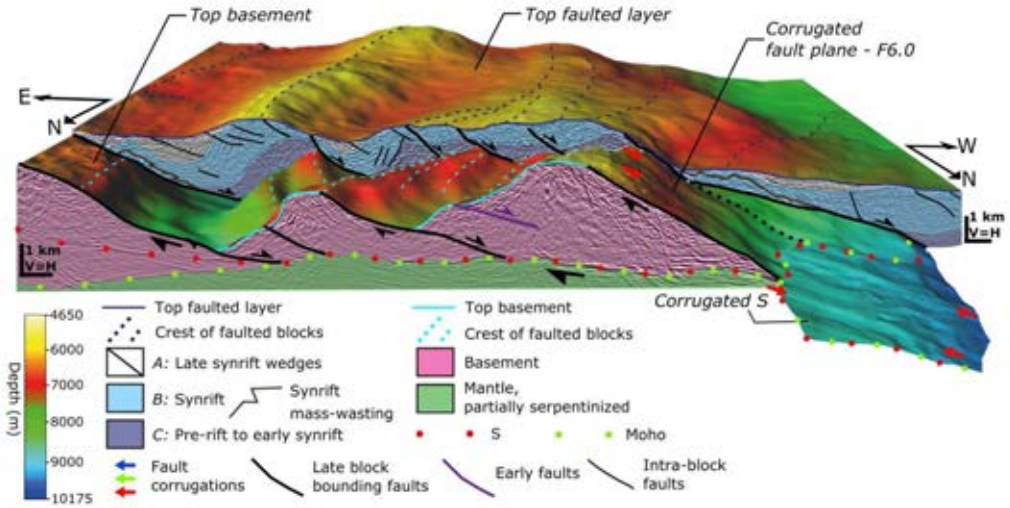

Figure 5.10: *Block figure showing the key observations from interpretation of the surfaces and faults within 3D Galicia seismic volume. Note view is looking south. Top faulted layer is equivalent to base post-rift.*

Chapter 6

3D Fault Analysis

Similar techniques to those used to understand fault growth in less extended basins have been employed to determine the development of faults on the hyperextended Galician margin. A 3D study of fault displacements has never been undertaken on a hyperextended margin and this study will highlight how faults interact both along strike, perpendicular to strike, in the down dip direction, and with an underlying possible detachment fault. Taking the idea of fault growth into the hyperextended zone may shed new light onto the applicability of current models. It is worth noting that displacement backstripping (Chapman and Meneilly, 1991) (also see Section 2.8.4) commonly used in sedimentary basins (Jackson et al., 2017) was not used in this analysis. In sedimentary basins there is an almost an *a priori* assumption that basement is transferred up from deeper levels, on a hyperextended margin the structural level of fault initiation and maximum slip is uncertain. Therefore the displacement was simply plotted rather than subtracting displacement from a shallower horizon.

6.1 Fault heave analysis

Displacement measured on adjacent faults can be used to determine the amount of thinning or extension of the crust (see, for example Davis and Kusznir, 2004; Reston and McDermott, 2014; Walsh and Watterson, 1992; Jackson and Rotevatn, 2013, and Section 2.6). Additionally,

and especially pertinent when considering the use of a 3D seismic reflection data, measuring displacement indicates how faults interact spatially either along strike or in the tectonic transport direction. Furthermore, the changes in displacement at different structural levels within the data can indicate the temporal evolution and kinematics of the tectonic deformation occurring (see Section 2.8).

On the hyperextended portion of the Galicia margin which is covered by the 3D dataset, the most revealing measurement of deformation within the continental crust is fault heave. Although fault throw is often used to measure fault displacement and analyse fault interaction, where the analysis is focused on determining the amount of extension, throw is not a relevant measurement. Measuring heave allows for a direct measure of the amount of extension that has taken place.

Fault heaves were measured by interpreting both hangingwall and footwall cut offs (Section 3.2.2) on three structurally significant interpreted horizons:

- top acoustic basement level (see Section 4.2.3 and Figure 4.17)
- the top of 'Package A' described (Chapter 5 and Figure 4.16)
- the top of the syn-rift sediments on the base post-rift unconformity (see Section 4.2.1 and Figure 4.12)

These heave measurements were performed on the present day block-bounding faults interpreted to be the last generation of faulting. The most recent large offset faults have resulted in the current passive margin architecture. The most recent faults are interpreted as ones that show an offset at the base post-rift unconformity level. These most recent faults were also determined visually on seismic images as having significant offset and lateral extent within the 3D data.

Figures 4.17, 4.16 and 4.12 show a fault system that is somewhat more complex than simple, linear N-S trending blocks, especially if previous phases of faulting are considered (see Figure 4.10). The faults and fault blocks above S die out or merge laterally and extension is accommodated on a network of faults that interact (connect) both along strike and perpendicular to strike (Figure 5.10).

Figure 6.1 shows the lines within the data that were used to measure fault heave on the three interpreted horizons. To investigate the mechanism of break-up fault heaves were measured on an arcuate tectonic transport direction along arbitrary lines through the seismic dataset. These arbitrary lines followed the directions of the corrugations seen on the S reflector and shown in Figures 4.8, 4.17 and 4.20. These arbitrary lines are therefore parallel to the interpreted tectonic transport direction and approximately perpendicular to the faults, see inset rose diagram in Figure 6.1. Figure 6.2 shows the location of the mapped faults at each of three horizons on which the heave was measured.

The rationale for undertaking this heave analysis was in order to provide insight into the relative timings of motion on the faults and therefore the possible fault growth models that can be seen by the use of displacement profiles (Sections 2.8.2 and 2.8.4).

In addition to heaves measured along an arcuate transport direction, they were also measured in the inline direction. The results of these show a similar pattern however they provide a smaller heave, especially for 6.0 and other faults that trend more WNW-ESE. The results of these heave measurement are shown in Appendix I.

6.1.1 Heave at top acoustic basement

The easternmost fault set (closest to Iberia) consists of three directly linked faults (F3, F 3.1 and F4 - numbering after Ranero and Pérez-Gussinyé (2010) and one minor fault F3.2 (Figure 4.17). The blocks between F4 and F3 and between F3 and F3.1 pinch out southwards and northwards respectively: these faults are geometrically linked, the evolution of the faults as either coherent or isolated (Section 2.8) will be discussed in Section 7.5.

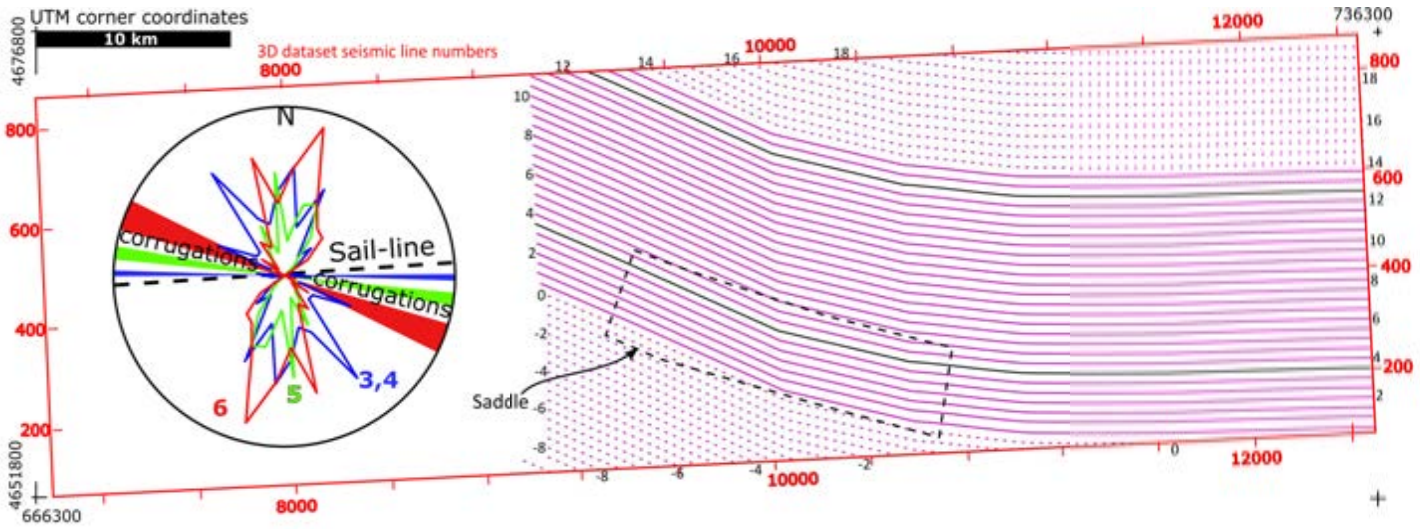

Figure 6.1: *Plan showing (pink) lines along which fault heave was measured. The lines are numbered according to the strike distance shown in Figures 6.3, 6.4, and 6.5. Broken lines indicate were only partial measurement was possible due to curved nature of the line, black lines refer to Figure 5.8*

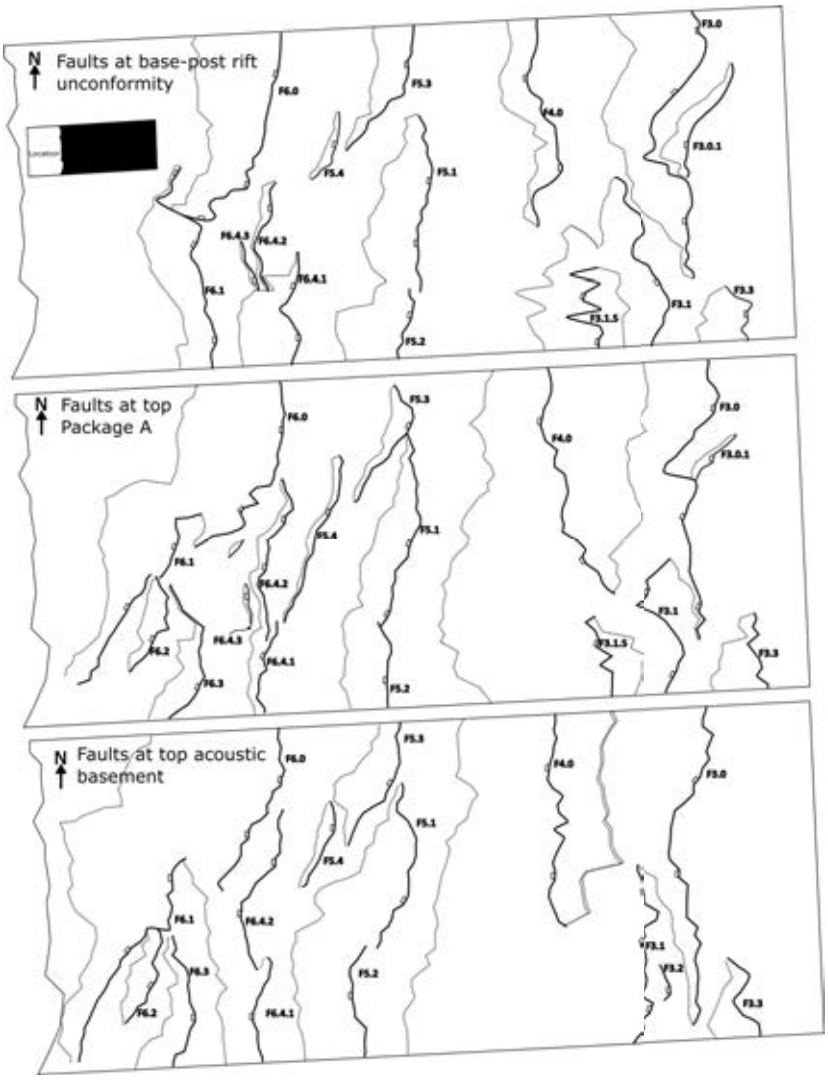

Figure 6.2: *Fault maps for each horizon on which faults were measured: base post-rift, Figure 6.5; top Package A, Figure 6.4; top acoustic basement, Figure 6.3. Inset shows location of map in dataset (Figure 3.3*

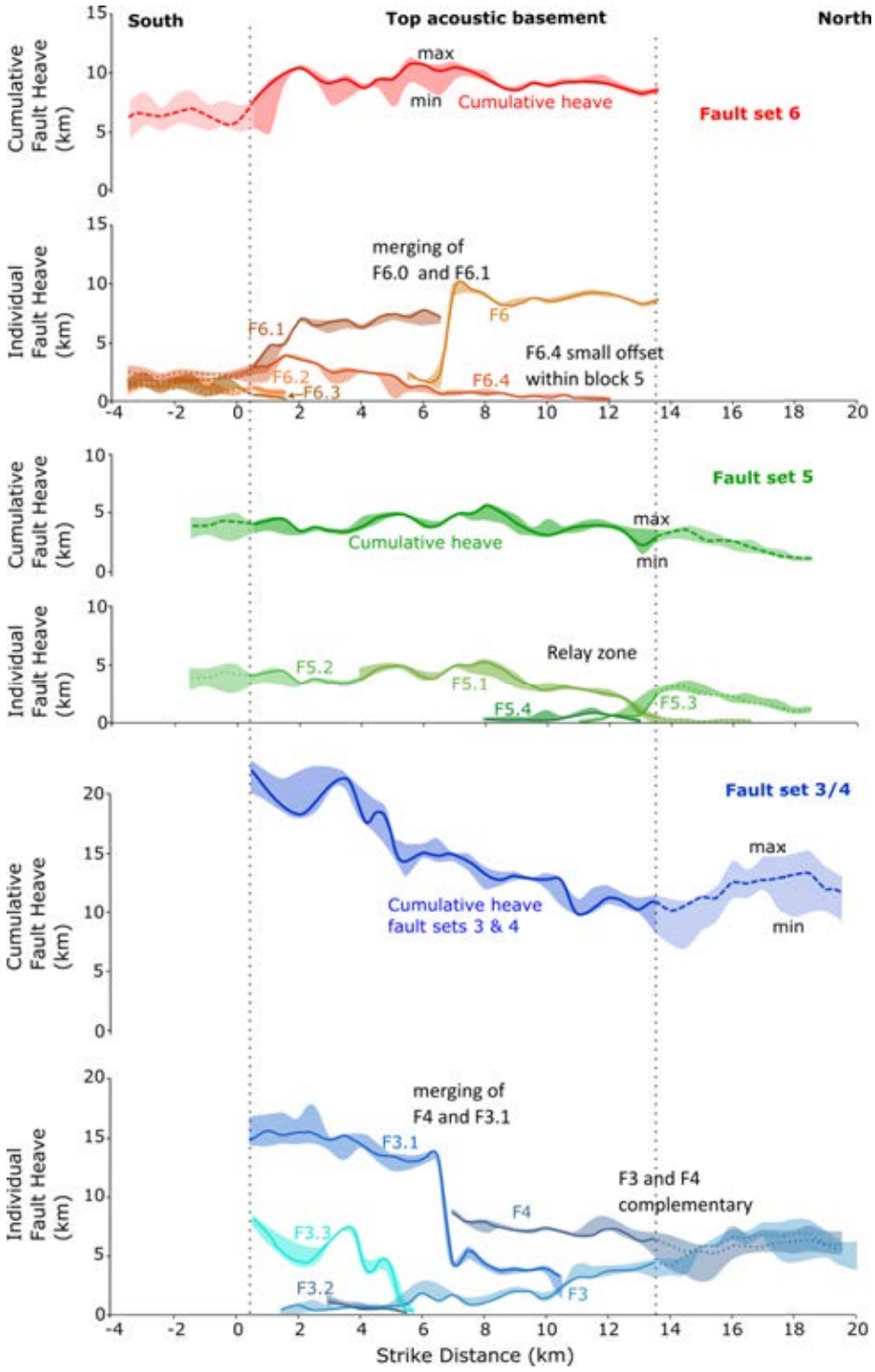

Figure 6.3: *Heaves measured at top acoustic basement level on an Arcuate tectonic transport direction (Figure 6.1). The shading gives uncertainty of heaves primarily from determining Footwall cutoffs (see Section 3.2.2, especially Figure 3.5). Vertical lines indicate where measurement was possible throughout the volume Figure 6.1.*

Fault set 3/4

Considering the measured heaves on these faults set 3-4 (Figure 6.3) it can be seen that as the heave on one fault decreases, it increases elsewhere. For example, at a strike distance of approximately 7 km, the heave on Fault 3.1 reduces drastically and suddenly by approximately 8 km (c. 60 percent from 13 km to 5 km); some of this extension is taken up by F3.0 as its heave increases gradually to the north from c. 2 km to 3 km over the space of 4 km strike distance, but this increase is insufficient to explain the reduction seen on F3.1. In the absence of any structure to account for this reduction in extension, it is necessary to invoke F4 as being part of the same phase of extension. Further than 7 km north it can be seen that as the heave on F4 gradually decreases, the heave on F3.0 gradually increases. Cumulative heave (shown with estimate of uncertainty) for fault set 3-4 remains steady, if decreasing from 15 km in the south to 12 km in the north. The geometrical linkages and the complementarity of the heaves (see Section 2.8, Figure 2.18VI) all indicate that F3, F3.1, F3.2 and F4 were active simultaneously, rather than sequentially (F3 then F4) as previously suggested on the basis of 2D data (Ranero and Pérez-Gussinyé, 2010).

It is necessary to note that *simultaneously* used here does not necessarily mean that faults were actively slipping at the same instant of time or same individual (a)seismic slip event, rather that, over a period of geological time there was an interplay of slip events on the complementary faults.

Fault set 5

Moving oceanward to Block 4, F5.1 marks the start of another fault set. Faults within this fault set, 5 (5.1, 5.2, 5.3, 5.4) strike NNE-SSW and are seen to directly link or geometrically interact and are *en echelon*. Faults set 5 also have complementary heaves maintaining a cumulative lateral displacement of approximately 4.5 km across the dataset with, again, a slight decrease to the north (Figure 4.17). The consistent heave and level of fault linkage lead to the interpretation of the faults being simultaneously active. Working from the south the heave on F5.2 is

directly transferred to F5.1 which reduces, at a strike distance of 8km, with the reduction in heave transferred to F5.4 and then 5.3. Cumulative heave remains steady across the volume. The relationships outlined for fault set 5 results in the same interpretation as for fault set 3-4: faults in this set were active simultaneously.

Fault set 6

Stepping oceanward once more; fault set 6 consists (F6.0, 6.1, 6.2, 6.3, 6.4) of laterally discontinuous faults that also trend NNE-SSW and are seen to link laterally (Figure 4.17). Figure 6.3, shows the heave on F6.1 increases by approximately 3 km between 2 and 6 km strike distance whilst the heave on F6.4 decreases by a similar amount, 3 km; these faults show complementary heaves indicating they were active at the same time. Where a 10 km heave on F6.0 stops abruptly at 6.5 km strike distance, the heave is transferred almost entirely onto F6.1; these faults show complementary heaves indicating they were active at the same time in order to ensure extension across the volume. Cumulative heave remains steady across the volume. Here again, it can be seen that the sum of the heaves remains approximately constant across the volume: as one fault dies out its displacement is transferred to neighbouring faults. Again this is interpreted as simultaneous slip on multiple faults.

Furthermore, the heave measurements highlight the presence of a fault that seems to link sets 5 and 6: fault 6.4 indicates that slip on each fault set may not itself be discrete but that there may be a period in the slip history where faults within different sets were moving (quasi)simultaneously as is seen in adjacent faults in currently tectonically active areas for either earthquakes or slow slip events (Stein, 1999; Peng and Gomberg, 2010).

The complementarity of faults heaves and the geometrical relationships of the faults at the top acoustic basement level demonstrate that extension of the pre-thinned continental crust above the S reflector migrated oceanward, but as sets of simultaneously active faults not as single sequential faults.

A further observation that the rapid reduction in heave of F6.0 and F3.1 occurs at the same place, 7 km strike distance (Figure 6.3). If it were not for the spatial distance between these

two faults there would be a strong case for complementarity. This 7 km point is also consistent with where the northward reduction in total cumulative heave begins, however this reduction is much less pronounced in any of the single fault set cumulative heaves. To add to these two observations on the heave plots the 7 km strike distance flow line lies through the centre of the 'saddle' (see Section 4.1.1). The saddle, the rapid reduction in fault heaves and the fact that only one major fault west of the breakaway faults (see Figure 4.17 cuts across the saddle (F6.4) suggests that there are two tectonic terranes, one to the NE of the saddle the other to the SW. F6.4 is itself made of parallel, linked fault strands (Section 4.2.3), that are seen as individual faults at higher structural levels.

6.1.2 Heave at top of package A

Heaves were also measured at the top of package A (Figure 4.16 and Figure 6.4). As package A is interpreted as being pre-rift to early syn-rift, west of Faults 3.0 and 3.1 and east of fault set 6 it is seen as a persistent negative polarity reflector that runs parallel to the interpreted top acoustic basement surface (see Figures 4.2 and 4.3). West of fault set 6, the top package A horizon can be interpreted but does not have the same distinctive seismic signature; see Chapter 5 for a discussion on this important marker horizon. This uncertainty means that the measurement of heave on this horizon on F6.0 and F6.1 would have a theoretical maximum that matches that of heave at top acoustic basement, however, for the sake of this analysis we have used the interpretation that the package does exist west of F6.0 and F6.1.

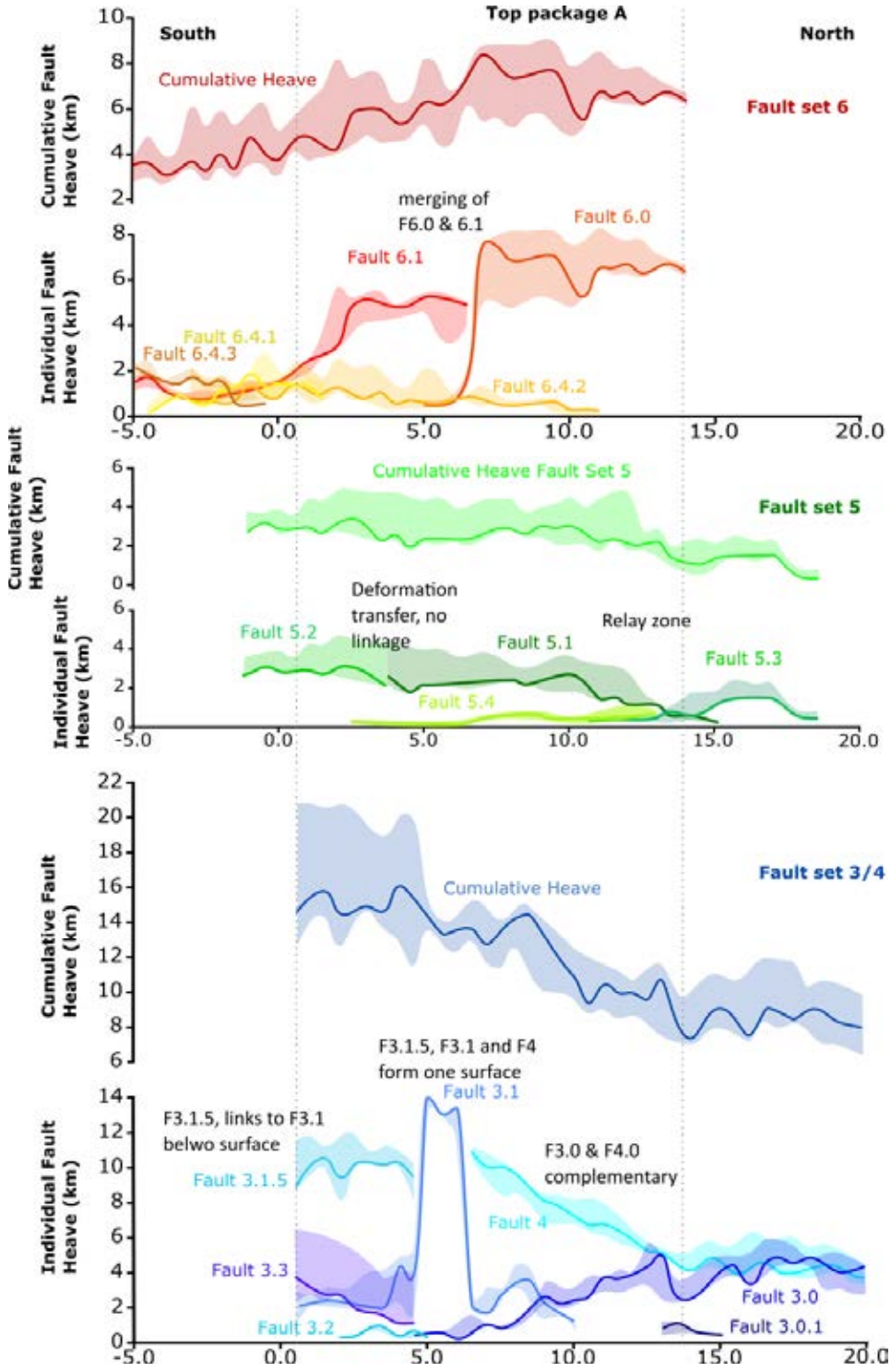

Figure 6.4: *Heaves measured at the top of sedimentary package A, pre-rift or early syn-rift, on an arcuate tectonic transport direction (Figure 6.1). The shading gives uncertainty of heaves primarily from determining footwall cutoffs (see Section 3.2.2, especially Figure 3.5. . Vertical lines indicate where measurement was possible throughout the volume Figure 6.1.*

The depth map of the top of package A (Figure 4.16), incorporates fault hangingwall and footwall cutoffs and provides useful context with which to consider the implications of fault heave plots shown in Figure 6.4.

Starting with the faults sets close to the continental margin, there are two more faults that are seen to offset the top of Package A: F3.1.5 and 3.0.1 which connect down dip onto F3.1 and F3.0, respectively. This provides a more complex faults network than is seen for at top acoustic basement level. F4.0 shows a large increase in heave to the south during the pre-rift or early syn-rift period, suggesting that during this period extension was greater in the south.

Moving outboard to consider Fault set 5, a similar pattern of fault cutoffs exists as at top basement with a clear overlapping link between F5.1 and 5.4 in the central-north of the study area and the *en echelon* nature of F5.3 and 5.4. Faults 5.1 and F5.2 are laterally linked in the south with no or limited overstep. Considering fault set 6, there is a clear lateral connection between F6.0 and F6.1 that includes a rapid switch in the dominant fault evidenced by the sudden closure of fault cutoff polygons. F6.1, F6.2 and F6.3 are all expressed in the southern area and therefore all contribute to the extension seen st the top of Package A. Considering the heave plots (Figure 6.4) for the various fault families reveals a number of interesting features that are described in the following sections.

Fault set 3/4

The cumulative heave is seen to decrease steadily northwards by 7 km over a strike distance of 19 km (from 15 km and strike distance 0 km to 8 km at a strike distance of 19 km). The most striking feature is the rapid increase in heave attributed to F3.1 between strike distance 4.5 and 7 km. This is a result of the merging of F4 and F3.1 whilst the 'new' fault strand, F3.1.5, accommodates the strain within package A. F3.1.5 links with F3.1 within the acoustic basement.

This discussion highlights that the fault network is slightly more complex at top package A level compared to top acoustic basement. The interaction between Faults 3.0/3.1 and and Fault 4 is clear: as the heave of Fault 4 decreases southward faults 3.0/3.1 accommodate a similar amount of heave. Large maximum errors in the south can be partly explained by the complexity of the fault network and the merging of multiple fault planes. This strike linkage at high levels

of extensions would result in large amounts of damage in relay zones and around fault tips as propagation became retarded but displacement continued (see for example Cartwright et al., 1995, and Section 2.8). In addition there are a number of smaller faults within the hangingwall that splay off F3.1, increasing uncertainty of cuttoffs.

Fault set 5

Three laterally linked faults accommodate the majority of the heave across the width of the data (north-south). Fault 5.3 in the north, F5.2 in the south and F5.1 in the central area. Faults 5.1 and F5.2 are seen to link directly, whereas Faults 5.1 and 5.3 show an overstep of 4 km. Fault 5.4 contributes only approximately 0.5 km of heave and runs the majority of the central portion of the dataset as does F5.1.

The cumulative heave for Fault set 5 is relatively steady with a slight reduction around a strike distance of 13km where the most westerly faults in set 5 can no longer be measured as the heave goes outside the dataset.

Fault set 6

In the northern and central areas, heaves on fault set 6 are dominated by two faults that show clear complementarity, F6.0 and F6.1; F6.0 being the northernmost of the two. F6 has a laterally consistent heave of approximately 7 km between strike distances 7-14 km. At strike distance 7 km the heave on F6.0 rapidly diminishes to less than 1km as the extension is taken up by F6.1, but the heave on F6.1 is only 5 km, suggesting a stepped reduction in overall heave to south at a strike distance of 7 km. At strike distance of approximately 2 km, the heave on F6.1 reduces to approximately 2 km with the extension being accommodated on F6.2 and F6.3. Fault 6.4 has a long lateral extent but with limited heave (approximately 1 km, increasing to 2 in the south). In the south therefore a number of discrete strike parallel faults separated by 2-3 km (when considered in a section taken perpendicular to the tectonic transport direction) are seen to offset the base post rift level. These faults splay southward but link to the north, forming a single fault plane (6.0). Contrary to cumulative heaves seen in the Fault sets 3/4 and 5, heaves are seen to reduce to the south at the base post rift level. This reduction is gradual by 3-4 km of heave over a strike distance of approximately 12 km, but also has two distinct steps of 1-2 km at strikes

distances of 2 and 7 km. It is worth of note here that the top of package A could not be directly followed into the hangingwall of fault set 6, due to the extreme deformation seen within the syn-rift especially in on the southern potion of Block 5. Interpretation was undertaken using seismic characteristics. Given the limited syn-rift sediment on the top of Block 5 (footwall of F6) it may be the case that the top package A horizon is absent and that the top acoustic basement heave of 5 km is more representative of the displacement (Figure 6.3).

6.1.3 Heave at base post rift unconformity level

Fault heaves were also measured at the base post-rift unconformity level (which is for each half graben is the top of the syn-rift). The nature of this horizon (i.e. representing the end of the extension associated with the rifting) means that it captures the fault displacement at the palaeoseafloor prior to any later flexural rotation resulting from faulting further outboard or later thermal subsidence, see Section 4.2.1.

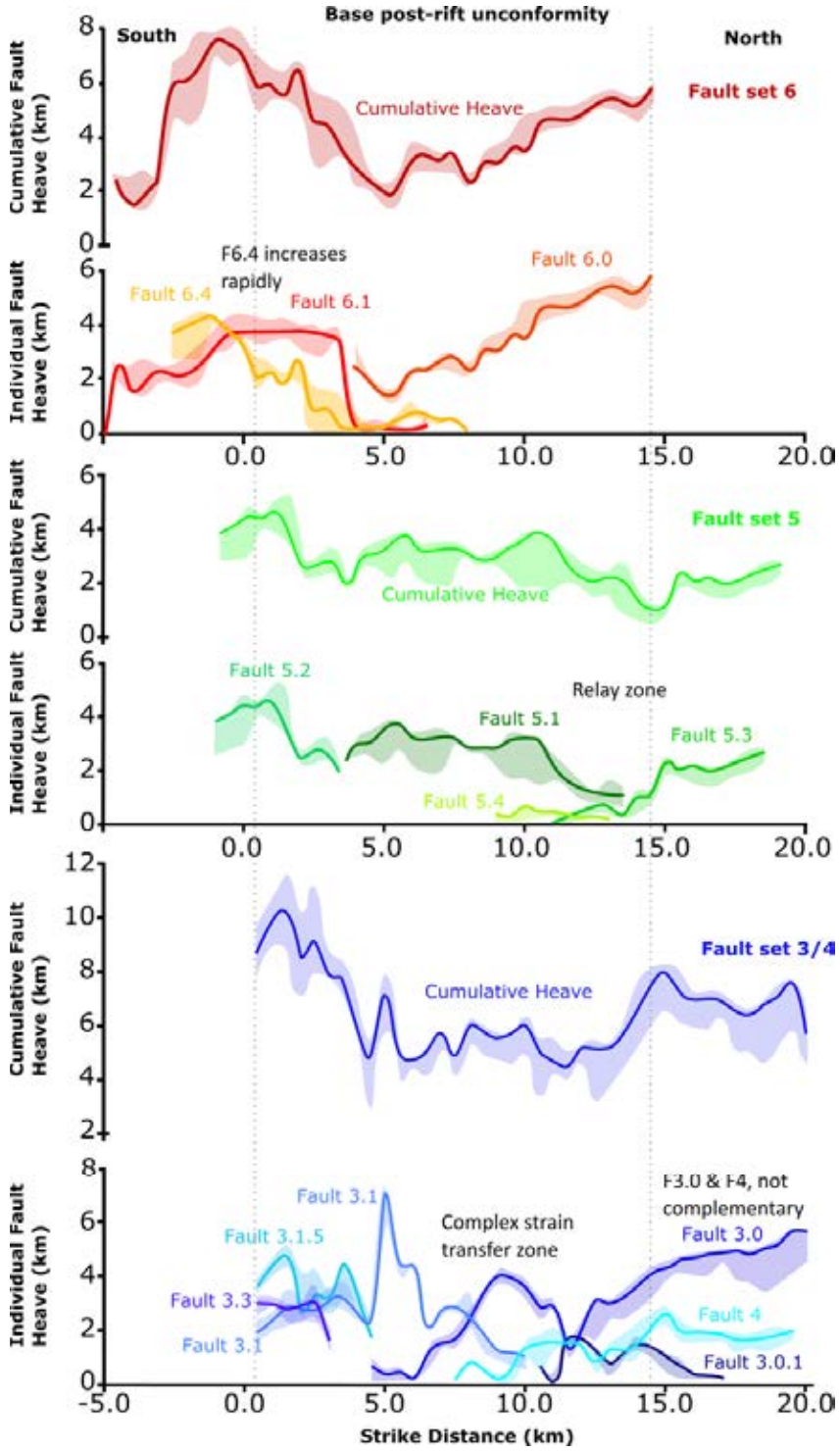

Figure 6.5: *Heaves measured at base of post rift on an arcuate tectonic transport direction (Figure 6.1). The shading gives uncertainty of heaves primarily from determining footwall cutoffs (see Section 3.2.2, especially Figure 3.5. Vertical lines indicate where measurement was possible throughout the volume Figure 6.1.*

Figure 4.12 shows the fault hanging wall and footwall cutoffs that were mapped by interpreting the seismic sections in the 3D dataset. A number of faults (numbered) that do not exist within the acoustic basement are shown to display displacement at this level. The heaves mapped in Figure 4.12 at the base post rift level are plotted in Figure 6.5.

Fault set 3/4

In the north of the area there is a clear complementary relationship between F3.0 and F4 and F3.0.1 (the latter a fault that is not seen to offset basement and is barely expressed in the early syn-rift, top package A). As heaves on Faults 3.0, 3.0.1 and 4 decline to the south heave is taken up by F3.1 and then F3.2 and F3.3 south of strike distance 5 km. One very distinctive feature of heave at this level is the high heave at strike distance 5 km, which is also recognised a the top of Package A (see Figure 6.4).

There is a increase of cumulative heave moving south from 7 - 10 km, however the central area shows heaves to be consistently around 5 km. The complex and complementary nature of the heaves measured on each fault results in an irregular heave along strike for this fault set, an aspect that will be returned to in Section 6.3.

Fault set 5

At the base post rift level the relationships of the faults are broadly similar to those seen at the top of package A (Figure 6.4): F5.3 in the north oversteps F5.1 at its southern end. F5.1 in turn links laterally with F5.2 in the south. F5.4 is much less laterally extensive (only 4 km) with limited heave ($<$0.5 km). The cumulative heave for fault set 5 increases to the south from approximately 2.5 km to 4 km, but this increase is far from gradual; two significant heave minima occur at strike distance 14 km and 4 km where F5.3 and F5.1, and F5.1 and F5.2 link, respectively. These minima suggest isolated fault growth (Figure 2.20).

Fault set 6

As with previously discussed heave graphs at lower structural levels, there is a clear lateral link from F6.0 in the north to F6.1 in the south at a strike distance of 4 - 5 km. The role of F6.4 at this level in considerable more than that seen at lower structural level and also shows complementarity with F6.0 in the north.

The presence of two roughly parallel faults in the south results in a cumulative heave for fault set 6 that increases from approximately 5 km in the north to 7-8 km in the south, however as with Fault set 3/4 there is a distinctive minimum in the central portion of the dataset where faults link.

6.1.4 Heave at different structural levels

In order to analyse the interaction and propagation of faults both laterally (along strike) and vertically (in the dip direction), it is informative to compare heaves at the different structural levels.

Individual faults

Figure 6.6 shows this comparison for the main block bounding faults in the study area.
For F3.0 and F4.0 in the north of data volume (strike distances 12-20 km) heave at TAB level are approximately 2 km more than at either top package A of BPR the level, as would be expected for upward propagation. For F4.0 the heave at BPR level reduces to the south whilst for top package A it increases until it is measured as being higher than at TAB level at a strike distance of 10 km. For F3.0 south of strike distance 12 km, the heave for all three horizons is similar and decreases (as displacement is passed on to F3.1) at the same rate, with heave at the BPR level being more variable. The southernmost fault of this set, F3.1 (and F3.1.5 at top package A and BPR level), also shows the largest heave at the TAB level, but only marginally more than that on top package A. In the southern part of the volume (0 - 6 km strike distance) heave at BPR level is only half of the 14 km seen at TAB level.

Fault set 5 shows much more modest heaves (maximum 4 km) than other fault sets. A consistent pattern is seen where TAB heave is larger or equal to that seen at the BPR (the structurally highest level measured), consistent with propagation from depth, apart from in the very north of the data volume.

BPR heave in turn is predominantly higher than that seen at top package A level. This pattern of heave between BPR and top package A is more difficult to reconcile with models of

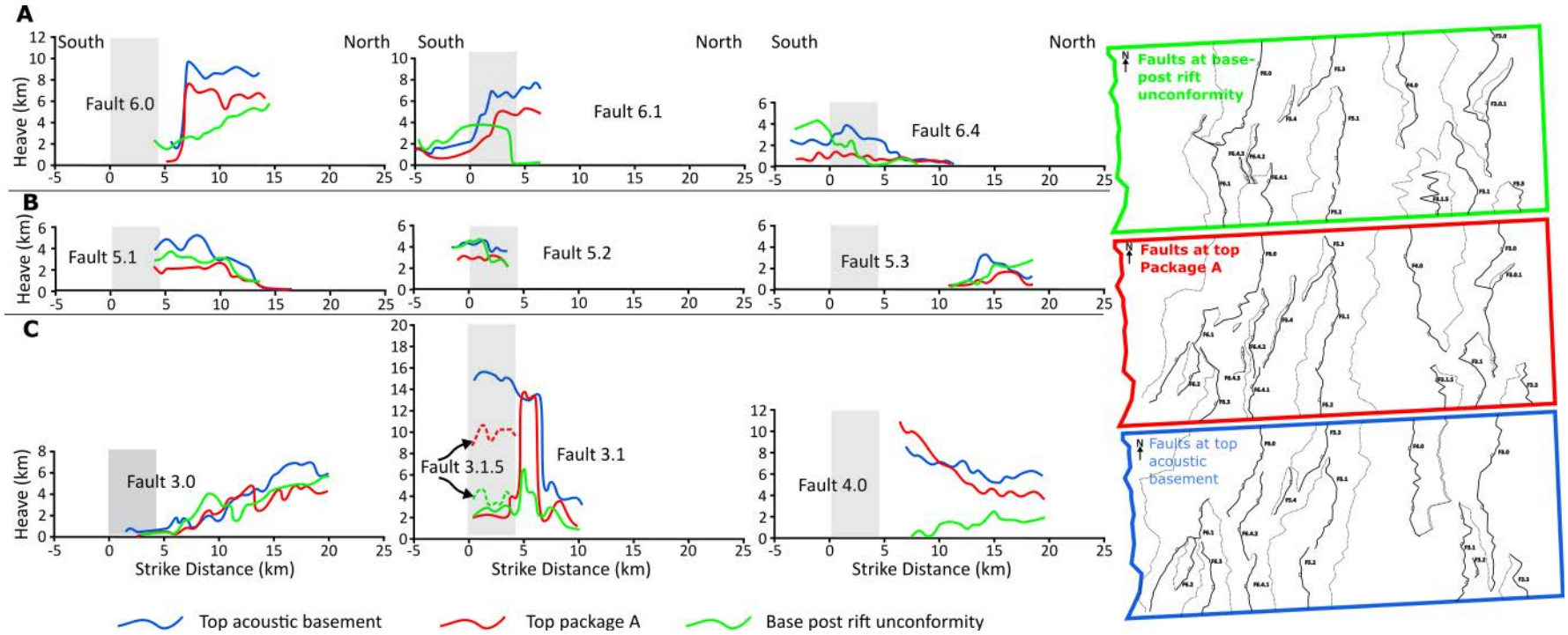

Figure 6.6: *Heaves at different structural levels shown for individual faults measured on an arcuate tectonic transport direction. Grey box marks the extent of the saddle.*

fault growth and displacement (see Figure 2.18I). At least three possible scenarios may produce this pattern. First, two initially distinct faults formed at two different structural levels one in the acoustic basement and one in the upper syn-rift. As these faults grow the link vertically eventually offsetting the mid-structural level, but by a lesser amount. Second, a fault at a deep structural level initially offsets all structural levels. The upper portion of the fault only is then reactivated in response to a localised deformation event in the late syn-rift. Third, the location of initiation of the fault and its displacement maxima shifts over time as the fault interacts with other faults.

Fault set 6 shows a pattern of heave at the different structural levels where heave at TAB level is predominantly higher than at top package A level. The heave at top package A is only inplaces larger than at base post-rift level. Looking at individual faults: F6.0, in the north of the dataset shows a simple relationship where the deepest structural level has the largest heave and shallowest has the least. It is also worth noting that the decrease in heave to the south of top package A is steadier than that seen at the other two levels, which decrease suddenly at strike distance 6 km where F6.0 merges into F6.1 (see Figure 4.17). F6.1 and F6.4 have a heave at TAB level which is consistently 1.5-2 km larger than that seen on top package A. Heave at the BPR level, however, increases toward the south on both faults from a strike distance of 4 km. At a strike distance of 0 heave on the BPR becomes the largest heave, up to 4 km on F6.4 compared to c. 2 km for heave at TAB level. The basic pattern of fault displacement seen on F6.0 can be explained by a standard model of elliptical fault growth (see Figure 2.18) if the maximum displacement on the fault is at or below top acoustic basement level.

Cumulative heave

In addition to the heave measured on individual faults at different structural levels Figure 6.7 shows the cumulative heave for each fault set. These cumulative plots reduce the complexities seen on individual faults and reveal the patterns described above with more clarity.

Working from the proximal margin, the cumulative heave on fault set 3/4 (6.7C) shows a clear pattern: heave at TAB is predominantly 1-2 km higher than at top package A level, heave

at base post-rift is approximately half that seen at TAB level. The pattern is slight different north of strike distance 15 km. Where TAB heave is still the largest and BPR is approximately half, however heave at Top package A is lower than in south. The northern section therefore shows a clear relationship: deeper structural levels having the largest heave and the shallowest structural level having the least heave.

Cumulative heave on Fault set 5 (Figure 6.7B) shows that heave at top acoustic basement level is largest by approximately 2 km, heave at the two lower structural levels is similar. Cumulative heave on Fault set 6 (Figure 6.7A) shows deeper structural levels having the largest heave and the shallowest structural level having the least. This breaks down a little between strike distances of -3 to 3 km where heave at the base post rift level was the largest.

The cumulative heave plot for all faults (Figure 6.7D) clearly indicates that within the 3D Galicia dataset, deeper structural levels having the largest heave and the shallowest structural level have the least heave. Areas outwith strike distances 0 - 14 km should not be considered as due to the arcuate tectonic transport direction not all fault sets could be measured in these areas (Figure 6.1).

A striking feature of the heave for all faults (cumulative) Figure 6.7 is the reduction in cumulative heave of 4.5 - 5 km in the central portion of the plot (ignoring heave measured along lines partly outside the data volume, e.g., dashed lines in Figure 6.1). This reduction in the heave may reflect northward propagation of the rifting.

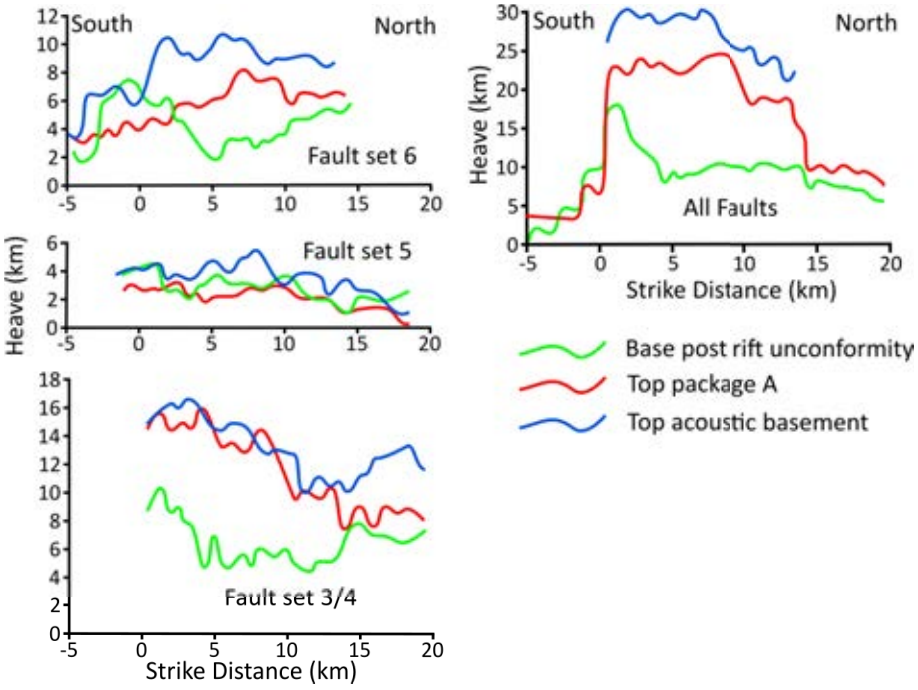

Figure 6.7: *Heaves at different structural levels shown for individual faults measured on an arcuate tectonic transport direction. Grey box marks the extent of the saddle.*

6.2 Fault scaling

Many of the block-bounding faults seen within the dataset extend outside of it (e.g. F6.1, F4.0 F3.0) those that are within the dataset (e.g. F6.1, F5.1, F5.4) are often kinematically linked to other faults so treating them as single faults may give them an unusually high displacement/length ratio. Fault displacements for these F6.1, F5.1, F5.4 are 11.2, 1.1 and 5.3 km, respectively. These displacements are derived from the measured heave but adjusted (increased) to provide an estimate of a displacement along the fault surface, dipping at 20°, the approximate dip of the faults imaged in the dataset (Figure 5.8). These three faults are plotted on the D/L graph of Kim and Sanderson (2005) in Figure 6.8, along with a displacement range of 1-10 km. The range of 1-10km displacement would at the best fit line for normal faults suggest fault lengths of 70-500 km. Although most faults interpreted in the dataset extend out of the block it is clear that given the nature of lateral variation that faults are unlikely to be more than a few 10's of kms. Faults in the hyperextended zone therefore do not show the usual scaling criteria of normal faults.

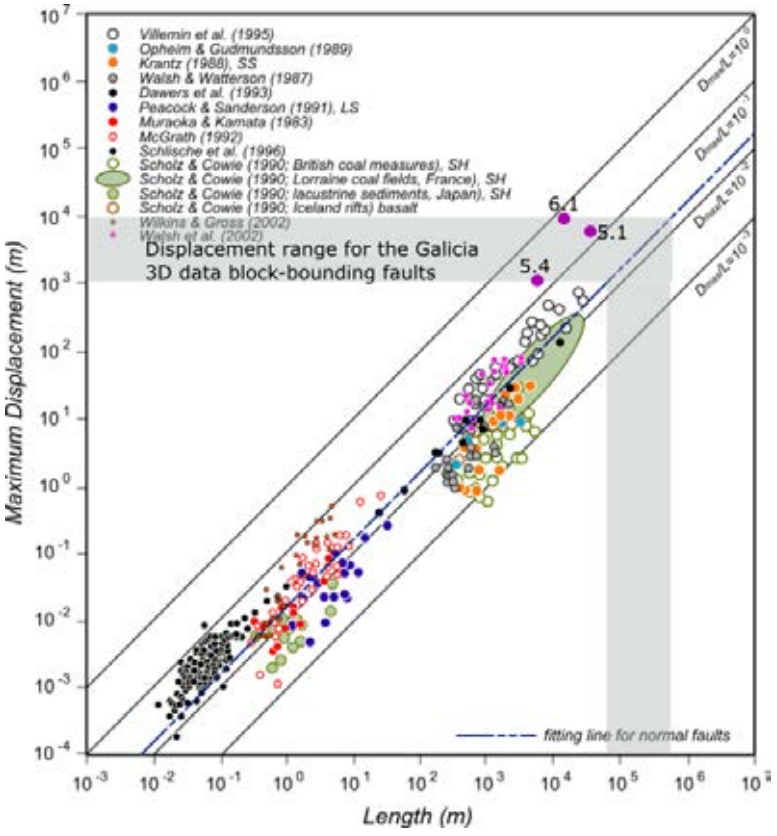

Figure 6.8: *Displacement length plot showing the block-bounding faults that occur entirely within the seismic dataset, grey shaded bands mark the maximum displacement seen for faults from the heave plots to give estimates of the lengths of these faults.*

6.3 Summary of heave analysis

A number of useful observations and interpretations can be made from the analysis of heaves on the faults within the Galicia dataset, these are:

- The heave relationships between some of the faults suggests simultaneous movement of faults, these can be faults along strike but can also be perpendicular to strike (for example F3.0 and F4). Broadly simultaneous fault activity is not uncommon within rift basins prior to localisation of faulting (Cowie et al., 2005).
- Where faults do link along strike, rapid strain transfer is seen (e.g. Faults 6.0 and 6.1)
- Faults in set 5 have lower heave compared to other sets.
- The saddle marks a zone of reduction in displacement to the north.
- The synrift contains faults that show offset at this level only (i.e. not in the basement); these faults connect to the larger block-bounding faults at depth and show how faulting increases in complexity within the the syn-rift due to continued deformation.
- Heave is highest at deeper structural levels
- There is some uncertainty for heave at top package A level, it may be more appropriate to use displacement seen at top acoustic basement level

Chapter 7

Discussion

The following section provides a discussion on the limitations of the data and the results presented. This is followed by a brief review of uncertainties of the current paradigm of magma-poor rifted margins with respect to continental break-up. Simple tests of the various mechanisms of break-up are then presented. The key results from the observation and analysis presented in this work are then discussed to highlight the contribution of this work to enhance our understanding of continental break-up at the Galicia margin. Finally, the implications for break-up at other magma-poor passive margins are discussed.

7.1 Limitations of results

The 3D Galicia data provides excellently imaged structures over a hyperextended margin. However, a number of important factors limit the results presented here. Much of the analysis undertaken has been derived from interpreting horizons within the seismic data that are assumed to represent geological surfaces: sedimentary units, unconformities, acoustic basement, detachment faults or crust mantle boundary. The high resolution dataset reduces the uncertainty and compared to other data, the interpretations are well constrained, several uncertainties are, however, worthy of note:

- The top acoustic basement in the southern portion of the data volume, between fault set 6

and the Peridotite Ridge (Figures 4.1 and 4.4), is less well constrained than in other areas.

- The interpretation of the top package A horizon west of fault set 6 is less certain as it cannot be directly traced from the other half grabens (due to the large offsets), but is interpreted based on the nature of seismic characteristics and its relationship with the underlying basement

- Other than for top package A, it was not possible to trace syn-rift horizons between half grabens with sufficient confidence to allow more complete mapping of the syn-rift. This was not because of a lack of reflectors with sufficient lateral extent but rather that reflectors did not pass over faults or that the level of deformation was such that relatively small offset faulting within fault blocks reduced the ability to trace reflectors (Figure 5.2).

- The trace of some of the faults within the basement was less clear due to a lack of acoustic impedance contrast and the heavily deformed nature of the hyperextended margin (Figure 4.10).

Continental break-up is a lithospheric scale process. The observations presented here are based on deformation seen within the continental crust and at the crust-mantle interface (the S reflector). Whilst recognising lithospheric scale effects, such as rotation of blocks due to unloading, these results allow us to directly address processes occurring at a deeper lithospheric level. The high level of deformation seen within the dataset has produced structures that are very complex; mapping them in 3D is therefore also very complex. Despite the high resolution seismic data, we dot not have the evidence in terms stratigraphy to fully understand the timings of the system.

The time to depth conversion undertaken for the dataset only uses vertical changes in the seismic data and does not take into account ray-path bending effects. Given the laterally discontinuous nature of the high velocity acoustic basement this may create artefacts on surfaces, especially the S reflector (as this underlies the other surfaces) so any topographic effects need to be considered with caution. However, the different velocity models were trialled and used velocities that agreed with tomographic and full waveform inversion models (Bayrakci et al., 2016;

Davy et al., 2017). In addition the topographic features seen on S, for instance where the faults connect, are also seen as features on the amplitude maps and are narrower (sharper) features than the longer wavelength velocity pull-up effects seen on the time structure maps.

7.2 Uncertainties of the current paradigm

The conceptual models of break-up (Figure 2.8) highlight a number of possible uncertainties that may, if resolved, inform the mechanisms of break-up. The current paradigm of magma-poor continental margins has at its core the idea that distinctive domains on a margin were generated by specific processes operating at a given stage of the rift's evolution. One of the missing factors, however, is the mechanism of final breakup. Breakup occurs between necking, i.e. embrittlement of the crust and coupling of deformation between brittle upper crust and mantle (Pérez-Gussinyé and Reston, 2001) and the long lived exhumation of the mantle (Lavier and Manatschal, 2006). It is unclear if break-up is a distinctly different from these processes. Most mechanisms invoke some form of simple shear structure such as a detachment fault, although the angle of slip on this is detachment is debated. Furthermore, the reduction in strength that enables displacement on a simple shear structure is also uncertain and may be thermally induced (for example Brune et al., 2014), due to mineral alteration (for example Reston and Pérez-Gussinyé, 2007c) or fluid pressure (Floyd et al., 2001).

One way to solve this uncertainty would be to explain why, in the migrating fault models, do the faults that form in the hanging wall of the currently active fault suddenly stop forming. Is it simply an increased amount of offset that is produced over a particular period of time? Does it require the offset to be equal to the thickness of the crust (therefore breaking the crust)? Or is it a change in the rate bought about by a switch to a more oblique rifting (Brune et al., 2016), in this portion of the Galicia margin possibly related to the influence of the triple junction (Figure 1.16, Sibuet et al. 2007).

7.3 Testing the Mechanisms

It is possible to test the various mechanisms proposed for final break-up using absolute or relative ages of the syn-rift sediments deposited in the half grabens formed by the faults (see Section 2.5, by the cross-cutting relationships of faults and geometries seen within /between the crustal blocks. Figure 2.8 shown in Chapter 2 outlined current models of crustal breakup, including the presence of the crust-mantle boundary below the tilted fault blocks (S reflector). These models can be considered as three end-member mechanisms of break-up (see Figure 7.1). These three end members are defined by the relative motion on the the faults (including any underlying detachment). All faults active at the same time (Figure 7.1**a**), the active fault migrating oceanward (**b**), and the movement on faults focusing oceanward (**c**). It is worth considering how these end-members relate to previous conceptual models (Figure 2.8). The *all faults active* end-member (Figure 7.1**a**) can be related to early ideas of low angle detachment faults (for example see Lister et al., 1986; Boillot, Winterer et al., 1988). The geometries may also represent proximal portions of gravity slide models (Figure 2.8D) and, furthermore, the geometries also reflect those seen in models of depth-depedent thinning when the plastic lower crust has been removed (Figure 2.8A-II), but with depth-dependent thinning, no explanation for the presence of the underlying ocean dipping detachment is required. The *active fault migrating* end-member equates with the rolling hinge (Buck, 1988a; Lavier and Manatschal, 2006; Choi et al., 2013) and sequential faulting models (Ranero and Pérez-Gussinyé, 2010) (see also Figure 2.8B). The *faults focusing* end-member (see McDermott and Reston, 2015) derives from aspects of the polyphase faulting model (Reston, 2005) and highlights the important of the margin scale and recognises that break-up occurs on a section of crust that has undergone earlier rifting. The originally distributed faulting gradually (or in stages) focuses toward the incipient margin (see Figure 2.8C). Such focusing does not rule out the development of a detachment especially in the distal margin.

One of the benefits of having 3D seismic data is that it is possible to map reflectors (a geophysical representation of sedimentary units which give relative age) over a large area; the Galicia data therefore offers a unique opportunity at an hyperextended margin to map out syn-rift

horizons. However, the relative heights of the rotated basement blocks and the heavily deformed nature of the syn-rift means that tracing individual reflectors between half grabens was not possible with the degree of certainty required. Despite this uncertainty important evidence is avaiable to test the different end member mechanisms mechanisms (Figure 7.1) these are outlined below.

For all faults to be active at the same time (Figure 7.1a) the top of the syn-rift would be of the same age. Additionally, fault blocks would be tilted at a similar angle throughout the lower crust and would have relatively planar surfaces. Neither of these tests are clearly met from observations of the Galicia 3D data presented here. Moreover, the sheer extent of brittle deformation seen in the tilted fault blocks and the cross cutting faulting both within the basement and outwith, suggests this end-member is not applicable to break-up. Important in excluding the gravity slide model in particular, is the lack of both compressional deformation and chaotic facies seen in the distal portion of the data (for example see Calvès et al., 2015).

For the active fault migrating end-member (Figure 7.1b) the majority of, and all of the latest syn-rift sediments, would young oceanward as seems to be the case from within the Galicia dataset, with the diachronous nature of the base post-rift horizon supporting the results of drilling (see Section 1.3.3). The same argument of latest syn-rift younging oceanward also supports the focusing faults model (Figure 7.1c). The evidence from drilling during ODP leg 103, summarised in Figure 7.2, provides the only age data we have for sediments on the margin and these provide a picture of diachroneity. It is also clear that there is significant deformation in the fault blocks that could result from the back rotation of the fault blocks (as in the rolling hinge and to a lesser extent sequential faulting).

There are a number of wedge-shaped fault blocks where the faults are not expressed at the base post-rift level and therefore do not represent the most recent phase of faulting. Adding to this the presence of flat tops to some of the blocks (Figure 4.17) suggests that there are a number of cross-cutting faults. The high level of deformation seen within the fault blocks and overlying syn-rift sediments and complex geometries of the syn-rift sediments especially in the more distal blocks (for example B5, see Figures 4.1 and 4.10) taken with the earlier stages of faulting provide

evidence for the focusing of deformation end-member shown in Figure 7.1.

It is important however that it is recognised that these three models represent end-member mechanisms of break-up. It is possible that as hyperextension occurred and continued in the the latter stages of rifting, these mechanisms may have acted at different stages. For example structural heterogeneities generated during earlier phases of extension produced by the focusing deformation end-member will impact on the propagation of faults and the deformation seen in the hanging wall and footwall of rolling hinge of sequential faulting models.

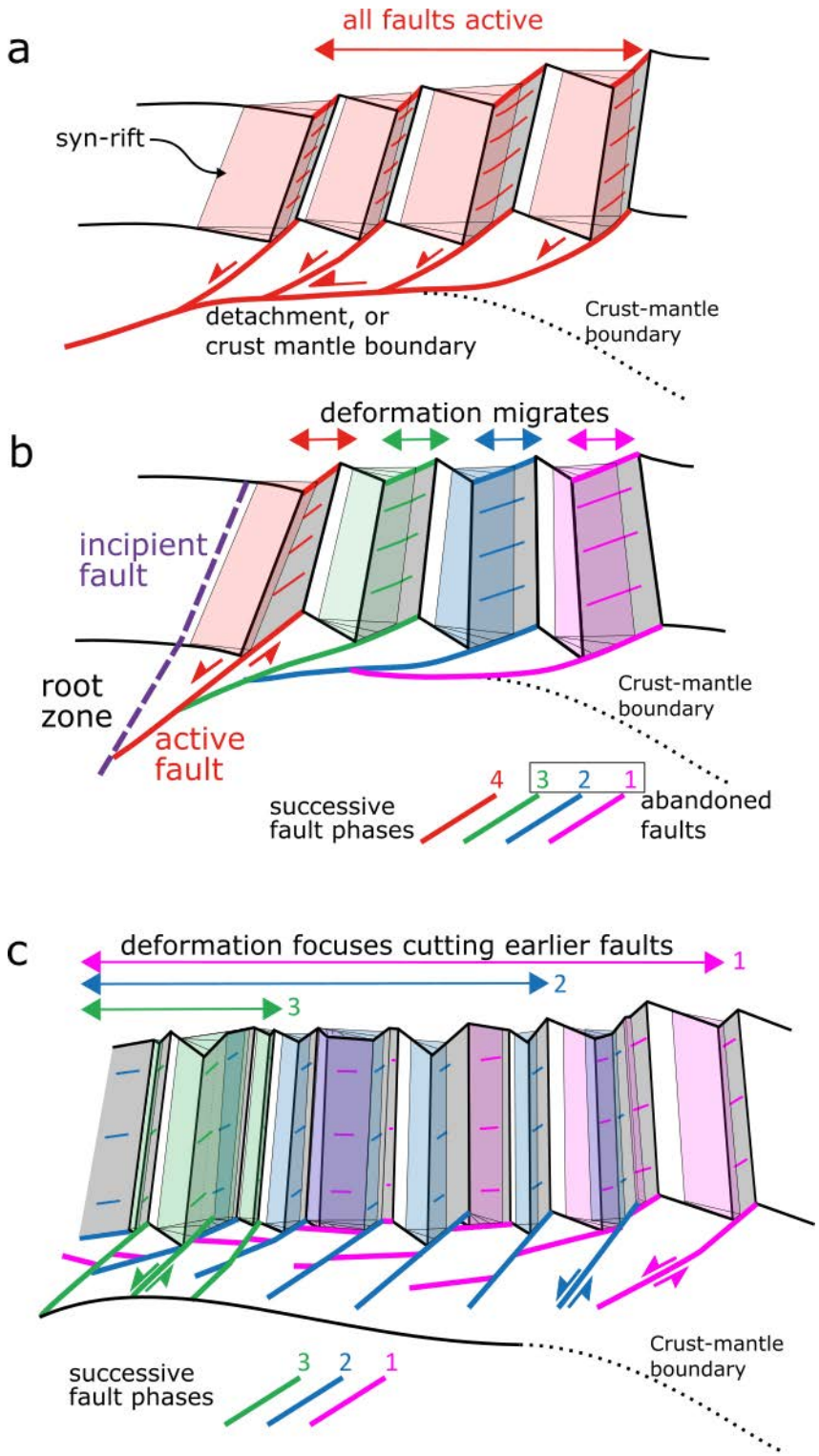

Figure 7.1: *End-member mechanisms of break-up of the continental crust derived from conceptual ideas shown in Figure 2.8*

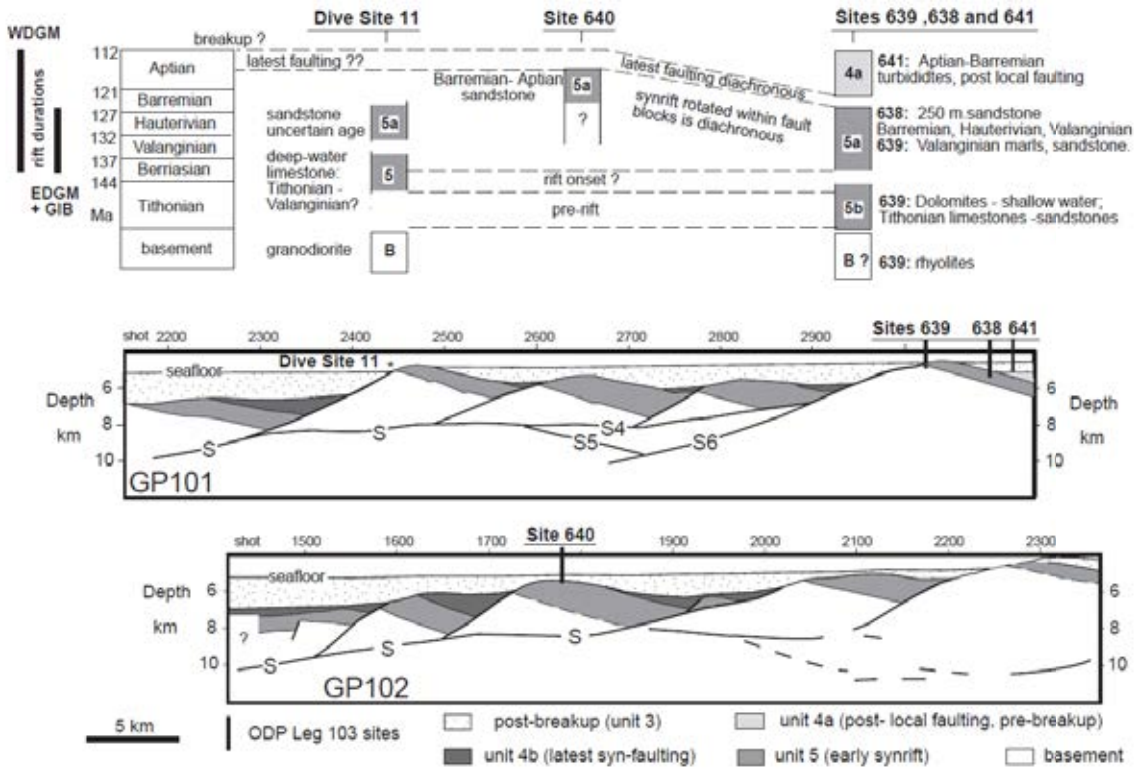

Figure 7.2: *Diagrammatic representation of stratigraphy drilled from the top of different fault blocks derived from ODP Leg 103 originally shown as Figure 1.8. The diachronous nature of the latest syn-rift, that youngs oceanward, supports the migrating fault and focusing fault models (Figure 7.1b and c)*

7.4 Key observations

A number of important observations based on the horizon and fault interpretations from the 3D Galicia data presented in this work require a more detailed consideration, these include:

- Nature of the S reflector
- Lateral variation of fault blocks
- The nature of the saddle

7.4.1 S reflector

The presence of corrugations as slip indicators seen in the data agree with those highlighted by Schuba et al. (2018). The results shown here on time, amplitude and depth maps (Figures 4.8, 4.21 and 4.20, respectively) for the S reflector and also on the amplitude maps of fault surfaces forming top basement (Figure 4.18) provide much more certainty on the presence of slip on the S. That these corrugations can be traced from S onto fault planes and rival those seen at compressional margins (Edwards et al., 2018) in terms of clarity and length (3-5 km), suggests a cumulative slip on the S. In addition to the corrugations seen in the various maps of the S reflector, the depth and amplitude maps of S also show a clear link with high amplitude areas and subtle changes in the topography of S, respectively. The high amplitudes may be a result of either seismic tuning effects, variations in the amount of serpentinite (Bayrakci et al., 2016), or the presence of cataclasites (Reston et al., 2007b; Schuba et al., 2018). The changes in the topography of S may result from the intersection of faults surfaces that are evolving into detachment surface. If the rolling hinge model is invoked, then once S has rotated due to unloading there comes a point where mechanically it might be easier to form another fault, generating a change in the topography of S. This change in topography is best seen (see Figures 4.20 and 4.21) on F5.1, F5.3 (in the north) F4.0 and an unnamed fault west of F5.2 that is not expressed at the BPR level and is therefore interpreted as being an earlier phase of faulting. That this change in the topography of S is not necessarily seen along the length of a fault or on all faults suggests that

displacement may initiate locally on the S surface which then suggests that faulting that leads to break-up initiates and propagates up from the S, acting as a detachment. Evidence from the angles of slip presented in Section 5.3 suggest that S was slipping at 20-26° and the faults at 38-45° suggesting an angle between them of 18-19°, which may well have been changed due to subsequent rotation and deformation.

7.4.2 Lateral variation and complexity of blocks/surfaces

The size of the blocks does not simply decrease oceanward on this part of the Galician margin which suggests that the 2D sequential faulting model (Ranero and Pérez-Gussinyé, 2010) needs significant refinement.

Block 3, which tapers to the south, has very limited syn-rift sediments and that the faults that bound each side of it merge into a single fault plane requires an explanation, given that its foot-wall fault is one of the breakaway faults. This suggests that fault set 3/4 was an overstepping relay with a relatively high aspect ratio (see Childs et al., 2016). The mini-ridge seen in the fault surface (see Figures 7.3 and 7.4) would then be the remnant of a fault that continues southward out of the data volume (and was able to cut slightly deeper due evolving embrittlement (Pérez-Gussinyé and Reston, 2001). The northern end of F3.1 therefore acted as a breaching structure, onto fault 3.0. Fault 4 in the north either propagated as an isolated fault southward or linked by increased displacement (coherent fault, see Figure 2.20) with the the southern fault at the 'jog' in the depth of the basement at the tip of the fault 4.0. The continuous surface suggests that these structures developed in part simultaneously, an interpretation supported by the complementary heaves (see Section 7.5).

The limited syn-rift seen on top of Block 3 suggests that movement on F3.0 may have been later than on F3.1 and 4.0 but this would require deformation to be stepping back onto the continent rather than focusing toward the rift and seems problematic in terms of kinematics, but does not rule it out. The displacement on fault set 3/4 is larger than seen on other faults, with a correspondingly wider graben (except for F6.0), suggesting that the breakaway faults may form from a different mechanism. The heavy dissection of the crust west of the breakaway faults may

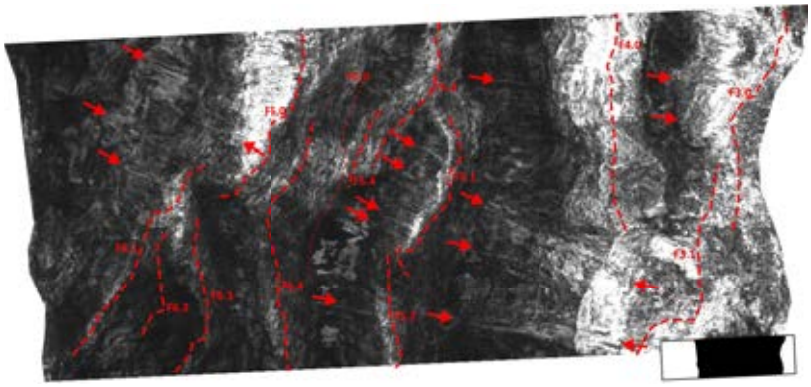

Figure 7.3: *Amplitude map of the top acoustic basement (originally shown as Figure 4.18). Note the high amplitudes of seen to the west of F4.0 showing the rotation and lack of syn-rift on this block (B3) and the high amplitude ridge that extends southward from F4.0.*

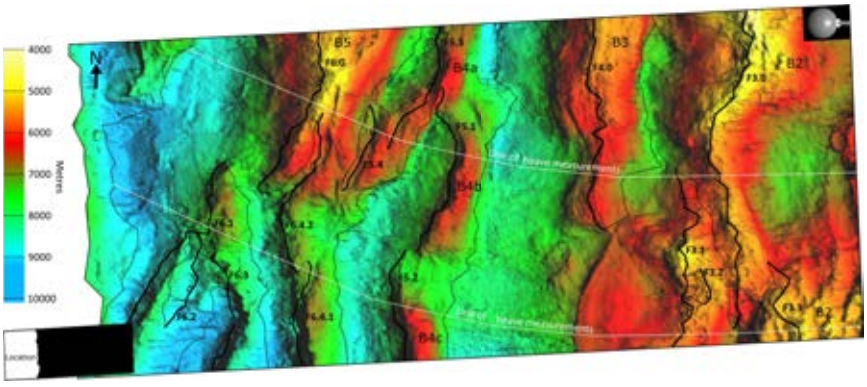

Figure 7.4: *Depth map of the top acoustic basement (originally shown as Figure 4.17). Note the small scarp/ridge south of F4.0 and the relay structure between F3.0 and F3.1*

be a consequence of crustal embrittlement and coupling, allowing serpentinisation of the mantle and the development of weak serpentinite faults which develop into the S detachment, inducing more fault nucleation and propagation up into the crust. This process is also suggested by the increasing presence of new faults in the structurally higher horizons that link to ones at deeper levels, and the more complex geometries and interactions at higher structural levels compared to the relatively linear fault traces seen on the S. This localised weakening may result in basement windows, which under more traditional models of propagating faults and continuous blocks would form strips of exhumed mantle rather than windows that are surrounded by basement. It is also noteworthy that the basement windows lie on the line of the saddle. It is to this enigmatic feature which the discussion now turns.

7.4.3 The Saddle

The saddle (Figure 4.13) seems to provide a demarcation between a northern/north-east and southern/south-west section in terms of the structures seen within the dataset. Considering the more proximal portion of the dataset (west of the breakaway faults) to the S/SW the faults and blocks trend predominantly N-S whereas to the N/NW the structures are rotated clockwise by c. 30° to trend NNW-SSE (Figure 7.4). Only F6.4.4 can be seen to cross the saddle, and where it does so it has change of strike to match those of the other faults on each side of the saddle. Also of note is that the amount of crust is significantly less to the S/SW of the saddle, this may just be a fact that to north of the data volume lies the Galicia Bank. The orientation of the saddle matches that seen on the corrugations on S on the fault surfaces (Figure 6.1). It also lies on the line of the large displacement seen on F3.1 to the east. Possible explanations for the saddle are inheritance: that it lies on the line of a previous structure. It may also be a minor transfer zone with deformation difficult to pass across it. This would account for the change in structural trend but not account for F6.4.2. The separation of the basement blocks (albeit not complete) and the extensional deformation of the syn-rift sediments above blocks 4b and 4c in the saddle suggest that it is a an inherited structure that was also influencing the rifting. No (N-S) displacement across the zone can be evidenced.

7.5 A refined mechanism of break-up

By synthesising observations from the syn-rift geometries, sediment isopachs and displacement profiles (Figures 4.1, 5.2, 5.6, 5.7 and 6.7) it is possible to ascertain aspects of how the faults developed on the margin.

An important feature seen from the displacement (heave) profile plots is the complementary nature of the faults. Where one fault displacement declines and another one increases indicates the faults must be acting together in in order to maintain the a consistent extension. Where faults are interacting (linking or beginning to link), displacements for each fault begin to decrease to account for displacement by the other fault. This fault interaction is seen to be the case for faults F3.0 and F4.0 in the central portion of data volume for heave measured at top acoustic basement and within the syn-rift (top package A) at strike distances 7-14 km (Figure 6.3). Given that these faults are linked to form one surface in the south, these faults are therefore considered to be acting simultaneously for some period of their growth, a common occurrence in rift basins prior to localisation (Cowie et al., 2005).

The relatively linear plots of cumulative heave for all fault sets at top acoustic basement and top package A (early syn-rift) levels suggests that during extension the length of the fault remained steady and was therefore acting as a coherent fault (see Section 2.8 and Figure 2.20). During the later syn-rift, as measured at the base post rift level, the dips in cumulative heave where faults link suggests that this was a period of propagation and possible linkage. This linkage is highlighted by the presence of new faults linked to ones at deeper levels.

For fault set 3/4 at all levels, and for fault sets 5 and 6 at the base post rift level, there is a significantly increased displacement in the south which is also reflected in the isopach maps for package A and B that show thicker sediments in the south indicating increased extension in the south.

The relationship of syn-rift sediments to faults provides methods for assessing fault growth (Jackson et al., 2017). Isopachs generated in the syn-rift highlight that faults were linked early but had distinct depocentres that merged and migrated as the fault grew, often migrating closer

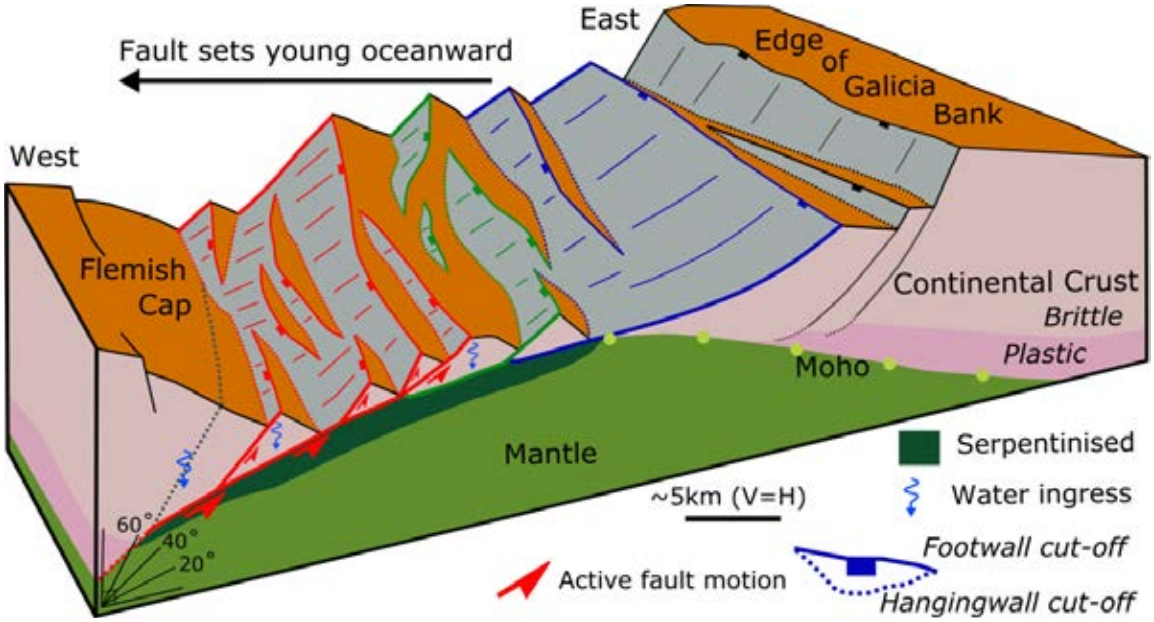

Figure 7.5: *Conceptual 3D Block model explaining the final breakup of the Galicia Margin*

to the fault over time, but not directly adjacent to the fault (see Section 5.2).

The displacement profiles plotted (Figure 6.7) to compare the cumulative heave of fault sets at different structural levels show a consistent pattern of higher displacement at lower structural levels. This pattern suggests that faults are propagating from depth, in this case that can only be from the S reflector or lower. This strongly favours the migrating fault mechanisms of break-up, specifically the rolling hinge model (Figures 2.8C and Figure 2.9).

A revised model, an adaptation of the the rolling hinge model to incorporate a third dimension is presented in Figure 7.5. The rationale for the revised mechanism of break-up is derived directly from observations based on the 3D data. The components that needed to be included are:

- a consistently present, yet variable S reflector
- basement windows, exhumed mantle surrounded by fault bounded blocks
- corrugations on S reflector that match those seen on Fault 6.0
- corrugations extend up dip on to faults landward of their intersection (for example F6.0-S)
- heave plots suggest complementarity of some faults

- numerous faults initiate on a weakened (serpentinised) lithospheric (mantle)

The revised model suggests break-up when the two areas of brittle failure, in the embrittled crust and in the strong lithospheric mantle (Lavier and Manatschal, 2006) connect via the detachment fault, in the case of the Galicia margin this is the S reflector. Final break-up occurrs in the north of the dataset by the large offset seen on F6.0 and by numerous faults connected laterally and at depth (on the S) in the south.

7.6 Implications for magma-poor margins

Previous models of faulting and syn-rift sediments based on 2D seismic lines could not incorporate the lateral variation now recognised by the interpretation of the 3D data presented here. However, field data (Epin and Manatschal, 2017) does recognise the possibilities of lateral connection of structures and sedimentary sequences (Masini et al., 2012), but lacks the coverage of scale and exposure to fully realise them. Future studies of magma-poor margins should recognise the scale of brittle deformation and the variability of structures both between tilted blocks and within blocks. Relatively simple models of break-up do not recognise the complexity seen in the Galicia 3D. It is also clear that within the spectrum of margin types (magma-rich to magma poor) that the complexity of break-up seen in Galicia can help identify novel thinking when considering break-up with the addition of even small amounts of magma entering a system that is clearly so deformed.

An explanation for the large sediment accumulations, deeper grabens and deeper S reflector in the south, and the larger displacement shown by the heave analysis in the south of the data would be a rotational opening. Such rotational opening has been shown using analogue models (Molnar et al., 2017) and is also recognised at other margins (Koehn et al., 2008; McClusky et al., 2010) and plate boundaries (Klein et al., 2005). Rotational opening resulting in V-shaped basins are also seen elsewhere in the north Atlantic (Peron-Pinvidic and Manatschal, 2010): the Galicia margin may represent a small v-shaped basin.

The idea of a V-shaped opening is explored using data presented here. By taking normals to

the tangents of the line of the corrugations (Figure 6.1) seen on the S and fault surfaces, gives a pole of rotation just to the south of the Galicia Bank. This is approximately 75 km north of the seismic data volume. The bathymetry of the Galicia bank does indeed show a V shape (scissor) as shown on Figure 7.6 (Lymer et al., 2016). A similar idea can be developed by considering the cumulative heave measured on the margin (Figure 6.7) and extrapolating the reduction in heave to zero, this gives a pole approximately 50 km north of the seismic data volume Figure 7.7.

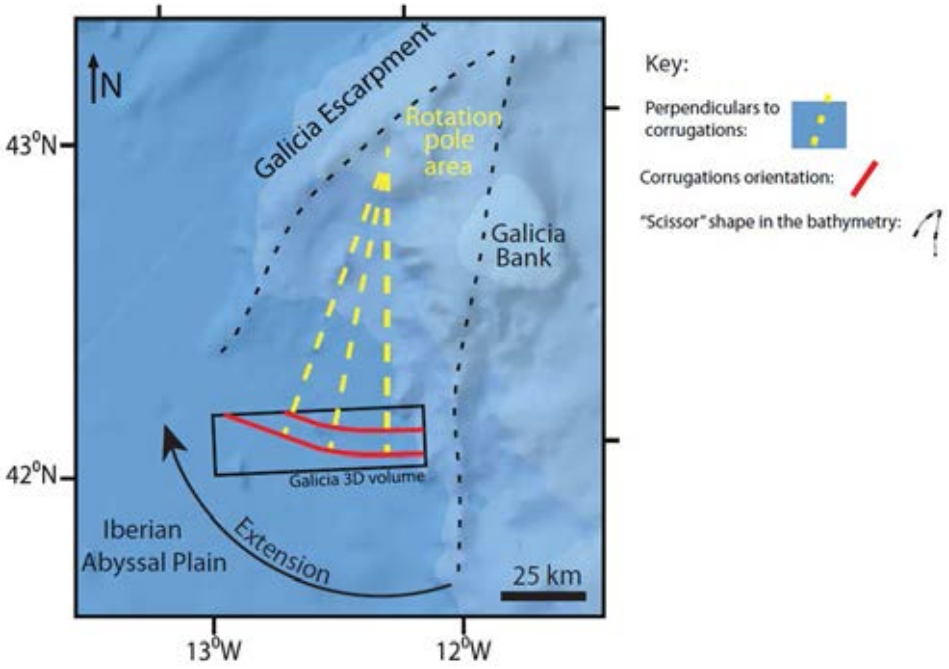

Figure 7.6: *Using fault-slip indicators to determine poles of rotation*

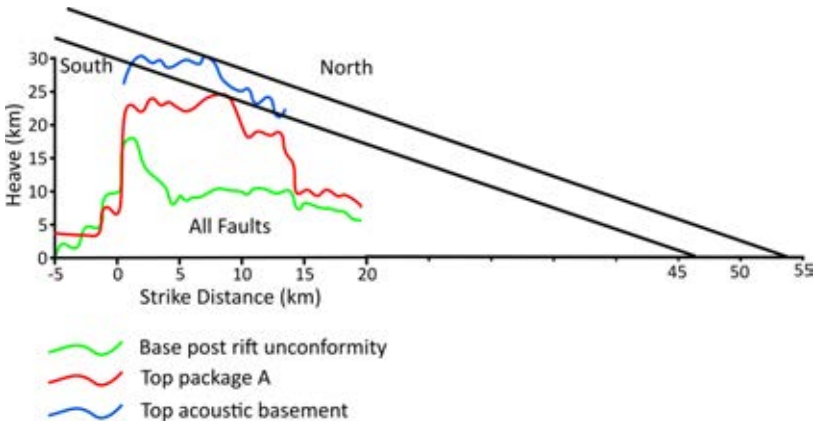

Figure 7.7: *Extending the northward displacement profile to a point of no extension (Lymer et al., 2016)*

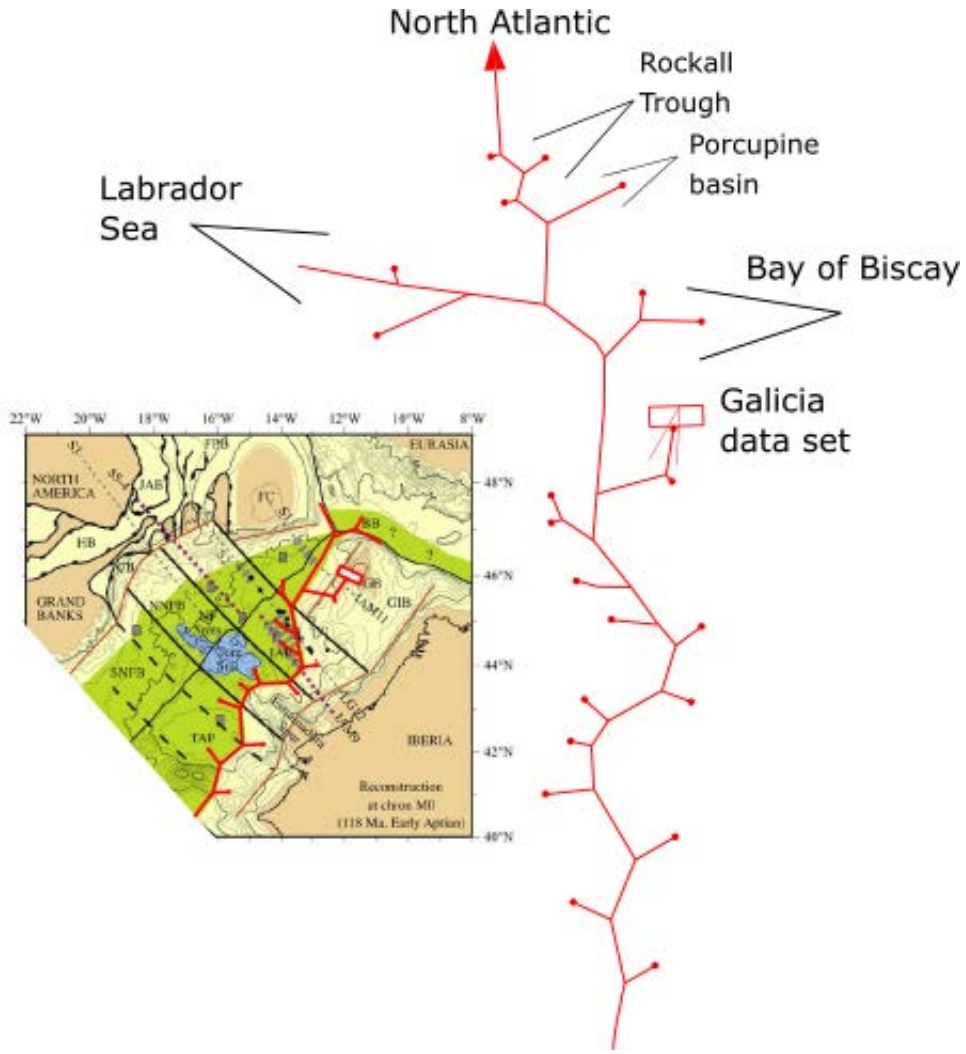

Figure 7.8: *Conceptual idea of propagating rifts being nascent triple junctions, failed arms of which result in V-shaped basins*

Taking this idea beyond the simply V-shaped basins and the Galicia margin. The rotation of structures seen in the mini 'V-shaped' basin may occur as a result of propagation front of oceanic spreading to the constantly forming proto-triple junctions, but one of the arms failing, resulting in a series of V-shaped basins (Figure 7.8). An additional possibility is the rotation (or change of direction) as a response to propagation of the proto-mid-Atlantic ridge and an change of stress orientation as the zone of ultra slow spreading stepped westward to the site of the North Atlantic-Biscay Triple Junction (Figure 1.16 and inset in Figure 7.8).

Chapter 8

Conclusions

8.1 Concluding remarks

The Galician margin is the most studied magma-poor passive margin. The relatively low sediment thicknesses and the absence of known igneous bodies means that high resolution seismic imaging is possible. 2D seismic imaging to date has revealed the margin to consist of tilted fault blocks of continental crust at least partially underlain by a bright reflector (the S) and a ocean-continent transition zone at least 100 km wide. The margin has been used to compare both field evidence of uplifted former passive margins, primarily from the Alps, and numerical modelling simulations of lithospheric breakup. Drilling has also constrained some of the rocks types seen on margin, notably exhumed mantle and granodioritc/rhyolitic core to tilted faults blocks. Drilling has also revealed that, in general, the extensional deformation at the margin focused oceanward over time.

Despite being the most studied margin in the world the mechanism of breakup at the Galician margin, and therefore all magma-poor passive margins, is still debated.

The work presented here used a 3D seismic reflection dataset acquired in the summer of 2013 to interpret faults and structurally relevant surfaces to help resolve the mechanism of break-up. In addition, displacement analysis on the main faults was also undertaken.

The observations and interpretation presented outline a number of key findings:

- The tilted blocks and faults that form them are much more laterally variable than previously thought or demonstrated.
- The faults form coherent networks of kinematically linked faults
- Slip indicators have been imaged for the first time on the S reflector, highlighting its role as a detachment.
- The same slip indicators have been imaged on S, and can can be traced from S onto faults to show that they acted simultaneously
- Heave analysis on faults also suggests simultaneous movement of faults
- The lateral variability seen may be a result of changing tectonic transport directions over time possibly as a result of rotational opening

The work presents a refined 3D rolling hinge model in which faults initiate at different points on a serpentinised crust-mantle boundary (to form the S reflector) and then propagate up through the crust. It is expected that other magma-poor margins are also variable and any future research should bear this variability in mind.

There are implications of the research for the deep water exploration of hydrocarbons. In particular the lateral variability may strongly influence heat flow models, and therefore the understanding of when source rocks enter the oil window. Furthermore, the complex nature of brittle faulting will severely impact on the flow of fluids in the syn-tectonic sequences and, via polygonal faults into post-rift sequences. The present sedimentation on the sea floor at the Galician margin is still influenced by the 3D tectonic architecture and has therefore influences the sedimentary architecture since rifting ceased, highlighting the importance of structures on such margins on possible source and reservoir rocks.

Academic implications include the new ability, from the interpretation of the syn-rift presented in the work (and the supporting interpretations), to plan an academic drilling leg to constrain the absolute ages of the rifting at the margin.

8.2 Recommendations for further research

A number of lines of further work are considered appropriate:

- As mentioned above important further work would include the development of sites for a drilling cruise.
- Restoration of the seismic lines will further constrain the timing and mechanisms of breakup.
- 3D restoration of horizons may also elucidate changes in strain over at different relative times.
- Interpretation of the early post-rift unconformities may highlight interesting thermal subsidence history (and other history) of the margin.
- The large dataset of interpreted syn-kinematic faults could provide an interesting dataset on fault scaling at an hyperextended margin.
- The use of fracture network software, such as *Fraqpaq*, would open up the a line of enquiry for establishing the hydrogeology of the margin to determine the possible rate of water ingress and therefore serpentinisation and elemental cycling seen both during rifting and at present day.

Bibliography

Alves, T., Bell, R., Jackson, C.-L. and Minshull, T. (2014), 'Deep-water continental margins: geological and economic frontiers', *Basin Research* **26**(1), 3–9.

Anderson, E. (1905), 'The dynamics of faulting', *Transactions of the Edinburgh Geological Society* **8**(3), 387–402.

Anderson, E. M. (1951), *The Dynamics of Faulting and dyke formation with applications to Britain*, Hafner Pub. Co.

Axen, G. J. and Bartley, J. M. (1997), 'Field tests of rolling hinges: Existence, mechanical types, and', *Journal of Geophysical Research* **102-B9**, 20515–20537.

Bacon, M., Simm, R. and Redshaw, T. (2007), *3-D seismic interpretation*, Cambridge University Press.

Barker, P. and Burrell, J. (1977), 'The opening of Drake Passage', *Marine geology* **25**(1-3), 15–34.

Barnes, A. E. (2007), 'A tutorial on complex seismic trace analysis', *Geophysics* **72**(6), W33–W43.

Barnett, J., Mortimer, J., Rippon, J., Walsh, J. and Watterson, J. (1987), 'Displacement geometry in the volume containing a single normal fault', *T he American Association of Petroleum Geologists Bulletin* **71**(8), 925–937.

Barton, P. and Wood, R. (1984), 'Tectonic evolution of the North Sea Basin: crustal stretching and subsidence', *Geophysical Journal International* **79**(3), 987–1022.

Bayrakci, G., Minshull, T., Sawyer, D., Reston, T. J., Klaeschen, D., Papenberg, C., Ranero, C., Bull, J., Davy, R., Shillington, D. et al. (2016), 'Fault-controlled hydration of the upper mantle during continental rifting', *Nature Geoscience* **9**(5), 384.

Beltrando, M., Zibra, I., Montanini, A. and Tribuzio, R. (2013), 'Crustal thinning and exhumation along a fossil magma-poor distal margin preserved in corsica: A hot rift to drift transition?', *Lithos* **168**, 99–112.

Boillot, G., Comas, M. C., et al. (1988), 'Preliminary results of the Galinaute cruise: dives of the submersible nautile on the western Galicia margin, Spain', *Proceedings Ocean Drilling Programme, Science Results* **103**, 37–51.

Boillot, G., Féraud, G., Recq, M. and Girardeau, J. (1989), 'Undercrusting by serpentinite beneath rifted margins', *Nature* **341**(6242), 523.

Boillot, G., Recq, M. and Winterer, E L al., e. (1987), 'Tectonic denudation of the upper mantle along passive margins: a model based on drilling results (ODP Leg 103, western Galicia margin, Spain)', *Tectonophysics* **132**(4), 335–342.

Boillot, G., Winterer, E. L. and Meyer, A W al., e. (1987), Proceedings of the Ocean Drilling Programme initial reports 103, Report.

Boillot, G., Winterer, E. et al. (1988), '45. Drilling on the Galicia margin: Retrospect and Prospect 1'.

Brun, J. and Beslier, M. (1996), 'Mantle exhumation at passive margins', *Earth and Planetary Science Letters* **142**(1-2), 161–173.

Brune, J. N. and Ellis, M. A. (1997), 'Structural features in a brittle-ductile wax model of continental extension', *Nature* **387**, 67–70.

Brune, S., Heine, C., Clift, P. D. and Pérez-Gussinyé, M. (2017), 'Rifted margin architecture and crustal rheology: reviewing Iberia-Newfoundland, central South Atlantic, and South China Sea', *Marine and Petroleum Geology* **79**, 257–281.

Brune, S., Heine, C., Perez-Gussinye, M. and Sobolev, S. S. (2014), 'Rift migration explains continental margin asymmetry and crustal hyperextension', *Nature Communications* p. 5014.

Brune, S., Williams, S. E., Butterworth, N. P. and Müller, R. D. (2016), 'Abrupt plate accelerations shape rifted continental margins', *Nature* **536**(7615), 201.

Buck, W. R. (1988a), 'Flexural rotation of normal faults', *Tectonics* **7**(5), 959–973.

Buck, W. R., Lavier, L. L. and Poliakov, A. N. (1999), 'How to make a rift wide', *Philosophical Transactions-Royal Society of London Series A Mathematical Physical And Engineering Sciences* pp. 671–689.

Buck, W. R., Martinez, F., Steckler, M. S. and Cochran, J. R. (1988), 'Thermal consequences of lithospheric extension: Pure and simple', *Tectonics* **7**(2), 213–234.

Calvès, G., Huuse, M., Clift, P. D. and Brusset, S. (2015), 'Giant fossil mass wasting off the coast of west india: the nataraja submarine slide', *Earth and Planetary Science Letters* **432**, 265–272.

Cann, JR Blackman, D. et al. (1997), 'Corrugated slip surfaces formed at North Atlantic ridge-transform intersections', *Nature* **385**, 329–332.

Cartwright, J., Trudgill, B. and Mansfield, C. (1995), 'Fault growth by segment linkage: an explanation for scatter in maximum', *Journal of Structural Geology* **17**(9), 1319–1326.

Chapman, T. and Meneilly, A. (1991), 'The displacement patterns associated with a reverse-reactivated, normal growth fault', *Geological Society, London, Special Publications* **56**(1), 183–191.

Chew, D. M. (2001), 'Basement protrusion origin of serpentinite in the Dalradian', *Irish Journal of Earth Sciences* pp. 23–35.

Chew, D. M. and Strachan, R. A. (2014), 'The Laurentian Caledonides of Scotland and Ireland', *Geological Society, London, Special Publications* **390**(1), 45–91.

Chew, D. M. and van Staal, C. R. (2014), 'The ocean-continent transition zones along the Appalachian-Caledonian margin of Laurentia: Examples of large-scale hyperextension during the opening of the Iapetus Ocean', *Geoscience Canada* **41**, 165–185.

Childs, C., Holdsworth, R. E., Jackson, C. A.-L., Manzocchi, T., Walsh, J. J. and Yielding, G. (2017), 'Introduction to the geometry and growth of normal faults', *Geological Society, London, Special Publications* **439**, SP439–23.

Childs, C., Manzocchi, T., Nicol, A., Walsh, J., Soden, A., Conneally, J. and Delogkos, E. (2016), 'The relationship between normal drag, relay ramp aspect ratio and fault zone structure', *Geological Society, London, Special Publications* **439**, SP439–16.

Childs, C., Nicol, A., Walsh, J. J. and Watterson, J. (2003), 'The growth and propagation of synsedimentary faults', *Journal of Structural geology* **25**(4), 633–648.

Choi, E., Buck, W. R., Lavier, L. L. and Petersen, K. D. (2013), 'Using core complex geometry to constrain fault strength', *Geophysical Research Letters* **40**(15), 3863–3867.

Claringbould, J. S., Bell, R. E., Jackson, C. A.-L., Gawthorpe, R. L. and Odinsen, T. (2017), 'Pre-existing normal faults have limited control on the rift geometry of the northern North Sea', *Earth and Planetary Science Letters* **475**, 190 – 206.

Clark, S. A., Sawyer, D. S., Austin, J. A., Christeson, G. L. and Nakamura, Y. (2007), 'Characterising the Galicia Bank-southern Iberia Abyssal Plain rifted margin segment boundary using multichannel seismic and ocean bottom seismometer data', *Journal of Geophysical Research* **112**, B03408.

Cowie, P. A., Underhill, J. R., Behn, M. D., Lin, J. and Gill, C. E. (2005), 'Spatio-temporal evolution of strain accumulation derived from multi-scale observations of late jurassic rifting in the northern North Sea: A critical test of models for lithospheric extension', *Earth and Planetary Science Letters* **234**(3-4), 401–419.

Cowie, P. and Scholz, C. (1992a), 'Physical explanation for the displacement-length relationship for faults using a post-yeild fracture mechanics model', *Journal of Structural Geology* **14**, 1133–1148.

Cowie, P. and Scholz, C. (1992b), 'Displacement-length scaling relationship for faults: data synthesis and', *Journal of Structural Geology* **14**, 1149–1156.

Davis, M. and Kusznir, N. (2004), *Depth-dependent lithospheric stretching at rifted continetal margins*, Columbia Universtiy Press, NY, pp. 92–136.

Davy, R., Morgan, J. V., Minshull, T., Bayrakci, G., Bull, J., Klaeschen, D., Reston, T., Sawyer, D. S., Lymer, G. and Cresswell, D. (2017), 'Resolving the fine-scale velocity structure of continental hyperextension at the deep Galicia margin using full-waveform inversion', *Geophysical Journal International* **212**(1), 244–263.

Dawers, N. and Anders, M. (1995), 'Displacement-length scaling and fault linkage', *Journal of Structural Geology* **17**(5), 607–614.

Dawers, N. H., Anders, M. H. and Scholz, C. H. (1993), 'Growth of normal faults: Displacement-length scaling', *Geology* **21**, 1107–1110.

de Charpal, O., Montadert, L., Guennoc, P. and Roberts, D. G. (1978), 'Rifting, crustal attenuation and subsidence in the Bay of Biscay', *Nature* **275**, 706–711.

Dean, S., Sawyer, D. and Morgan, J. (2015), 'Galicia Bank ocean-continent transition zone: new seismic reflection constraints', *Earth and Planetary Science Letters* **413**, 197–207.

Doré, T. and Lundin, E. (2015), 'Hyperextended continental margins—knowns and unknowns', *Geology* **43**(1), 95–96.

Driscoll, N. W. and Karner, G. D. (1998), 'Lower crustal extension across the northern Carnarvon Basin, Australia: Evidence for an eastward dipping detachment', *Journal of Geophysical Reasearch* **103-B3**, 4975–4991.

Druet, M., Muñoz-Martín, A., Granja-Bruña, J., Carbó-Gorosabel, A., Acosta, J., Llanes, P. and Ercilla, G. (2018), 'Crustal structure and continent-ocean boundary along the Galicia continental margin (NW Iberia): insights from combined gravity and seismic interpretation', *Tectonics* pp. 1576–1604.

Duretz, T., Petri, B., Mohn, G., Schmalholz, S., Schenker, F. and Müntener, O. (2016), 'The impor-

tance of structural softening for the evolution and architecture of passive margins', *Scientific reports* **6**, 38704.

Edwards, J. H., Kluesner, J. W., Silver, E. A., Brodsky, E. E., Brothers, D. S., Bangs, N. L., Kirkpatrick, J. D., Wood, R. and Okamoto, K. (2018), 'Corrugated megathrust revealed offshore from costa rica', *Nature Geoscience* **11**(3), 197.

Egan, S., Buddin, T., Kane, S. and Williams, G. (1997), Three-dimensional modelling and visualisation in structural geology: new techniques for the restoration and balancing of volumes, *in* 'Proceedings of the 1996 Geoscience Information Group Conference on Geological Visualisation. Electronic Geology Special Volume', Vol. 1, pp. 67–82.

Elliott, D. (1976), 'A discussion on natural strain and geological structure-the energy balance and deformation mechanisms of thrust sheets', *Phil. Trans. R. Soc. Lond. A* **283**(1312), 289–312.

Epin, M.-E. and Manatschal, G. (2017), 3D architecture, importance of inheritance and structural evolution of an extensional detachment system related to crustal thinning and exhumation: example of the Err detachment (SE Switzerland).

Epin, M.-E., Manatschal, G. and Amann, M. (2017), 'Defining diagnostic criteria to describe the role of rift inheritance in collisional orogens: the case of the Err-Platta nappes (Switzerland)', *Swiss Journal of Geosciences* **110**(2), 419–438.

Etheridge, M. A., Symonds, P. A. and Lister, G. S. (1988), *Application of the detachment model to reconstruction of conjugate passive margins*, American Association of Petroleum Geologists Memoir 46, pp. 23–40.

Finch, E. and Gawthorpe, R. (2017), 'Growth and interaction of normal faults and fault network evolution in rifts: insights from three-dimensional discrete element modelling', *Geological Society, London, Special Publications* **439**(1), 219–248.

Floyd, J., Mutter, J., Goodliffe, A. and Taylor, B. (2001), 'Evidence for fault weakness and fluid flow within an active low-angle normal fault', *Nature* **411**(6839), 779.

Fossen, H. and Rotevatn, A. (2016), 'Fault linkage and relay structures in extensional settings—a review', *Earth-Science Reviews* **154**, 14–28.

Franke, D. (2013), 'Rifting, litosphere breakup and volcanism: Comparison of magma-poor and volcanic rifted margins', *Marine and Peteoluem Geology* **42**, 63–87.

Froitzheim, N. and Eberli, G. P. (1990), 'Extensional detachment faulting in the evolution of a tethys passive continental margin, eastern Alps, Switzerland', *Geological Society of America bulletin* **102**(9), 1297–1308.

Gerya, T. (2009), *Introduction to numerical geodynamic modelling*, Cambridge University Press.

Giba, M., Walsh, J. and Nicol, A. (2012), 'Segmentation and growth of an obliquely reactivated normal fault', *Journal of Structural Geology* **39**, 253 – 267.
URL: *http://www.sciencedirect.com/science/article/pii/S019181411 20001 32*

Granot, R., Dyment, J. and Gallet, Y. (2012), 'Geomagnetic field variability during the cretaceous normal superchron', *Nature Geoscience* **5**(3), 220.

Hopper, J. R., Funck, T., Tucholke, B. E., Larsen, H. C., Holbrook, W. S., Louden, K. E., Shillington, D. and Lau, H. (2004), 'Continental breakup and the onset of ultraslow seafloor spreading off Flemish Cap on the Newfoundland rifted margin', *Geology* **32**(1), 93–96.

Huismans, R. and Beaumont, C. (2011), 'Depth-dependent extension, two stage breakup and cratonic underplating at rifted margins', *Nature* **473**, 74–78.

Huismans, R. S. and Beaumont, C. (2002), 'Asymmetric lithospheric extension: The role of frictional plastic strain softening inferred from numerical experiments', *Geology* pp. 211–214.

Huismans, R. S. and Beaumont, C. (2003), 'Symmetric and asymmetric lithosphere extension: Relative effects of frictional-plastic and viscous strain softening', *Journal of Geophysical Reseach* **108**, B10 2496.

Huismans, R. S. and Beaumont, C. (2014), 'Rifted continental margins: The case for depth-dependent extension', *Earth and Planetary Science Letters* **407**, 148–162.

Jackson, C. A.-L., Bell, R. E., Rotevatn, A. and Tvedt, A. B. M. (2017), 'Techniques to determine the kinematics of synsedimentary normal faults and implications for fault growth models', *Geological Society, London, Special Publications* **439**(1), 187–217.

Jackson, C. A.-L. and Rotevatn, A. (2013), '3D seismic analysis of the structure and evolution of a salt-influenced normal fault zone: a test of competing fault growth models', *Journal of Structural Geology* **54**, 215–234.

Jackson, C., Gawthorpe, R. and Sharp, I. (2006), 'Style and sequence of deformation during extensional fault-propagation folding: examples from the Hammam Faraun and El-Qaa fault blocks, Suez rift, Egypt', *Journal of Structural Geology* **28**(3), 519–535.

Jackson, J. and White, N. (1989), 'Normal faulting in the upper continental crust: observations from regions of active extension', *Journal of Structural Geology* **11**(1-2), 15–36.

Kane, S., Williams, G., Buddin, T., Egan, S. and Hodgetts, D. (1997), Flexural-slip based restoration in 3d, a new approach, *in* '1997 AAPG Annual Convention Official Program A', Vol. 58.

Khalil, S. M. and McClay, K. R. (2017), '3D geometry and kinematic evolution of extensional fault-related folds, NW Red Sea, Egypt', *Geological Society, London, Special Publications* **439**(1), 109–130.

Kim, Y.-S. and Sanderson, D. J. (2005), 'The relationship between displacement and length of faults: A review', *Earth-Science Reviews* **68**, 317–334.

Klein, E. M., Smith, D. K., Williams, C. M. and Schouten, H. (2005), 'Counter-rotating microplates at the Galapagos Triple Junction', *Nature* **433**, 855.

Koehn, D., Aanyu, K., Haines, S. and Sachau, T. (2008), 'Rift nucleation, rift propagation and the creation of basement micro-plates within active rifts', *Tectonophysics* **458**(1-4), 105–116.

Krahmann, G., Brandt, P., Klaeschen, D. and Reston, T. (2008), 'Mid-depth internal wave energy off the Iberian peninsula estimated from seismic reflection data', *Journal of Geophysical Research: Oceans* **113**(C12).

Krawczyk, C., Reston, T., Beslier, M. and Boillot, G. (1996), '38. Evidence for detachment tectonics on the Iberia Abyssal Plain rifted margin', *Proceedings-ocean Drilling Program Scientific Results* pp. 3–26.

Kusznir, N. J., Hunsdale, R., Roberts, A. M. and Team-iSIMM (2005), Norwegian margin depth-dependent stretching, *in* A. G. Dore and B. A. Vining, eds, 'Petroleum Geology: North-West Europe and Global Perspectives—Proceedings of the 6th Petroleum Geology Conference', Geological Society, London.

Kusznir, N. J. and Karner, G. D. (2007), Continental lithospheric thinning and breakup in response to upwelling divergent flow:application to the Woodlark, Newfoundland and Iberia margins, *in* 'Imaging, mapping and modelling continental lithosphere extension and breakup', Geological Society of London Special Publication 282, pp. 389–419.

Kusznir, N. J., Marsden, G. and Egan, S. S. (1991), A flexral-cantilever simple-shear/pure-shear model of continental lithosphere extension: Applications to the Jeanne d'Arc Basin, Grand Banks and Viking Graben, North Sea, *in* 'The Geometry of Normal Faults, Gological Society of London Special Publication 56', pp. 41–60.

Lavier, L. L., Buck, W. R. and Poliakov, A. N. (1999), 'Self-consistent rolling-hinge model for the evolution of large-offset low-angle normal faults', *Geology* **27**, 1127–1130.

Lavier, L. L. and Manatschal, G. (2006), 'A mechanism to thin the continental lithosphere at magma-poor margins', *Nature* **440**, 324–3328.

Lentini, M. R., Fraser, S. I., Sumner, S. and Davies, R. j. (2010), 'Geodynamics of the central south atlantic conjugate margins: Implications for hydrocarbon potential', *Petroleum Geoscience* **16**, 217–229.

Leythaeuser, T., Reston, T. J. and Minshull, T. (2005), 'Waveform inversion of the s reflector west of spain: Fine structure of a detachment fault', *Geophysical research letters* **32**(22).

Li, L., Clift, P., Stephenson, R. and Nguyen, H. (2014), 'Non-uniform hyper-extension in advance

of seafloor spreading on the Vietnam continental margin and the SW South China Sea', *Basin Research* **26**(1), 106–134.

Lister, G. S., Etheridge, M. A. and Symonds, P. A. (1986), 'Detachment faulting and the evolution of passive margins', *Geology* **14**, 246–250.

Long, J. J. and Imber, J. (2012), 'Strain compatibility and fault linkage in relay zones on normal faults', *Journal of Structural Geology* **36**, 16 – 26.
URL: *http://www.sciencedirect.com/science/article/pii/S019181411 1002240*

Lymer, G., Cresswell, D., Reston, T., Bull, J. and Sawyer, D. (2016), Corrugations on the s reflector west of spain: Kinematic implications., *in* 'American Geophysical Union Fall Meeting, T41E-3005'.

Lymer, G., Cresswell, D., Reston, T., Bull, J., Sawyer, D., Morgan, J., Stevenson, C., Causer, A., Minshull, T. and Shillington, D. (2018), The development of detachment faulting during 3D, continental breakup. Manuscript submitted for publication.

Manatschal, G. (2004), 'New models for evolution of magma-poor rifted margins based on a review of data and concepts from West Iberia and the Alps', *International Journal of Earth Science* **93**, 432–466.

Manatschal, G. and Bernoulli, D. (1999), 'Architecture and tectonic evolution of non-volcanic margins: Present-day Galicia and ancient Adria', *Tectonics* **18**(6), 1099–1119.

Manatschal, G., Froitzheim, N., Rubenach, M. and Turrin, B. D. (2001), *The role of detachment faulting in the foirmation of an ocean-continent transition; Insights form the Iberian Abyssal Plain*, Geological Socety of London, London, pp. 405–428.

Manatschal, G., Lavier, L. and Chenin, P. (2015), 'The role of inheritance in structuring hyper-extended rift systems: Some considerations based on observations and numerical modeling', *Gondwana Research* **27**(1), 140–164.

Manatschal, G. and Müntener, O. (2009), 'A type sequence across an ancient magma-poor ocean–continent transition: the example of the western Alpine Tethys ophiolites', *Tectonophysics* **473**(1-2), 4–19.

Manatschal, G., Müntener, O., Lavier, L., Minshull, T. and Péron-Pinvidic, G. (2007), Observations from the Alpine Tethys and Iberia–Newfoundland margins pertinent to the interpretation of continental breakup, Vol. 282, Geological Society of London, pp. 291–324.

Marrett, R. and Allmendinger, R. W. (1992), 'Amount of extension on" small" faults: An example from the viking graben', *Geology* **20**(1), 47–50.

Masini, E. and Manatschal, G. (2014), 'The Err detachment in SE Switzerland: a witness of how continents break apart', *International Journal of Earth Sciences: Geologische Rundschau* **103**(1), 121.

Masini, E., Manatschal, G. and Mohn, G. (2013), 'The Alpine Tethys rifted margins: Reconciling old and new ideas to understand the stratigraphic architecture of magma-poor rifted margins', *Sedimentology* **60**, 174–196.

Masini, E., Manatschal, G., Mohn, G. and Unternehr, P. (2012), 'Anatomy and tectono-sedimentary evolution of a rift-related detachment system: The example of the Err detachment (central Alps, SE Switzerland)', *GSA Bulletin* **124**(9/10), 1535–1551.

Masini, E., Manatschal, G., Tugend, J., Mohn, G. and Flament, J.-M. (2014), 'The tectono-sedimentary evolution of a hyper-extended rift basin: the example of the Arzacq-Mauleon rift system (western Pyrenees, SW France)', *International Journal of Earth Science* **103**, 1569–1596.

Maus, S., Barckhausen, U., Berkenbosch, H., Bournas, N., Brozena, J., Childers, V., Dostaler, F., Fairhead, J., Finn, C., Von Frese, R. et al. (2009), 'Emag2: A 2–arc min resolution earth magnetic anomaly grid compiled from satellite, airborne, and marine magnetic measurements', *Geochemistry, Geophysics, Geosystems* **10**(8).

McClusky, S., Reilinger, R., Ogubazghi, G., Amleson, A., Healeb, B., Vernant, P., Sholan, J.,

Fisseha, S., Asfaw, L., Bendick, R. et al. (2010), 'Kinematics of the southern Red Sea–Afar triple junction and implications for plate dynamics', *Geophysical Research Letters* **37**(5).

McDermott, K. and Reston, T. (2015), 'To see, or not to see? rifted margin extension', *Geology* **43**(11), 967–970.

McKenzie, D. (1978), 'Some remarks on the development of sedimentary basins', *Earth and Planetary Science Letters* **40**, 25–32.

Mohn, G., Karner, G. D., Manatschal, G. and Johnson, C. A. (2015), 'Structural and stratigraphic evolution of the Iberia-Newfoundland hyper-extended rifted margin: a quantitative modelling approach', *Geological Society, London, Special Publications* **413**(1), 53–89.

Mohn, G., Manatschal, G., Beltrando, M., Masini, E. and Kusznir, N. (2012), 'Necking of continental crust in magma-poor rifted margins: Evidence from the fossil Alpine Tethys margins', *Tectonics* **31**, TC1012.

Mohn, G., Manatschal, G., Müntener, O., Beltrando, M. and Masini, E. (2010), 'Unravelling the interaction between tectonic and sedimentary processes during lithospheric thinning in the Alpine Tethys margins', *International Journal of Earth Sciences* **99**(1), 75–101.

Molnar, N., Cruden, A. and Betts, P. (2017), 'Interactions between propagating rotational rifts and linear rheological heterogeneities: Insights from three-dimensional laboratory experiments', *Tectonics* **36**(3), 420–443.

Murillas, J., Mougenot, D., Boillot, G., Comas, M. C., Banda, E. and Mauffret, A. (1990), 'Structure and evolution of the Galicia Interior Basin (Atlantic western Iberian continental margin)', *Tectonophysics* **184**, 297–319.

Murphy, J. B. and Nance, R. D. (2013), 'Speculations on the mechanisms for the formation and breakup of supercontinents', *Geoscience Frontiers* **4**(2), 185–194.

Naliboff, J. B., Buiter, S. J., Péron-Pinvidic, G., Osmundsen, P. T. and Tetreault, J. (2017), 'Complex fault interaction controls continental rifting', *Nature communications* **8**(1), 1179.

Naliboff, J. and Buiter, S. J. (2015), 'Rift reactivation and migration during multiphase extension', *Earth and Planetary Science Letters* **421**, 58–67.

Nance, R. D. and Murphy, J. B. (2013), 'Origins of the supercontinent cycle', *Geoscience Frontiers* **4**(4), 439–448.

Nance, R. D., Murphy, J. B. and Santosh, M. (2014), 'The super continent cycle: A retrospective essay', *Gondwana Research* **25**, 4–29.

Newman, R. and White, N. (1997), 'Rheology of the continental lithosphere inferred from sedimentary basins', *Nature* **385**(6617), 621.

Nicol, A., Childs, C., Walsh, J. J., Manzocchi, T. and Schöpfer, M. P. J. (2017), 'Interactions and growth of faults in an outcrop-scale system', *Geological Society, London, Special Publications* **439**(1), 23–39.

Nicol, A., Walsh, J., Watterson, J. and Gillespie, P. (1996), 'Fault size distributions m are they really power-law?', *Journal of Structural Geology* **18**(2/3), 191–197.

Osmundsen, P. and Ebbing, J. (2008), 'Styles of extension offshore mid-norway and implications for mechanisms of crustal thinning at passive margins', *Tectonics* **27**(6).

Peacock, D. (2002), 'Propagation, interaction and linkage in normal fault systems', *Earth Science Reviews* **58**, 121–142.

Peacock, D. and Sanderson, D. (1994), 'Geometry and development of relay ramps in normal fault systems', *American Assosciation of Petroleum Geologists Bulletin* **78**(2), 147–165.

Peng, Z. and Gomberg, J. (2010), 'An integrated perspective of the continuum between earthquakes and slow-slip phenomena', *Nature Geoscience* **3**(9), 599.

Pérez-Gussinyé, M. (2013), A tectonic model for hyperextension at magma-poor rifted margins: an example from the west Iberia-Newfoundland conjugate margins, Vol. 369, Geological Society of London, pp. 403–427.

Pérez-Gussinyé, M., Morgan, J. P., Reston, T. J. and Ranero, C. R. (2006), 'The rift to drift transition at non-volcanic margins: Insights from numerical modelling', *Earth and Planetary Science Letters* **244**, 458–473.

Pérez-Gussinyé, M., Ranero, C. R. and Reston, T. J. (2003), 'Mechanisms of extsension at nonvolcanic margins: Evidence from the Galicia Interior Basin, west of Iberia', *Journal of Geophysical Research* **108**(B5), 2245.

Pérez-Gussinyé, M. and Reston, T. J. (2001), 'Rheological evolution during extension at nonvolcanic rifted margins' onset of serpentinization and development of detachments leading to continental breakup', *Journal of Geophysical Research* **106**(B3), 3961–3975.

Pérez-Gussinyé, M., Reston, T. J. and Phipps Morgan, J. (2001), Serpentinization and magmatism during extension at non-volcanic margins: the effect of initial lithospheric structure, *in* 'Non-Volcanic Rifting of Continental Margins: A Comparison of Evidence from Land and Sea. Geological Society, London, Special Publications 187', The Geological Society of London, London, pp. 551–576.

Peron-Pinvidic, G. and Manatschal, G. (2009), 'The final rifting evolution at deep magma-poor passive margins from Iberia-Newfoundland: A new point of view', *International Journal of Earth Science* **98**, 1581–1597.

Peron-Pinvidic, G. and Manatschal, G. (2010), 'From microcontinents to extensional allochthons: witnesses of how continents rift and break apart?', *Petroleum Geoscience* **16**, 189–197.

Peron-Pinvidic, G., Manatschal, G., Minshull, T. and Sawyer, D. (2007), 'Tectonosedimentary evolution of the deep Iberia-Newfoundland margins: Evidence for a complex breakup history', *Tectonics* **26**, TC2011.

Peron-Pinvidic, G., Mantaschal, G. and Osmundsen, P. T. (2013), 'Structural comparisons of archytypal Atlantic rifted margins: A review of observations and concepts', *Marine and Petroleum Geology* **43**, 21–47.

Pindell, J., Graham, R. and Horn, B. (2014), 'Rapid outer marginal collapse at the rift to drift transition of passive margin evolution, with a Gulf of Mexico case study', *Basin Research* **26**, 1–25.

Prada, M., Watremez, L., Chen, C., O'Reilly, B. M., Minshull, T. A., Reston, T. J., Shannon, P. M., Klaeschen, D., Wagner, G. and Gaw, V. (2017), 'Crustal strain-dependent serpentinisation in the Porcupine Basin, offshore Ireland', *Earth and Planetary Science Letters* **474**, 148–159.

Puttock, S. H. (2015), Polygonal faulting in post rift sediment of the Galicia margin, Mastersthesis, University of Birmingham.

Ranero, C. R. and Pérez-Gussinyé, M. (2010), 'Sequntial faulting explains the asymmetry and extension discrepancy of conjugate margins', *Nature* **468**, 294–298.

Resor, P. G. and Meer, V. E. (2009), 'Slip heterogeneity on a corrugated fault', *Earth and Planetary Science Letters* **288**(3-4), 483–491.

Reston, T. (1990), 'Mantle shear zones and the evolution of the northern North Sea basin', *Geology* **18**(3), 272–275.

Reston, T. J. (1996), 'The S reflector west of galicia: The seismic signature of a detachment fault', *Geophysical Journal International* **127**, 230–144.

Reston, T. J. (2005), 'Polyphase faulting during the development of the west galicia rifted margin', *Earth and Planetary Science Letters* **237**, 561–576.

Reston, T. J. (2007a), 'Extension discrepancy at North Atlantic non-volcanic rifted margins: Depth dependent stretching or unrecognised faulting?', *Geology* **35**(4), 367–370.

Reston, T. J. (2009*a*), 'The extension discrepancy and syn-rift subsidence deficit at rifted margins', *Petroleum Geoscience* **15**(3), 217–237.

Reston, T. J. (2009*b*), 'The strucutre, evolution and symmetry of the magma-poor rifted margins of the north and central Atlantic: A synthesis', *Tectonophysics* **468**, 6–27.

Reston, T. J., Leythauser, T., Booth-Rea, G., Sawyer, D., Klaeschen, D. and Long, C. (2007b), 'Movement along a low-angle normal fault: The S Reflector west of Spain', *Geochemistry, Geophysics, Geosystems - G3* **8**(6).

Reston, T. J. and McDermott, K. G. (2011), 'Successive detachment faults and mantle unroofing at magma-poor rifted margins', *Geology* **39**(11), 1071–1074.

Reston, T. J. and McDermott, K. G. (2014), 'An assessment of the cause of the extension discrepancy with reference to the west Galicia margin', *Basin Research* **26**, 135–153.

Reston, T. J. and Pérez-Gussinyé, M. (2007c), 'Lithospheric extension from rifting to continental breakup at magma-poor margins: rheology, serpentinisation and symmetry', *International Journal of Earth Sciences* **96**(6), 1033–1046.

Reston, T. and Manatschal, G. (2011), Rifted margins: Building blocks of later collision, *in* 'Arc-Continent Collision', Springer, pp. 3–21.

Reston, T., Pennell, J., Stubenrauch, A., Walker, I. and Perez-Gussinye, M. (2001), 'Detachment faulting, mantle serpentinization, and serpentinite-mud volcanism beneath the Porcupine Basin, southwest of Ireland', *Geology* **29**(7), 587–590.

Roche, V., Homberg, C., van der Baan, M. and Rocher, M. (2017), 'Widening of normal fault zones due to the inhibition of vertical propagation', *Geological Society, London, Special Publications* **439**(1), 271–288.

Rutter, E. H. (1986), 'On the nomenclature of mode of failure transitions in rocks', *Tectonophysics* **122**, 381–387.

Sandwell, D. T., Müller, R. D., Smith, W. H., Garcia, E. and Francis, R. (2014), 'New global marine gravity model from CryoSat-2 and Jason-1 reveals buried tectonic structure', *Science* **346**(6205), 65–67.

Savva, D., Meresse, F., Pubellier, M., Chamot-Rooke, N., Lavier, L., Po, K. W., Franke, D., Steuer,

S., Sapin, F., Auxietre, J. et al. (2013), 'Seismic evidence of hyper-stretched crust and mantle exhumation offshore Vietnam', *Tectonophysics* **608**, 72–83.

Sawyer, D. S., Whitmarsh, R. B., Klaus, A. and al., e. (1994), Proceedings of Pcean Drilling Programme - Initial Reports 149, Report.

Schlishe, R., Yooung, S., Ackerman, R. and Gupta, A. (1996), 'Geometry and scaling relations of a population of very small rift-related normal faults', *Geology* **24**(8), 683–686.

Scholz, C. and Cowie, P. (1990), 'Determination of total strian from faulting using slip measurements', *Nature* **346**, 837–839.

Schuba, C. N., Gray, G. G., Morgan, J. K., Sawyer, D. S., Shillington, D. J., Reston, T. J., Bull, J. M. and Jordan, B. E. (2018), 'A low-angle detachment fault revealed: Three-dimensional images of the S-Reflector fault zone along the Galicia passive margin', *Earth and Planetary Science Letters* **492**, 232–238.

Sclater, J. G. and Christie, P. A. (1980), 'Continental stretching: An explanation of the post-mid-cretaceous subsidence of the central north sea basin', *Journal of Geophysical Research: Solid Earth* **85**(B7), 3711–3739.

Sibuet, J.-C. (1992), 'New constraints on the formation of the non-volcanic continental Galicia-Flemish Cap conjugate margins', *Journal of the Geological Society* **149**(5), 829–840.

Sibuet, J.-C., Srivastava, S. and Manatschal, G. (2007), 'Exhumed mantle-forming transitional crust in the Newfoundland-Iberia rift and associated magnetic anomalies', *Journal of Geophysical Research: Solid Earth* **112**(B6).

Sillitoe, R. H. (2003), 'Iron oxide-copper-gold deposits: an Andean view', *Mineralium Deposita* **38**(7), 787–812.

Stein, R. S. (1999), 'The role of stress transfer in earthquake occurrence', *Nature* **402**(6762), 605.

Sutra, E. and Manatschal, G. (2012), 'How does continental crust thin in a hyperextended rifted margin? insights from the Iberia Margin', *Geology* **40**(2), 139–142.

Sutra, E., Manatschal, G., Mohn, G. and Unternehr, P. (2013), 'Quantification and restoration of extensional deformation along the western iberia and newfoundland rifted margins', *Geochemistry, Geophysics, Geosystems G3* **14**, 2575–2597.

Taner, M. T., Koehler, F. and Sheriff, R. (1979), 'Complex seismic trace analysis', *Geophysics* **44**(6), 1041–1063.

Tankard, A. J. and Balkwill, H. R. (1989), *Extensional Tectonics and Stratigraphy of the North Atlantic Margin: Introduction*, American Association of Petroleum Geologists Memoir 46, pp. 1–6.

Tetreault, J. and Buiter, S. (2017), 'The influence of extension rate and crustal rheology on the evolution of passive margins from rifting to break-up', *Tectonophysics* .

Torabi, A. and Berg, S. (2011), 'Scaling of fault attributes', *Marine and Petroleum Geology* **28**, 1444–1460.

Tucholke, B. E. and Sibuet, J.-C. (2007), *Leg 210 Synthesis: Tectonic, magmatic anf sedimentary evolution of Newfoundland-Iberia rift*, Vol. 10, Ocean Drilling Program, College Station TX, pp. 1–56.

Tucholke, B. E. and Sibuet, J.-C. (2012), 'Problematic plate reconstruction', *Nature Geoscience* **5**(10), 676.

Tugend, J., Manatschal, G. and Kusznir, N. (2015), 'Spatial and temporal evolution of hyperextended rift systems: Implication for the nature, kinematics, and timing of the iberian-european plate boundary', *Geology* **43**(1), 15–18.

Tugend, J., Manatschal, G., Kusznir, N., Masini, E., Mohn, G. and Thinon, I. (2014), 'Formation and deformation of hyperextended rift systems: Insights from rift domain mapping in the Bay of Biscay-Pyrenees', *Tectonics* **33**(7), 1239–1276.

Tullis, T. E., Horowitz, F. G. and Tullis, J. (1991), 'Flow laws of polyphase aggregates from end-member flow laws', *Journal of Geophysical Research: Solid Earth* **96**(B5), 8081–8096.

Twiss, R. J. and Moores, E. M. (2007), *Structural geology, (Second Edition)*, Macmillan.

Téllez, F., Matias, L. M., Córdoba, D. and Mendes-Victor, L. A. (1993), 'Structure of the crust in the schistose domain of Galicia-Tras-os-Montes (NW Iberian peninsula)', *Tectonophysics* **221**(1), 81 – 93.

Vann, I. R. (1985), 'Structural geology: To stretch a continent', **316**.

Vauchez, A., Barruol, G. and Tommasi, A. (1997), 'Why do continents break-up parallel to ancient orogenic belts?', *Terra Nova* **9**(2), 62–66.

Vink, G. E., Morgan, W. J. and Zhao, W.-L. (1984), 'Preferential rifting of continents: A source of displaced terranes', *Journal of Geophysical Research SE* **89**, 10072–10076.

Walsh, J. J. and Watterson, J. (1989), 'Displacement gradients on fault surfaces', *Journal of Structural Geology* **11**(3), 307–316.

Walsh, J. J. and Watterson, J. (1991), 'Geometric and kinematic coherence and scale effects in normal fault systems', *Geological Society, London, Special Publications* **56**(1), 193–203.

Walsh, J., Nicol, A. and Childs, C. (2002), 'An alternative model for the growth of faults', *Journal of Structural Geology* **24**, 1669–1675.

Walsh, J. and Watterson, J. (1987), 'Distributions of cumulative displacement and seismic slip on a single normal', *Journal of Structural Geology* **9**(8), 1039–1046.

Walsh, J. and Watterson, J. (1988), 'Analysis of the relationship between displacements and dimensions of faults', *Journal of Structural Geology* **10**(3), 239–247.

Walsh, J. and Watterson, J. (1992), 'Populations of faults and fault displacements and their effects on estimates', *Journal of Structural Geology* **14**(6), 701–712.

Watterson, J. (1986), 'Fault dimensions, displacements and growth', *Pure and Applied Geophysics* **124**(1-2), 365–373.

Watts, A. B. (2001), *Isostasy and Flexure of the Lithosphere*, Cambridge University Press.

Wernicke, B. (1985), 'Uniform-sense normal simple shear of the continental lithosphere', *Canadian Journal of Earth Science* **22**(1), 108–125.

Wernicke, B. (1995), 'Low-angle normal faults and seismicity: A review', *Journal of Geophysical Research: Solid Earth* **100**(B10), 20159–20174.

Wernicke, B. and Axen, G. J. (1988), 'On the role of isostasy in the evolution of normal fault systems', *Geology* **16**, 848–851.

White, N. (1990), *Does the uniform stretching model work in the North Sea?*, Publ Int Lithos Prog 181, pp. 217–239.

White, N. and McKenzie, D. (1988), 'Formation of the "steer's head" geometry of sedimentary basins by differential stretching of the crust and mantle', *Geology* **16**, 250–253.

Whitmarsh, R. B., Beslier, M.-O., Wallace, P. J. and al., e. (1998), Proceedings of Ocean Drilling Programme Initial Reports 173, Report.

Whitmarsh, R. B., Dean, S. M. and Minshull, T. A. (2000), 'Tectonic implications of exposure of lower continental crust beneath the Iberia Abyssal Plain, northeast Atlantic ocean: Geophysical evidence', *Tectonics* **19**(5), 919–942.

Whitmarsh, R. B., Manatschal, G. and Minshull, T. A. (2001), 'Evolution of magma-poor continental margins from rifting to seafloor spreading', *Nature* **413**, 150–153.

Wilson, J. T. (1963), 'Hypothesis of Earth's behaviour', *Nature* **198**, 925–9.

Wilson, J. T. (1968), 'Static or mobile Earth: The current scientific revolution', *Proceedings of the American Philosophical Society* **112**(5), 309–320.

Wilson, R. C. L., Hiscott, R. N., Willis, M. G. and Gradstein, F. M. (1989), *The Lusitanian Basin of west-central Portugal: Mesozoic and Tertiary tectonic, stratigraphic and subsidence history*, AAPG Memoir 46, pp. 341–362.

Wilson, R. C., Manatschal, G. and Wise, S. (2001), *Rifting along non-volcanic passive margins: stratigraphic and seismic evidence from the Mesozoic successions of the Alps and western Iberia*, Geological Society, London.

Wood, R. and Barton, P. (1983), 'Crustal thinning and subsidence in the North Sea', *Nature* **302**, 134–136.

Yielding, G., Needham, C. and Jones, H. (1996), 'Sampling of fault populations using sub-surface data: a review', *Journal of Structural Geology* **18**(2-3), 135–146.

Yilmaz, Ö. (2001), *Seismic data analysis*, Vol. 1, Society of Exploration Geophysicists Tulsa.

Zhang, P., Slemmons, D. and Mao, F. (1991), 'Geometric pattern, rupture termination and fault segmentation of the Dixie Valley-Pleasant Valley active normal fault system, Nevada, U.S.A.', *Journal of Strucutural Geology* **13**(2), 165–176.

Ziegler, P. A. (1989), *Evolution of the north Atlantic - An overview*, Amercian Association of Petroleum Geologists, pp. 111–130.

Appendix

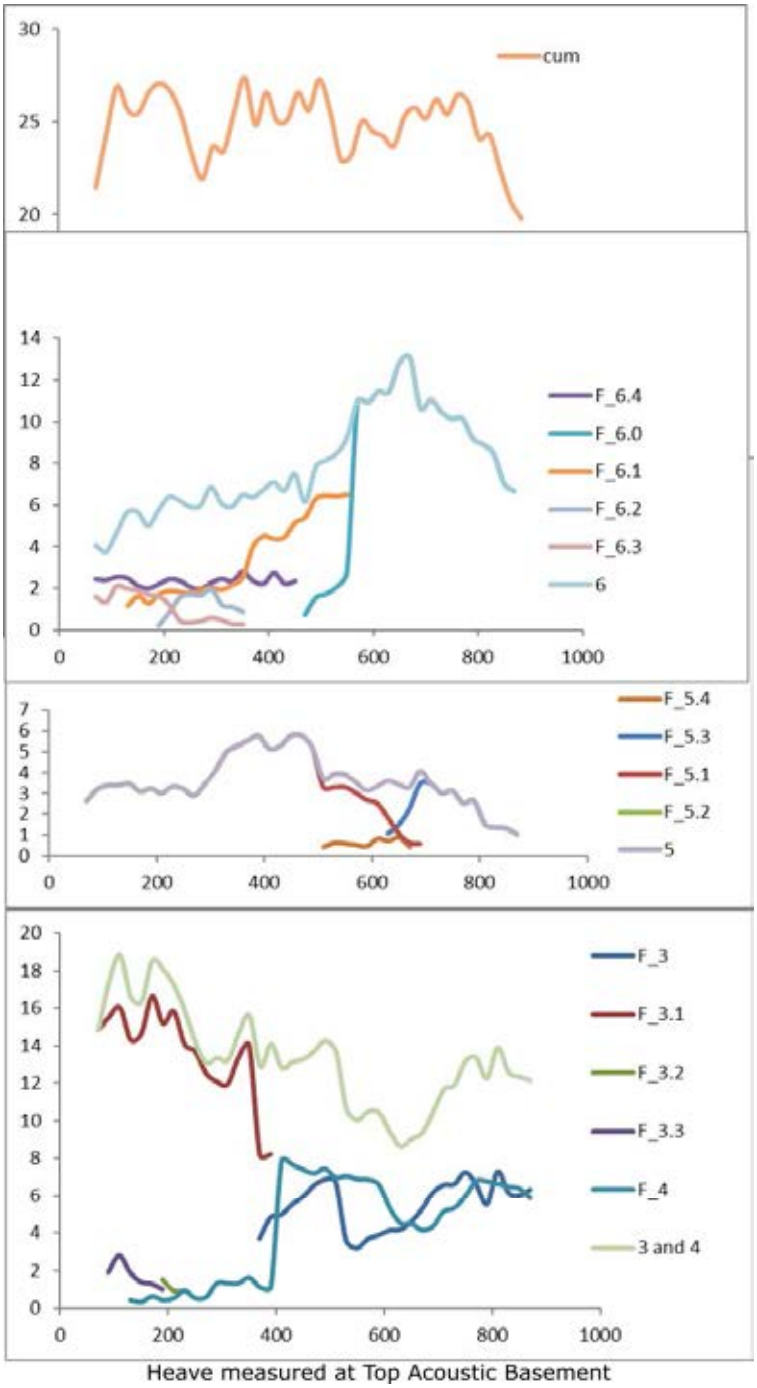

Heave measured at Top Acoustic Basement

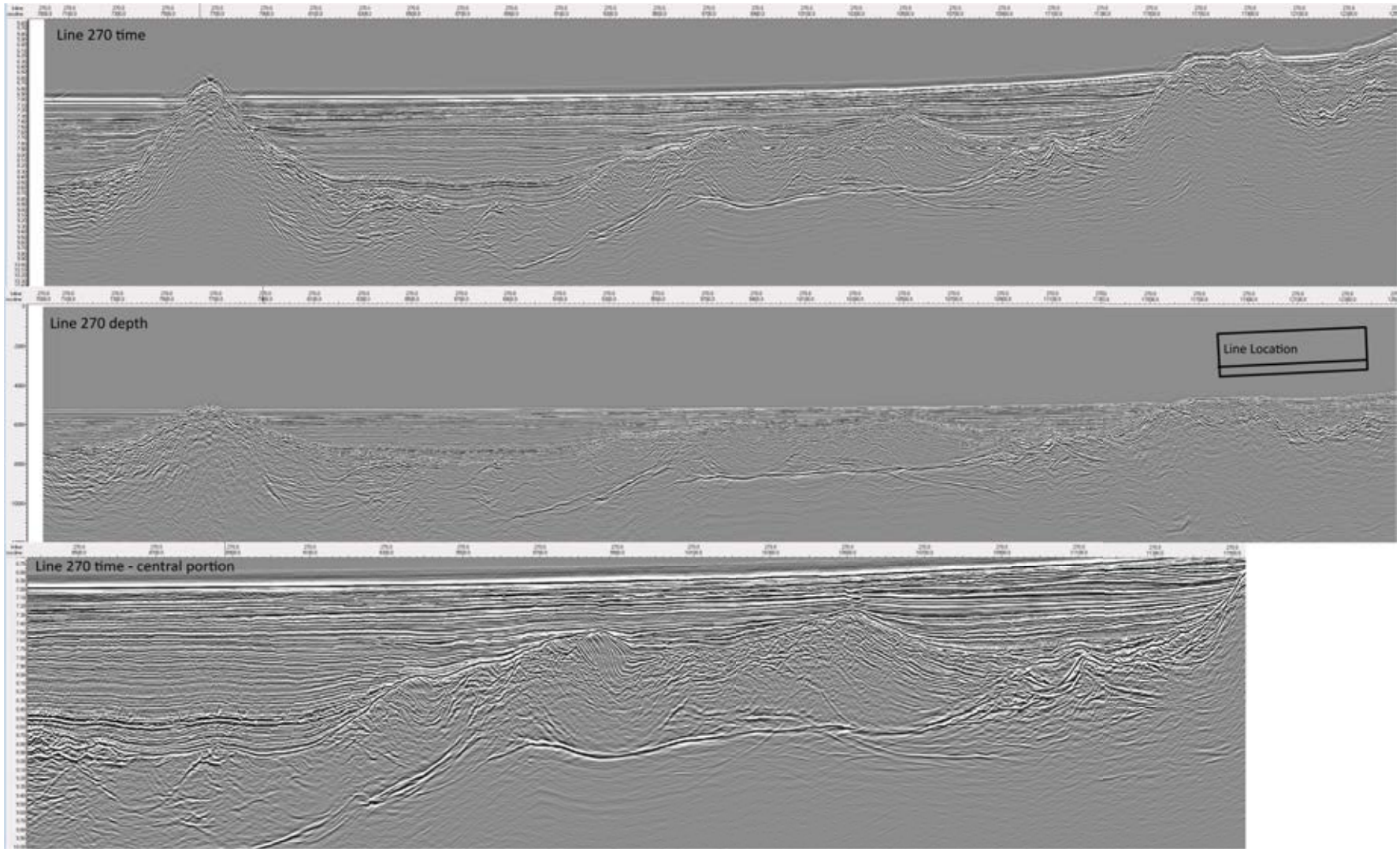
Line 270 time
Line 270 depth
Line Location
Line 270 time - central portion

Figure 8.1

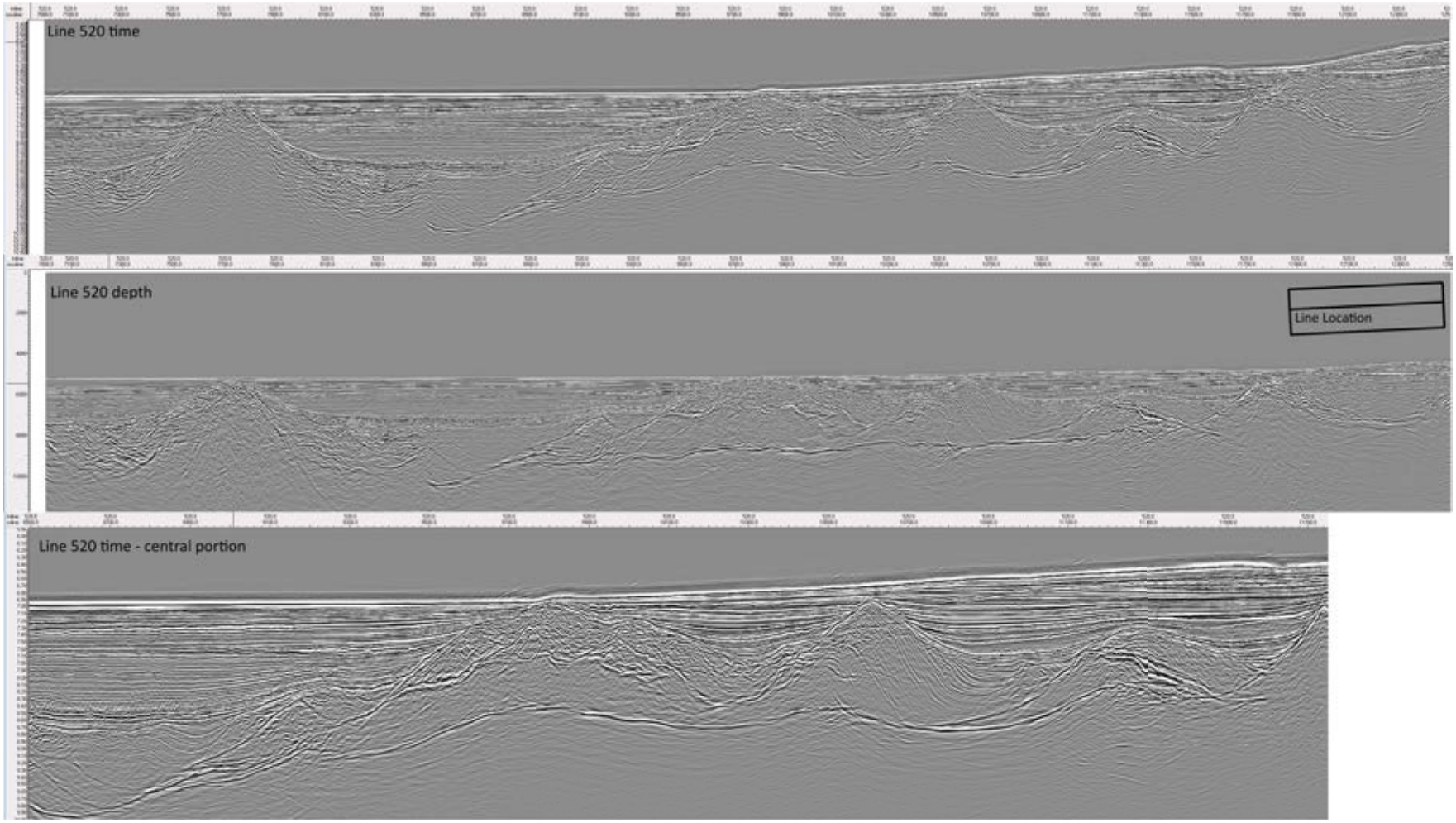
Line 520 time
Line 520 depth
Line Location
Line 520 time - central portion

Figure 8.2

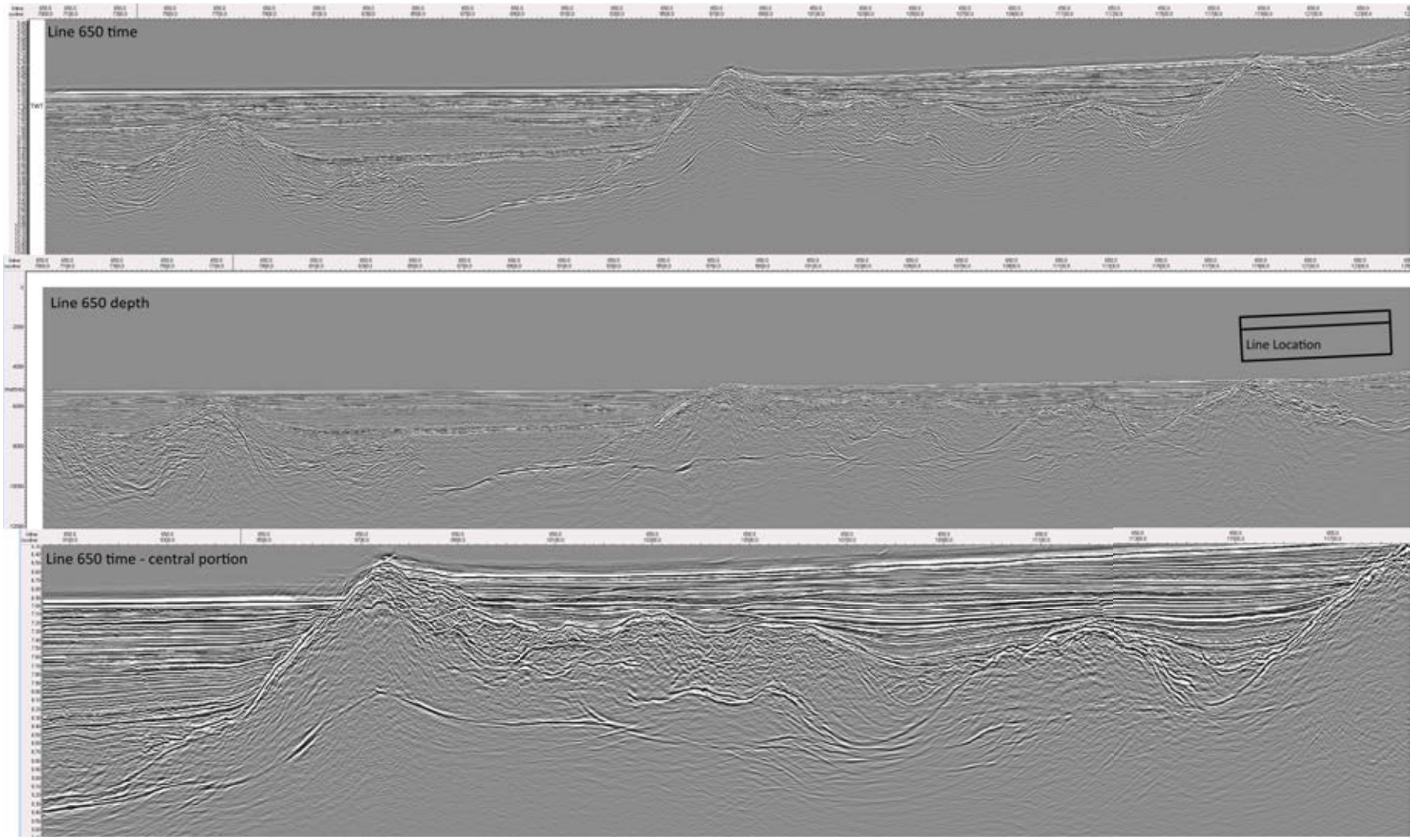
Line 650 time
Line 650 depth
Line Location
Line 650 time - central portion

Figure 8.3